# Combining Catalytic Chain Transfer Polymerisation and Post-Polymerisation Functionalisation for the Preparation of Functional Materials


By José-Chris Abi Saleh

A thesis submitted in partial fulfilment of the requirements of the degree of

Doctor of Philosophy in Chemistry

Department of Chemistry

University of Warwick

June 2021

*"Our virtues and our failures are inseparable, like force and matter. When they separate, man is no more"* – Nikola Tesla

*"Ce sont les Grecs qui nous ont légué le plus beau mot de notre langue : le mot " enthousiasme" - du grec "en théo", un Dieu intérieur"* – Louis Pasteur
(It is the Greeks who gave us the most beautiful word in our language: the word “enthusiasm”, from the word “theo”; a god inside)

*"It does, for example, no good to offer an elegant, difficult and expensive process to an industrial manufacturing chemist, whose ideal is something to be carried out in a disused bathtub by a one-armed man who cannot read, the product being collected continuously through the drain hole in 100% purity and yield"* – Sir John Cornforth

# Table of Contents

# List of Figures, Schemes and Tables

## Abbreviations

| | |
|---|---|
| %AOWP | Percentage agent on weight of pigment |
| AA | Acrylic acid |
| ACN | Acetonitrile |
| ACVA | 4,4′-Azobis(4-cyanopentanoic acid) |
| AIBN | Azobisisobutyronitrile |
| ATRP | Atom transfer radical polymerization |
| BET | Brunauer–Emmett–Teller |
| CB | Carbon black |
| CCTP | Catalytic chain transfer polymerisation |
| CHT | Cyclohexanethiol |
| CoBF | Bis[(difluoroboryl)dimethylglyoximato]cobalt(II) |
| CTA | Chain transfer agent |
| CTAC | Cetyltrimethylammonium chloride |
| CuAAC | Azide-alkyne Huisgen cycloaddition |
| DBN | 1,5-Diazabicyclo[4.3.0]non-5-ene |
| DBU | 1,8-Diazabicyclo(5.4.0)undec-7-ene |
| DCE | Dichloroethane |
| DCM | Dichloromethane |
| DCTB | Trans-2-[3-(4-tert-Butylphenyl)-2-methyl-2-propenylidene]malononitrile |
| DDA | Dodecylamine |
| DDT | Dodecanethiol |
| DLS | Dynamic light scattering |
| DMAP | 4-Dimethylaminopyridine |

| | |
|---|---|
| DMF | Dimethylformamide |
| dmg | Dimethyl glyoxime |
| DMPP | Dimethylphenyl phosphine |
| DMSO | Dimethyl sulfoxide |
| DP | Degree of polymerisation |
| DSC | Differential scanning calorimetry |
| DTGA | Derivative thermogravimetric analysis |
| EA | Ethylamine |
| EGDMA | Ethylene glycol dimethacrylate |
| EHA | 2-Ethylhexyl acrylate |
| ESI | Electrospray |
| ESI-MS | Electrospray-mass spectrometry |
| ETA | Ethanolamine |
| EtOAc | Ethyl acetate |
| FRP | Free-radical polymerisation |
| FT-IR | Fourier transform-infra red |
| GBP | British pound sterling |
| GC-FID | Gas chromatography-flame ionisation detection |
| GlyMA | Glycerol monomethacrylate |
| GMA | Glycidyl methacrylate |
| GPC | Gel permeation chromatography |
| HEMA | Hydroxyethyl methacrylate |
| HIPE | High internal phase emulsion |
| HT | Hexanethiol |
| IBOA | Isobornyl acrylate |

| | |
|---|---|
| IPA | Isopropyl alcohol |
| i-PT | Iso-propylthiol |
| IR | Infra-red |
| MALDI-ToF | Matrix assisted laser desorption ionization-time of flight mass spectrometry |
| MAOS | Microwave-assisted organic synthesis |
| MB | Mill base |
| MEA | 2-Methoxyethyl acrylate |
| MeOH | Methanol |
| MMA | Methyl methacrylate |
| MWCNT | Multi-walled carbon nanotube |
| NA | Nonylamine |
| NMP | Nitroxide-nediated polymerisation |
| NMR | Nuclear magnetic resonance |
| NT | Nonanethiol |
| ODT | Octadecanethiol |
| Pdi | Polydispersity |
| PEG | Polyethylene glycol |
| PEO | Polyethylene oxide |
| PET | Phenylethyl thiol |
| PS | Polystyrene |
| RAFT | Reversible addition−fragmentation chain-transfer |
| RDRP | Reversible-deactivation radical polymerization |
| RNA | Ribonucleic acid |
| ROMP | Ring-opening metathesis polymerisation |

| | |
|---|---|
| SEM | Scanning electron microscopy |
| SI | Supplementary information |
| TDT | Tetradecane thiol |
| TEA | Triethylamine |
| TEM | Transmission electron microscopy |
| TGA | Thermogravimetric analysis |
| THF | Tetrahydrofuran |
| TPMD | Tetraethyl-2,2′-[1,4-phenylenebis(methanyl-ylidene)]dimalonate |
| UV | Ultraviolet |
| V-601 | Dimethyl 2,2'-azobis(2-methylpropionate) |
| VOC | Volatile organic content |

## Acknowledgments

I want to, first and foremost, thank Prof. David Haddleton. He has, during my time in his group, been an excellent mentor. His philosophies of “just do it” and general intellectual curiosity are ones that every researcher should strive for. He always led by example and always put people first.

I would also like to thank Dr Ahmed Eissa for his guidance, as well as Dr Andrew Shooter, Dr Stuart Richards, Robert Jennings and Elliot Coulbeck from Lubrizol. They have always been helpful and encouraging throughout my PhD.

PhDs are the result of several years of painstaking work, but they are never truly only one person’s work. Many members of the Haddleton group, past and present, have given me help or advice.

The cobalt squadron: George Patias, Spyros Efstathiou and Ataula Shegiwal have been there from the very start. Atty’s teasing and jokiness made the long days in the lab much easier. George started his PhD at the same time as I did. His good mood was always contagious and he was always willing to lend a hand (with experimental work or TEM). Spiros, sharing his project’s ups and downs, never failed to get a laugh out of me. The trip to San Diego with those three people is something I will never forget. For that and much more, I want to sincerely thank all three of them.

During these four years James Town, Despina Coursari, Ellis Hancox, Lucas Al-Shok and Dan Lester were always around for coffee, lunch, discussions about science at the Chestnut Tree, video games, music, or just general banter. They are all very good friends and skilled scientists for whom I have tremendous respect.

My PhD year consisted of seven people: Gavin Kirby, Yujin Chang, Mohammed Aljuaid, Arkadios Marathianos, Yongguang Li, George and myself. It has been a pleasure to work and learn alongside those people; I wish them all the best in their future endeavours.

In my first year, I was put in an office with people I did not know, but who turned out to become good friends: Samuel Lawton, Patrick de Jong and Rachel Hand. At the time, they were all wrapping up their own thesis and, as I am writing these acknowledgments in the middle of various Covid lockdowns, I can only look back and have respect for them, finishing their thesis in very packed offices full of noisy first years.

The French crew Marjolaine Thomas, Fannie Burgevin and Sophie Laroque were always my glimpse of France in the UK. Satu Häkkinen and Marco Turano my Lubrizol acolytes, Stefania Moro who always was up for philosophical discussions over pints of beer and Tom Floyd with whom I explored the depths of Los Angeles. Many more people deserve thanks, and these acknowledgements could go on for pages because they have all made this PhD a once-in-a-lifetime experience.

Finally, I would like to thank Eliza Komisenko, she has seen me through months of lockdown, thesis writing, and viva revisions. She has always been there for me through thick and thin, and her incredible support means the world to me.

Je suis parti de France en 2016 pour venir faire mon master à l’université de Warwick. Je ne savais pas que je finirais par rester afin de poursuivre un doctorat dans le groupe du Professeur Haddleton. Être loin de ma famille n’a pas été facile, mais je voudrais remercier mon frère et ma sœur, Karl et Karelle pour leur soutien à distance et leurs encouragements.

Enfin, rien de ce que je n’ai pu faire pendant ces quatre dernières années n’aurait pu être possible sans l’aide de mes parents. Jean et Sophie Abi Saleh. Il ne se passe pas un jour sans qu'ils fassent tout leur possible pour aider leurs enfants. Ils sont travailleurs, généreux et aimants. Aucun mot ne pourrait exprimer ma gratitude. Cette thèse est entièrement dédiée à eux.

Jose-Chris Abi Saleh (a.k.a Chris Atkins)

## Declaration

Experimental work contained in this thesis is original research carried out by the author, unless otherwise stated, in the Department of Chemistry at the University of Warwick, between October 2017 and June 2021. No material contained herein has been submitted for any other degree, or at any other institution.

Results from other authors are referenced in the usual manner throughout the text.

Date:

_____

José-*Chris Abi Saleh*

## Abstract

The initial objective of this thesis was to synthesis amphiphilic polymethacrylates under the umbrellas of catalytic chain transfer polymerisation and click-chemistry that could then be used as dispersing agents in carbon black waterborne suspensions. Three generations of dispersants were iteratively synthesised and tested.

MKI and MKII (*chapter 1*) dispersants were prepared through the polymerisation of glycidyl methacrylate and glycerol monomethacrylate respectively. In the former, amphiphilic polymers were prepared using an optimised one-pot dual post-polymerisation consisting of Michael-thiol addition of commercially available hydrophobic mercaptans, followed by microwave-assisted epoxide ring-opening. It was found that most polymers were fully functionalised within a 3-hour window, with minimal side-reactions. For MKII dispersants, the epoxide ring-opening step was bypassed, with Michael-thiol additions reaching full conversion within 5 minutes

The third generation, MKIII (*chapter 2*), allowed us to consider various aspects of our protocol and how to improve its environmental friendliness. Glycerol monomethacrylate synthesis was carried out in green solvents such as IPA. Functionalisation of the macromonomers was subsequently investigated with amines, through aza-Michael addition, under three synthetic pathways: catalysed, catalyst-free, and catalyst-free microwave-assisted (MAOS). This allowed the investigation of various reaction conditions and, two final dispersant candidates with nonyl- and dodecylamine anchors were prepared through catalyst-free MAOS.

The various amphiphilic polymethacrylates' (MKI: 12 candidates, MKII: 8 candidates and MKIII: 2 candidates) performance as stabilising agent in carbon black waterborne pigment suspensions were tested in chapter 4. In our investigations, stabilising segment with a molecular weight of 1-2.5 kDa were determined to provide better stabilisation. Furthermore, it was not only found that linear aliphatic anchors would adsorb better onto the surface of other pigment than any other type of anchor, but also that these dispersants would outperform commercially available products.

We also wished to investigate new applications of CCTP (*chapter 5*). To this end, EGDMA-based branched CCT-macromonomers were integrated as crosslinkers into polyHIPE formulations. The use of various acrylate propagation promoters such as 2-ethylhexyl acrylate (EHA), isobornyl acrylate (IBOA) and 2-methoxyethyl acrylate (MEA) was shown to both facilitate the photochemical curing of the HIPEs and to impart material properties to the products. Scanning electron microscopy (SEM) was used to explore the morphology of the materials. Surface wettability experiments were conducted to evaluate the hydrophilicity of the polyHIPEs' surface and, compression tests were used to investigate the influence of the branching density of the CCTP macromonomers, as well as the nature of promoters on the mechanical properties of the prepared polyHIPEs.

# **Chapter 1**:

## Literature Review

## 1.1 A Brief History of Polymers

Polymers can be defined as natural or synthetic macromolecules that are multiples of smaller, simpler building block units called monomers. Polymer science is a relatively new field, only dating back a century.[1] Naturally occurring biopolymers on the other hand, are as old as life itself, appearing in the first prokaryotic cells under the form of RNA around 3.8 billion years ago.[2]

Most other naturally occurring polymers include for instance polysaccharides (starch,[3] cellulose,[4,5] chitin[6]…), natural rubber (polyisoprene[7]), or amino acid based-polymers (silk fibre,[7] collagen[8]…). These same natural polymers have been used throughout human history to shape our ancestors' daily lives: pre-dynastic Egyptians used flax fabric to create linen cloths (3800 BCE). The Kiribati people of Micronesia used coconut fibres to build sturdy and resistant armours. Natural rubber was used by Mesoamerican civilisations for ritualistic ballgames (1650 BCE). The book "*De Orbe Nuovo*" (1516) by Pietro Martire D'Anghiera first reported the exceptional properties of natural rubber, but it was the demonstration by Charles Marie de La Condamine to the Académie Royale des Sciences in Paris in 1736 that really sparked the interest in the study of these materials.[9] A hundred years later, Charles Goodyear would introduce the vulcanisation process that requires the heating of rubber with sulfur containing compounds, that would then go on to be used in the manufacture of car tires.

Although extensively used, many chemists did not fully identify or even accept the concept of polymers. The term *polymers* itself was introduced by Berzelius in 1832 to describe what he thought to be $C_6H_6$, a compound he considered a polymer of ethyne $C_2H_2$.[10,11] We have now, however, come to understand that he was actually describing

an olefin mixture with octane as the compositional average. Berthelot and Holleman later refined the definition to include chemical bodies made up of as little as two repeat units, which could also be reacted to yield the starting reagents.[11]

Herman Staudinger, with his 1920 publication "*Uber Polymerisation*", laid the foundations for the modern understanding of polymers, by explaining his views on the polymerisation process.[12] Since then, polymer science has evolved into a fully-fledged field and is intricately intertwined with the technological innovations of the 21st century.

## 1.2 Radical Polymerisations

### 1.2.1 Free-Radical Polymerisation

Free-radical polymerisation (FRP) is a chain-growth polymerisation process, which, as its name suggests, is based on the reactivity of radical species, which can be obtained from a radical generating source, or initiator. Macromolecules are formed by the successive reaction of vinyl bond-containing monomers, the typical structure of which is shown in figure 1.1. Polymerisable monomers with these reactive centres generally have a stabilising substituent ($R_4$), with most other substituents generally being hydrogens. Also listed are monomers frequently encountered in the literature (styrene, methyl (meth)acrylate, vinyl chloride for example).


**Figure 1.1** Structure of polymerisable monomer containing at least one vinyl bond.

| Monomer | $R_1$ | $R_2$ | $R_3$ | $R_4$ | References |
|---|---|---|---|---|---|
| Ethylene | H | H | H | H | 13,14,15,16 |
| Methyl methacrylate | H | H | $CH_3$ | $COOCH_3$ | 17,18,19,20 |
| Vinyl alcohol | H | H | H | OH | 21,22,23,24 |
| Vinyl chloride | H | H | H | Cl | 25,26,27,28 |
| Styrene | H | H | H | Ph | 29,30,31,32 |

**Table 1.1** Example of widespread commercial monomers used in free-radical polymerisation.

The number of additions determines the degree of polymerisation and growth is eventually halted by the bi-molecular reaction of two growing macromolecules, preventing the further addition of monomer.

These steps, known as *initiation*, *propagation* and *termination*, underpin free-radical polymerisation, and are discussed separately in more depth below.

#### *1.2.1.1 Initiation*

The initiation process of FRPs can be divided into two separate events: (i) decomposition of the initiator and (ii) formation of initiating radicals.

Multiple types of initiator are available. Which type is used will depend on the reaction conditions, but the entire polymerisation process relies on the effective dissociation of the initiator, scheme 1.1.

1. *Redox initiation*:

$$ROOR + M^{2+} \rightarrow M^{3+} + RO^{-} + RO^{\bullet}$$

2. *Photolysis*:

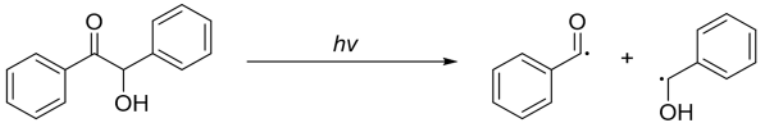


3. *Radiolysis*:

$$I + \gamma \rightarrow I^{\cdot +} + e^{-}$$

4. *Thermal initiation: Azo and peroxide compounds*:

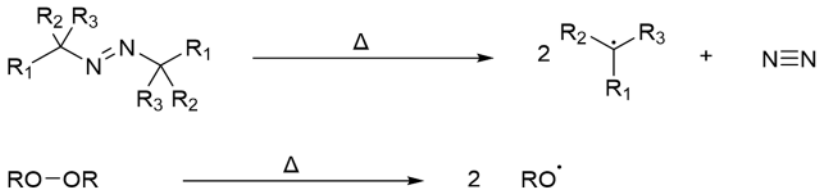


**Scheme 1.1** Methods for the generation of radical species used in FRP.

One of the oldest methods of production of radical species is the reduction of hydrogen peroxide by metal salts, known as Fenton's reagent when ferrous sulfate is used.[33] In redox systems the same process is employed, or adapted, through the use of peroxides[34,35] or persulfates[36,37] where, by way of a single-electron transfer step, O-O bonds are cleaved to yield a free radical entity able to initiate polymerisation.[38,39]

Electromagnetic radiation, UV/visible light or ionizing radiation, can also be manipulated to generate radicals. Photolytic initiation can be conducted at low temperatures in solvent-free conditions and is often employed in cross-linking processes. This is the case in 3D printing technology where photo-FRP is preferred.[40] Radiolysis, with β- or γ particles sources can be used to generate radicals, but also tend to form a wide array of ionic species.[41]

Thermal initiation, however, is by far the most widely encountered method of generating radicals in polymer chemistry. The best initiators for thermal initiation are the so-called peroxide,[42,43] where the low dissociation energy of the O-O bond favours

the homolytic cleavage of the peroxide bond, and azo initiators, whose decomposition is driven by the formation of stable nitrogen molecules.[44]

Radicals are, in general, reactive transient species that will either start a polymer chain or undergo side-reactions. When radicals are formed, they are surrounded by a "cage" consisting of solvent and monomer. This is of particular importance in the case of thermal initiations where two radicals are formed. Should the radicals fail to escape the solvent cage in a timely manner, a mutual deactivation of both initiating radicals can occur, without polymerisation having been initiated, scheme 1.2.

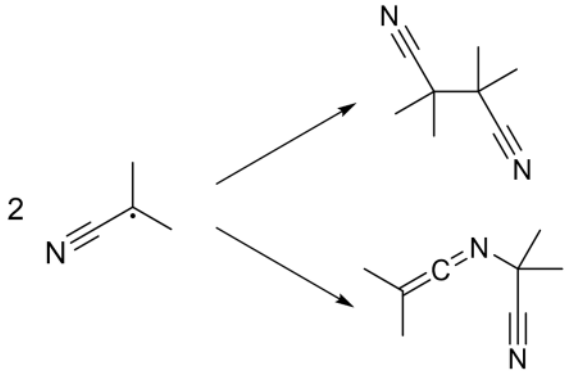


**Scheme 1.2** Bimolecular side reactions that can occur between two initiating radicals (here from AIBN) within the solvent cage.

To quantify how efficiently those radicals initiate polymerisation, we can evaluate *initiator efficiency*, *f*, where:

$$f = \frac{\text{radicals incorporated into polymers}}{\text{radicals formed by initiator}} \qquad \text{(eqn. 1)}$$

Should the initiating radicals be able to exit the solvent cage, they will be able to react with a close-by monomer that can then undergo propagation.

#### *1.2.1.2 Propagation*

Propagation is the bimolecular process that enables increase in chain length through the repeated addition of monomers. There are two possible reaction sites on mono- ($R_1$ = $R_2$ = $R_3$ = H, $R_4$ = Y) or disubstituted ($R_1$ = $R_2$ = H, $R_3$ = X, $R_4$ = Y) monomers: carbon a (tail) or b (head), figure 1.1. Head-to-tail (H-T) additions are favoured both on steric grounds, but also on electrostatic, as $R_4$ is usually an electron withdrawing group.

With each monomer addition, a new *chiral centre* is formed. The regularity, or lack thereof, in the arrangement of those successive chiral centres is an important parameter that can influence the physical properties of the polymer. This is called tacticity. Three different tacticities can be defined: polymers where there is no prevailing order are atactic. When successive chiral centres have the same configuration they are isotactict and, finally, when the configuration alternates between each sides of the plane of the polymer backbone, polymers are described as syndiotactic. In theory, propagation could carry on until termination and produce linear macromolecules, however many side-reactions can compromise the chain length and structure of polymers.

#### *1.2.1.3 Termination*

The reactions with which growth is terminated happen through the interaction of two adjacent macroradicals, $P_n^*$ and $P_m^*$, under one of two scenarios. The first, *combination*, sees two polymeric chains react together to create a single chain, with a degree of polymerisation equal to the sum of its two constituting chains, and a head-head configuration at the point of combination. The second, referred to as

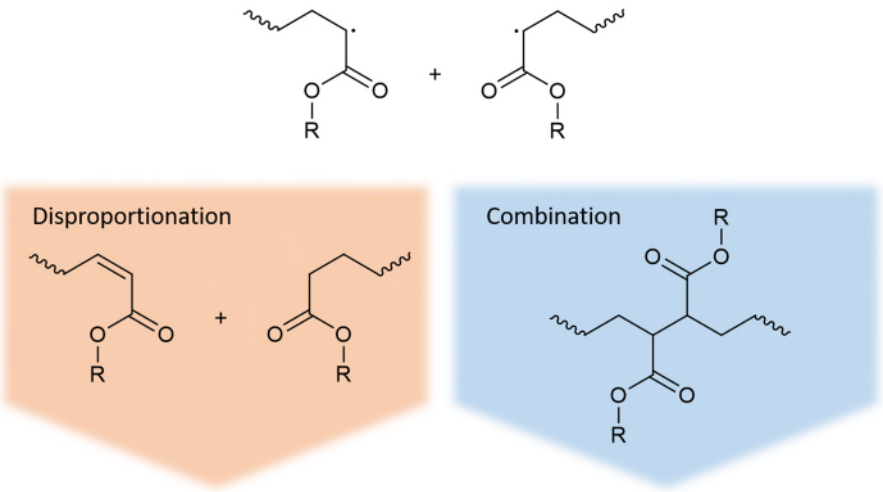


**Figure 1.2** Termination pathways encountered in FRP.

*disproportionation*, happens when a proton atom is abstracted from one chain to another resulting in two *dead* polymers, one with a terminal vinyl bond and one saturated chain end, figure 1.2.

#### *1.2.1.4 Kinetics*

The three steps and rates of the free-radical polymerisation process can be summarised as:

*Initiation*

$I \rightarrow 2R^*$

$R^* + M \rightarrow M^*$

$$R_i = 2k_d f[I]$$

(eqn 2)

*Propagation*

$P_n^* + M \rightarrow P_{n+1}^*$

$$R_p = k_p[P_n^*][M]$$

(eqn 3)

*Termination by disproportionation*

$P_n^* + P_m^* \rightarrow P_n^= + P_m$

*Termination by combination*

$P_n^* + P_m^* \rightarrow P_n P_m$

$$R_t = 2k_t[P_n{}^*]^2$$

With $k_t = k_{t,c} + k_{t,d}$

(eqn 4)

The decomposition of the initiator is the rate-controlling step during initiation, the secondary step occurring much more rapidly. In $R_i$, the "2" is introduced because for each initiator molecule, two radicals are created, and *f* refers to the initiator efficiency. For termination, both combination and disproportionation are in competition and $k_t$ takes both pathways into account.

An equilibrium between generation and consumption of radicals is eventually reached during polymerisation. This allows the assumption of a steady-state, where the concentration of radicals does not vary significantly within short timeframes, meaning:

$$R_i - R_t = 0$$

$$<=> \ 2k_d f[I] - 2k_t[P^*]^2 = 0$$

$$<=> \ [P^*] = \sqrt{\frac{k_d f[I]}{k_t}}$$

Substituting this into the general rate of propagation equation, we obtain:

$$R_p = k_p \sqrt{\frac{k_d f[I]}{k_t}}[M] \qquad \text{(eqn. 5)}$$

#### *1.2.1.5 Chain Transfer*

Chain transfer is another major event in FRP, beyond normal termination, which limits chain growth. Its reaction can be written as:

$$P_n^* + XH \rightarrow P_nH + X^*$$

$$R_{tr} = k_{tr}[P_n^*][XH] \qquad \text{(eqn 6)}$$

where the growing centre is terminated via transfer of a hydrogen atom from a compound XH that can be monomer, solvent molecules or impurities. The reaction also yields a new radical species, here denoted $X^*$, able to re-initiate polymerisation. These mechanisms of chain transfer lower the overall molecular weight of polymers.

In most cases, chain-transfer is undesirable, but the process can be harnessed to control molecular weights through the deliberate introduction of chain transfer agents (CTA). This is a relatively facile, industrially viable method to manipulate the size of polymers. The use of thiol and halides, in particular, has been reported since the 1940's with their application being first investigated by Frank Mayo and co-workers.[45,46]

Chain transfer reactions can be characterised by their chain transfer constant, $C_s$, equal to the ratio of transfer to propagation rate constant, such that:

$$C_s = \frac{k_{tr}}{k_p} \qquad \text{(eqn 7)}$$

The higher the $C_s$, the more likely a radical is to undergo chain-transfer rather than to propagate. With this, we can write that the average degree of polymerisation will be equal to the ratios of the rate of polymerisation to the rates of chain-altering event (termination and chain transfer), with:

$$\overline{DP_n} = \frac{R_p}{R_t + R_{tr}} = \frac{k_p[P_n^*][M]}{2k_t[P_n^*]^2 + k_{tr}[P_n^*][XH]} \qquad \text{(eqn 8)}$$

$$<=> \frac{1}{\overline{DP_n}} = \frac{2k_t[P^*]}{k_p[M]} + \frac{k_{tr}[XH]}{k_p[M]} = \frac{2k_t}{k_p[M]}\sqrt{\frac{k_d f[I]}{k_t}} + \frac{k_{tr}[XH]}{k_p[M]}$$

It is important to note that the term $k_{tr}$ encompasses *all* chain transfer events, *i.e.* transfer to monomer, solvent, impurity or chain transfer agent, as such:

$$\frac{1}{\overline{DP_n}} = \frac{2k_t}{k_p[M]}\sqrt{\frac{k_d f[I]}{k_t}} + \frac{k_{tr,M}[M]}{k_p[M]} + \frac{k_{tr,Sol}[S]}{k_p[M]} + \frac{k_{tr,I}[I]}{k_p[M]} + \frac{k_{tr,CTA}[CTA]}{k_p[M]}$$

$$\frac{1}{\overline{DP_n}} = \frac{2k_t}{k_p[M]}\sqrt{\frac{k_d f[I]}{k_t}} + C_m + C_{Sol}\frac{[S]}{[M]} + C_I\frac{[I]}{[M]} + C_S\frac{[CTA]}{[M]} \qquad \text{(eqn 9)}$$

Generally, the rate of polymerisation is scarcely affected by chain transfer. This is because of the relatively minute concentrations of the species involved in chain

transfer processes but, as previously mentioned, CTAs can be purposely introduced within polymerisation systems to artificially manipulate molecular weights.[47] The last term in equation 9, then becomes of importance:

$$\frac{1}{\overline{DP_n}} = \frac{2k_t}{k_p[M]}\sqrt{\frac{k_d f[I]}{k_t}} + C_S\frac{[CTA]}{[M]} \quad \text{(eqn 10)}$$

An equation that can be simplified to:

$$\frac{1}{\overline{DP_n}} = \frac{1}{DP_0} + C_S\frac{[CTA]}{[M]} \quad \text{(eqn 11)}$$

Equation 11, referred to as Mayo equation relates the degree of polymerisation at various chain transfer agent loading, $DP_n$, with the degree of polymerisations without added CTA, $DP_0$. This equation yields a linear plot of $1/DP_n$ against [CTA]/[M], the slope of which is equal to the chain transfer constant. Examples of $C_s$ values for commonly encountered CTAs such as dodecyl thiol or carbon tetrachloride typically stand at 0.70 and 0.0122 (for MMA and styrene at 60 °C respectively).[48–50]

Chain transfer to small reaction constituent is pervasive; but transfer to dead polymer can also be widespread in FRPs. This usually occurs at higher conversions and influences the topology of polymers by introducing branching to the system. Short branches radiating from the structure are a result of backbiting, a rearrangement where the radical carrying carbon transfers the activity to the backbone, five/six carbons back. Alternatively, long branching is observed when the transfer occurs intermolecularly.

The use of traditional CTAs, while able to influence the degree of polymerisation, can nevertheless require high amounts of either thiols or halides to yield effective control, which can lead to concerns over CTA toxicity, smell, or colour. Catalytic chain

transfer polymerisation, on the other hand, makes use of catalyst with $C_s$ values several orders of magnitude higher than traditional CTAs.

## 1.2.2 Catalytic Chain Transfer Polymerisation

### *1.2.2.1 Initial Development and Overview of CCTP*

Catalytic chain transfer polymerisation (CCTP) offers an efficient and attractive alternative pathway to the regulation of molecular weights of polymers.[51–54] The technique was developed in the mid 1970's in Russia by Smirnov and Marchenko. Their work, meant as a continuation of Gelii Ponomarev's work on metal transition metal-containing compounds, initially aimed at investigating cobalt porphyrins' catalytic activity in the redox decomposition of peroxy initiators in radical polymerisations. However, and after much experimentation, it was concluded that cobalt porphyrins would instead reliably and reproducibly inhibit the polymerisation of MMA, without affecting the rate of polymerisation. The polymerisations would display all the signs of "normal" free radical, bar for the fact that the resulting polymers had, respectively, a proton and an olefinic insaturation in the α and ω positions, figure 1.3. [55–58]

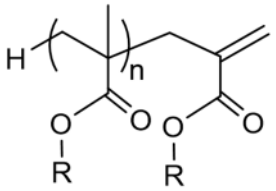


**Figure 1.3** Typical structure of CCTP-made polymer.

Outside of the Russian patent literature however, the technique gained little traction in the West at its inception as early Soviet and American (from the Glidden paint company) patents prevented further public disclosure.[24,59–61]

### *1.2.2.2 Catalysts*

One of the early pitfalls of CCTP was the cost of the catalysts. The low natural abundance of cobalt porphyrins (figure 1.4, A) made the removal of the catalyst from the polymeric material a necessary, but costly process.[54] To this day, cobalt porphyrins can cost up 130 GBP per 500 mg of product. Many catalysts were tested, particularly by A. Gridnev.[52,54] One of the most important breakthroughs, and the one subject of the aforementioned Soviet patents, came in the form of the cobaloxime catalysts. As described by Gridnev himself, cobaloximes, the structure of which is shown in figure 1.4 (B), were an order of magnitude more CCTP active than porphyrins, with chain transfer constants up to $10^3$-$10^5$,[62–64] but also markedly less toxic and with little colour. This activity of cobaloximes is unique in that most other transition metal based catalysts (Cu, Fe, Ni, Zn, Rh, Mn, Pd, Mg, Pt, Sn, U),[52,54,57] or even other cobalt-based complexes, showed no activity whatsoever, except for some complexes of chromium and molybdenum which showed reduced catalytic activity.[65–67] One of the principal

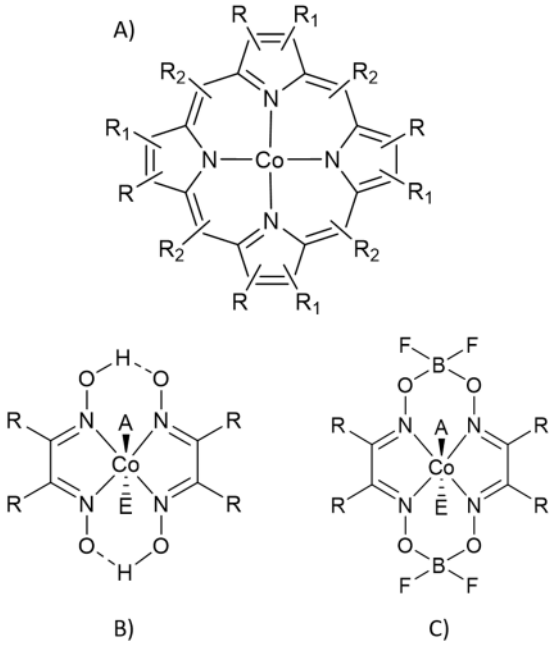


**Figure 1.4** Cobalt porphyrin (A). Typical unbridged (B) and bridged (C) structures of the low spin cobaloxime CCTP catalyst.

drawbacks of the catalysts, however, was the hydrolytic instability. Unless used in an inert, glove-box, atmosphere, equatorial OHO bridge could be partially hydrolysed, disrupting the compound's catalytic activity, scheme 1.3.[68]

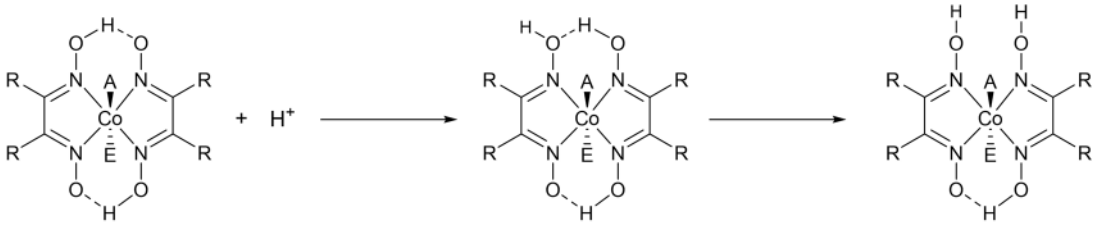

**Scheme 1.3** Hydrolysis of the dimethylglyoxime planar ligand of cobaloxime catalysts.

This issue can nevertheless avoided by introducing $BF_2$ bridges, as was shown by Janowicz and co-workers. This made the catalyst stable in most environments, as well as easy to handle under aerobic conditions (figure 1.4, C).[69]

Cobaloximes are octahedral complexes made up of two axial ligands A (monoanionic) and E (electron-donating, coordinative bound Lewis base), as well as a tetradentate glyoxime ligand that makes up the square planar base of the catalyst.

The glyoximes' substituents, as well as the axial ligands can be modified to suit the experimental conditions but retain catalytic activity, with examples of the various investigated catalysts/monomer/solvent combinations given in table 1.2.

| Catalyst | R | Solvent | $C_s$ |
|---|---|---|---|
| Cobaloxime | Me | Butanone | 27 000 |
| | $C_6H_5$ | Butanone | 7 200 |
| | $MeC_6H_4$ | THF | 25 000 |
| | $tBuC_6H_4$ | THF | 21 000 |
| | $MeC_6H_4$ | THF | 16 000 |

**Table 1.2** Chain transfer constants of a range of cobaloxime catalysts for the polymerisation of MMA in various solvents. Adapted from reference 47.

The reaction conditions (solvent, monomer, A, E, planar substituents) also contribute towards the catalytic activity, but their effect is measured through the chain transfer constant.

#### *1.2.2.3 Mechanism*

The majority of CCT polymerisations are thermally initiated in the presence of an azo initiator as peroxide initiators lead to an oxidation of cobaloximes that locks them in their inactive L-Co(III) oxidation state. Since the inception of CCTP, three mechanisms have been proposed:

Mechanism 1:

*Step 1*: Activation of propagating radical

$$P_n^* + LCo \leftrightarrow [P_n - LCo]$$

*Step 2*: Monomer abstraction of proton

$$[P_n - CoL] + M \rightarrow LCo + P_1^* + P_n^=$$

Mechanism 2:

*Step 1*: Michaelis-Menten activation of monomer

$$LCo + M \leftrightarrow [M - LCo]$$

*Step 2*: Chain transfer and re-initiation

$$[M - LCo] + P_n^* \rightarrow P_1^* + P_n^= + LCo$$

Mechanism 3:

*Step 1*: chain transfer and hydride generation

$$P_n^* + LCo(II) \rightarrow P_n^= + LCo(III)H$$

*Step 2*: Cobalt(III) hydride re-initiation

$$LCo(III)H + M \rightarrow LCo(II) + M^*$$

The first two involve the activation of macroradicals or monomers respectively. The monomer was however shown by Heuts *et al.*[70] to not participate in hydrogen abstraction, ruling out the first mechanism. The second requires the formation of a monomer-cobaloxime mechanism, which would make the polymerisation highly dependent on monomeric concentration. theoretically, this would equate to CCT being less likely as the reaction proceeds and the monomer reserves are depleted, and this theory has been refuted.[55,71] The more widely accepted third mechanism was demonstrated by A. Gridnev, Smirnov, O'Driscoll and co-workers and is shown in more details in scheme 1.4.[51,52,54,70,72–74] In this mechanism, a hydrogen atom is first abstracted from the carbon in the α-position to the radical centre of the polymeric radical. This produces a vinyl terminated polymer and a reactive cobalt-hydride cobalt hydride complex able to re-initiate polymerisation through the transfer of hydrogen to an unreacted monomer.

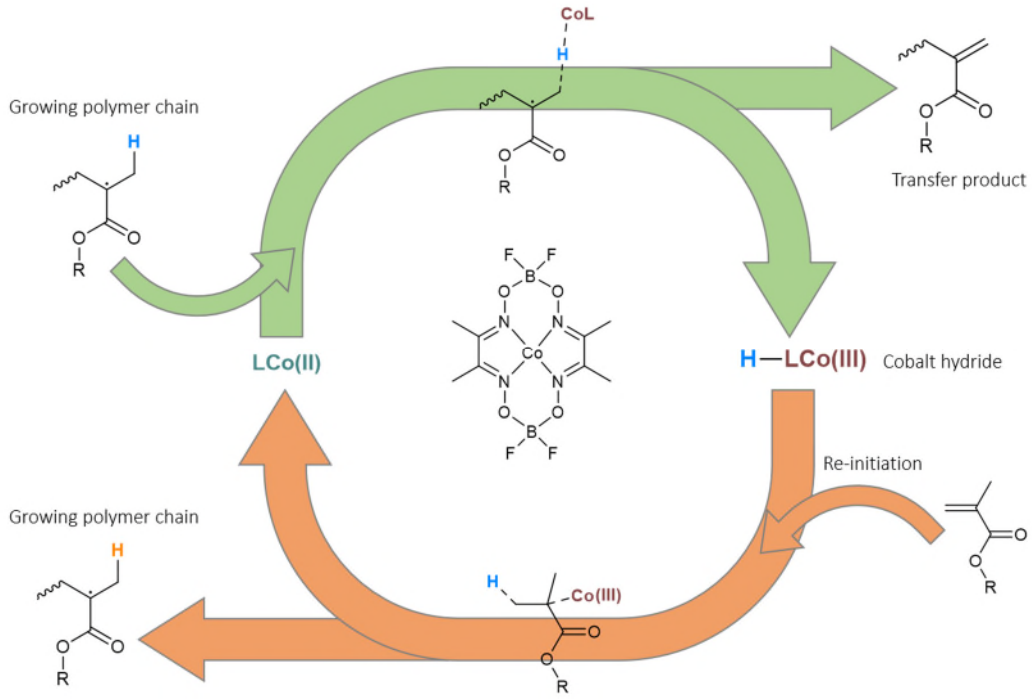


**Scheme 1.4** Currently accepted mechanism of CCTP.

The chain transfer process can further be broken down into three steps[75]:

$$P_n^* + LCo(II) \underset{k_{-1}}{\overset{k_1}{\rightleftharpoons}} [P_n^* - LCo(II)]$$

$$R_1 = k_1[P_n^*][LCo(II)] \quad \text{(eqn 9)}$$

$$\text{and } R_{-1} = k_{-1}[P_n^* - LCo(II)] \quad \text{(eqn 10)}$$

$$[P_n^* - LCo(II)] \xrightarrow{k_{tr}} P_n^{=} + LCo(III)H$$

$$R_{tr} = k_{tr}[P_n^* - LCo(II)] \quad \text{(eqn 11)}$$

$$LCo(III)H + M \xrightarrow{k_{rein}} M^* + LCo(II)$$

$$R_{rein} = k_{rein}[LCo(III)H][M] \quad \text{(eqn 12)}$$

Assuming a steady-state for $[P_n^* - Co(II)]$, we can write:

$$\frac{d[P_n^* - Co(II)]}{dt} = R_1 - R_{-1} - R_{tr} = 0$$

$$<=> [P_n^* - LCo(II)] = \frac{k_1}{k_{-1} + k_{tr}}[P_n^*][LCo(II)]$$

Which, if subbed into $R_{tr}$, provides us with an equation for the rate of chain transfer:

$$R_{tr} = \frac{k_{tr}k_1}{k_{-1}+k_{tr}}[P_n^*][LCo(II)] \quad \text{(eqn 13)}$$

### *1.2.2.4 Monomers*

In order to be viable options for CCT polymerisation, monomers need to be able to facilitate proton transfer. In most case, this means having an α-methyl group. In such case, monomers are said to be CCTP active. This is as during the polymerisation, propagating tertiary radicals formed from methacrylates and other α-methyl monomers, lead to the formation of a labile Co-C bond that will be able to yield to the cobalt hydride and polymeric product. In contrast, acrylates or styrenic monomers form very stable Co-C bonds that are inactive for CCTP, figure 1.5.

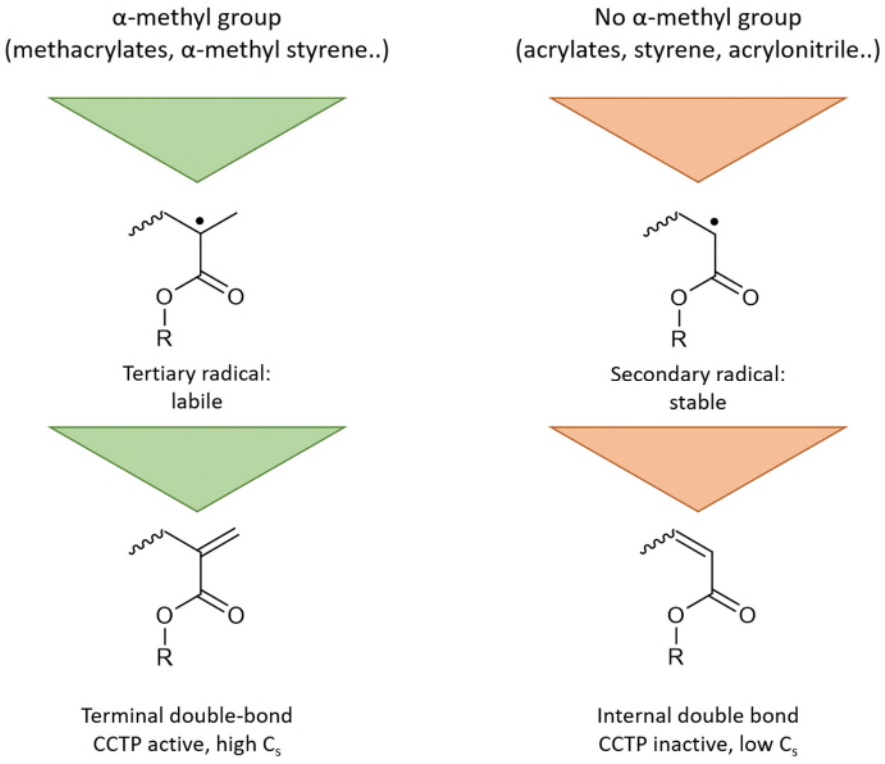


**Figure 1.5** Classification of common monomers' CCTP activity and resulting CCTP product.

## 1.3 Click Reactions

Click-chemistry is, today, an integral part of polymer science. The term "click-chemistry" was first introduced by Sharpless and co-workers in the late 1990's to describe a class of modular reactions that could be used that would simplify the, often overcomplicated synthesis of biomimetic compounds used in the pharmaceutical industry.[76,77]

At its core, the concept of click-chemistry englobes a family of reactions that share several properties: they must achieve high yields, be regio- and stereo-selective, yield a single product that is easy to purify *via* non chromatographic methods, whilst being carried out in benign solvents under ambient temperatures and/or atmospheric conditions. Click-reactions have been categorised into 4 different classes: (i) cycloadditions of unsaturated species (Huisgen cycloadditions,[78–81] Diels–Alder addition[82,83]), (ii) carbonyl chemistry,[77] (iii) nucleophilic substitutions (ring-opening reactions[84]) and (iv) addition to carbon-carbon unsaturation (Michael additions[85–88]) and a few examples of such reactions are shown in scheme 1.5.

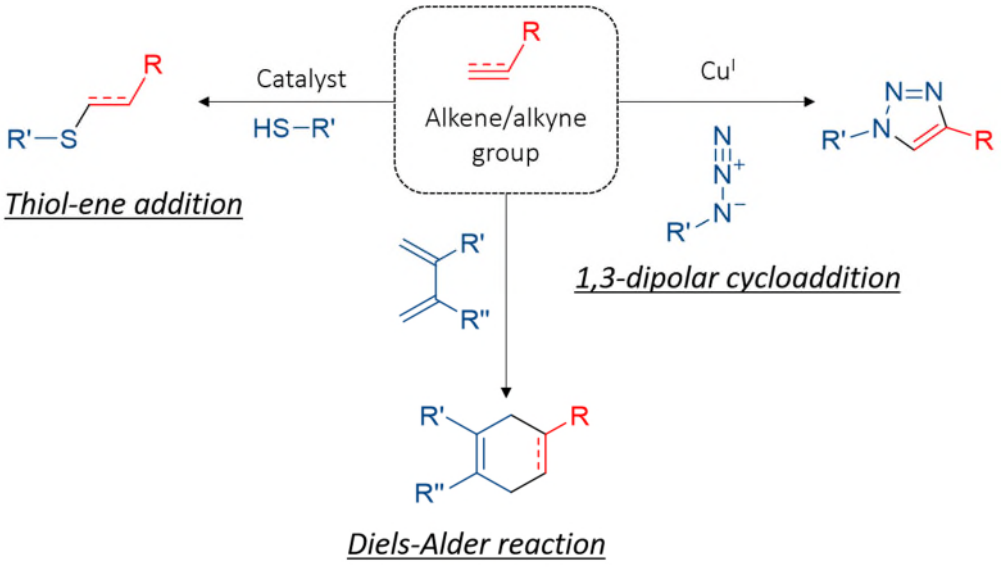


**Scheme 1.5** Example of commonly used "click" reactions.

### 1.3.1 Michael Additions

Michael additions were named after Arthur Michael who, in the late 1880's, sought to find an explanation to the formation of cyclopropane derivatives during the reaction between diethyl 2,3-dibromopropionate and diethyl sodiomalonate that was observed by Conrad and Guthzeit.[89] The reaction, and historic definition Michael addition, involves a carbon-carbon bond forming conjugate addition reaction in which an enolate nucleophile is reacted with the β carbon of an α,β-unsaturated carbonyl.[87,90] This definition can, however, be extended to encompass reactions whereby a strong nucleophile, or Michael donor, attacks an α,β-unsaturated carbonyl, or Michael acceptor. Since then, reactions with oxygen-,[91–94] selenium-,[95] and phosphorus-centered[96–98] nucleophiles as Michael-donors have also been described.

#### *1.3.1.1 Michael-thiol Additions*

The most encountered reaction of this subclass is the Michael-thiol addition, which was first reported in the 1960's by Allen *et al*.[99] and have since been of great interest to polymer chemists for being usable with a great variety of monomers: (meth)acrylates, acrylamides, vinyl sulfones, or even maleimides.[100–105]

Two catalytic pathways are available. The first, base-catalysed Michael-thiol addition, relies on non-nucleophilic bases such as TEA, DBU or DBN. As illustrated in scheme 1.6, the role of these catalyst is to deprotonate the thiol reagent.[106–109] This generates a nucleophilic thiolate intermediate that can undergo Michael-addition onto the electron-deficient vinyl bond. One of the main factors of the base-catalysed Michael-thiol addition is the strength of the base. With strong bases, the concentration of thiolate is equal to that of the catalyst but with weak bases, the concentration will depend on the acid-base equilibrium.

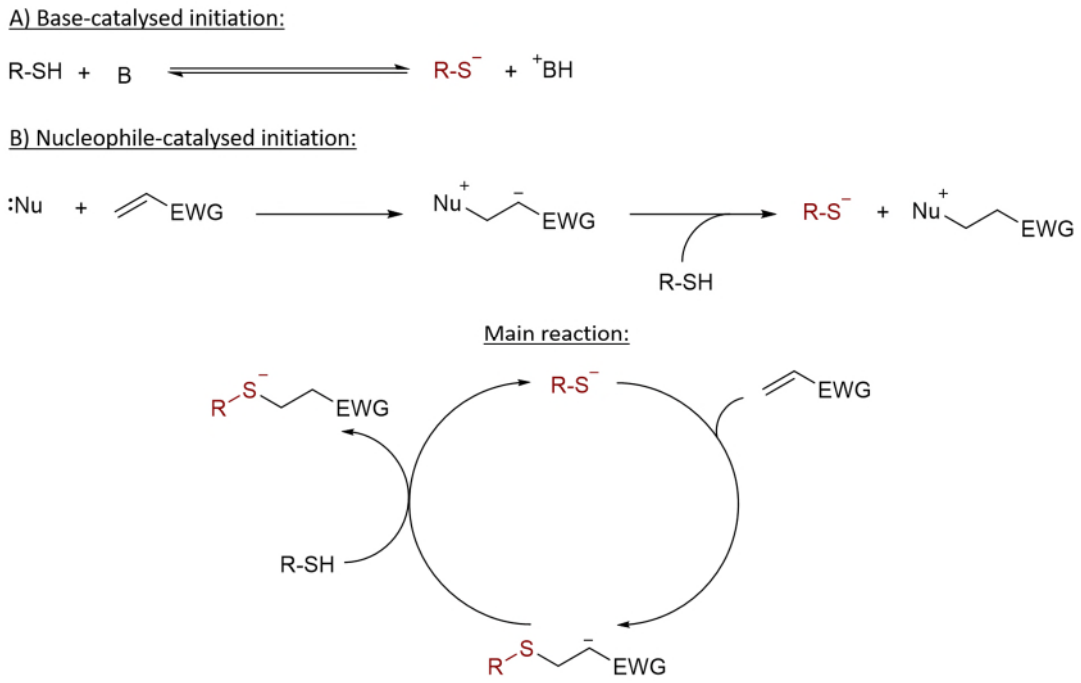


**Scheme 1.6** Base and nucleophile-catalysed Michael-thiol addition mechanism. Adapted from ref 81.

The reaction is also susceptible to the presence of protic sources, water or alcohol, which can interfere with the base catalyst.

One of the main factors that influences base-catalysed Michael-thiol addition is the $pK_a$ of the thiol, which will regulate the acid/base equilibrium, but this dependency, however, be circumvented with N- or P- centered nucleophiles (DMPP, DMAP, trialkylphosphine etc…) catalysts, which constitutes the second catalytic pathway.[64,84,106,108,110] The first step, the reaction between the catalyst and an electron-poor vinyl bond, results in a zwitterionic intermediate, able to next deprotonate the thiol.

In both cases, once the negatively charged thiolate is generated in the reaction medium, a reaction with a vinyl bond to form a deprotonated Michael adduct occurs. The adduct is then neutralized by the interaction with another thiol, thus establishing a reactive cycle typical of Michael-thiol additions.

The thiolate nucleophilic attack is the rate-limiting step and can be written as:

$$R_{MTA} = k[R - S^-][vinyl] \quad \text{(eqn. 14)}$$

With $[R - S^-]$ and [vinyl] the respective concentrations of thiolate and vinyl bond. The former's definition can however be expanded when dealing with base-catalysed additions as the concentration of thiolate will depend on the dissociation constant. As such, we have:

$$K_{eq} = \frac{[R{-}S^-][BH^+]}{[R{-}SH][B]} \quad \text{(eqn. 15)}$$

and so for base-catalysed reactions:

$$R_{BCMTA} = kK_{eq}\left(\frac{[B]}{[BH^+]}\right)[R - SH][vinyl] \quad \text{(eqn. 16)}$$

### *1.3.1.2 Aza-Michael Additions*

Another iteration of the Michael addition, the aza-Michael addition, makes use of amines.[111–113] The reaction between an amine-centered nucleophile and an α,β-unsaturated carbonyl, namely ammonia and mesityl oxide, was first reported by Sokoloff and Latschinoff almost a decade before Arthur Michael described the reactions that would later be named after him.[114]

The use of aza-Michael reactions offers several additional advantages. If used with a catalyst, a strong base such as DBU, the reaction occurs through a mechanism similar to that of base-catalysed Michael-thiol addition but the reaction is also possible in a more interesting environment whereby more basic amines act as their "own" catalyst, following a mechanism proposed by Shooshtari *et al.*,[115] scheme 1.7, although this

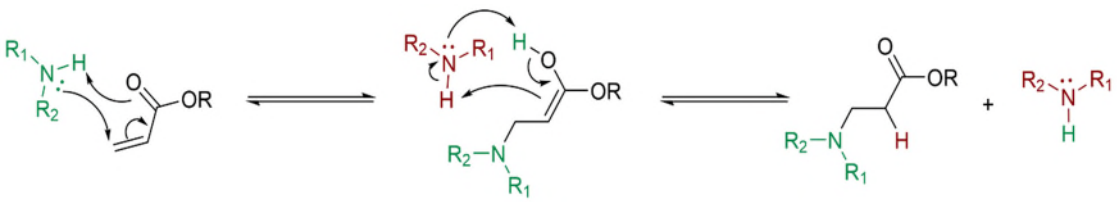


**Scheme 1.7** Proposed mechanism of catalyst-free aza-Michael addition.

mechanism is still debated.[116,117] Moreover, amines can be preferable to malodorous thiols, reactions can occur using multiple combinations of often inexpensive Michael donors (aliphatic,[118] aromatic[119] etc..) and Michael acceptors such as (meth)acrylates,[120–126] or amides among others.[113,127–129] It is an important reaction that could enable an easy access to β-amino carbonyl derivatives and which can prove relevant in the synthesis of biologically relevant molecules.[124,130]

### 1.3.2 Epoxide Ring-Opening

Epoxides are three membered rings containing an oxygen atom. Their reactivity stems from the inherent strain that all three membered rings are subject to. This makes them particularly susceptible to base or acid-catalysed nucleophilic attacks, with Sharpless likening them to "spring loaded" rings.[77] These nucleophilic attacks overwhelmingly proceed through an $S_N2$ mechanism, scheme 1.8.

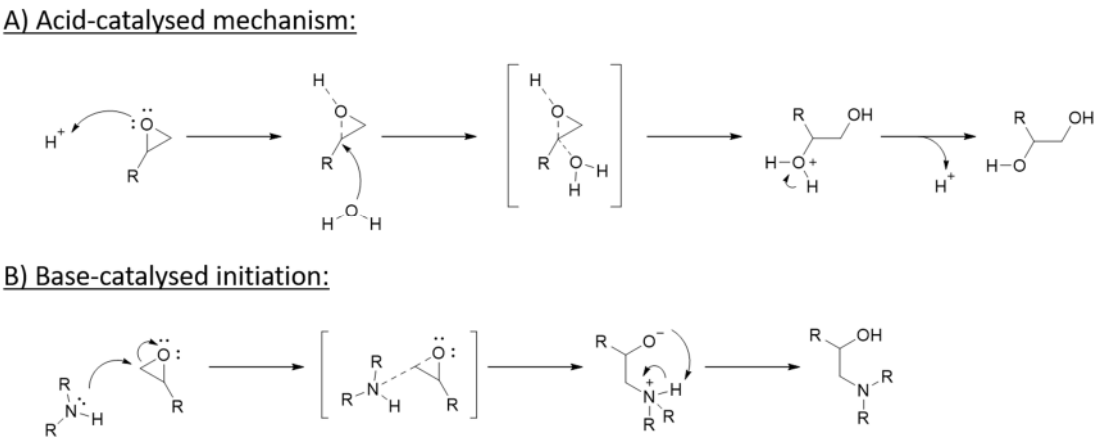


**Scheme 1.8** Acid and base-catalysed mechanisms of epoxide ring-opening. Adapted from ref 78.

Polymers with epoxide containing side-chains can be obtained through the polymerisation of glycidyl (meth)acrylate.[84] The monomer's low-cost and general stability have attracted a great deal of attention. It is, for instance, commonly encountered in the production of epoxy resins.[131,132] Polymers of GMA can be

obtained using both free-radical (FRP, CCTP) and reversible-deactivation radical polymerisation (ATRP, RAFT, NMP) techniques[84,133–137] and, through the availability of the pendant strained-three membered rings for nucleophilic ring-opening reactions. McEwan *et al.*[137] investigated the versatility afforded by the combination of CCTP and click-chemistry. During the study, the authors evaluated several routes leading to the complete functionalisation of epoxide containing poly(glycidyl methacrylate) CCT-polymers. Various amine and/or thiol compounds were reacted with both the terminal vinyl groups and epoxide side-chains using hydroamination or Michael-thiol addition alongside epoxide ring-opening.

Similarly, Zhang *et al.*[138] used CCTP to polymerise GMA. The multi-handle polymers were subsequently modified by reacting benzyl mercaptans with the ω-vinyl ends. The

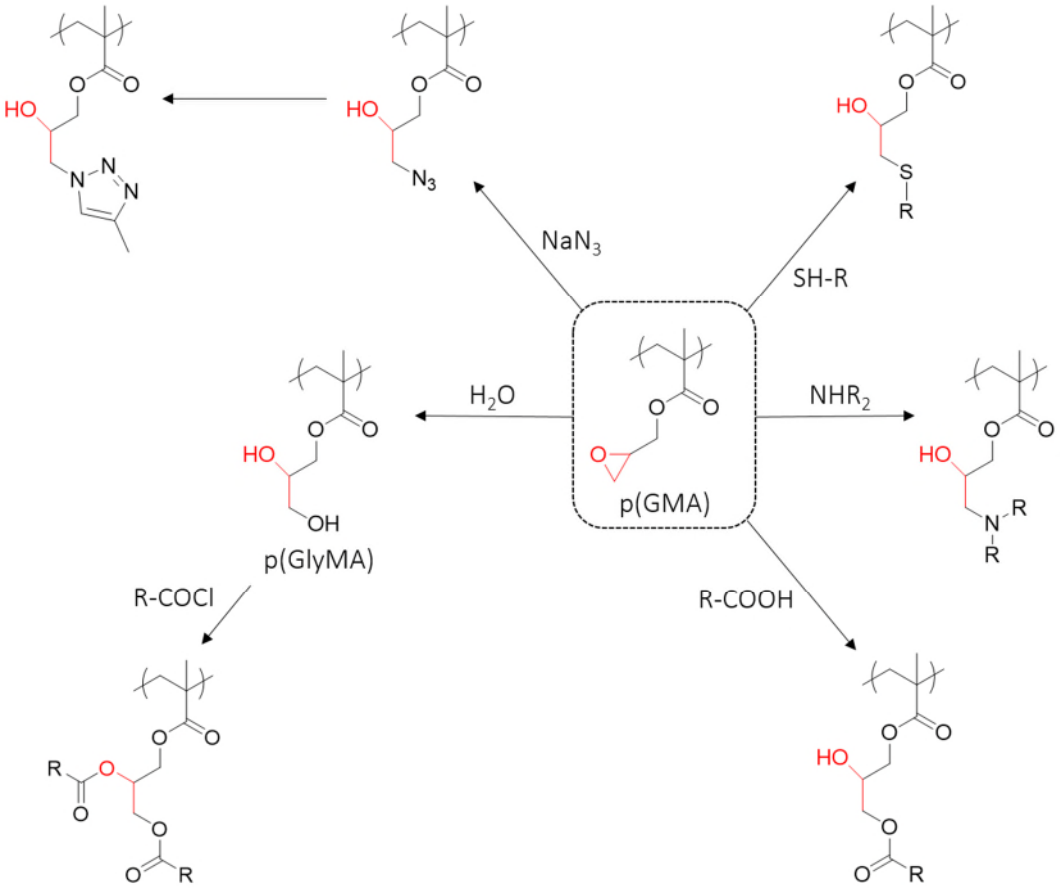


**Scheme 1.9** Post-polymerisation modifications of p(glycidyl monomethacrylate).

epoxy side-chains' reactivity was harnessed by dual-functionalisation using a combination of epoxide ring-opening using sodium azide, which was immediately followed by a copper catalysed alkyne azide coupling (CuAAC) reaction between the azide-polymers and alkyne carbohydrates to yield linear glycopolymers. Common to both these papers is the presence of epoxy functional monomer glycidyl methacrylate, which as can be seen from scheme 1.9, open up a host of possibilities for preparing functional polymers.

## 1.4 Microwave-Assisted Organic Synthesis

### 1.4.1 Principles of Microwave Heating

A rule of thumb in chemical synthesis states that, for every 10 °C increase, the reaction time is halved (adapted from Arrhenius' law). Traditional heating in organic and material sciences, is external and achieved using oil or water baths.

Microwave-assisted organic synthesis, or MAOS, on the other hand, relies on the use of microwaves. These are electromagnetic irradiations found between IR and radio

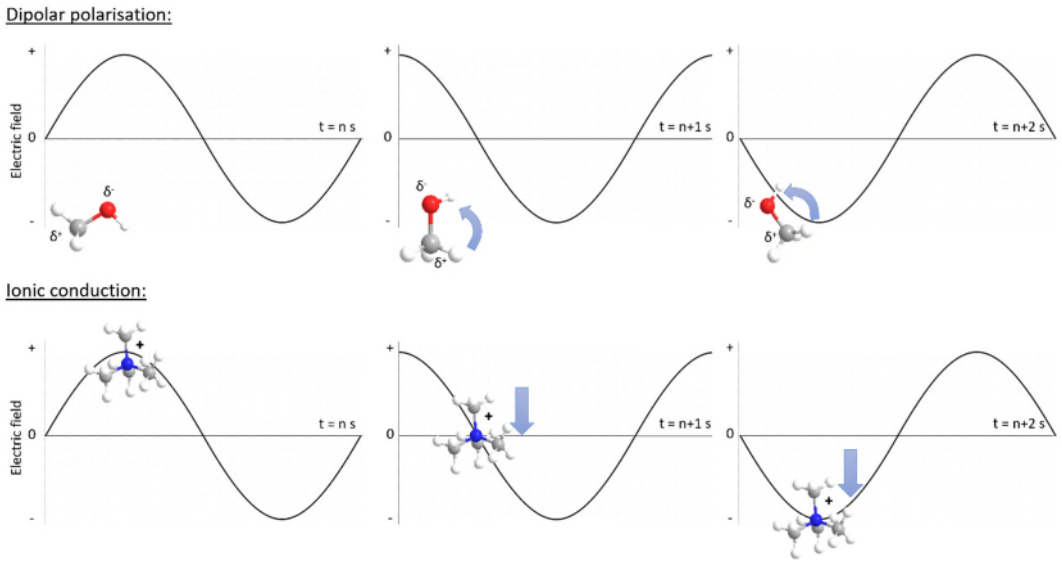


**Figure 1.6** Processes of dielectric heating (dipolar polarisation and ion conduction) occurring during microwave heating.

frequencies from 0.3 to 300 GHz. As the name suggests, electromagnetic waves are made up of an electric and magnetic field, with the former being responsible for the observed heating effect, also known as dielectric heating effect.

There are two mechanisms that take place, figure 1.6:[139,140]

(i) Dipolar polarization: for dipolar polarization to occur, at least one of the compounds in the reaction vessel must be a dipole (i.e., have a dipole moment); this often will be the solvent. In that case the molecule will, when microwaves are being applied, align itself with the electric field. However, because the field oscillates, solvent molecules will be in a constant state of attempting to realign themselves with the field, which results in the production of heat by molecular friction.

(ii) If a molecule is charged (positively or negatively), it will be subject to ionic conduction, in which case molecules oscillate back and forth following the microwave field. This mechanism is generally considered more efficient at production of heat, which stems from the collisions between molecules.

When possible, MAOS has shown to be much more efficient than traditional heating. This is because heat is generated internally and ensures that the sample is heated homogenously, unlike traditional heating where the heat source is external and wall effects can occur.

### 1.4.2 Microwave Instruments

With the development of modern microwave reactors came several innovations. Nowadays, most scientific reactors come with, among others, an optic fibre temperature probe, pressure control, continuous power regulation, post-reaction cooling, built-in magnetic stirring capabilities and explosion proof cavities.

In domestic, just like scientific microwave instruments, the microwave source generally is a magnetron that converts the kinetic energy created by the oscillation of electrons into electromagnetic waves, here, microwaves.[141]

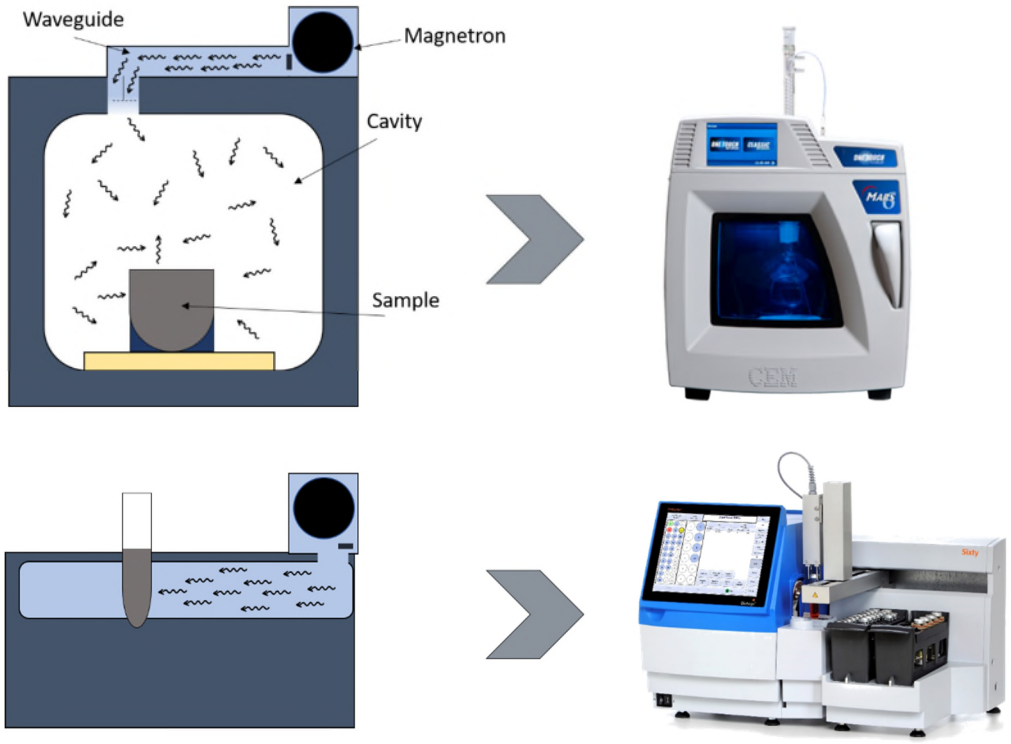


**Figure 1.7** Microwave reactor designs: multi- (top) and monomodal (bottom) instruments.

In practice, reactors vary by size, cavity design, type (batch/flow),[142–145] but the most important factor to consider is the mode of the reactor, which will impact the other parameters. There are two modes that can be used, figure 1.7. The first, based on domestic reactors, is described as multimodal.[146,147] Multimodal instruments are usually designed with large cavities, making them able to run multiple reactions in parallel and allow for larger reaction volumes to be carried out (300 µL to 100 mL). Those reactors can have one or two magnetrons and the waves are directed to the cavity by a waveguide and distributed randomly within the cavity by a mode stirrer. These microwaves are then able to bounce around the metallic walls of the cavity, thus interacting with the sample in a disorganised manner. The other instruments, so called monomodal,[147–151] have smaller, more compact cavities; the microwaves are focused

into a homogenous wave field with a single reaction vessel placed in the waveguide. This generates a high-density microwave field, but the vial sizes are typically smaller (2-5, 10-20 mL); this makes those reactors ideal for small, laboratory scales reactions.

## 1.5 Theory of Pigment Dispersion

### 1.5.1 Pigments

Pigment, dye, dyestuff or colorant are words often used interchangeably to describe colour-bearing substances. By definition however, pigments differ from dyes as they are for the most part insoluble in the application medium, usually water. Most of us would be familiar with the Lascaux caves paintings that were produced more than 20 000 years ago.[152] Early humans used crudely water-dispersed pigments such as iron oxides (red and yellow), charcoal (black) pigments to apply to their bodies, or create cave wall paintings.[153] Semi-precious stones (Lapis lazuli and Malachite) could be, for instance, ground down to produce intense blue or green powders. A similar grinding process was employed with the True Indigo plant to produce, as its name suggests, indigo powder. Throughout history, pigments were largely produced from natural sources (plants, minerals and animals), and the first modern synthetic pigment, Prussian blue, was likely only discovered around 1710.[154]

Nowadays, pigments are near ubiquitous in our lives. The global synthetic pigment market is valuated at $41 billion in 2021 and set to reach $46 billion by 2025,[155] with applications in plastics,[156–158] cosmetics[159,160] and fabrics.[161] Commonly, pigments are integrated within coatings and paints for use, for instance in the automotive industry. These paints can be applied for both exteriors and interiors of cars, and are used not

**Figure 1.8** Pigment powders, from left to right: carbon black, diarylide yellow, titanium dioxide, iron oxide and chromium oxide.

only for aesthetic purposes, but also protective purposes.[162] The paint industry constitutes around 60% of global pigment consumption.[163]

Pigments can classified within two subgroups, organic and inorganic pigments. The formers are made of organic elements (carbon, nitrogen, hydrogen, oxygen)[164,165] while the later are largely based on inorganic compounds.[166–169] Typical examples of organic pigments are carbon black (C, black),[170–175] diarylide pigments (a family of yellow diazos pigments),[176] Quinacridone ($C_{20}H_{12}N_2O_2$, magenta)[176] or Indanthrene ($C_{28}H_{14}N_2O_4$, blue).[177] In contrast, metallic oxides such as titanium dioxide ($TiO_2$, white),[178–182] iron oxide ($Fe_2O_3$, brownish red),[183] cobalt blue ($Al_2CoO_4$, blue)[184] or chromium oxide ($Cr_2O_3$, green)[185,186] provide instances of available inorganic pigments, figure 1.8.

### 1.5.2 The Dispersion Process

Pigments are generally sold as more or less fine powders but different substructures can be defined. The smallest undividable pigment entities are called *primary particles*

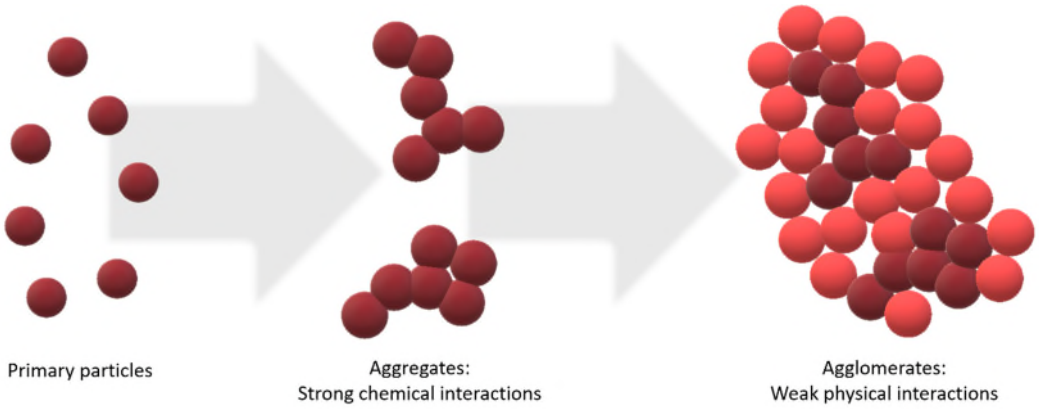


**Figure 1.9** Typical structure of pigment powder agglomerates.

(10-300 nm), also referred to as nodules, but are scarcely observed. During the pigment manufacturing process, nodules frequently become chemically bound through covalent bonds to form clusters referred to *aggregates* (85-500 nm). *Agglomerates* (1-1000 nm) can finally be formed through the weak, physical (Van der Waals, hydrophobic) interactions that occur between aggregates and nodules, figure 1.9. The goal of the dispersion process is to break down these agglomerates down to aggregates and, ideally, primary particles. This is a critical step of paint manufacturing because some of the key properties of coatings for instance haze and tinting strength, that increase with the fineness and homogeneity of the pigment particles distribution within the dispersion medium. The dispersion of pigments is arguably the most important part of paint manufacturing, and can generally be divided into three steps:

*Step 1: Wetting*

Agglomerates, these clusters of primary particles and aggregates, do not constitute a homogenous phase. There is air and moisture in the space between particles.[187] The first step of the dispersion process, the so-called *wetting* step, occurs when the powder is introduced in the dispersion medium, which is concomitant with the partial removal

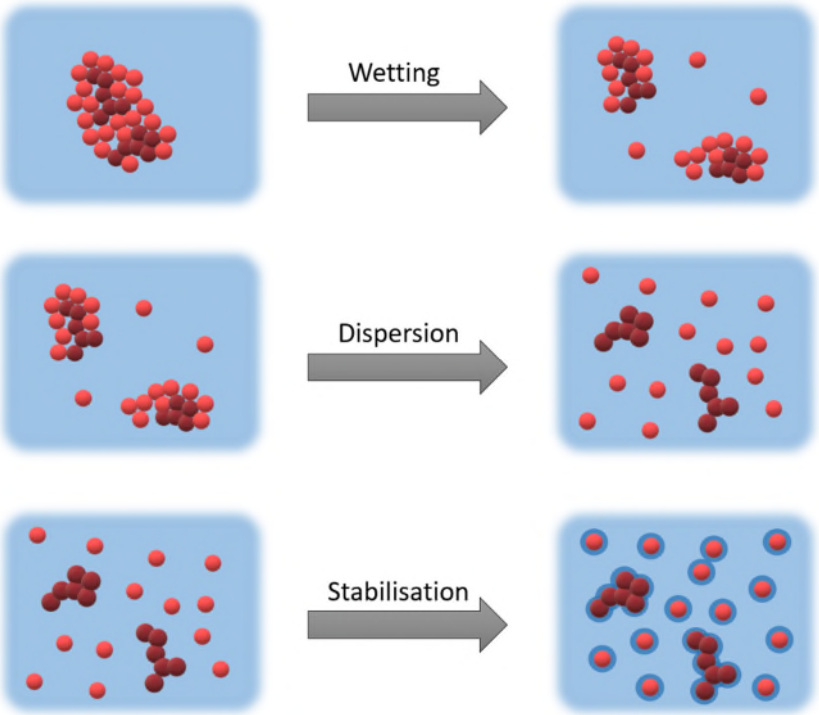


**Figure 1.10** Steps of the pigment dispersion process.

of the entrapped air/moisture and its replacement with dispersion medium. Figure 1.10 illustrates the change from the pigment/air interface, to pigment/medium interface. Generally, the amount of wetting that occurs depends on the geometry of the primary particles, as well as the chemical composition, viscosity and surface tension of the dispersion medium.

*Step 2: Dispersion*

It is during the *dispersion* step that agglomerates and flocculates are broken down through the application of mechanical – impact and shear – forces to the system. It is also during this step that full wetting is achieved.

*Step 3: Stabilisation*

As the agglomerates are ground down, this increases the surface area of the pigment exposed to the dispersion medium, which is a thermodynamically disfavoured state of higher energy.[188] Particles will in turn flocculate, a process whereby the finely ground particles clump together due to the attractive London-van der Waals forces, to reduce the overall energy of the system. Dispersing additives can however be used to stabilise the system after grinding and prevent flocculation. The production of high-quality pigmented coatings relies on the homogeneous distribution of pigment particles throughout the solution. As such, the role of the dispersing agent is to sterically, electrostatically, or electrosterically stabilise the dispersed particles. Failure to effectively do so would result in a variety of defects occurring either before the application of the paint (particle flocculation), but also after application with gloss reduction, hazing, or orange peeling among others, figure 1.11.

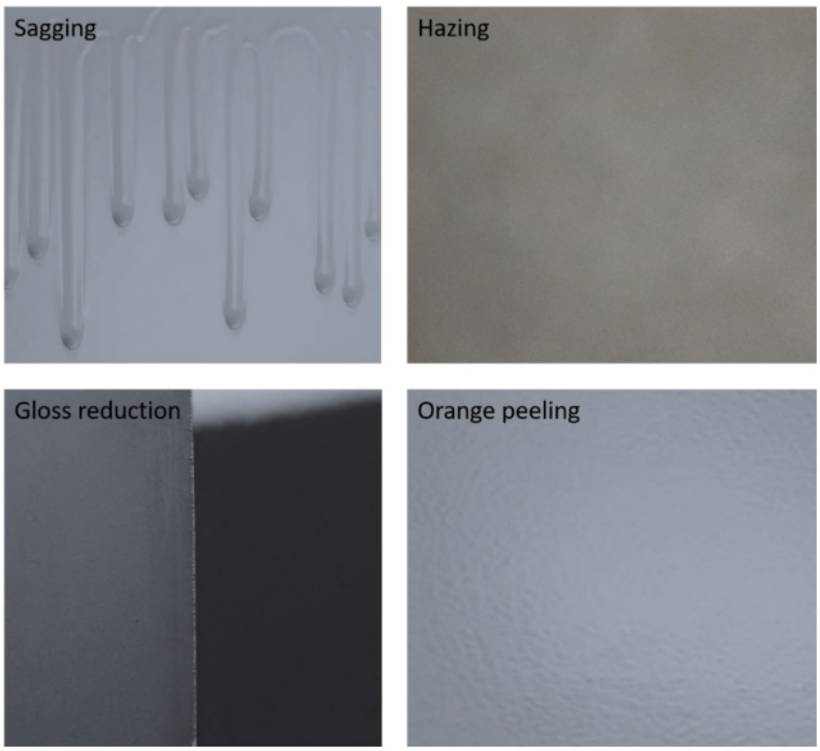


**Figure 1.11** Examples of paint and coating defects that can occur in non-optimised formulations.

### 1.5.3 Pathways to Stabilisation

In a well-dispersed system, pigment particles will, much like colloid particles, be subjected to Brownian motion, meaning they will frequently encounter and collide with one another. Unrestricted, this would eventually lead to a complete flocculation of the system. Alternatively, it is possible to introduce sources of electrostatic or steric repuslion as seen on figure 1.12.[187]

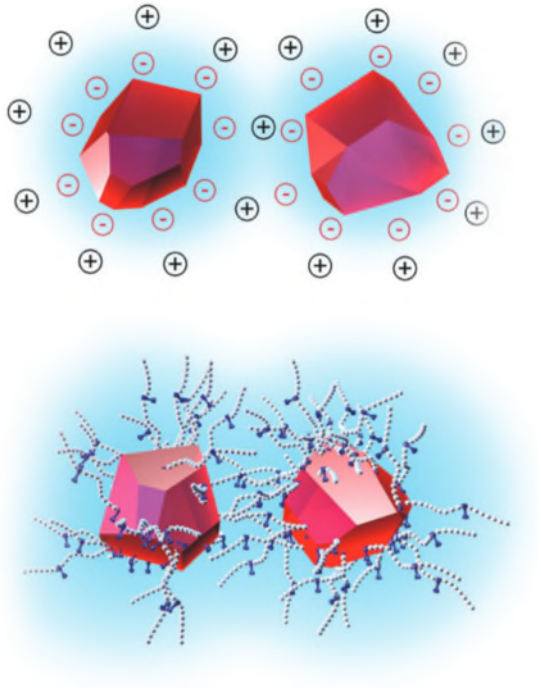

**Figure 1.12** Electrostatic (top) and steric (bottom) stabilisation of pigment dispersions. Figure obtained from BASF's "little helpers love great achievements Practical Guide to Dispersing Agents".

#### *1.5.2.1 Electrostatic Stabilisation*

In aqueous systems, electrostatic stabilisation is particularly relevant for particles that have a surface charge, something that is often the case with inorganic pigments, or have been made to display a surface charge through the adsorption of a polyelectrolyte to the surface.[106,181]

Charges can either be positive or negative, but due to the required neutrality of the system, an ionic cloud of opposite and equal charge forms around the dispersed particles. Any one cloud is formed of two layers: the stern layer is the internal layer present at the particle/water interface. It is strongly bound to the surface and neutralizes the surface's charge. The second layer, or diffuse layer, is made up of ions attracted to the first layer. When two neighbouring particles approach one another, the two equally charged and overlapping clouds create a repulsive electrostatic force, able to overcome the London-Van der Waals attractive forces. Electrostatic stabilisation is however susceptible to variations in pH, and is also essentially restricted to aqueous

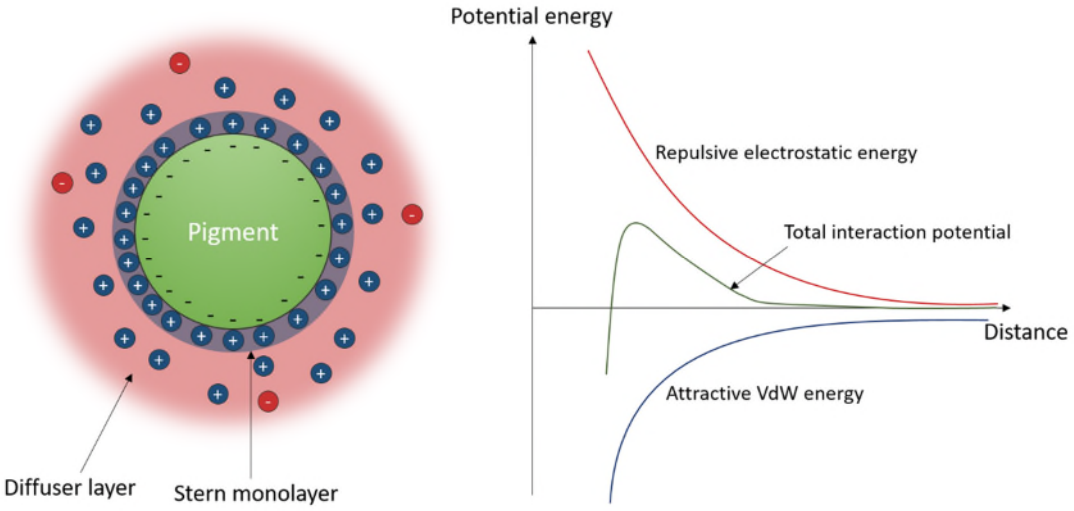


**Figure 1.13** Electric double layer (left) around a pigment particle consisting of the inner Stern layer and the outer diffuse layer and corresponding attractive, repulsive and total potential curves (right).

systems. Titanium dioxide dispersion is a regularly encountered topic in the literature. $TiO_2$ is indeed a major pigment, with a market value of 18.55 billion dollars in 2021 that is used in paints, coatings, cosmetics and paper making.[163,166,178,181,189,190] The pigment is often stabilised with ionic dispersants; Farrokhpay *et al.*[166] for instance found that $TiO_2$-based paints showed higher gloss and improved pigment stabilisation

when dispersed alongside "polyacrylic acid or carboxylate/hydroxyl-modified polyacrylamide". Cobalt blue was also more effectively stabilised by ionic dispersion, such as with a copolymer of acrylic and itaconic acids, as was shown by Peymannia *et al*.[191]

#### *1.5.2.2 Steric Stabilisation*

Alternatively, repulsion forces can also be generated using steric stabilisation. Segments of polymers, anchoring groups, can be adsorbed onto the surface of the pigments by non-covalent forces, with the remaining group ideally being fully solvated within the dispersion medium (aqueous or organic). This stabilisation can be brought on by linear amphiphilic or triblock copolymers, but also comb, brush or star polymers.[172,192–196] When two stabilised particles approach one another, the solvated segments' mobility become restricted. This loss of degrees of freedom results in an unfavourable reduction of the overall entropy. This entropic barrier prevents further attraction of the particles and, the additional rise in osmotic pressure increase repels the particles away from each other.

## 1.6 References

1 H. Frey and T. Johann, *Polym. Chem.*, 2019, **11**, 8–14.

2 K. Kawamura, in *Evolution, Origin of Life, Concepts and Methods*, Springer International Publishing, 2019, pp. 3–30.

3 P. Dandekar, R. Jain, T. Stauner, B. Loretz, M. Koch, G. Wenz and C. M. Lehr, *Macromol. Biosci.*, 2012, **12**, 184–194.

4 E. C. C. Santos, T. Kaldeus, D. B. Senoro, E. Malmström and A. Hult, *J. Environ. Sci. Manag.*, 2020, **23**, 48–64.

5 A. E. Alexakis, J. Engström, A. Stamm, A. V. Riazanova, C. J. Brett, S. V. Roth, P.-O. Syrén, L. Fogelström, M. S. Reid and E. Malmström, *Green Chem.*, 2021, **23**, 2113–2122.

6 E. S. Abdou, K. S. A. Nagy and M. Z. Elsabee, *Bioresour. Technol.*, 2008, **99**, 1359–1367.

7 M. Tang, R. Zhang, S. Li, J. Zeng, M. Luo, Y.-X. Xu and G. Huang, *Angew. Chemie*, 2018, **130**, 16062–16066.

8 W. He, Z. W. Ma, T. Yong, W. E. Teo and S. Ramakrishna, *Biomaterials*, 2005, **26**, 7606–7615.

9 J. C. Long, *Rubber Chem. Technol.*, 2001, **74**, 493–508.

10 D. Feldman, *Des. Monomers Polym.*, 2008, **11**, 1–15.

11 S. C. Rasmussen, *Ambix*, 2018, **65**, 356–372.

12 H. Staudinger, *Berichte der Dtsch. Chem. Gesellschaft (A B Ser.*, 1920, **53**, 1073–1085.

13 S. Kumar, A. K. Panda and R. K. Singh, *Resour. Conserv. Recycl.*, 2011, **55**, 893–910.

14 S. Shen, A. Henry, J. Tong, R. Zheng and G. Chen, *Nat. Nanotechnol.*, 2010, **5**,

251–255.

15 M. Gardette, A. Perthue, J. L. Gardette, T. Janecska, E. Földes, B. Pukánszky and S. Therias, *Polym. Degrad. Stab.*, 2013, **98**, 2383–2390.

16 S. Ronca, in *Brydson's Plastics Materials: Eighth Edition*, Elsevier Inc., 2017, pp. 247–278.

17 S. S. Haas, G. M. Brauer and G. Dickson, *J. Bone Jt. Surg. - Ser. A*, 1975, **57**, 381–391.

18 H. Liu, D. Liu, F. Yao and Q. Wu, *Bioresour. Technol.*, 2010, **101**, 5685–5692.

19 R. Gautam, R. D. Singh, V. P. Sharma, R. Siddhartha, P. Chand and R. Kumar, *J. Biomed. Mater. Res. - Part B Appl. Biomater.*, 2012, **100B**, 1444–1450.

20 P. Anguita-Alonso, M. S. Rouse, K. E. Piper, D. J. Jacofsky, D. R. Osmon and R. Patel, *Clin. Orthop. Relat. Res.*, 2006, **445**, 239–244.

21 T. Liu, C. Jiao, X. Peng, Y. N. Chen, Y. Chen, C. He, R. Liu and H. Wang, *J. Mater. Chem. B*, 2018, **6**, 8105–8114.

22 X. Wang, X. Liu, H. Yuan, H. Liu, C. Liu, T. Li, C. Yan, X. Yan, C. Shen and Z. Guo, *Mater. Des.*, 2018, **139**, 372–379.

23 X. Zhang, T. Liu, T. V. Sreekumar, S. Kumar, V. C. Moore, R. H. Hauge and R. E. Smalley, *Nano Lett.*, 2003, **3**, 1285–1288.

24 M. Mirzababaei, A. Arulrajah, S. Horpibulsuk, A. Soltani and N. Khayat, *Geotext. Geomembranes*, 2018, **46**, 646–655.

25 M. I. Ali, S. Ahmed, G. Robson, I. Javed, N. Ali, N. Atiq and A. Hameed, *J. Basic Microbiol.*, 2014, **54**, 18–27.

26 Y. Bai, Z. Wang, C. Wu, R. Xu, F. Wu, Y. Liu, H. Li, Y. Li, J. Lu and K. Amine, *ACS Appl. Mater. Interfaces*, 2015, **7**, 5598–5604.

27 N. Wang, A. Raza, Y. Si, J. Yu, G. Sun and B. Ding, *J. Colloid Interface Sci.*,

2013, **398**, 240–246.

28 Y. Zhang, F. Zhang, Z. Yang, H. Xue and D. D. Dionysiou, *J. Catal.*, 2016, **344**, 692–700.

29 G. Chen, C. Wu, W. Weng, D. Wu and W. Yan, *Polymer (Guildf).*, 2003, **44**, 1781–1784.

30 X. Fu and S. Qutubuddin, *Mater. Lett.*, 2000, **42**, 12–15.

31 D. E. Hill, Y. Lin, A. M. Rao, L. F. Allard and Y. P. Sun, *Macromolecules*, 2002, **35**, 9466–9471.

32 T. Maharana, Y. S. Negi and B. Mohanty, *Polym. - Plast. Technol. Eng.*, 2007, **46**, 729–736.

33 C. Walling, *Acc. Chem. Res.*, 1975, **8**, 125–131.

34 P. Garra, F. Morlet-Savary, C. Dietlin, J. P. Fouassier and J. Lalevée, *Macromolecules*, 2016, **49**, 9371–9381.

35 P. Garra, A. Kermagoret, A. Al Mousawi, F. Dumur, D. Gigmes, F. Morlet-Savary, C. Dietlin, J. P. Fouassier and J. Lalevée, *Polym. Chem.*, 2017, **8**, 4088–4097.

36 S. Bednarz, A. Błaszczyk, D. Błazejewska and D. Bogdał, *Catal. Today*, 2015, **257**, 297–304.

37 X. Y. Du, J. Shen, J. Zhang, L. Ling, C. F. Wang and S. Chen, *Polym. Chem.*, 2018, **9**, 420–427.

38 R. G. R. Bacon, *Q. Rev. Chem. Soc.*, 1955, **9**, 287–310.

39 A. S. Sarac, *Prog. Polym. Sci.*, 1999, **24**, 1149–1204.

40 J. Lalevée and J.-P. Fouassier, *Photopolymerisation Initiating Systems*, Royal Society of Chemistry, Cambridge, 2018.

41 E. J. Henley and C. C. Ng, *J. Polym. Sci.*, 1959, **36**, 511–517.

42 E. T. Denisov, T. G. Denisova and T. S. Pokidova, in *Handbook of Free Radical Initiators*, John Wiley & Sons, Inc., Hoboken, NJ, USA, 2005, pp. 129–282.

43 I. Chodák and E. Zimányová, *Eur. Polym. J.*, 1984, **20**, 81–84.

44 E. T. Denisov, T. G. Denisova and T. S. Pokidova, in *Handbook of Free Radical Initiators*, John Wiley & Sons, Inc., Hoboken, NJ, USA, 2005, pp. 303–358.

45 R. A. Gregg, D. M. Alderman and F. R. Mayo, *J. Am. Chem. Soc.*, 1948, **70**, 3740–3743.

46 F. R. Mayo, *J. Am. Chem. Soc.*, 1948, **70**, 3689–3694.

47 F. R. Mayo, *J. Am. Chem. Soc.*, 1943, **65**, 2324–2329.

48 J. L. O'Brien and F. Gornick, *J. Am. Chem. Soc.*, 1955, **77**, 4757–4763.

49 F. Jahanzad, M. Kazemi, S. Sajjadi and F. A. Taromi, *Polymer (Guildf).*, 1993, **34**, 3542–3544.

50 M. H. George and P. F. Onyon, *Trans. Faraday Soc.*, 1963, **59**, 134–140.

51 J. P. A. Heuts, G. E. Roberts and J. D. Biasutti, Aust. J. Chem., 2002, **55**, 381–398.

52 A. A. Gridnev and S. D. Ittel, *Chem. Rev.*, 2001, **101**, 3611–3659.

53 S. Slavin, K. McEwan and D. M. Haddleton, in *Polymer Science: A Comprehensive Reference, 10 Volume Set*, 2012, **3**, 249–275.

54 A. Gridnev, *J. Polym. Sci. Part A Polym. Chem.*, 2000, **38**, 1753–1766.

55 B. R. Smirnov, V. D. Plotnikov, B. V. Ozerkovskii, V. P. Roshchupkin and N. S. Yenikolopyan, *Polymer Science U.S.S.R*, 1981, **23**, 2807-1816.

56 B. R. Smirnov, A. P. Marchenko, V. D. Plotnikov, A. I. Kuzayev and N. S. Yenikolopyan, *Polymer Science U.S.S.R*, 1981, **23**, 1169-1178.

57 N. S. Enikolopyan, B. R. Smirnov, G. V. Ponomarev and I. M. Belgovskii, *J. Polym. Sci. A1.*, 1981, **19**, 879–889.

58 L. V Karmilova, G. V Ponomarev, B. R. Smirnov and I. M. Bel'govskii, *Russian Chemical Reviews*, 1984, **53**, 132-139.

59 US Pat., 4,680,354, 1987.

60 US Pat., 4,526,945, 1985.

61 Rospatent, SU664434A1, 1977.

62 G. Patias, A. M. Wemyss, S. Efstathiou, J. S. Town, C. J. Atkins, A. Shegiwal, R. Whitfield and D. M. Haddleton, *Polym. Chem.*, 2019, **10**, 6447–6455.

63 K. G. Suddaby, D. R. Maloney and D. M. Haddleton, *Macromolecules*, 1997, **30**, 702–713.

64 K. A. McEwan and D. M. Haddleton, *Polym. Chem.*, 2011, **2**, 1992–1999.

65 E. Le Grognec, J. Claverie and R. Poli, *J. Am. Chem. Soc.*, 2001, **123**, 9513–9524.

66 US Pat., 4,746,713, 1988.

67 G. P. Abramo and J. R. Norton, *Macromolecules*, 2000, **33**, 2790–2792.

68 A. A. Gridnev, *Polym. J.*, 1992, **24**, 613–623.

69 US Pat., US4694054A, 1987.

70 J. P. A. Heuts, D. J. Forster and T. P. Davis, *Macromol. Rapid Commun.*, 1999, **20**, 299–302.

71 B. R. Smirnov, A. P. Marchenko, G. V. Korolev, I. M. Bel'govskii and N. S. Yenikolopyan, *Polymer Science U.S.S.R.*, 1981, **23**, 1158-1168.

72 A. A. Gridnev, S. D. Ittel, M. Fryd and B. B. Wayland, *J. Chem. Soc. Chem. Commun.*, 1993, **12**, 1010–1011.

73 A. A. Gridnev, S. D. Ittel, B. B. Wayland and M. Fryd, *Organometallics*, 1996, **15**, 5116–5126.

74 R. A. Sanayei and K. F. O'Driscoll, *J. Macromol. Sci. Part A - Chem.*, 1989,

**26**, 1137–1149.

75 S. C. J. Pierik, PhD thesis, Technische Universiteit Eindhoven, 2002.

76 W. Xi, T. F. Scott, C. J. Kloxin and C. N. Bowman, *Adv. Funct. Mater.*, 2014, **24**, 2572–2590.

77 H. C. Kolb, M. G. Finn and K. B. Sharpless, *Angew. Chemie - Int. Ed.*, 2001, **40**, 2004–2021.

78 J. A. Opsteen and J. C. M. Van Hest, *Chem. Commun.*, 2005, **0**, 57–59.

79 W. H. Binder and C. Kluger, *Macromolecules*, 2004, **37**, 9321–9330.

80 B. Helms, J. L. Mynar, C. J. Hawker and J. M. J. Fréchet, *J. Am. Chem. Soc.*, 2004, **126**, 15020–15021.

81 G. Mantovani, V. Ladmiral, L. Tao and D. M. Haddleton, *Chem. Commun.*, 2005, **0**, 2089–2091.

82 B. Gacal, H. Durmaz, M. A. Tasdelen, G. Hizal, U. Tunca, Y. Yagci and A. L. Demirel, *Macromolecules*, 2006, **39**, 5330–5336.

83 H. Durmaz, B. Colakoglu, U. Tunca and G. Hizal, *J. Polym. Sci. Part A Polym. Chem.*, 2006, **44**, 1667–1675.

84 E. M. Muzammil, A. Khan and M. C. Stuparu, *RSC Adv.*, 2017, **7**, 55874–55884.

85 V. S. Khire, T. Y. Lee and C. N. Bowman, *Macromolecules*, 2007, **40**, 5669–5677.

86 C. Lluch, J. C. Ronda, M. Galiá, G. Lligadas and V. Cádiz, *Biomacromolecules*, 2010, **11**, 1646–1653.

87 D. P. Nair, M. Podgórski, S. Chatani, T. Gong, W. Xi, C. R. Fenoli and C. N. Bowman, *Chem. Mater.*, 2014, **26**, 724–744.

88 A. Genest, D. Portinha, E. Fleury and F. Ganachaud, *Prog. Polym. Sci.*, 2017,

**72**, 61–110.

89 M. Conrad and M. Guthzeit, *Berichte der Dtsch. Chem. Gesellschaft*, 1884, **17**, 1185–1188.

90 T. Tokoroyama, *European J. Org. Chem.*, 2010, **2010**, 2009–2016.

91 H. Yang, J. Zhang, Y. Zuo, Y. Song, W. Huang, L. Jiang, Q. Jiang, X. Xue and B. Jiang, *Macromol. Chem. Phys.*, 2019, **220**, 1900147.

92 H. Yang, Y. Zuo, J. Zhang, Y. Song, W. Huang, X. Xue, Q. Jiang, A. Sun and B. Jiang, *Polym. Chem.*, 2018, **9**, 4716–4723.

93 Q. Jiang, Y. L. Zhang, Y. Du, M. Tang, L. Jiang, W. Huang, H. Yang, X. Xue and B. Jiang, *Polym. Chem.*, 2020, **11**, 1298–1306.

94 C. F. Nising and S. Bräse, *Chem. Soc. Rev.*, 2008, **37**, 1218–1228.

95 D. Tanini, S. Scarpelli, E. Ermini and A. Capperucci, *Adv. Synth. Catal.*, 2019, **361**, 2337–2346.

96 F. Palacios, C. Alonso and J. M. de los Santos, *Chem. Rev.*, 2005, **105**, 899–931.

97 D. Enders, A. Saint-Dizier, M. I. Lannou and A. Lenzen, *European J. Org. Chem.*, 2006, **2006**, 29–49.

98 M. Moreno, G. Lligadas, J. C. Ronda, M. Galià and V. Cádiz, *J. Polym. Sci. Part A Polym. Chem.*, 2013, **51**, 1808–1815.

99 C. F. H. Allen, J. O. Fournier and W. J. Humphlett, *Can. J. Chem.*, 1964, **42**, 2616–2620.

100 J. S. Brown, A. W. Ruttinger, A. J. Vaidya, C. A. Alabi and P. Clancy, *Org. Biomol. Chem.*, 2020, **18**, 6364–6377.

101 A. B. Lowe, *Polym. Chem.*, 2014, **5**, 4820–4870.

102 A. D. Baldwin and K. L. Kiick, *Polym. Chem.*, 2013, **4**, 133–143.

103 Y. Suzuki, T. Higashihara, S. Ando and M. Ueda, *Eur. Polym. J.*, 2010, **46**, 34–41.

104 R. Matsuno, K. Takami and K. Ishihara, *Langmuir*, 2010, **26**, 13028–13032.

105 A. H. Khan, J. K. Cook, W. J. Wortmann, N. D. Kersker, A. Rao, J. A. Pojman and A. T. Melvin, *J. Biomed. Mater. Res. - Part B Appl. Biomater.*, 2020, **108**, 2294–2307.

106 G. Z. Li, R. K. Randev, A. H. Soeriyadi, G. Rees, C. Boyer, Z. Tong, T. P. Davis, C. R. Becer and D. M. Haddleton, *Polym. Chem.*, 2010, **1**, 1196–1204.

107 M. Li, P. De, S. R. Gondi and B. S. Sumerlin, *J. Polym. Sci. Part A Polym. Chem.*, 2008, **46**, 5093–5100.

108 S. H. Frayne, R. R. Murthy and B. H. Northrop, *J. Org. Chem.*, 2017, **82**, 7946–7956.

109 A. O. Konuray, F. Liendo, X. Fernández-Francos, À. Serra, M. Sangermano and X. Ramis, *Polymer (Guildf).*, 2017, **113**, 193–199.

110 W. Xi, C. Wang, C. J. Kloxin and C. N. Bowman, *ACS Macro Lett.*, 2012, **1**, 811–814.

111 A. Y. Rulev, *Russ. Chem. Rev.*, 2011, **80**, 197–218.

112 J. L. Vicario, D. Badía, L. Carrillo, J. Etxebarria, E. Reyes and N. Ruiz, *Org. Prep. Proced. Int.*, 2005, **37**, 513–538.

113 A. Genest, D. Portinha, E. Fleury and F. Ganachaud, *Prog. Polym. Sci.*, 2017, **72**, 61–110.

114 T. Tokoroyama, *European J. Org. Chem.*, 2010, **2010**, 2009–2016.

115 K. A. Shooshtari and M. Van De Mark, *Polym. Prepr.*, 2001, **42**, 458–459.

116 G. B. Desmet, D. R. D'Hooge, P. S. Omurtag, P. Espeel, G. B. Marin, F. E. Du Prez and M. F. Reyniers, *J. Org. Chem.*, 2016, **81**, 12291–12302.

117 M. Bláha, O. Trhlíková, J. Podešva, S. Abbrent, M. Steinhart, J. Dybal and M. Dušková-Smrčková, *Tetrahedron*, 2018, **74**, 58–67.

118 S. M. Sarkar, T. Sultana, T. K. Biswas, M. L. Rahman and M. M. Yusoff, *New J. Chem.*, 2016, **40**, 497–502.

119 A. Ying, Q. Zhang, H. Li, G. Shen, W. Gong and M. He, *Res. Chem. Intermed.*, 2013, **39**, 517–525.

120 G. Bartoli, M. Bosco, E. Marcantoni, M. Petrini, L. Sambri and E. Torregiani, *J. Org. Chem.*, 2001, **66**, 9052–9055.

121 L. Bai, P. Qv and J. Zheng, *J. Mater. Sci.*, 2020, **55**, 14045–14057.

122 G. González, X. Fernández-Francos, À. Serra, M. Sangermano and X. Ramis, *Polym. Chem.*, 2015, **6**, 6987–6997.

123 N. Azizi and M. R. Saidi, *Tetrahedron*, 2004, **60**, 383–387.

124 J. Zhang, C. Wang, C. Wang, W. Shang, B. Xiao, S. Duan, F. Li, L. Wang and P. Chen, *J. Chem. Technol. Biotechnol.*, 2019, **94**, 3981–3986.

125 H. Zhang, Y. Zhang, L. Liu, H. Xu and Y. Wang, *Synthesis (Stuttg).*, 2005, **2005**, 2129–2136.

126 N. Naga, S. Fujioka, D. Inose, K. Ahmed, H. Nageh and T. Nakano, *RSC Adv.*, 2019, **10**, 60–69.

127 S. Verma, S. L. Jain and B. Sain, *Org. Biomol. Chem.*, 2011, **9**, 2314–2318.

128 A. Y. Rulev, H. Kotsuki and J. Maddaluno, *Green Chem.*, 2012, **14**, 503–508.

129 M. Schmider, E. Müh, J. E. Klee and R. Mülhaupt, *Macromolecules*, 2005, **38**, 9548–9555.

130 L. W. Xu and C. G. Xia, *European J. Org. Chem.*, 2005, **2005**, 633–639.

131 J. Zhang, K. Kato, Y. Uyama and Y. Ikada, *J. Polym. Sci. Part A Polym. Chem.*, 1995, **33**, 2629–2638.

132 Q. Tang, B. Wang, Y. Shi, L. Song and Y. Hu, *Ind. Eng. Chem. Res.*, 2013, **52**, 5640–5647.

133 M. Rosales-Guzmán, O. Pérez-Camacho, R. Torres-Lubián, S. Harrisson, U. S. Schubert, C. Guerrero-Sánchez and E. Saldívar-Guerra, *Macromol. Chem. Phys.*, 2018, **219**, 1800084.

134 A. Métafiot, J. F. Gérard, B. Defoort and M. Marić, *J. Polym. Sci. Part A Polym. Chem.*, 2018, **56**, 860–878.

135 P. J. Docherty, M. J. Derry and S. P. Armes, *Polym. Chem.*, 2019, **10**, 603–611.

136 N. V. Tsarevsky, S. A. Bencherif and K. Matyjaszewski, *Macromolecules*, 2007, **40**, 4439–4445.

137 K. A. McEwan, S. Slavin, E. Tunnah and D. M. Haddleton, *Polym. Chem.*, 2013, **4**, 2608–2614.

138 Q. Zhang, S. Slavin, M. W. Jones, A. J. Haddleton and D. M. Haddleton, *Polym. Chem.*, 2012, **3**, 1016–1023.

139 C. O. Kappe, A. Stadler and D. Dallinger, in *Microwaves in Organic and Medicinal Chemistry, 2nd Edition*, 2012, pp. 9–39.

140 D. M. P. Mingos and D. R. Baghurst, *Chem. Soc. Rev.*, 1991, **20**, 1–47.

141 Y. Blanchard, G. Galati and P. Van Genderen, *IEEE Antennas Propag. Mag.*, 2013, **55**, 244–254.

142 J. R. Schmink, C. M. Kormos, W. G. Devine and N. E. Leadbeater, *Org. Process Res. Dev.*, 20010, **14**, 205–214.

143 T. N. Glasnov and C. O. Kappe, *Chem. - A Eur. J.*, 2011, **17**, 11956–11968.

144 M. C. Bagley, R. L. Jenkins, M. C. Lubinu, C. Mason and R. Wood, *J. Org. Chem.*, 2005, **70**, 7003–7006.

145 I. R. Baxendale, C. M. Griffiths-Jones, S. V. Ley and G. K. Tranmer, *Chem. -*

*A Eur. J.*, 2006, **12**, 4407–4416.

146 A. Stadler, B. H. Yousefi, D. Dallinger, P. Walla, E. Van Der Eycken, N. Kaval and C. O. Kappe, *Org. Process Res. Dev.*, 2003, **7**, 707–716.

147 D. Santos, E. C. L. da Rocha, R. L. M. Santos, A. J. Cancelas, E. Franceschi, A. F. Santos, M. Fortuny and C. Dariva, *Sep. Purif. Technol.*, 2017, **189**, 347–356.

148 D. Bogdal, P. Penczek, J. Pielichowski and A. Prociak, *Adv. Polym. Sci.*, 2003, **163**, 193–263.

149 S. M. Budy, M. Khan, X. Chang, S. T. Iacono and D. Y. Son, *J. Polym. Sci.*, 2020, **58**, 2774–2783.

150 F. Fan, C. Cai, L. Gao, J. Li, P. Zhang, G. Li, C. Li and G. Yu, *Polym. Chem.*, 2017, **8**, 6709–6719.

151 C. Koopmans, M. Iannelli, P. Kerep, M. Klink, S. Schmitz, S. Sinnwell and H. Ritter, *Tetrahedron*, 2006, **62**, 4709–4714.

152 A. Leroi-Gourhan, *Sci. Am.*, 1982, **246**, 104–112.

153 J. R. Barnett, S. Miller and E. Pearce, in *Optics and Laser Technology*, Elsevier, 2006, vol. 38, pp. 445–453.

154 J. Bartoll, *9th Int. Conf. NDT Art, Jerusalem Isr. 25-30 May 2008*, 2008, 25–30.

155 T. B. R. Company, *Global Synthetic Pigments Market Data And Industry Growth Analysis*, 2021.

156 V. S. Vishnu, G. George, V. Divya and M. L. P. Reddy, *Dye. Pigment.*, 2009, **82**, 53–57.

157 E. M. Angelin, S. França de Sá, M. Picollo, A. Nevin, M. E. Callapez and M. J. Melo, *J. Raman Spectrosc.*, 2021, **52**, 145–158.

158 R. M. Christie, *Polym. Int.*, 1994, **34**, 351–361.

159 J. Choksi, J. Vora and N. Shrivastava, *Indian J. Microbiol.*, 2020, **60**, 379–382.

160 C. Menozzi-Smarrito and S. Smarrito, J. Cosmet. Dermatol., 2021, **20**, 2667–2668.

161 B. Mahltig, J. Zhang, L. Wu, D. Darko, M. Wendt, E. Lempa, M. Rabe and H. Haase, *J. Coatings Technol. Res.*, 2017, **14**, 35–55.

162 A. S. H. Makhlouf, in *Handbook of Smart Coatings for Materials Protection*, Elsevier Inc., 2014, pp. 121–131.

163 S. Farrokhpay, *Adv. Colloid Interface Sci.*, 2009, **151**, 24–32.

164 Y. F. Lan and J. J. Lin, *Dye. Pigment.*, 2011, **90**, 21–27.

165 S. Lelu, C. Novat, C. Graillat, A. Guyot and E. Bourgeat-Lami, *Polym. Int.*, 2003, **52**, 542–547.

166 S. Farrokhpay, G. E. Morris, D. Fornasiero and P. Self, *J. Coatings Technol. Res.*, 2006, **3**, 275–283.

167 V. S. Vishnu, S. Jose and M. L. Reddy, *J. Am. Ceram. Soc.*, 2011, **94**, 997–1001.

168 S. Butylina, O. Martikka and T. Kärki, *Polym. Degrad. Stab.*, 2015, **120**, 10–16.

169 S. Jose and M. L. Reddy, *Dye. Pigment.*, 2013, **98**, 540–546.

170 H. Sis and M. Birinci, *Colloids Surfaces A Physicochem. Eng. Asp.*, 2009, **341**, 60–67.

171 M. Okazaki and N. Tsubokawa, *J. Dispers. Sci. Technol.*, 2000, **21**, 511–524.

172 D. J. Growney, O. O. Mykhaylyk, T. Derouineau, L. A. Fielding, A. J. Smith, N. Aragrag, G. D. Lamb and S. P. Armes, *Macromolecules*, 2015, **48**, 3691–3704.

173 H. Kim, K. Park and M. Y. Lee, *Toxicol. Res.*, 2012, **28**, 209–216.

174 H. Ridaoui, A. Jada, L. Vidal and J. B. Donnet, *Colloids Surfaces A Physicochem. Eng. Asp.*, 2006, **278**, 149–159.

175 Y. Lin, T. W. Smith and P. Alexandridis, *Langmuir*, 2002, **18**, 6147–6158.

176 S. Q. Lomax and T. Learner, *J. Am. Inst. Conserv.*, 2006, **45**, 107–125.

177 I. Chaari, M. Feki, M. Medhioub, J. bouzid, E. Fakhfakh and F. Jamoussi, *J. Hazard. Mater.*, 2009, **172**, 1623–1628.

178 P. V Liddell and D. V Boger, *Ind. Eng. Chem. Res.*, 1994, **33**, 2437–2442.

179 S. Creutz and R. Jérôme, *Prog. Org. Coatings*, 2000, **40**, 21–29.

180 J. Clayton, *Pigment Resin Technol.*, 1998, **27**, 231–239.

181 S. Farrokhpay, G. E. Morris, D. Fornasiero and P. Self, *Powder Technol.*, 2010, **202**, 143–150.

182 J. R. C. Costa, C. Correia, J. R. Góis, S. M. C. Silva, F. E. Antunes, J. Moniz, A. C. Serra and J. F. J. Coelho, *Prog. Org. Coatings*, 2017, **104**, 34–42.

183 L. Dengxin, G. Guolong, M. Fanling and J. Chong, *J. Hazard. Mater.*, 2008, **155**, 369–377.

184 M. Yoneda, K. Gotoh, M. Nakanishi, T. Fujii and T. Nomura, *Powder Technol.*, 2018, **323**, 574–580.

185 S. Sangeetha, R. Basha, K. J. Sreeram, S. N. Sangilimuthu and B. Unni Nair, *Dye. Pigment.*, 2012, **94**, 548–552.

186 G. Wei, J. Qu, Z. Yu, Y. Li, Q. Guo and T. Qi, *Dye. Pigment.*, 2015, **113**, 487–495.

187 C. Agbo, W. Jakpa, B. Sarkodie, A. Boakye and S. Fu, *J. Dispers. Sci. Technol.*, 2018, **39**, 874–889.

188 D. H. Everett, *Basic Principles of Colloid Science*, 1988.

189 Grand View Research, *Titanium Dioxide Market Trends Analysis Report, 2021-2028,* 2021.

190 S. Farrokhpay, G. E. Morris, D. Fornasiero and P. Self, *Colloids Surfaces A Physicochem. Eng. Asp.*, 2005, **253**, 183–191.

191 M. Peymannia, A. Soleimani-Gorgani, M. Ghahari and M. Jalili, *Ceram. Int.*, 2015, **41**, 9115–9121.

192 D. T. Nguyen, *J. Coatings Technol. Res.*, 2007, **4**, 295–309.

193 J. Y. T. Chong, X. Mulet, L. J. Waddington, B. J. Boyd and C. J. Drummond, *Soft Matter*, 2011, **7**, 4768–4777.

194 J. Y. T. Chong, X. Mulet, A. Postma, D. J. Keddie, L. J. Waddington, B. J. Boyd and C. J. Drummond, *Soft Matter*, 2014, **10**, 6666–6676.

195 R. Gref, V. Babak, P. Bouillot, I. Lukina, M. Bodorev and E. Dellacherie, *Colloids Surfaces A Physicochem. Eng. Asp.*, 1998, **143**, 413–420.

196 G. P. Lokhande and R. N. Jagtap, *Prog. Org. Coatings*, 2016, **90**, 359–368.

# **Chapter 2**:

# Michael-thiol Reactions for the Synthesis of Linear Amphiphilic Polymethacrylates

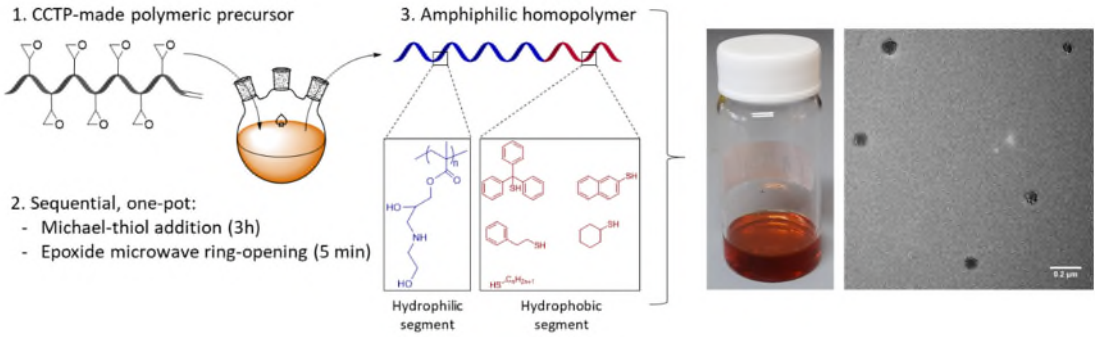


*Data in this chapter has been published:*

C. J. Atkins, G. Patias, J. S. Town, A. M. Wemyss, A. M. Eissa, A. Shegiwal and D. M. Haddleton, Polym. Chem., 2019, **10**, 646–655.

## 2.1 Introduction

The synthesis and behaviour of amphiphiles in solution has been the focus of numerous experimental[1–4] and theoretical[5–7] studies over the past few decades. Self-assembly, exemplified in nature by molecules such as phospholipids or cholesterol, occurs in order to reduce the overall free energy of a system by minimising interactions between water and hydrophobic moieties,[8] resulting in the formation of supra-molecular structures of varying morphologies, such as spherical micelles,[9,10] worm-like micelles,[11] and vesicles.[12]

Which of these morphologies is adopted can be generally predicted using the packing parameter, $p$,[13] defined as:

$$p = \frac{\nu_h}{a l_h} \qquad \text{(eqn. 1)}$$

where $\nu_h$ and $l_h$ represent the volume occupied and the maximum length of the hydrophobic chain, respectively, and $a$ the area of the hydrophilic head group.

Research into the self-assembly of synthetic macromolecules often focusses on their potential use in drug delivery systems,[14–16] but amphiphilic polymers have also found applications in bio-imaging,[17] food processing,[18] in the plastic industry as plasticisers[19] and in cleaning products as anti-redeposition agents[20] amongst others.

Of particular interest to this work is also the use of amphiphilic polymers as stabilisers for dispersed systems.[21–23] One such area of use being the stabilisation of pigments in waterborne paint formulations (discussed in depth in chapter 4), which has attracted the attention of multiple research groups.

For instance, Müller *et al.*[24] demonstrated the capacity of copolymers of methacrylic acid, styrene and acrylic esters to inhibit the corrosion of aluminium pigments within aqueous alkaline solutions. Other examples include an investigation by Leemans *et al.*[25] who reported the dispersion of carbon black in isododecane using polystyrene-

poly(stearyl methacrylate) block copolymer dispersants prepared by anionic polymerisation; and a study conducted by Saindane *et al.*[26] who dispersed titanium oxide ($TiO_2$) pigments using RAFT-made amphiphilic poly(ethyl acrylate)-poly(acrylic acid) block copolymers.

Developments in reversible-deactivation radical polymerisation (RDRP) techniques have allowed further advances towards the precise synthesis of functional amphiphilic polymers with the potential to be used in the aforementioned applications.[27–32] Ning *et al.*[33] have described the synthesis of biodegradable amphiphilic triblock copolymers using a combination of ring-opening polymerisation of $\varepsilon$-caprolactone and reversible addition–fragmentation chain transfer (RAFT) polymerisation of 2-(2-methoxyethoxy)ethyl methacrylate and ethylene glycol methacrylate. However, and despite academic interest in the synthesis and self-assembly of amphiphilic polymers, the implementation of RDRP within industrial settings has been increasing, but still is somewhat limited. This is a consequence of RDRP techniques often being difficult to

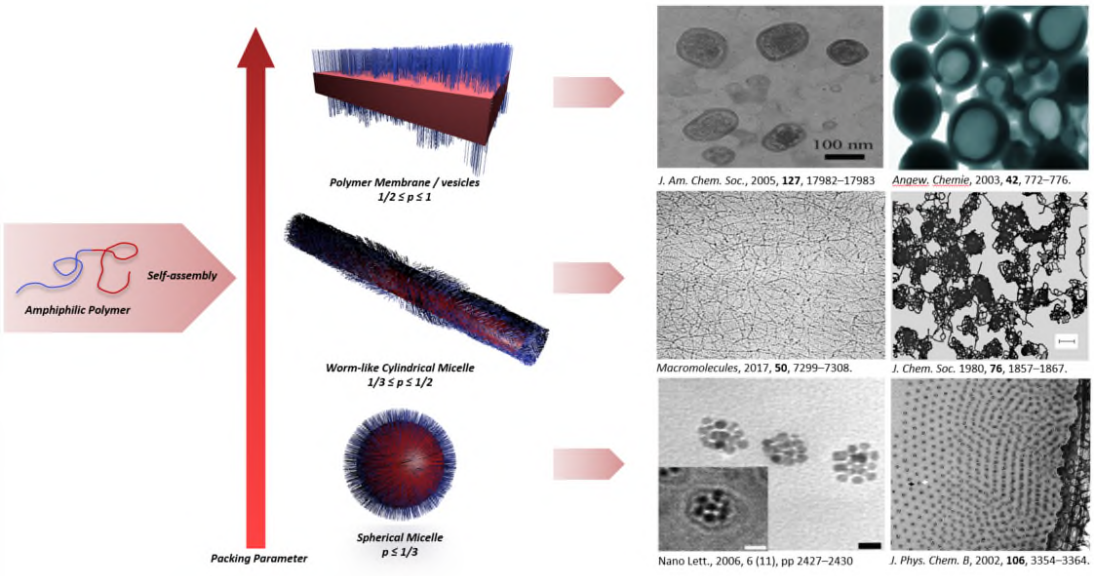


**Figure 2.1** Supra-molecular structures obtained by self-assembly of amphiphilic polymers in aqueous media. Morphologies can be predicted using the packing parameter, ρ, and observed with electron microscopy.

scale up due to oxygen sensitivity, or the production of polymers with chain transfer agent or halide end-groups which are often too difficult and/or expensive to remove from the final product.[34,35]

The use of industrially proven free-radical polymerisation techniques such as catalytic chain transfer polymerisation (CCTP), which allows for the synthesis of low molecular weight, vinyl-terminated oligomers or macromonomers, offers a potentially interesting alternative.[36,37] CCTP yields polymers terminated with vinyl ω-end groups. Typically, the low spin cobalt-(II) complexes are only required in ppm amounts relative to the concentration of monomer due to their extremely high chain transfer constants.[38–41] The process is highly adaptable, and polymers produced by CCTP have found direct applications within hair care,[42] as toner for printing applications,[43] and have also been used for the synthesis of low-VOC (Volatile Organic Compound) high solid coatings.[44] In general, however, CCT-prepared polymers have been increasingly used as intermediates in further chemistry strategies. Careful selection of the monomer, coupled with the presence of unsaturated chain-ends have made them ideal candidates for use alongside thiol-ene "click" chemistry.

In this chapter, a highly efficient post-polymerisation strategy is developed, allowing the production of amphiphilic polymers from a starting macromonomer within 3 hours. CCTP is used as the main reaction for the synthesis of intermediate macromonomers and Michael-thiol addition and epoxide ring-opening are investigated as post-polymerisation tools.

In the first part, hydrophobic p(GMA) polymers are prepared. Fully functionalised amphiphilic polymers are then obtained using a one-pot combination of hydrophobic

mercaptan Michael-addition and microwave-assisted epoxide ring-opening, constituting the MKI range of polymer.

As a comparison, hydrophilic polymers consisting of poly(glycerol monomethacrylate), p(GlyMA), are also prepared in a second part, and solely reacted with hydrophobic mercaptans, which are then classified within the MKII range.

In each case, a comparison of the influence of molecular weights of the polymers and clicked thiols is provided, alongside an investigation into the self-assembly behaviour and thermal properties of the different ranges.

This study was designed to provide a streamlined, potentially scalable method that allows the synthesis of amphiphilic polymethacrylates which could be utilised as stabilisers in the dispersion of carbon black pigments (chapter 4).

## 2.2 Results and Discussion

### 2.2.1 Catalyst Synthesis: $Co(dmgBF_2)_2(H_2O)_2$

Alexei Gridnev, in his 1989 paper,[45] reported the extremely high catalytic activity of low-spin cobalt(II) complexes as molecular weight regulators during the radical polymerisation of methacrylate monomers. Catalytic chain transfer polymerisation, or CCTP, is nowadays almost exclusively carried out using these cobaloxime complexes.

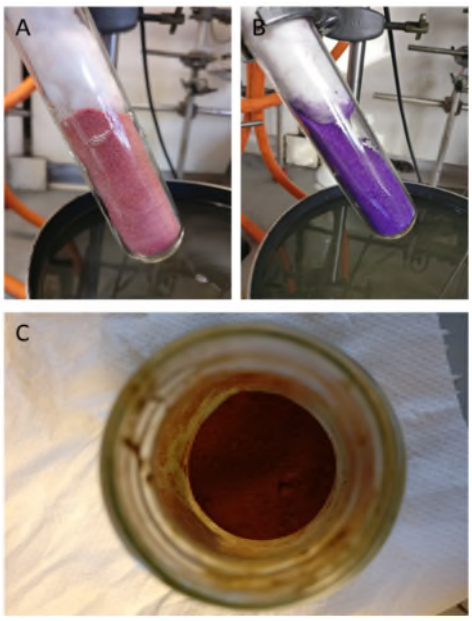


**Figure 2.2** Pictures of A) Cobalt(II) acetate tetrahydrate, B) Cobalt(II) acetate anhydride and C) dry CoBF powder.

Experimental conditions usually dictate the requirements for the structure of the CTA but by and large, the most used catalyst - and the one used in this work - is bis[(difluoroboryl)dimethylglyoximato]cobalt(II), or CoBF. The synthesis followed a two-step reaction pathway to the bridged structure presented in scheme 2.1. Cobalt(II)

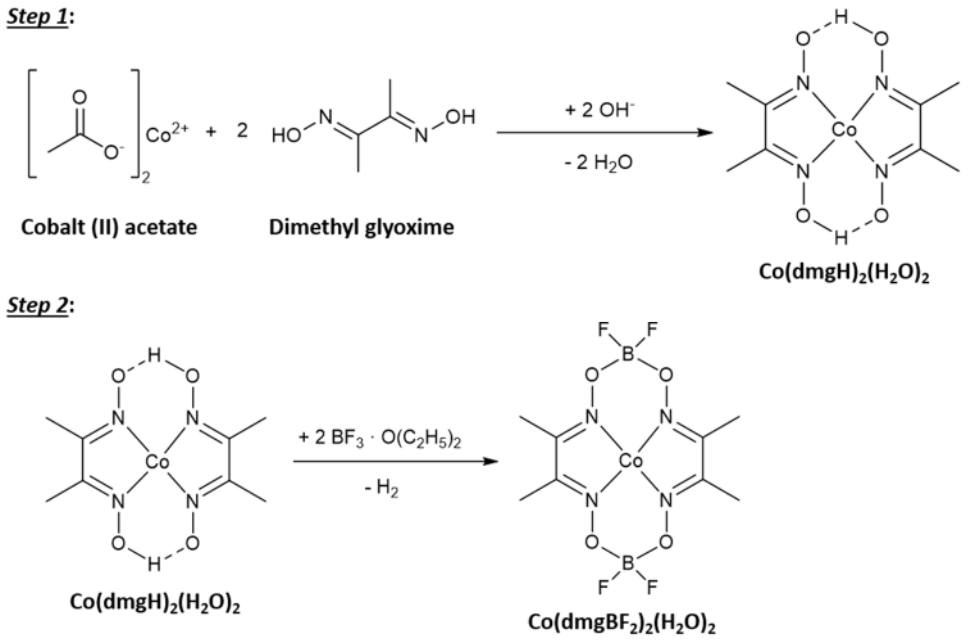


**Scheme 2.1** Synthetic pathway for the synthesis of $Co(dmgBF_2)_2(H_2O)_2$, or CoBF.

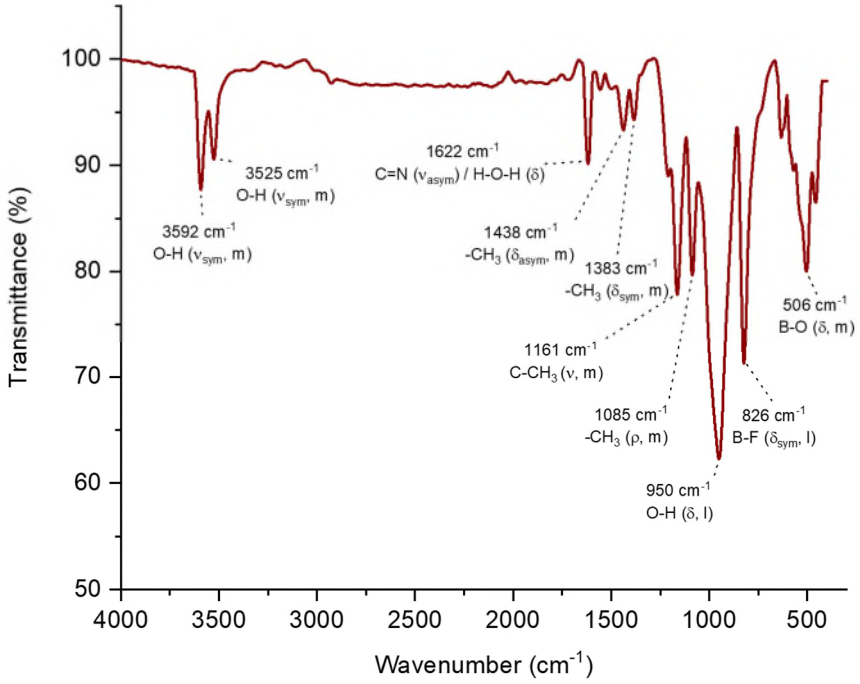


**Figure 2.3** FT-IR spectrum of CoBF at room temperature. ν = stretching, δ = deformation and ρ = rocking.

acetate anhydride was first reacted with dimethyl glyoxime to yield a $Co(dmgH)_2(H_2O)_2$ complex.

In order to increase the catalyst's hydrolytic and oxidative stability, a $BF_2$-capped derivative is often preferred.[46] This was achieved by mixing vigorously boron trifluoride etherate ($BF_3EtO_2$) with $Co(dmgH)_2(H_2O)_2$ whilst heating under an inert atmosphere.

The resulting powder had a dark brown / maroon colour, figure 2.2. Due to the paramagnetic nature of CoBF, $^1$H-NMR analysis was not possible. Multiple other techniques allowed us to nevertheless confirm the synthesis of the catalyst.

Figure 2.3 shows the IR spectrum of the reaction product. Identified peaks suggest the presence of the desired product.[47] The synthetic method that was carried out involved the recrystallization of CoBF in a solution of 80% water and 20% methanol. Consequently, a structure with axial water ligands is assumed. This is suggested by the presence of the two peaks at 3600 and 3530 $cm^{-1}$. These peaks correspond to,

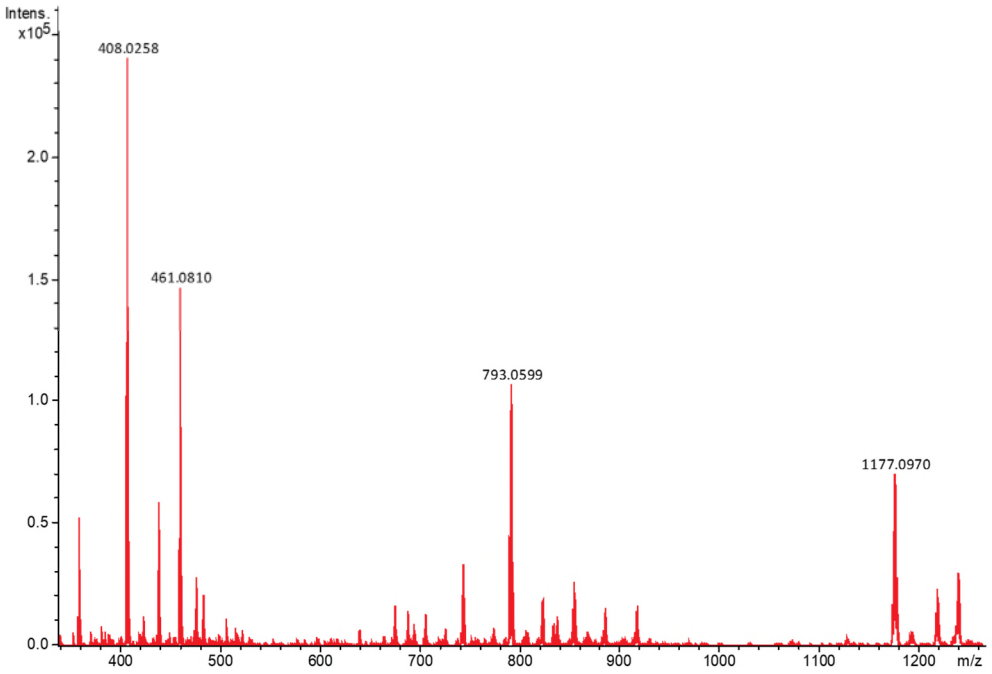


**Figure 2.4** ESI mass spectrum of CoBF.

respectively, lattice water ligands' asymmetric and symmetric stretching motion. As suggested by M. Duncan,[48] in the free gas water molecule the asymmetric:symmetric peak ratio is close to 18:1. However, and as is visible here, in water-containing metal complexes this ratio is closer to 1:1, an observation that is corroborated by Kazuo Nakamoto,[49] as well as Lawson and co-workers.[50]

CoBF has an octahedral structure and is chelated to a stable, planar tetradentate macrocyclic ligand with a π-system. The two lattice water molecules, however, are quite labile.[46] In mass spectrometry, while ESI is a soft ionisation technique, meaning the molecule's structural integrity is usually retained throughout the analysis, it is likely that both axial ligands were lost from the parent ion during the ionisation process.[51] The peaks shown in figure 2.4 indeed reveal the presence of water-less CoBF adducts at 408.0, 461.1, 793.1 and 1177.1 m/z ($[M+Na]^+$, $[M+2K+H]^+$, $[2M+Na]^+$ and $[3M+Na]^+$ respectively). The purity of the catalyst can nevertheless not be evaluated from the ESI. Small secondary peaks were visible on the ESI, but could

not be assigned. A comparison between a previous, “16 years old catalyst batch” and the freshly synthesised one could allow an indirect purity evaluation of the batches. The catalytic chain transfer constants of the catalysts were found to equal 34 800 and 49 700 for old and new CTAs respectively (for methyl methacrylate, MMA, in toluene, figure S2.2). Correlating with literature,[52] where the chain transfer constant of CoBF (for the same experimental conditions) was found to be between 41000 and 60000, we can infer that the new batch is within norm, while the older batch had lost some of its catalytic activity. This difference could partly be explained by a gradual degradation of the catalyst, but also by the impurities present in a given sample. ESI analysis (SI, figure S2.1) indeed showed that the old catalyst batch was contaminated, although the impurities could not be identified. While there was a difference in the calculated chain transfer constant, there did not seem to be a significant difference in the resulting polymeric products. Two identical reactions were carried out with the same catalytic loading, and both resulted in very similar products as can be seen from the NMR and GPC spectra, SI, figures S2.3, S2.4 and S2.5. The development of an HPLC methodology to help determine the degree of purity is underway.

## 2.2.2 Synthesis of Initial Main Framework CCTP Macromonomers

### *2.2.2.1 Poly(Glycidyl Methacrylate)*

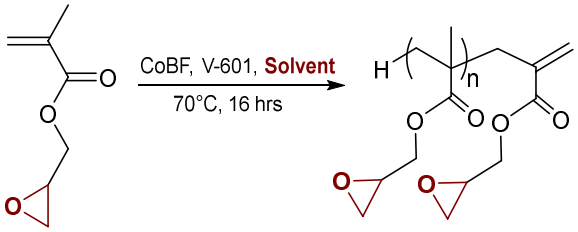


**Scheme 2.2** CCTP polymerisation conditions for the preparation of p(GMA).

The effect of solvents on the polymerisation of glycidyl methacrylate was investigated first. Under normal temperature and pressure conditions, the epoxide side-chains of p(GMA) are stable and do not show signs of side-reactions. Polymerisations were carried out with an azo initiator, V-601, at 70 °C for 16 hours.

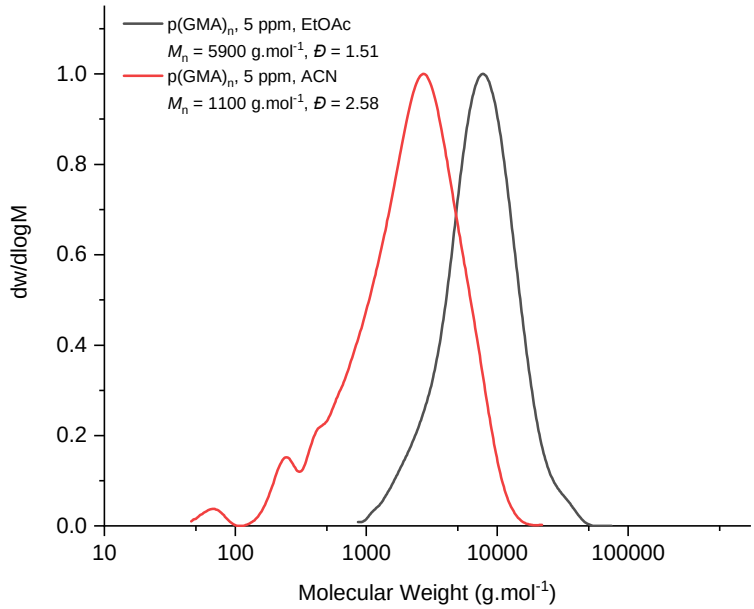


**Figure 2.5** GPC traces ($CHCl_3$, 50 °C) of GMA polymers prepared in ethyl acetate (grey) and acetonitrile (red).

Three different solvents were investigated, namely isopropyl alcohol (IPA), acetonitrile (ACN) and ethyl acetate (EtOAc), with a 5 ppm catalyst loading for each attempt.

EtOAc and ACN both led to the expected low molecular weight polymers as is evidenced by the GPC traces (figure 2.5) and, as can be seen from figure 2.6, infra-red analysis did not reveal the presence of any hydroxy peaks, confirming that neither solvent caused ring-opening of the epoxides.

This difference in resulting molecular weight is likely to stem from the chain transfer constants ($C_s$) of CoBF with GMA in both solvents. It is well reported that the solvent can have a drastic effect on the activity of the catalysts. The $C_s$ values were determined

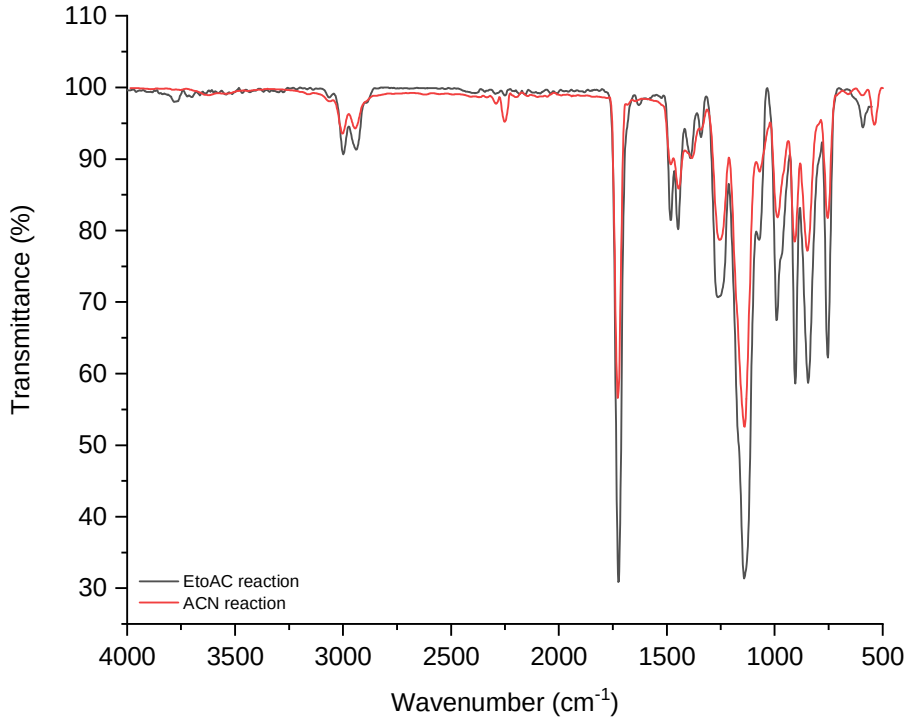


**Figure 2.6** Comparison of the FT-IR spectra of GMA polymers prepared by CCTP (5 ppm catalyst loading) in ethyl acetate (grey) and acetonitrile (red).

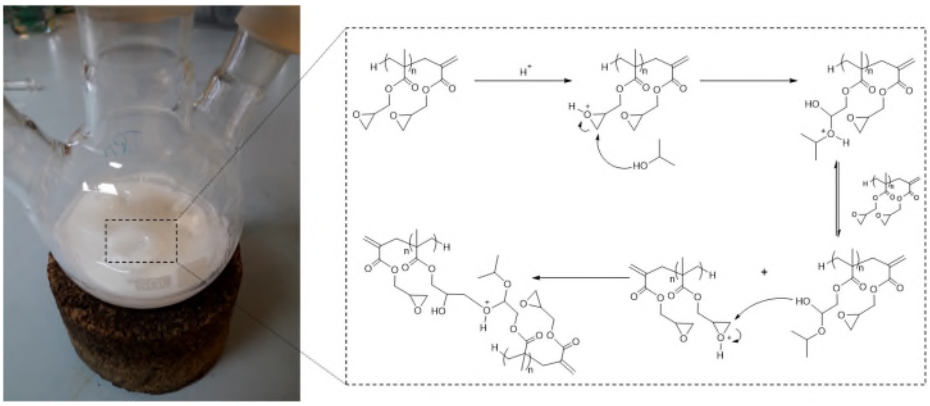

**Scheme 2.3** Polymerisation of GMA in a protic solvent, here IPA: picture of the crosslinked, solid product of the polymerisation (left). Crosslinking mechanism (right).

to be at approximatively 4750 and 7700 for EtOAc and ACN respectively (SI, figures S2.6 and S2.7).

The presence of protic solvents such as IPA, however, invariably led to ring-opening of the epoxides, followed by a cascade of reactions resulting in cross-linking of the system within 2 hours, which likely follows the mechanism shown in scheme 2.3, where an IPA molecule opens an epoxide moiety activated by a proton.

Acetonitrile was elected as main solvent for further polymerisations for its ability to dissolve a wider range of compounds than EtOAc, but also as it is less prone to side reaction such as hydrolysis or transesterification.[53]

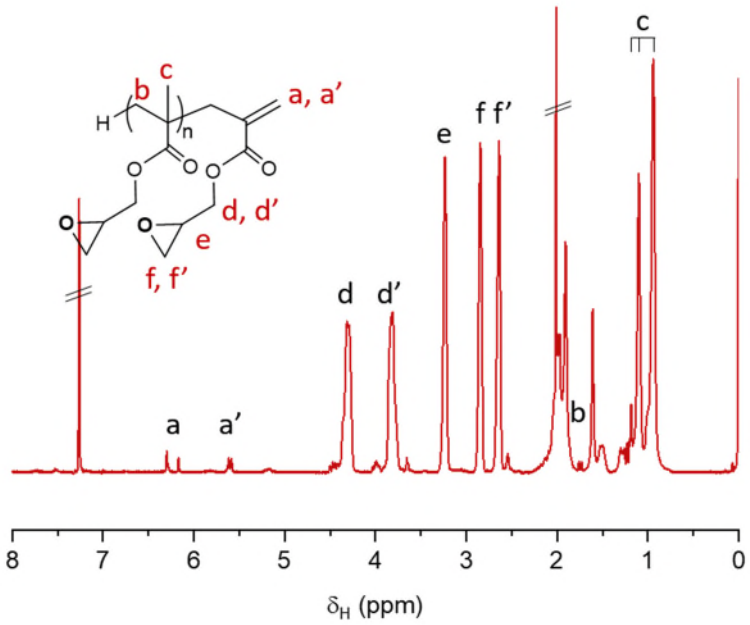


**Figure 2.7** $^{1}$H-NMR ($CDCl_3$, 400 MHz at 25 °C) spectrum of p(GMA) prepared by CCTP (catalyst loading: 5 ppm, $DP_{NMR}$ = 11).

Polymerisation reactions were subsequently scaled up to be carried out on a 70 g scale, table 2.1. Good control over molecular weights was observed by GPC at varying concentrations of catalyst (0.5, 2, 5 and 8 ppm) with conversions consistently reaching >95%, figure 2.8. As expected, molecular weights were found to decrease with increasing concentrations of CoBF. None of the polymerisation products showed signs of side-reactions, with no evidence for –OH functional groups observed by FT-IR spectroscopy, figure 2.9. Even with the presence of the $BF_2$ bridges, CoBF can be

| Entry | CoBF ppm | Conversion / % | $DP_{NMR}$ | $DP_{GPC}$ | $M_{n,GPC}$ / kg.mol$^{-1}$ | $M_{w,GPC}$ / kg.mol$^{-1}$ | $Đ$ |
|---|---|---|---|---|---|---|---|
| **1** | 0.5 | 98 | 230 | 270 | 17.60 | 76.84 | 4.36 |
| **2** | 2 | 98 | 43 | 51 | 6.70 | 14.50 | 2.17 |
| **3** | 5 | 96 | 11 | 17 | 2.60 | 4.92 | 1.87 |
| **4** | 8 | 95 | 7 | 12 | 0.95 | 3.70 | 2.32 |

**Table 2.1** CCTP p(GMA) batches synthesised for this study. $DP_{GPC} = M_{w,GPC}/(2M_0)$.

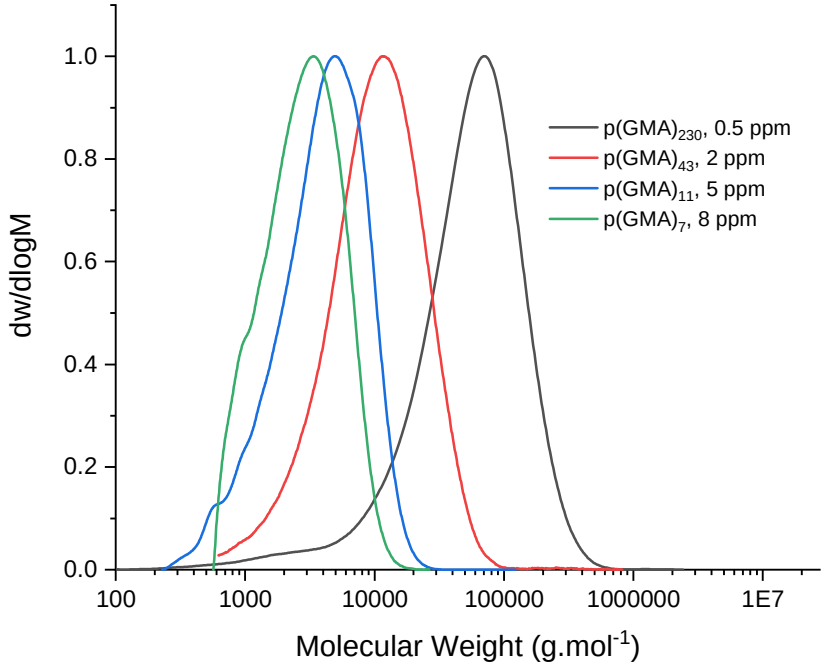


**Figure 2.8** Normalised GPC (DMF, 50 °C) traces comparison of p(GMA) batches **1**, **2**, **3** and **4** (respectively 0.5, 2, 5 and 8 ppm CoBF loading).

susceptible to acid hydrolysis or peroxide oxidation.[39] While unlikely to have a significant effect on the polymerisation of GMA, our group has previously described a protocol whereby a solution of CoBF in monomer is fed into the reaction mixture in order to maintain constant concentration of active catalyst.[54] Overall, the results demonstrate that the feeding of CoBF can allow the reactions to achieve high conversions and provide a solution to potential uncontrolled increase in dispersity, which can occur when the ratio of monomer to catalyst changes following monomer depletion or catalyst decomposition/degradation.

MALDI-ToF analysis, figure 2.10, of the products confirmed the presence of a polymer with a repeating unit of 142.16 Da, as expected from p(GMA), with a molecular weight distribution typical of free-radical polymers.

A −14 Da impurity was, however, also observed. ESI-MS of the GMA monomer (SI, figure S2.8) confirmed the presence of an unknown compound, which was hypothesised to stem from the monomer purity stated by the supplier (97%).

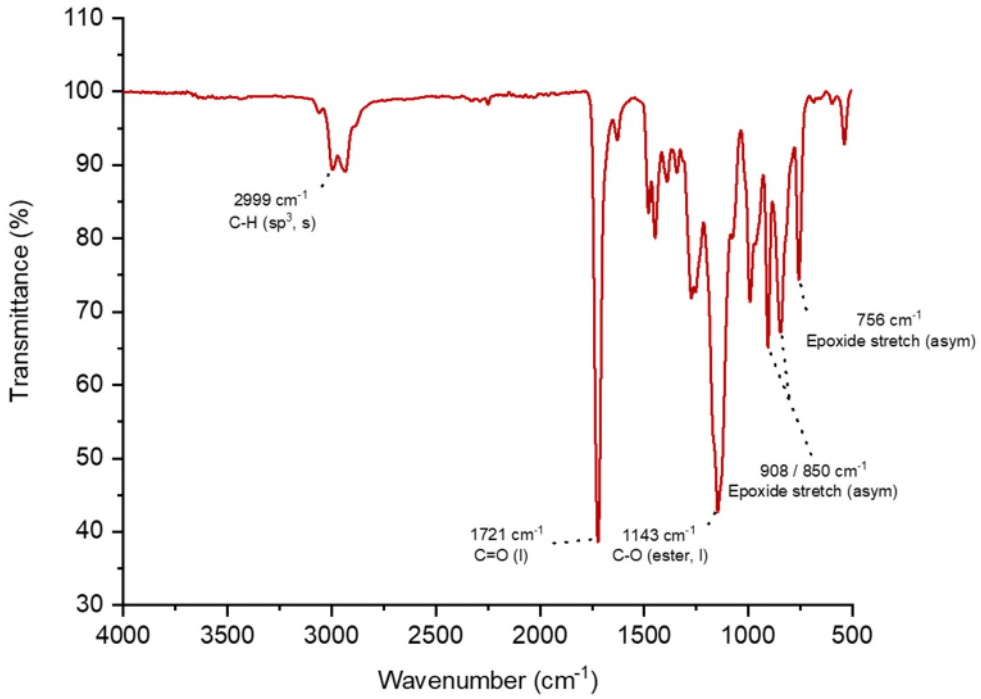


**Figure 2.9** FT-IR spectrum of $p(GMA)_{11}$ prepared by CCTP (catalyst loading: 5 ppm).

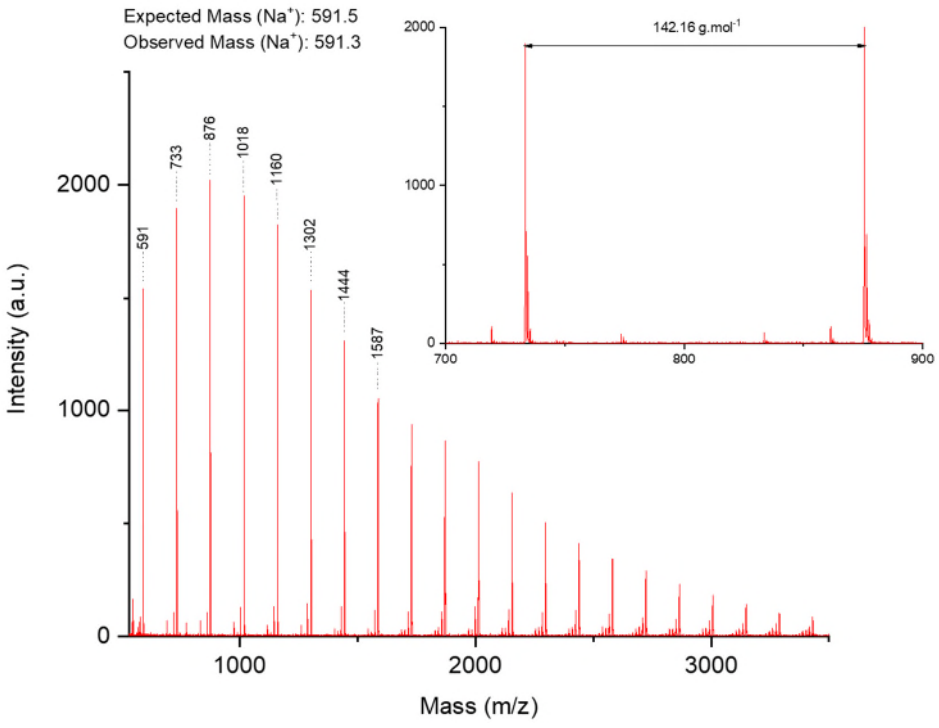


**Figure 2.10** MALDI-ToF spectrum of sample **2** with detailed zoom between 600 and 1000 Da.

### *2.2.2.2 Poly(Glycerol Monomethacrylate)*

Follwing the successful preparation of hydrophobic p(GMA), it was decided that it would be appropriate to investigate the preparation of hydrophilic CCT polymers. Glycerol monomethacrylate, GlyMA, is a hydrophilic specialty monomer useful in the preparation of hydrophilic networks or hydrogels. A typical example is its use as more hydrophilic alternative to HEMA in the preparation of soft contact lenses.[55] the monomer can be obtained by water-based ring-opening of GMA (discussed in chapter 3), or from the reaction between glycidol and methacrylic acid. As it is a methacrylic monomer of relatively high hydrophilicity, it was considered suitable for the preparation of a hydrophilic macromonomers for this work.

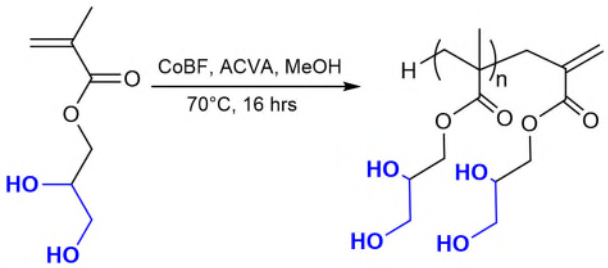


**Scheme 2.4** CCTP polymerisation conditions for the preparation of p(GlyMA).

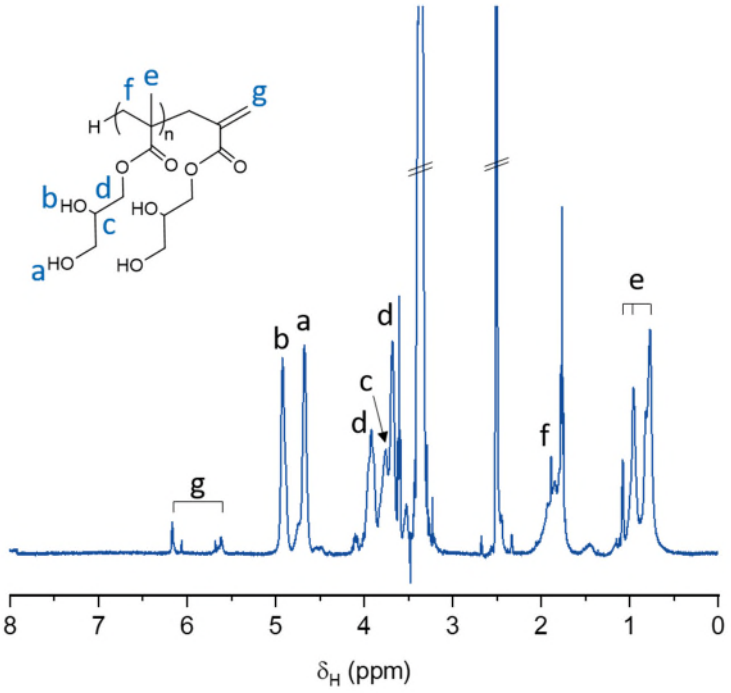


**Figure 2.11** $^{1}$H-NMR (DMSO-$d_6$, 400 MHz at 25 °C) spectrum of p(GlyMA)$_9$ prepared by CCTP.

| Entry | CoBF ppm | Conversion / % | $DP_{NMR}$ | $DP_{GPC}$ | $M_{n,GPC}$ / kg.mol$^{-1}$ | $M_{w,GPC}$ / kg.mol$^{-1}$ | $Đ$ |
|---|---|---|---|---|---|---|---|
| **1** | 20 | 95 | 94 | 68 | 15.0 | 21.9 | 1.45 |
| **2** | 30 | 98 | 50 | 36 | 8.3 | 11.6 | 1.43 |
| **3** | 40 | 98 | 9 | 4 | 1.4 | 3.9 | 2.66 |

**Table 2.2** CCTP p(GlyMA) batches synthesised for this study. ($M_n$ and $M_w$ were calculated from triple detection analysis). $DP_{GPC} = M_{w,GPC}/(2M_0)$.

The synthesis of p(GlyMA) was carried out in a similar manner to that of p(GMA). As there was no concern regarding potential side reactions, methanol was selected as solvent as it allowed for both monomer and polymer to be freely soluble, while being easier to remove than water. ACVA was chosen as initiator due to its relative solubility in methanol and availability. Initial experiments determining the chain transfer constant of the CCTP polymerisation of GlyMA in MeOH yielded a $C_s$ value of 539 (SI, figure S2.9). Three different 70 g batches were subsequently prepared and are reported in table 2.2.

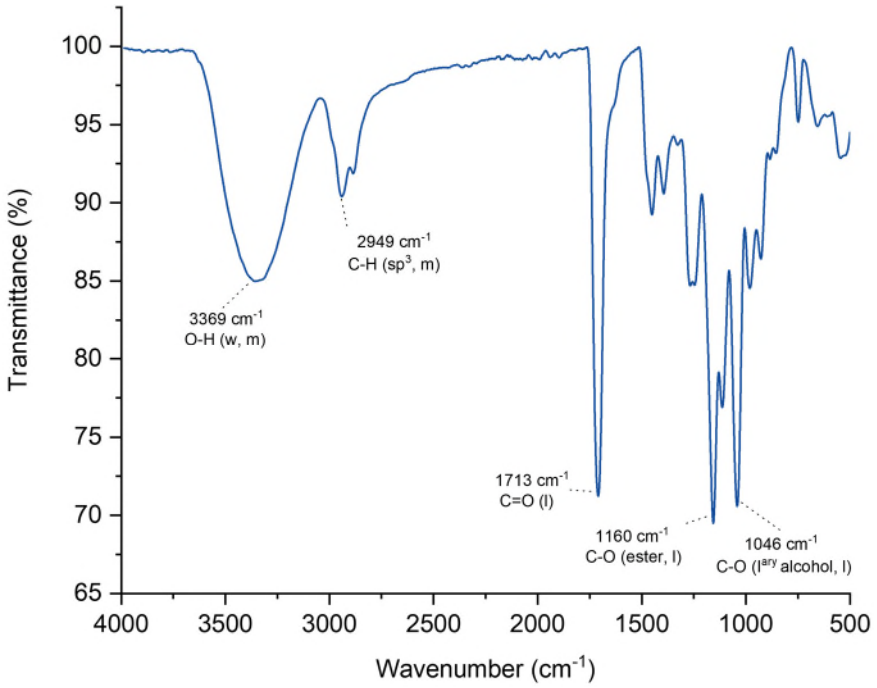


**Figure 2.12** FT-IR of p(GlyMA)$_9$ prepared by CCTP (batch **3**, catalyst loading: 40 ppm).

Generally, the trends that were observed with glycidyl methacrylate were also observed with glycerol monomethacrylate. A typical DMSO-$d_6$ $^1$H-NMR spectrum is shown in figure 2.11. The hydroxy groups' signals are typically found at 4.75 and 5 ppm, and are only visible in solvents where proton exchange does not occur. Thus, while $D_2O$ $^1$H-NMR are feasible, and a good indicator for amphiphilic polymers, as discussed later, the spectra cannot be considered as showing a full picture of the structure of the polymers.

The infra-red spectra from p(GMA) and p(GlyMA) were similar in most areas of the spectra except for the evident presence of the hydroxyl peaks at around 3300 cm$^{-1}$ for p(GlyMA), figure 2.12. GPC analyses indicated good dispersities for lower catalyst loading experiments (20/30 ppm, figure 2.13). This, however, is likely due to the precipitation purification process, whereby the lower molecular end-tail of the distribution is lost in the precipitation solvent (THF), leading to lower dispersities.

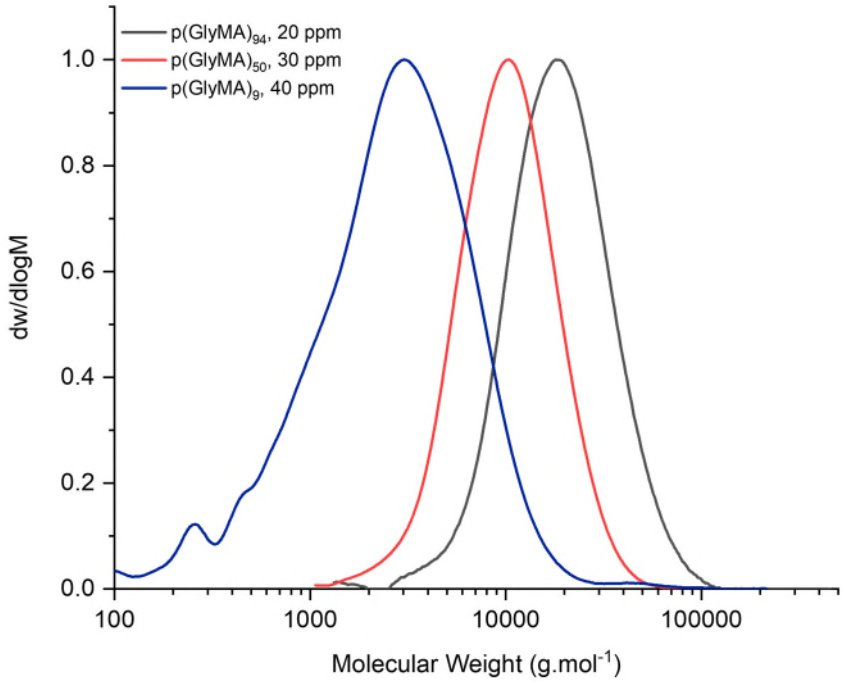


**Figure 2.13** Normalised triple-detection GPC (DMF, 50 °C) traces comparison of p(GlyMA) batches **1**, **2** and **3** (respectively 20, 30 and 40 ppm CoBF loading).

This hypothesis was confirmed with the higher catalyst loading polymerisations (40 ppm), where a non-negligible amount of product was lost in THF. The purification process for higher catalyst loading experiments (> 30 ppm) was optimised by carrying out precipitation where less polar solvents such as chloroform are preferred.

### 2.2.3 Post-Polymerisation Functionalisation of p(GMA), Preparation of the MKI Range

#### *2.2.3.1 Preliminary Investigation: Michael Addition Explorations, Solvent and Thiol Selection*

As described in chapter 1, Michael-thiol additions are some of the most widely encountered click reactions. They can be carried out through two different processes that, in principle, allow the formation of alkyl sulphides bonds.

They are catalysed by amines or phosphines (base or nucleophile-catalysed addition respectively), which are able to deprotonate thiols. The thiolate intermediates then react with the activated C=C bond.

Both mechanisms are versatile, and have historically been used in organic synthesis. Recently, however, they have increasingly been added to polymer chemists' toolbox, allowing for the post-polymerisation functionalisation of polymers.[56,57]

Here, the purpose of the fully functionalised polymers is to serve as amphiphilic polymethacrylate dispersants for carbon black and, due to the multitude of potential reaction conditions, a thorough investigation of the reaction conditions was required. Indeed, the carbon black pigment family is a diverse group of pigments but generally, all are produced from heavy oils with high aromatic hydrocarbons content, implying that the surface of the pigments has a high amount of aromaticity.

For this reason, preliminary investigations were conducted using hydrophobic compounds triphenylmethanethiol and 2-naphthalenethiol, as well as dodecanethiol (scheme 2.5). The working hypothesis was that aromatic anchor groups would adsorb onto the surface of the pigments more efficiently than aliphatic anchors due to π-π stacking and would thus provide better stabilisation to the dispersions.

Initial experiments were carried out between p(GMA) and the selected hydrophobic thiol moiety (1.2 equivalent) in DMSO as aprotic, hydrophobic solvent at room temperature, with dimethylphenylphosphine (DMPP) as catalyst, scheme 2.5. It was observed that, within 3 hours, only the reaction between

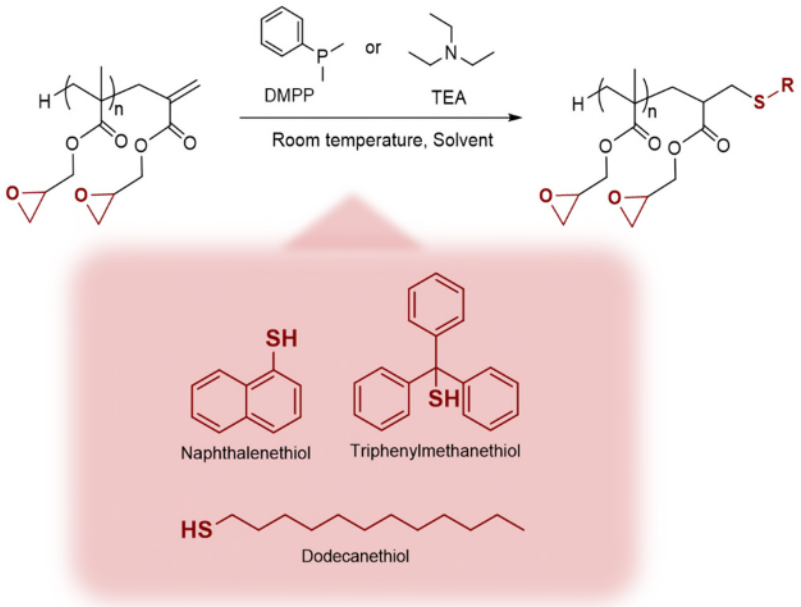


**Scheme 2.5** Michael-thiol addition of hydrophobic mercaptans onto p(GlyMA) CCTP polymers.

p(GMA) and dodecanethiol went to full conversion, showing a complete disappearance of the NMR-tracked vinyl peaks, figure 2.14 and S2.10, whilst lower yields were however observed with triphenylmethanethiol and 2-naphthalenethiol, plateauing around 65 and 75%.

In order to find an explanation for the divergence in observed yields, a switch from a nucleophilic Michael-thiol addition, with a phosphine, to a base-catalysed one with TEA was attempted. In both systems, the inherent mechanism remains the same, the

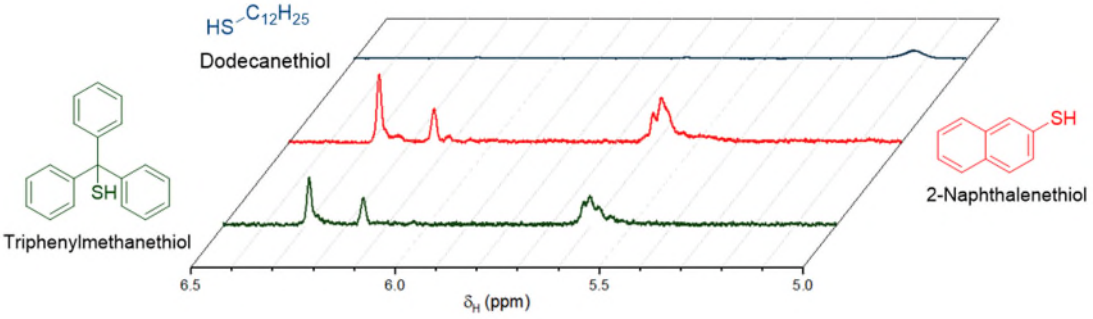


**Figure 2.14** Comparison of vinyl peaks between 5 and 6.5 ppm observed by $^{1}$H-NMR ($CDCl_3$) following Michael-thiol addition after 180 min of, from top to bottom: dodecanethiol, 2-naphthalenethiol and triphenylmethanethiol onto p(GMA) (with conversions of 100%, 75% and 65% respectively).

main difference being the way of generating the initial strong anion intermediates. The result should ultimately be the same. The NMR spectra of the attempts with naphthalenethiol as model reaction, however, showed almost no conversion of vinyl group after 15 hours of reaction at room temperature. Additionally, after 24 hours, there were little sign of epoxides being present within the mixture, figure S2.11. Evidence seemed to suggest that TEA instead played a role in side reactions, potentially between the epoxide side chain and thiol compounds, leading to a thiol-epoxy ring-opened system, as was shown by Gadwal *et al*.[58]

With DMPP, changing the reaction solvent to other common solvents such as DMF, DCM, dioxane or THF either did not lead to sufficient functionalisation of the vinyl groups with naphthalenethiol as a function of time and side-reactions, or reduced NMR vinyl peak visibility in the case of DCM (SI, figure S2.12). It was eventually hypothesised that increased steric hindrance and electronic stabilisation of the intermediates were the probable causes for the low conversions observed of, respectively, triphenylmethyl- and naphthalenethiol.

The reaction of dodecanethiol with p(GMA) reached full conversion within one hour. The reaction was repeated several times in order to test the consistency of the results and did show some inconsistencies with several reactions reaching noticeably lower functionalisation levels of 60 to 75%. DMPP is oxygen sensitive, being prone to oxidation and must be stored under inert gas. This sensitivity, combined with the relatively low quantities used, could play a role in this variation. The issue was avoided by purging the oxygen from all reaction vessels used thereafter.

While useful for the initial experiments, the high boiling point of DMSO made for a difficult product purification procedure. For this reason, other aprotic solvents were considered and acetonitrile, once again, proved to be an ideal candidate. It indeed

provided the opportunity to solubilise all reagents well, but also to run the dual functionalisation of p(GMA) in a one-pot fashion (discussed in part *2.2.3.4*). Reactions in acetonitrile proved as successful with complete disappearance of vinyl bonds, within an hour.

### *2.2.3.2 Further Study of the Michael-Thiol Addition of Hydrophobic Mercaptans to CCTP Macromonomers*

Using the explorative reactions discussed previously, it was decided to set the standard Michael-thiol addition reaction conditions as follows: Michael-thiol additions were to be carried out with DMPP as catalyst, in acetonitrile under an inert atmosphere at

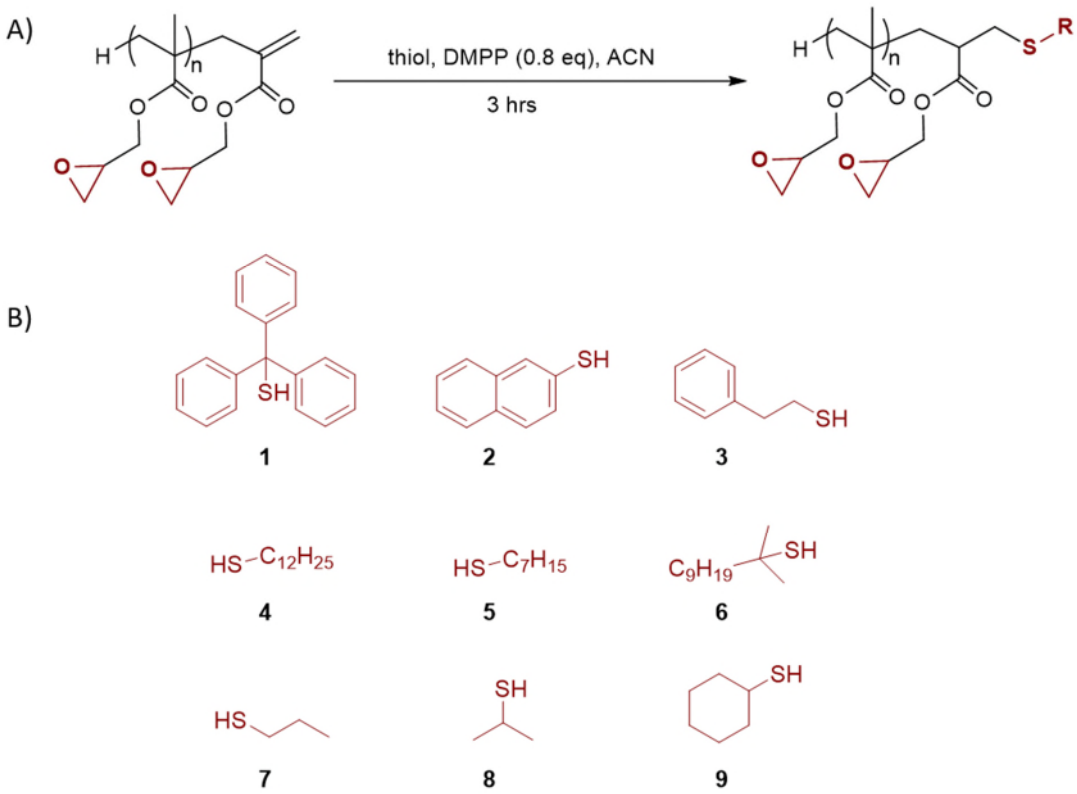


**Scheme 2.6** A) Final conditions for the Michael-thiol addition of hydrophobic mercaptans onto p(GMA) CCTP polymers and B) Commercially available thiols employed in this study: triphenylmethanethiol (**1**), 2-naphthalenethiol (**2**), phenylethylthiol (**3**), dodecanethiol (**4**), heptanethiol (**5**), tert-dodecanethiol (**6**), propanethiol (**7**), 2-propanethiol (**8**) and cyclohexanethiol (**9**).

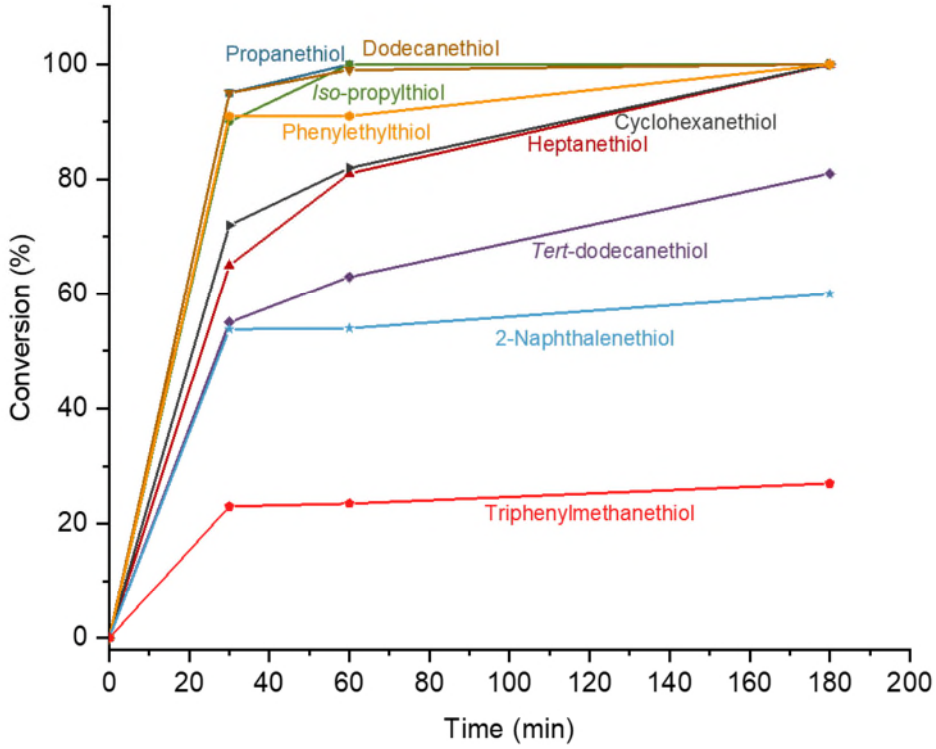


**Figure 2.15** NMR conversion data from vinyl peaks disappearance followed by $^{1}$H-NMR for the Michael-thiol addition of various hydrophobic thiols onto $p(GMA)_{11}$.

ambient temperature, with a 3-hour cut-off window. All reactions in this part were carried out on a 0.10 g scale of macromonomer, with 1.2 equivalents of thiols.

To investigate the reaction further, a screening of commercially available hydrophobic thiols was carried out, scheme 2.6. Most reactions reached yields ≥ 98% within 3 hours, figure 2.15.

Differences in reactivity were observed between iso-propylthiol and propanethiol, as well as between dodecanethiol and tert-dodecanethiol. Although each set comprised of isomers, differences were attributed to stereochemistry, the presence of methyl groups likely slowing down the rate of reaction, but not to the extent that was observed with the phenyl groups from triphenylmethanethiol. This observation was recently corroborated by the group of Christopher Bowman, who noted that increased thiol substitution during Michael-thiol addition led to the enolate being less able to

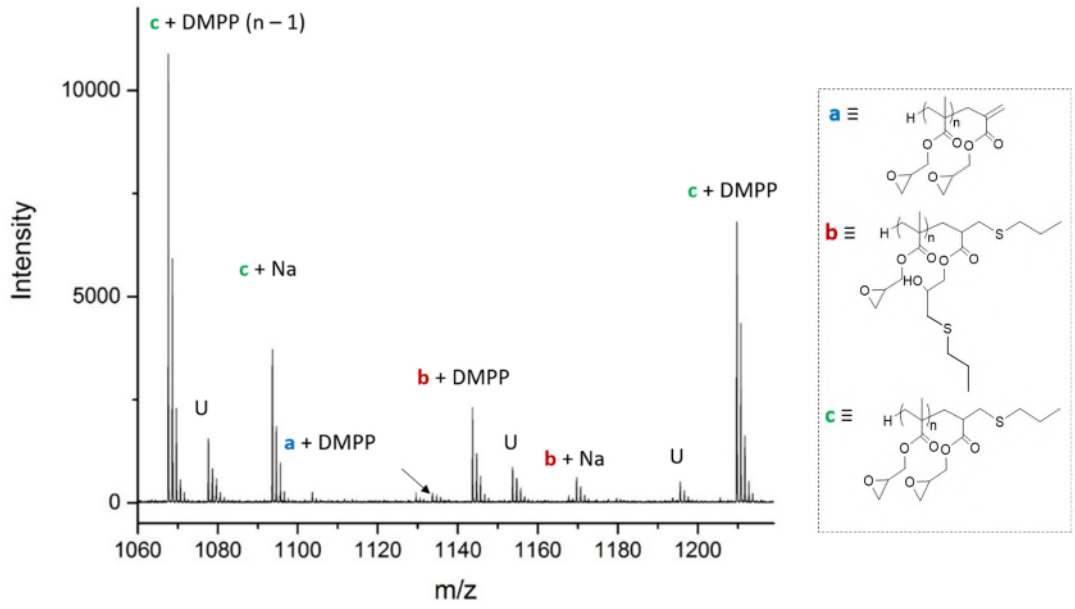


**Figure 2.16** MALDI-ToF spectrum of propanethiol-functionalised $p(GMA)_{11}$. Spectrum measured by Dr James S. Town.

deprotonate thiols, resulting in a decrease in the reaction rates (primary > secondary > tertiary).[59]

If left unpurified, full consumption of the epoxides arising from a range of side-reactions occurred after twelve hours. This is observed by NMR, with the disappearance of the three membered ring's peaks (SI, figure S2.13), which suggests a preferential reactivity of the thiols toward the olefinic bonds. Further MALDI-ToF analysis of the purified polymers showed that side-reactions between epoxide side-chains and thiols were negligible within the time frame of the reaction. For instance, with the propanethiol terminated p(GMA) (figure 2.16), we find a series matching the expected structure adducted with a single sodium (c + Na). This series, however, is not the series which has the highest intensity in the spectra. The main series of peaks suggest that residual DMPP is capable of ionising the sample (c + DMPP). We therefore propose a mechanism of adduction of DMPP onto the carbonyl group, although demonstration of the mechanism was considered beyond the scope of this project. Other minute impurities include evidence of a structure with a single ring-

opened terminal repeat unit epoxide due to thiol activation (b + Na, b + DMPP), and a very small peak related to the unreacted p(GMA) which maintained its unsaturated vinyl end group (a + DMPP). Interestingly, no phosphine-bridged by-products were observed. Frayne *et al.*,[60] whose 2018 paper studied the production of by-products during nucleophilic and base-catalysed Michael-thiol, also made this observations, even at equimolar amounts of phosphine catalyst. The authors stipulated that this could be due to kinetics *and* mechanistic considerations. Firstly, it seems that the thiolate reactions are significantly more rapid than the nucleophile reactions. Secondly, the lack of observable by-products could be due to several reactive pathways they report, whereby the thiolate salt by-product is reacted to yield the thio-bridged product.

### *2.2.3.3 Study of Epoxide Ring-Opening Reaction*

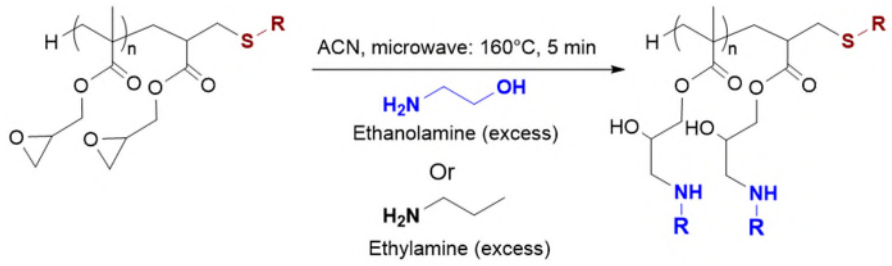


**Scheme 2.7**. General scheme of the epoxide ring-opening reactions investigated in this study.

Sharpless and co-workers defined epoxide ring-opening reactions as the opening of "spring-loaded rings" where protons are shuffled around.[61] This reaction is advantageous in that the opening of the strained cycle is thermodynamically favoured, and a wide array of nucleophilic compounds can be used. p(GMA) polymers are susceptible to both base or acid-catalysed ring-opening reactions to give access to functional polymers. Typically, these reactions are carried out with amines, during quite long reflux reactions, which can potentially last up to 24 hours in order to reach high degrees of functionalisation under inert conditions.[40] Microwave-assisted

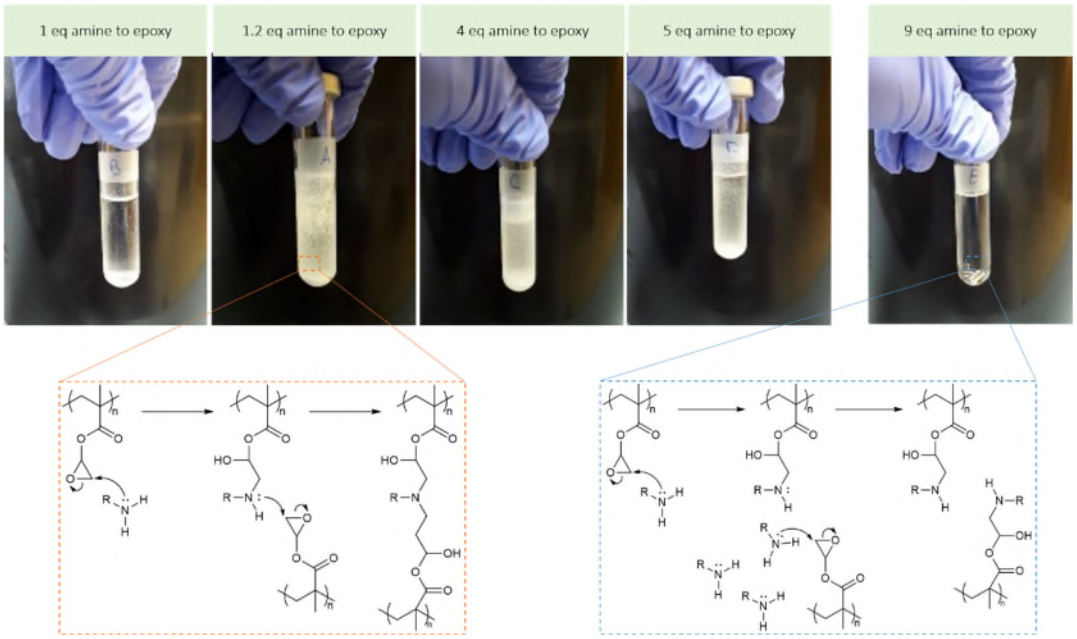


**Figure 2.17** Example of observed cross-linking and ring-opening reactions of p(GMA) with varying ratios of amine to epoxy groups with corresponding reaction pathways.

synthesis offers an elegant and efficient alternative, allowing for both a reduction in reaction times and for reactions to be carried out under aerobic conditions.

The reaction of ethylamine with $p(GMA)_{11}(DDT)$ polymers was studied as a model reaction. This was carried out in view of having no interference from other hydroxyl groups of hydrophilic amines during FT-IR studies (the use of ethanolamine is discussed later on). The microwave reactor was set to apply energy at lower rates to achieve a more controlled temperature increase. 1, 1.2, 3 and 5 equivalents of ethylamine to epoxy group were used separately. All led to the appearance of an insoluble, white solid, likely the result of intermolecular cross-linking. The issue was described by different research groups,[62] and is the result of the secondary amines undergoing another addition reaction to form tertiary amines, figure 2.17. The side-reaction can be prevented by either lowering reaction temperatures or utilising large excesses of amine. Consequently, reactions with 9-fold excess of amine were attempted and showed no visible sign of cross-linking. Ring-opening was observed

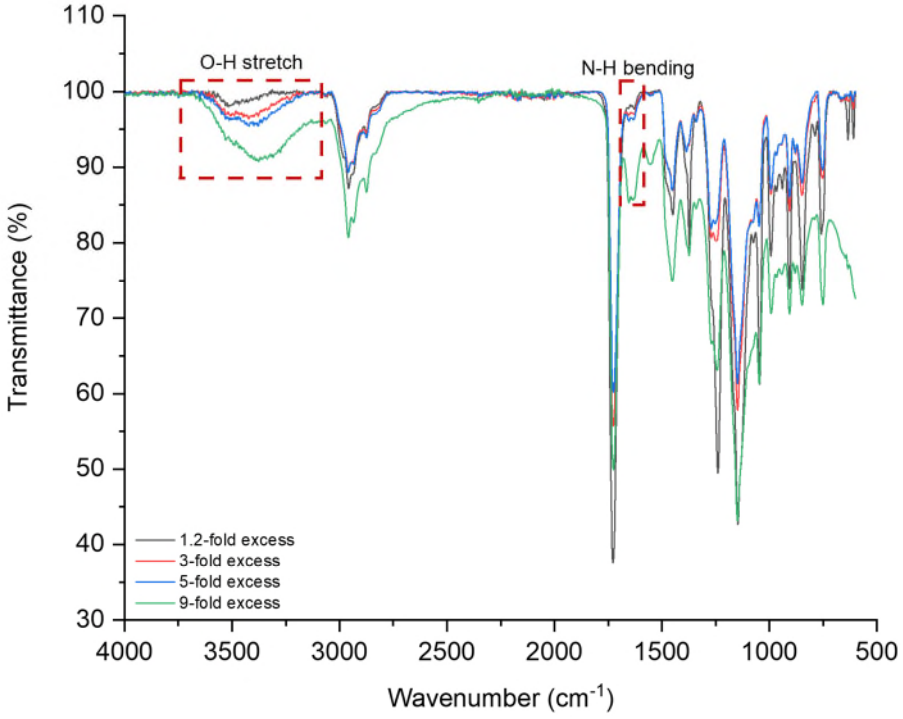


**Figure 2.18** Overlay of FT-IR spectra of $p(GMA)_{11}$ polymers ring-opened with varying quantities of ethylamine.

with the appearance, on the FT-IR spectra, of characteristic –OH and –NH peaks at around 3400 and 1620 $cm^{-1}$ respectively, figure 2.18. When cross-linking occurred, the latter peak remained negligible, albeit visible, due to the conversion of primary amines into tertiary amines, however, with the 9-fold excess both peaks became clearly visible. The success of the reaction can also be verified through the disappearance of the characteristic epoxide peaks at 908, 850 and 755 $cm^{-1}$, figure 2.19. Multiple combinations of temperature and time were explored, but it was found that running the reactions at 160 °C for 5-10 minutes offered the best compromise. The other advantage that was observed with the use of the microwave instruments was the ability to use higher temperatures. Indeed, under normal atmospheric pressure conditions, acetonitrile would be above its 82 °C boiling point. However, as microwave reactions are carried out in sealed environments, they are carried out under higher pressures than 1 atm, in this work approximately at a maximum of 15 bars

(equalling around 14.8 atm). This increases the boiling point of acetonitrile calculated using the following Clausius-Clapeyron relation:

$$ln\left(\frac{P_1}{P_2}\right) = -\frac{\Delta_{vap}H^{\circ}}{R}\left(\frac{1}{T_1} - \frac{1}{T_2}\right) \quad \text{(eqn. 2)}$$

With $P_1$ & $P_2$ the pressures (atm) in states 1 and 2, $\Delta_{vap}H^{\circ}$ the molar enthalpy of vaporization (33.4 kJ.mol$^{-1}$ in the case of acetonitrile[63]), $T_1$ and $T_2$ the boiling points (K) in states 1 and 2 and R the gas constant (J.mol$^{-1}$.K$^{-1}$). This equation rearranges to isolate $T_2$ to:

$$\frac{1}{T_2} = \frac{1}{T_1} - Rln\left(\frac{P_1}{P_2}\right).\frac{1}{-\Delta_{vap}H^{\circ}} \quad \text{(eqn. 3)}$$

Which indicates that the boiling of acetonitrile is approximately increased to 228 °C at 14.8 atm.

### *2.2.3.4 One-Pot Dual Functionalisation and analysis of the MKI range*

Subsequent to this study, a one-pot dual functionalisation of the p(GMA) polymers was attempted. This range of polymers being the first to be synthesised, the resulting amphiphilic polymethacrylates were classified in the MKI range. This nomenclature will be used in subsequent chapters. Four thiols were selected: one aromatic (phenylethylthiol; PET), one containing an aliphatic ring (cyclohexanethiol; CHT), as well as both a long and a short acyclic thiol (dodecanethiol, DDT and iso-propylthiol, i-PT). A library of twelve different polymers was subsequently produced using the developed procedures.

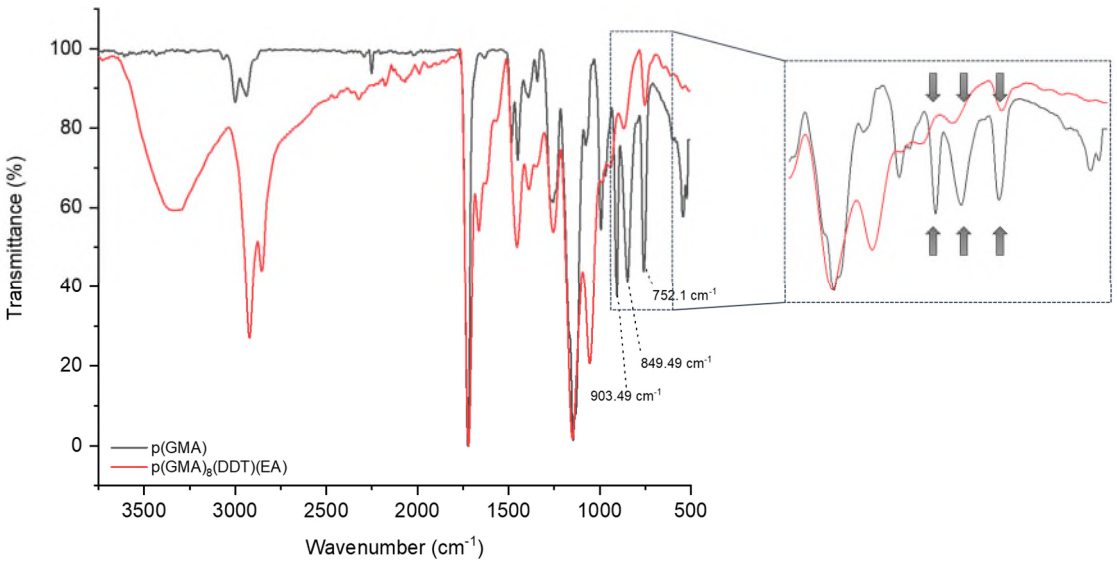


**Figure 2.19** Overlay of FT-IR spectra of unfunctionalised p(GMA), and polymers ring-opened with ethylamine, with a zoom between 1400 and 500 cm-1 showing the disappearance of the three characteristic epoxide peaks.

All experiments were carried out in a similar fashion as previously described in a sequential manner as a one-pot reaction with each thiol first reacted with p(GMA) polymers from batches **1**, **2** and **3**, and then ring-opened with ethanolamine. Reactions were conducted on larger, 5 g scales of macromonomer. Due to the larger scale, and a reduced headspace in the microwave vials, reactions in the microwave had to be heated to 120 °C for 30 minutes to avoid uncontrolled increase in internal pressure. However,

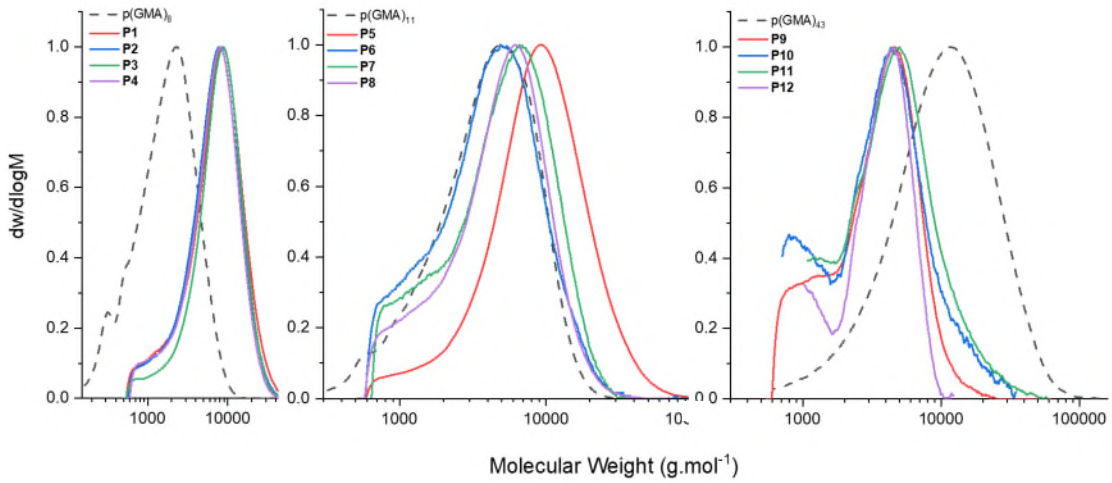


**Figure 2.20** GPC (DMF, 50 °C) comparison of polymers before and after functionalisation of **P1-P4**, **P5-P8** and **P9** to **P11**.

| Entry | Polymer | Thiol | MT-Add conversion / % | $M_{n,GPC}$ / g.mol$^{-1}$ | $Đ$ | Average size / d.nm[a] | Pdi (±)[a] |
|---|---|---|---|---|---|---|---|
| P1 | p(GMA)$_7$(DDT)(ETA) | HS—C$_{12}$H$_{25}$ | ≥99 | 4650 | 2.87 | 7.48 | 0.54 (0.14) |
| P2 | p(GMA)$_7$(CHT)(ETA) |  | ≥99 | 4540 | 1.83 | 121.65 | 0.30 (0.14) |
| P3 | p(GMA)$_7$(PET)(ETA) |  | 97 | 5260 | 1.72 | 119.43 | 0.41 (0.34) |
| P4 | p(GMA)$_7$(i-PT)(ETA) |  | ≥97 | 4510 | 1.80 | 101.42 | 0.35 (0.03) |
| P5 | p(GMA)$_{11}$(DDT)(ETA) | HS—C$_{12}$H$_{25}$ | ≥97 | 5850 | 2.00 | 8.60 | 0.26 (0.14) |
| P6 | p(GMA)$_{11}$(CHT)(ETA) |  | ≥97 | 2800 | 1.91 | 118.15 | 0.66 (0.06) |
| P7 | p(GMA)$_{11}$(PET)(ETA) |  | ≥97 | 3250 | 1.93 | 15.27 | 0.29 (0.01) |
| P8 | p(GMA)$_{11}$(i-PT)(ETA) |  | ≥97 | 3200 | 1.85 | 13.53 | 0.74 (0.14) |
| P9 | p(GMA)$_{43}$(DDT)(ETA) | HS—C$_{12}$H$_{25}$ | 96.1 | 2420 | 1.67 | 41.01 | 0.75 (0.21) |
| P10 | p(GMA)$_{43}$(CHT)(ETA) |  | 95.5 | 2560 | 1.97 | 11.36 | 0.51 (0.03) |
| P11 | p(GMA)$_{43}$(PET)(ETA) |  | 96.8 | 3530 | 1.73 | 6.16 | 0.80 (0.12) |
| P12 | p(GMA)$_{43}$(i-PT)(ETA) |  | 98.2 | 3000 | 1.35 | 9.66 | 0.51 (0.13) |

**Table 2.3** Amphiphilic polymers synthesised by post-polymerisation dual functionalisation. DDT = dodecanethiol, CHT = cyclohexanethiol, PET = phenylethylthiol, i-PT = iso-propylthiol, ETA = ethanolamine. [a]Determined by DLS.

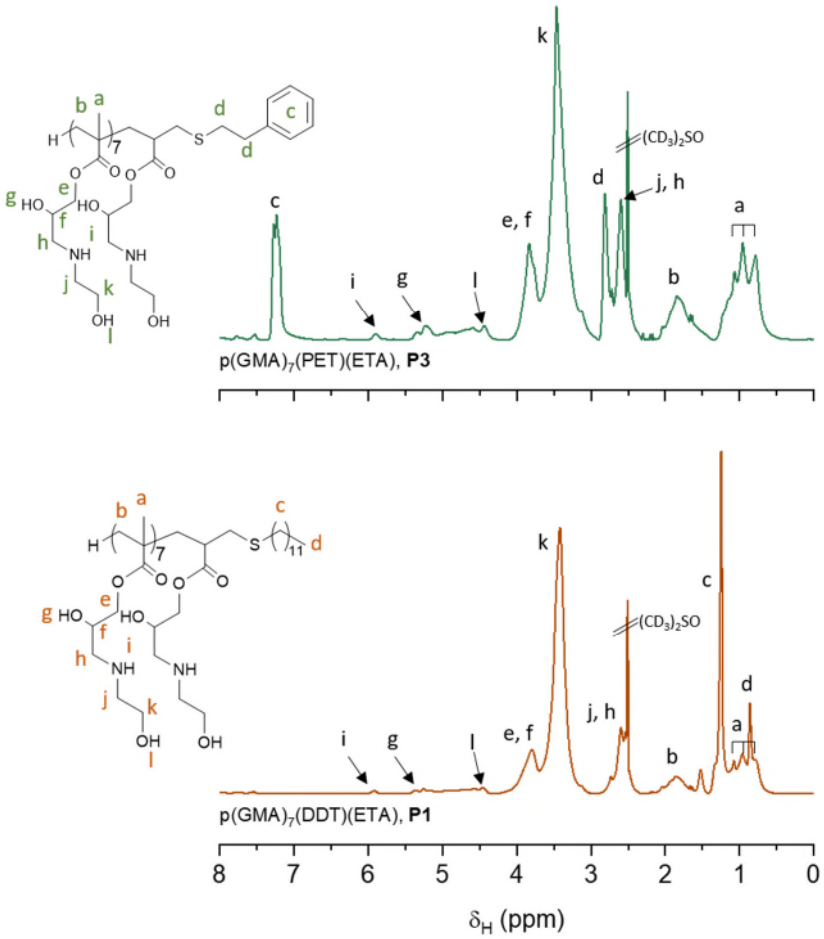


**Figure 2.21** Comparison of $^{1}$H-NMR (DMSO-$d_6$, 400 MHz at 25 °C)) of **P3** (top, green trace) and **P1** (bottom, brown trace).

both Michael-thiol addition and epoxide ring-opening produced polymers with high levels of thiol and amine functionalisation (table 2.3).

Functionalisation was first seen by GPC. The polymers were modified into a theoretically bigger structure, and the repeating unit modified into a hydrophilic one. We therefore expect a positive shift in molecular weight, but this is observed less and less as the molecular weight of the hydrophilic segment increases. One can suspect stationary phase interaction that increases with DP. It also seems that DMF, because the functionalised polymers can be eluted after the unfunctionalised polymer (with DP = 43 polymers), is not necessarily a good solvent for these amphiphilic polymers. It

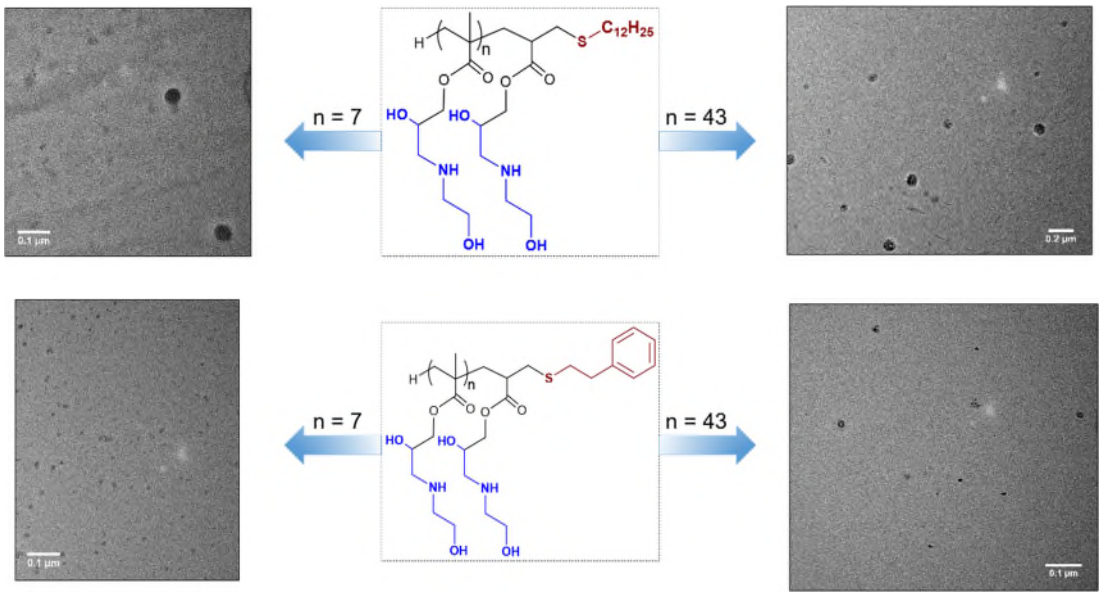


**Figure 2.22** TEM images of **P1**, **P3**, **P9** and **P11** (respectively: top left, bottom left, top right and bottom right) showing self-assembly onto carbon coated TEM copper grid. Images taken by Georgios Patias.

is, however, the only one that is available as both THF and chloroform lead to the precipitation of the polymers.

Figure 2.21 shows a comparison of the $^{1}$H-NMR spectra of **P1** and **P3**, both showing an absence of peaks corresponding to the vinyl peaks or cyclic epoxide functionalities, and confirming high levels of functionalisation. Hydroxyl and amine groups were, in both cases, visible at around 4.5 to 5.25 and 5.90 ppm, respectively. Further indications of ring opening were noticed from the merging of the $OCH_2$ peaks (e) and shift from 3.25 ppm to 4 ppm, overlapping with the methylene peak (d) from the opened epoxide. Moreover, differences were also observed from the different thiols used. For instance, **P1** showed dodecane methylene peaks at 1.25 ppm and methyl peak at 0.85 ppm; whilst **P3**, after reaction with phenylethylthiol, showed aromatic peaks at 7.30 ppm. Peaks from the hydrophobic segments also disappeared when ran in $D_2O$, a first indication of the self-assembly potential of the synthesised macromolecules and is discussed later.

This self-assembly was subsequently investigated using dynamic light scattering (DLS) and transmission electron microscopy (TEM). The dispersants were observed by TEM, all almost exclusively self-assembled into disperse micelles with sizes ranging from 10 to 30 nm in diameter, figure 2.22 and table 2.3. The type of clicked thiol and the size of the polymer did not seem to bear any significant influence on the observed morphologies.

From the DLS data in table 2.3, we see that **P1**, **P5** and **P9**, which were functionalised with dodecanethiol, showed an expected increase in size with increasing hydrophilic block size. The opposite trend is however observed for all other polymers sequences. The behaviour of amphiphilic polymers is expected to be intrinsically different when analysed under different conditions (in solution for DLS, and dried for TEM). PDis are within normal range for most analysed polymers, but the high average sizes of the self-assembled structures implies that some polymers could aggregate into undiscernible structures. We hypothesise that this could potentially be due to the nature of the clicked thiol, such as *iso*-propyl thiol, too small to drive self-assembly when the hydrophilic segment also has a degree of polymerisation $\leq 7$. In such case, DLS data can be considered unreliable.

As the hydrophobic block increases in size, the polymers progressively become more able to self-assemble into discernible structures. There therefore seems to be a threshold of size the hydrophobic block must reach to successfully drive self-assembly. Polymers containing longer dodecane chains behave and can be assimilated to di-block copolymers with polyethylene hydrophobic segments of degree of polymerisation $i = 12$ (or C12), with a self-assembly threshold that could lie around $i$

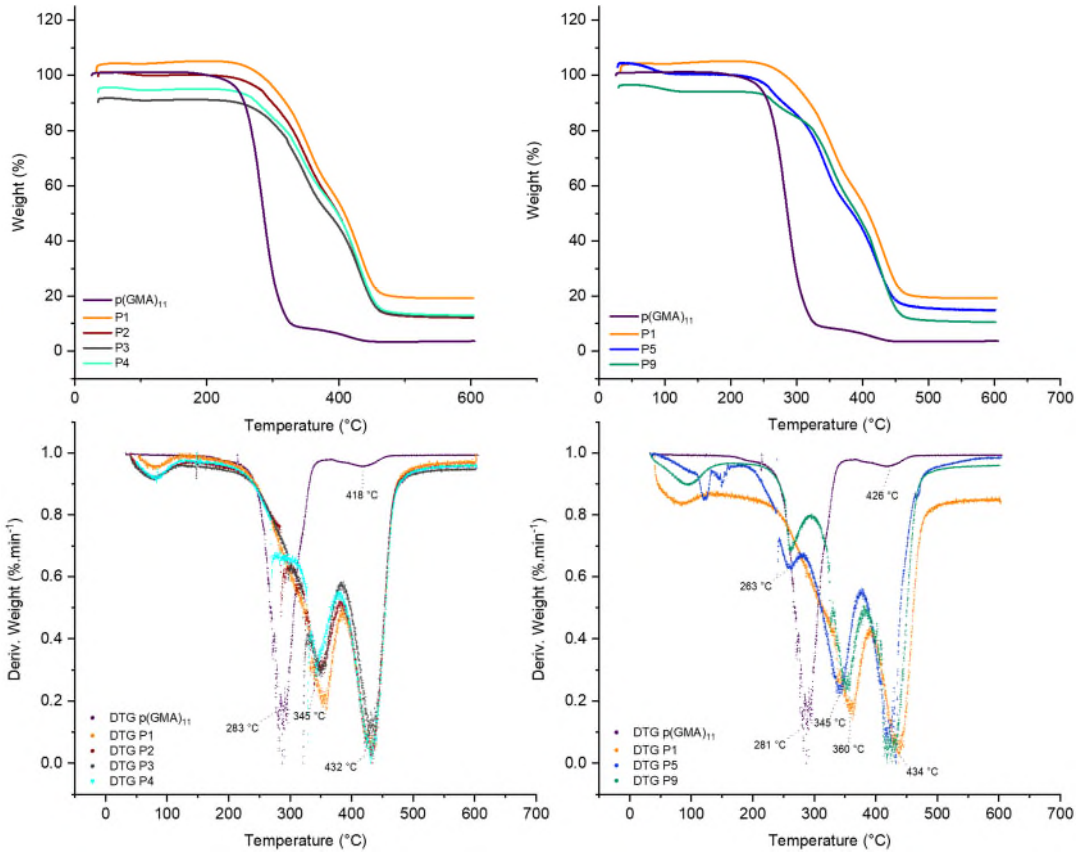


**Figure 2.23** Thermogravimetric (top row) and differential thermogravimetric (bottom row) data of similar hydrophilic block (**P1** to **P4**, left column) and similar hydrophobic block amphiphiles (**P1**, **P5** and **P9**, right column).

= 9-12 but more experiments are required to confirm this theory (discussed in part 2.2.4.1).

The behaviour of the polymers during thermal degradation was investigated using thermogravimetric analysis, figure 2.23. For all polymers, the TGA curves show a gradual degradation with an onset at around 250 °C, amounting to 10% remaining mass at 460 °C. Generally, the degradation of FRP-made polymethacrylates shows 3 characteristic steps. The first occurs at around 165 °C and is not always seen as it stems from the head-to-linkages (HH) breakage of polymers terminated by combination. Because of the presence of chain-transfer agents, this step not expected with CCT polymers. The second is the result of unsaturated chain ends-initiated degradation and is generally visible, as is the case here for $p(GMA)_n$, at around 280 °C. Finally the last

step is often observed > 400 °C and corresponds to random back-bone chain scission.[64–67]

Polymers **P1** to **P12** have a functionalised chain-end and do not contain HH linkages. As such, we should only expect the final step to occur. However, the DTGA curves reveal two clearly defined inflection points at around 345-360 and 435 °C. The second inflection is scarcely influenced by the type of thiol clicked or the molecular weight of the polymer, confirming that it is the random scission step. The first inflection point instead, seems to be more affected by these factors. We hypothesise the polymers undergo a retro-Michael reaction that yields both the thiol and the vinyl-terminated polymer that can subsequently undergo vinyl end-initiated degradation. The shifted inflection point then reflects the temperature at which retro-Michael reactions occur. This theory is also supported by the fact that, in some cases, a third peak is visible when polymers were not fully functionalised during Michael-thiol addition (95-98% conversion), with unreacted polymers able to undergo 2$^{nd}$ step degradation around the expected temperature (*note*: the term 2$^{nd}$ step is used in the broader sense of polymethacrylates degradation, even though HH linkages degradation is not observable). Interestingly, when analysing the degradation of the unfunctionalised polymer, we see that the vast majority of the product is degraded by vinyl-chain ends initiated degradation. This could be due to the shifted 2$^{nd}$ step degradation which can offer a “buffer”, suggesting the polymers are not entirely degraded by the time the instrument reaches the 3$^{rd}$ step temperature.

## 2.2.4 Post-Polymerisation of p(GlyMA), Preparation of the MKII Range

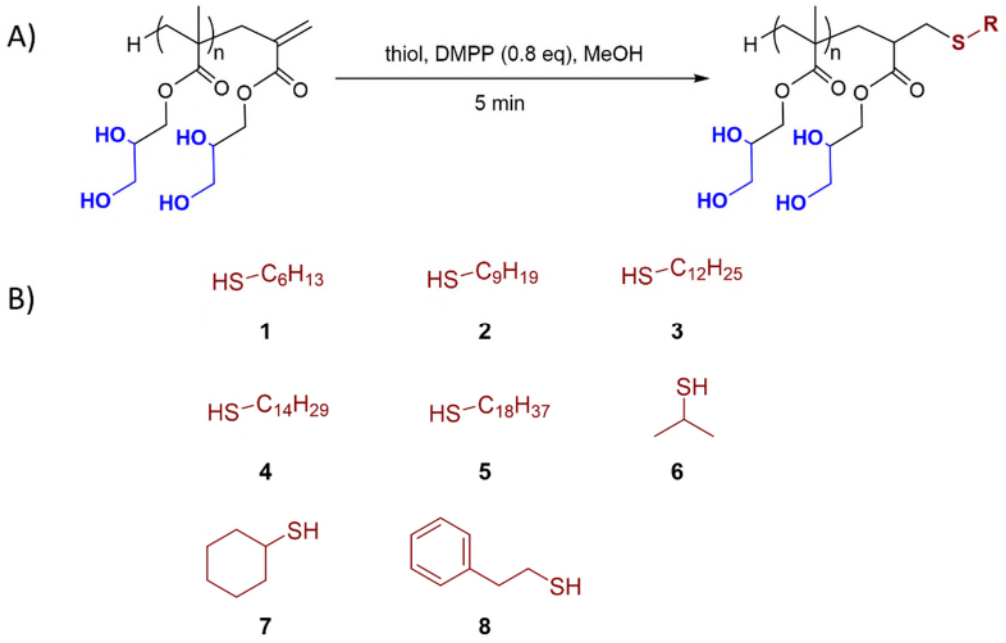


**Scheme 2.8** A) conditions for the Michael-thiol addition of hydrophobic mercaptans onto p(GlyMA) CCTP polymers and B) Commercially available thiols employed in this study: hexanethiol (1), nonanethiol (2), dodecanethiol (3), tetradecanethiol (4), octadecanethiol (5), 2-propanethiol (6), cyclohexanethiol (7) and phenylethylthiol (8).

| Entry | Polymer | Thiol | MT-Add conversion / % | $M_{n,GPC}$ / g.mol$^{-1}$ | $Đ$ | Average size / d.nm[a] | PDi (±)[a] | α[b] |
|---|---|---|---|---|---|---|---|---|
| Q1 | p(GlyMA)$_8$(PET) | 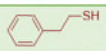 | >99 | 5140 | 1.60 | 167 | 0.71 (0.07) | 0.38 |
| Q2 | p(GlyMA)$_8$(CHT) |  | >99 | 5020 | 1.47 | 181 | 0.45 (0.04) | 0.34 |
| Q3 | p(GlyMA)$_8$(i-PT) |  | >99 | 6180 | 1 .48 | 106 | 0.36 (0.03) | 0.49 |
| Q4 | p(GlyMA)$_8$(HT) |  | >99 | 5560 | 1.34 | 79 | 0.51 (0.06) | 0.35 |
| Q5 | p(GlyMA)$_8$(NT) |  | >99 | 5720 | 1.35 | 188 | 0.61 (0.06) | 0.26 |
| Q6 | p(GlyMA)$_8$(DDT) |  | >99 | 5530 | 1.56 | 4.3 | 0.72 (0.13) | 0.29 |
| Q7 | p(GlyMA)$_8$(TDT) |  | >99 | 7650 | 1.32 | 5.7 | 0.78 (0.23) | 0.56 |
| Q8 | p(GlyMA)$_8$(ODT) |  | >99 | 2300 | 2.10 | 12 | 0.38 (0.04) | 0.21 |

**Table 2.4** Amphiphilic polymers synthesised by post-polymerisation single functionalisation. PET =phenylethylthiol, CHT = cyclohexanethiol, i-PT = iso-propylthiol, HT = hexanethiol, NT = nonanethiol, DDT = dodecanethiol, TDT = tetradecanethiol, ODT = octadecanethiol. [a]Determined by DLS in water, [b]determined by GPC in DMF.

The reactions reported here were carried out as previously reported in part *2.2.3.4*.

5 g sections from the 1.4 kDa p(GlyMA) batch were systematically dissolved in methanol in the presence of 0.8 equivalents of dimethylphenylphosphine (DMPP) catalyst and 1.02 equivalents of thiol. (The reason why other p(GlyMA) batches were not used is discussed in section 4.2.2.).

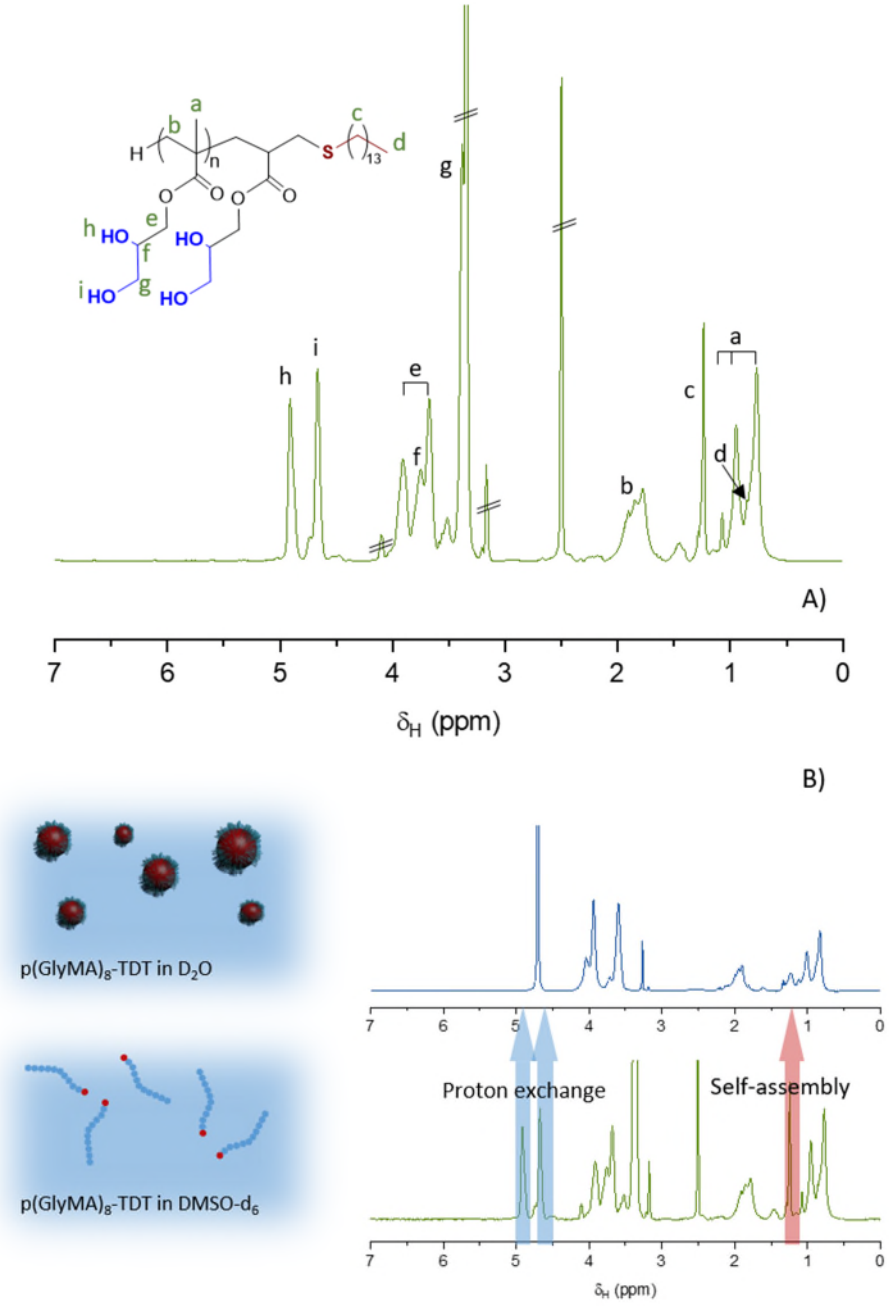


**Figure 2.24** A) $^{1}$H-NMR (DMSO-$d_6$, 400 MHz at 25 °C) of p(GlyMA)$_8$(TDT). B) $^{1}$H-NMR spectra of p(GlyMA)(TDT) in DMSO-$d_6$ (bottom) and $D_2O$ (top) with loss of peaks to proton exchange and self-assembly.

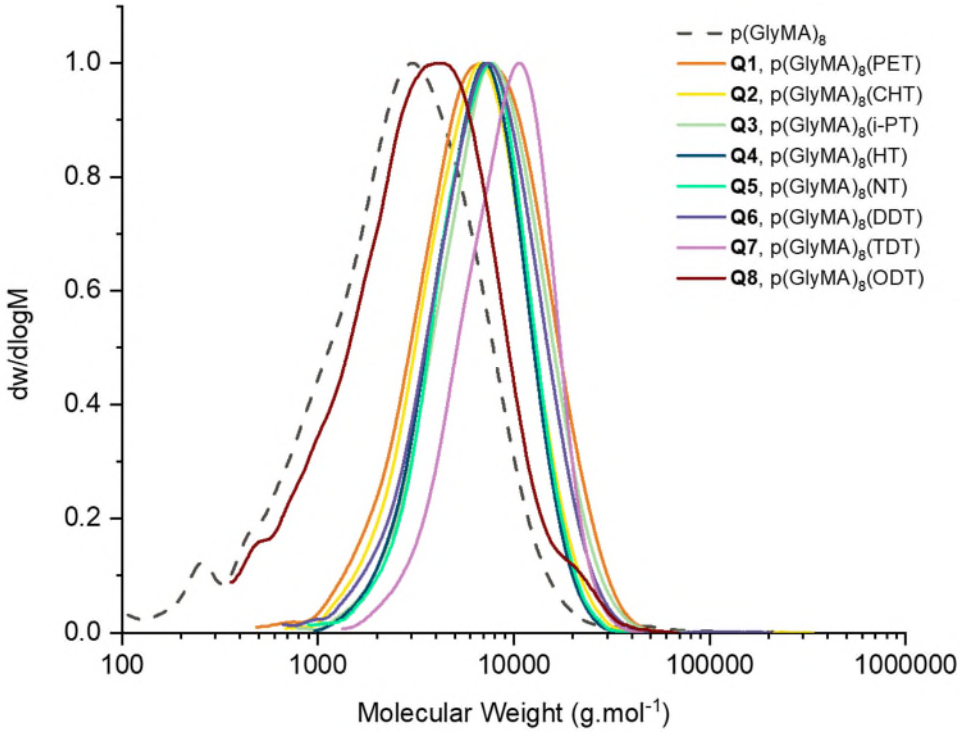


**Figure 2.25** GPC (DMF, 50 °C) comparison of polymers before and after functionalisation of **Q1** through to **Q8**.

Due to the efficiency of amphiphilic polymers containing linear aliphatic thiols anchors as pigment dispersant (discussed later), eight hydrophobic thiols were used, most of which were aliphatic, scheme 2.8. This was also performed as a way to investigate the optimum hydrophobic number of carbons to hydrophilic block degree of polymerisation. Octadecanethiol (ODT) is a solid at room temperature. Reactions with ODT were therefore carried out at 40 °C, above the melting point of the compound, so that it could be dispersed in MeOH.

Similarly to ODT, tetradecanethiol, while liquid at room temperature, was immiscible with methanol, and had to be dispersed. It is likely, that all hydrophobic thiols containing alkyl chains where the number of carbons is equal or higher than 15 would be immiscible in methanol.

For both of these compounds, fast stirring was necessary to increase the surface area of the insoluble thiol droplets. All reactions reached full conversion within five

minutes. This was a significant difference in comparison to the previous results where the reactions of hydrophobic thiols with p(GMA) would take from 1 to 3 hours to reach similar conversions. Li *et al*.[68] demonstrated that solvents exercise a very strong effect on Michael-thiol additions. In their paper, they state polar solvents as being more capable of stabilising the thiolate intermediate, thus making its formation more likely. Methanol is more polar than acetonitrile, something that could partly explain the differences in reaction time. Another reason could be the fact that the side chains of p(GlyMA) are more electron-withdrawing than the epoxides of p(GMA), which would also increase reaction rates.

Most functionalised polymers were purified by dialysis against methanol for 50 hours. Solvent was removed *in-vacuo* and the polymers dried. $P(GlyMA)_8(ODT)$ was purified by cooling down the reaction vessel with an ice bath and removing the solid thiol using Buchner filtration. Post-purification $^1$H-NMR showed that the functionalised polymers contained little to no vinyl bonds.

Furthermore, peaks from the clicked thiols were observed. A simple change of deuterated solvent from DMSO-$d_6$, where both blocks are soluble, to $D_2O$, where only the p(GlyMA) block is soluble provided a first proof of the success of the reaction, as exemplified with $p(GlyMA)_8(DDT)$, figure 2.24.

Figure 2.25 shows the GPC traces of all functionalised polymers with relation to the unreacted polymer. In all cases, noticeable shifts in molecular weights are observed. However, we can also see a difference in the behaviour of **Q8** whose shift is much less pronounced. GPC separates polymers not based on size but on the hydrodynamic volume of these polymers in the eluent. A look at the α values in table 2.4 reveals that, in DMF, p(GlyMA)$_8$(ODT) behaves more like a compact sphere, much more so than any other polymers. This could partly explain why it elutes quicker than other polymers and why there is a less clear shift on the chromatogram. A solution to

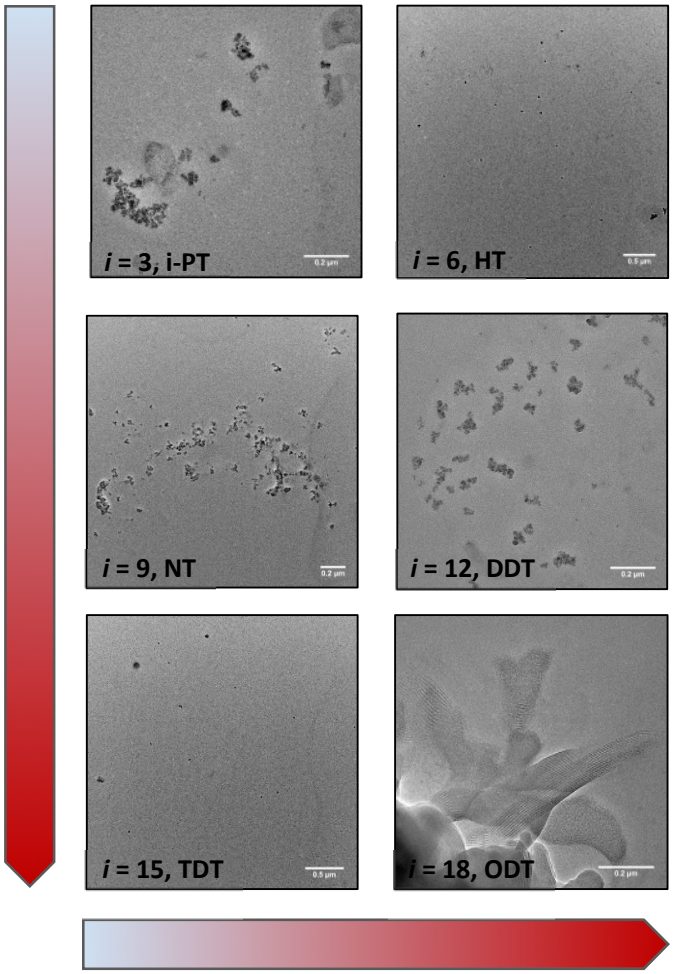


**Figure 2.26** TEM images of the MKII range amphiphilic polymethacrylates prepared using aliphatic and linear hydrophobic thiols. The number of carbons in the aliphatic chains is to increase from left to right, as well as top to bottom. Images taken by Georgios Patias

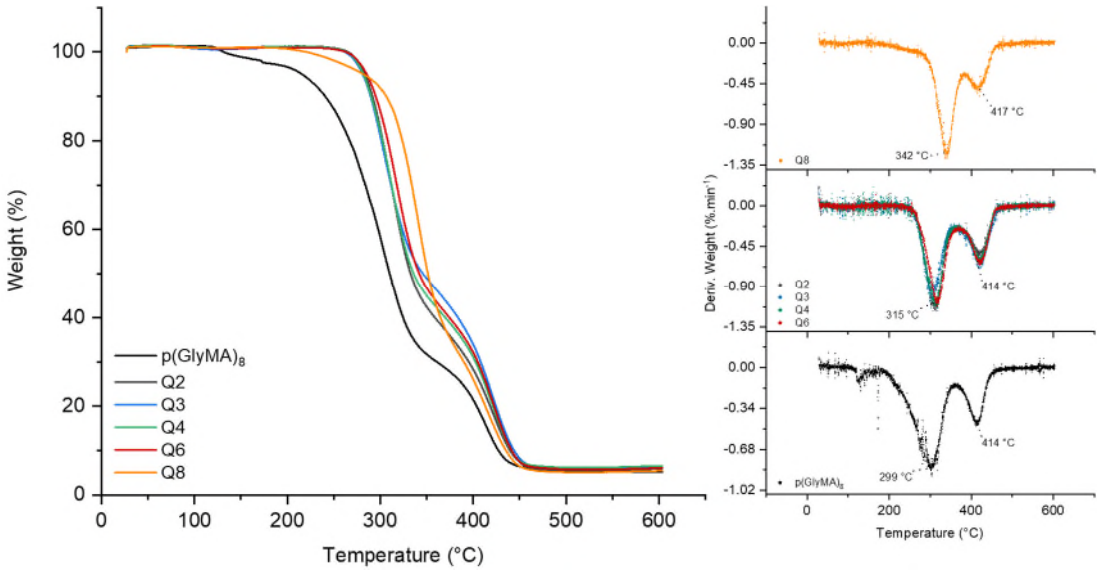


**Figure 2.27** Thermogravimetric (left) and differential thermogravimetric (right) data of p(GlyMA)$_8$ and representatives of the MKII dispersants category.

circumvent this would be to run the GPCs in another solvent, however these polymers were found to be only soluble in DMF. Notwithstanding, all polymers from the MKII range were found to self-assemble properly during TEM analysis, figure 2.26.

An interesting observation is that the trend that was observed previously with p(GMA) regarding the size threshold of the hydrophobic block can here be confirmed. Indeed, for the MKII range we have an identical hydrophilic block, but a varying hydrophobic aliphatic block with $i$ = 6, 9, 12, 15 and 18. We can also confirm that the requirement for distinct self-assembly is $i \geq 9$.

On the thermal degradation of the MKII range polymers, the same observations as were seen with the MKI range can be made here:

- 2 inflection points corresponding to vinyl-end initiated (300 to 342 °C) degradation and random chain scission (415 °C)
- Retro-Michael reaction occurs and fully reverse the Michael-thiol addition.
- The random-scission step is not influenced by the type of clicked thiol.

Linear aliphatic groups **Q2**/**3**/**4**/**6** chain do not seem to have an effect on the 2$^{nd}$ step's inflection point. **Q8**, which has an octadecane group, does show a significant increase in 2$^{nd}$ step temperature at 340 °C (instead of 315 °C for smaller aliphatic groups).

## 2.3 Conclusions

In the past, catalytic chain transfer polymerisation in combination with click chemistry has been used to developed functional polymers, but its application to the synthesis of amphiphilic polymers has, to our knowledge, been investigated.[40,69–71] We therefore set out to prepare different ranges of amphiphilic polymers using a scalable combination of catalytic chain transfer polymerisation and post-polymerisation modifications.

The synthesis of hydrophobic and hydrophilic polymers, respectively p(glycidyl methacrylate) and poly(glycerol monomethacrylate) was first investigated. The influence of the catalyst loading was evaluated and generally, we observed that ppm amounts of catalyst were required to significantly reduce the molecular weights of polymers (to 1.5-5 kDa) and that increasing concentrations of catalyst led to smaller polymers. Next, terminal vinyl bonds were reacted with a range of commercially available hydrophobic thiols through Michael-thiol addition and, in the case of p(GMA), was followed by a microwave-assisted epoxide ring opening step, in a one-pot fashion in the presence of ethanolamine. A library of 20 amphiphilic polymethacrylates was prepared, classified into MKI (synthesised from p(GMA)) and MKII (synthesised from p(GlyMA)) ranges. The structural, thermal and self-assembly behaviour of these polymers were then investigated using multiple techniques, namely NMR, DLS, GPC, TEM, TGA or MALDI-ToF.

# 2.4 Experimental

## 2.4.1 Additional Figures and Schemes

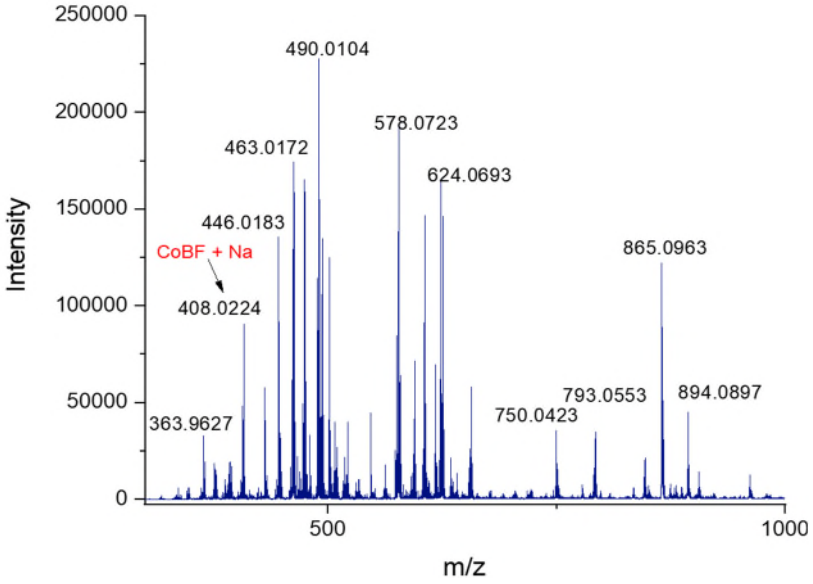


**Figure S2.1** ESI mass spectrum of a 16 year old CoBF catalyst sample.

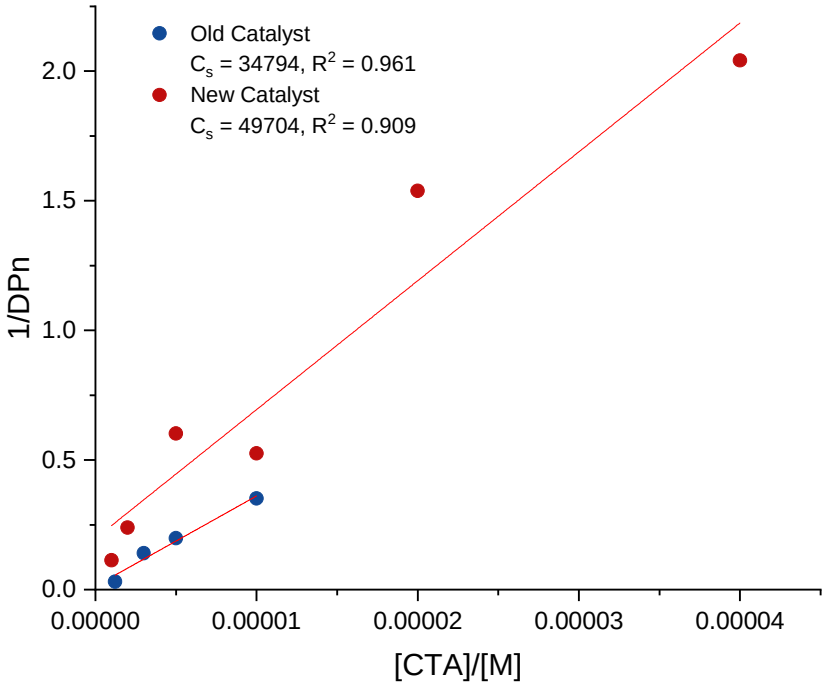


**Figure S2.2** Mayo plot for the measurement of the $C_s$ of CoBF with MMA/toluene with comparison between a newly prepared, and a 16-year-old batch. Old catalyst measurements carried out by Dr Ataulla Shegiwal.

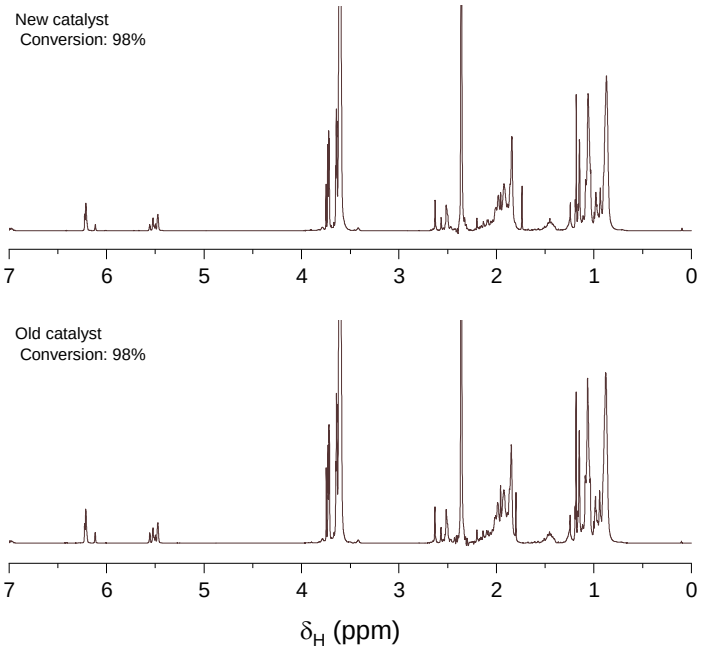


**Figure S2.3** $^{1}$H-NMR ($CDCl_3$, 300 MHz at 25ºC) spectra of two 5 ppm CCTP polymerisation reactions of MMA in toluene using either the new batch of CoBF, or the 16 year old batch.

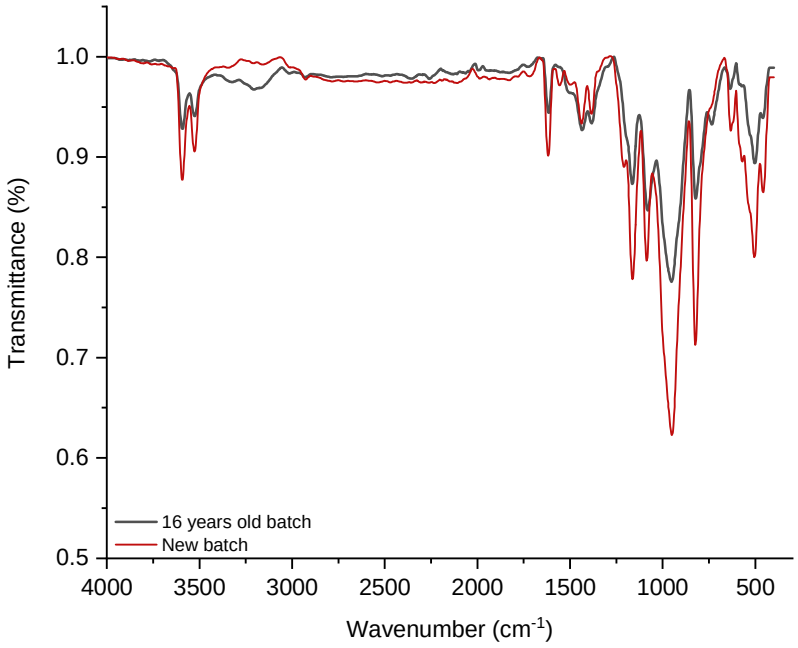


**Figure S2.4** FT-IR spectra of both the new batch of CoBF and the 16 year old batch.

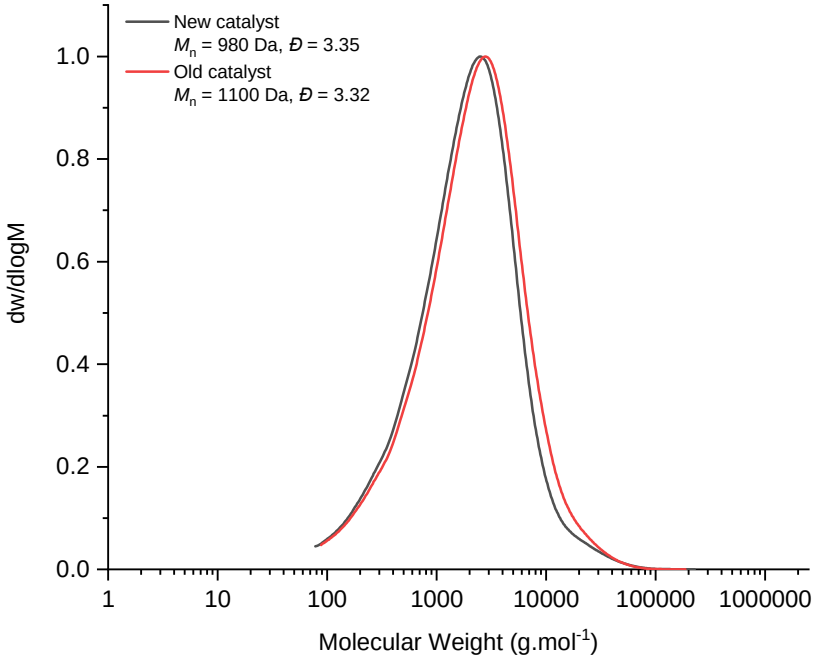


**Figure S2.5** GPC (DMF, 50 °C) spectra of two 5 ppm CCTP polymerisation reactions of MMA in toluene using either the new batch of CoBF, or the 16 year old batch.

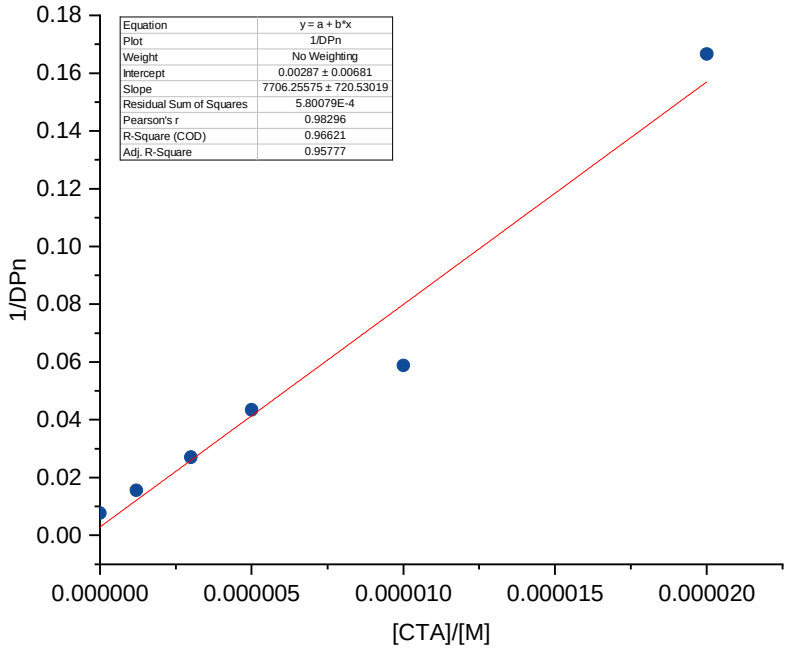


**Figure S2.6** Mayo plot for the measurement of the $C_s$ of CoBF with GMA and acetonitrile.

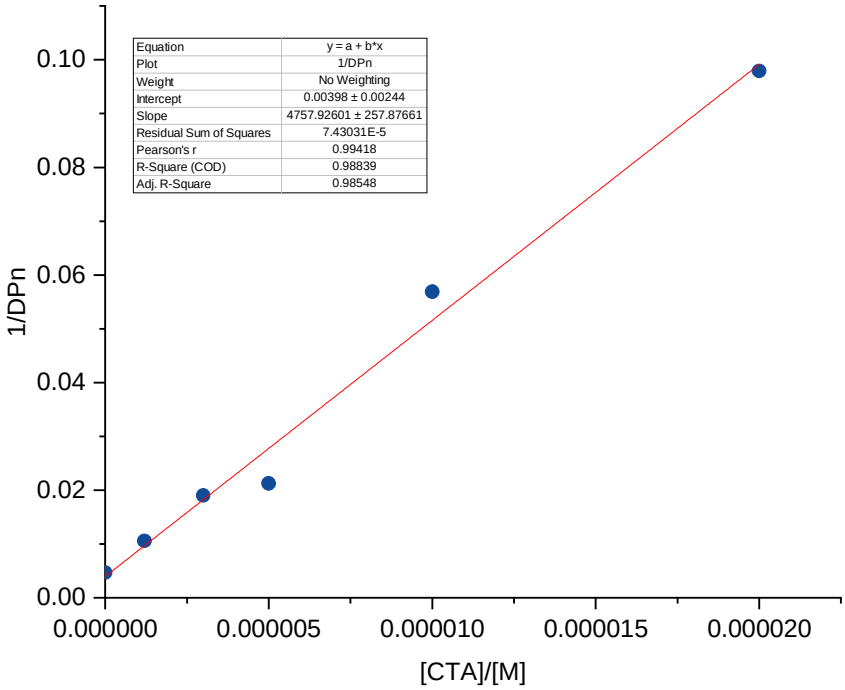


**Figure S2.7** Mayo plot for the measurement of the $C_s$ of CoBF with GMA and ethyl acetate.

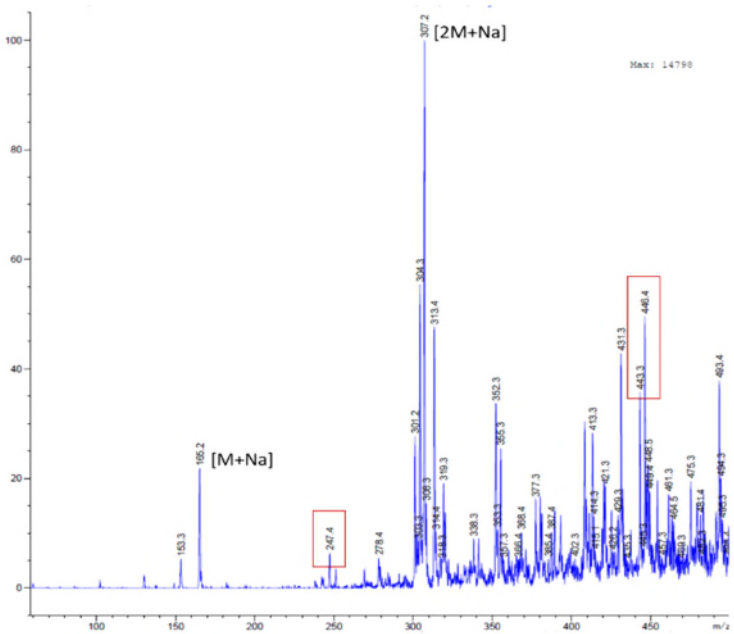


**Figure S2.8** ESI-MS spectrum of glycidyl methacrylate.

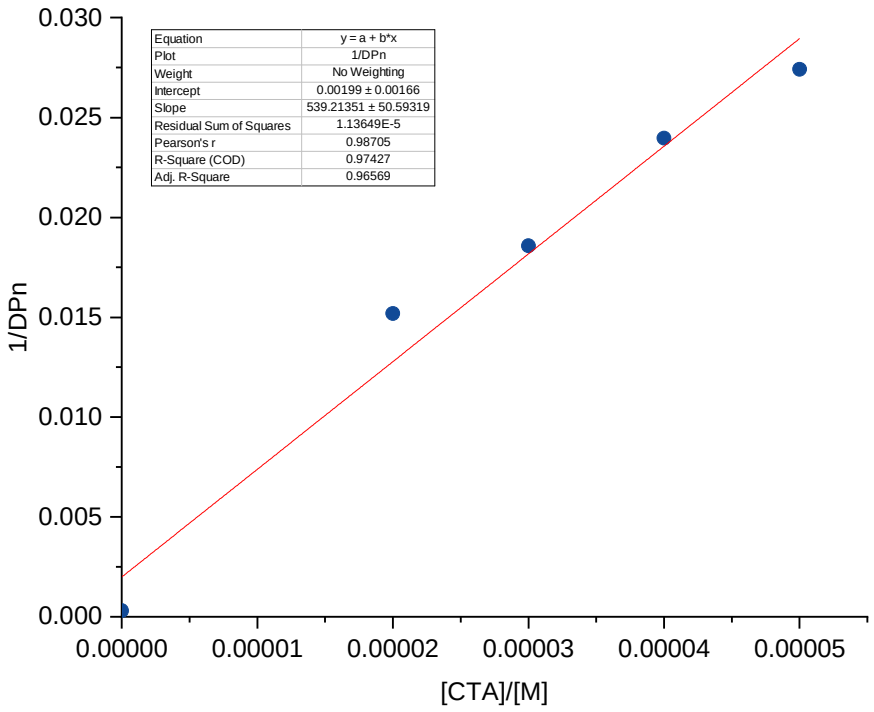


**Figure S2.9** Mayo plot for the measurement of the $C_s$ value of CoBF in GlyMA and methanol.

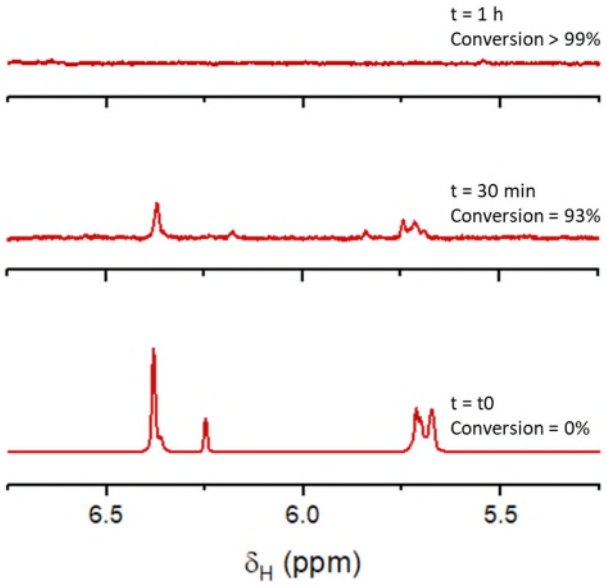


**Figure S2.10** Vinyl bond signals evolution after 30 and 60 min of the reaction between p(GMA) and dodecanethiol in DMSO-$d_6$.

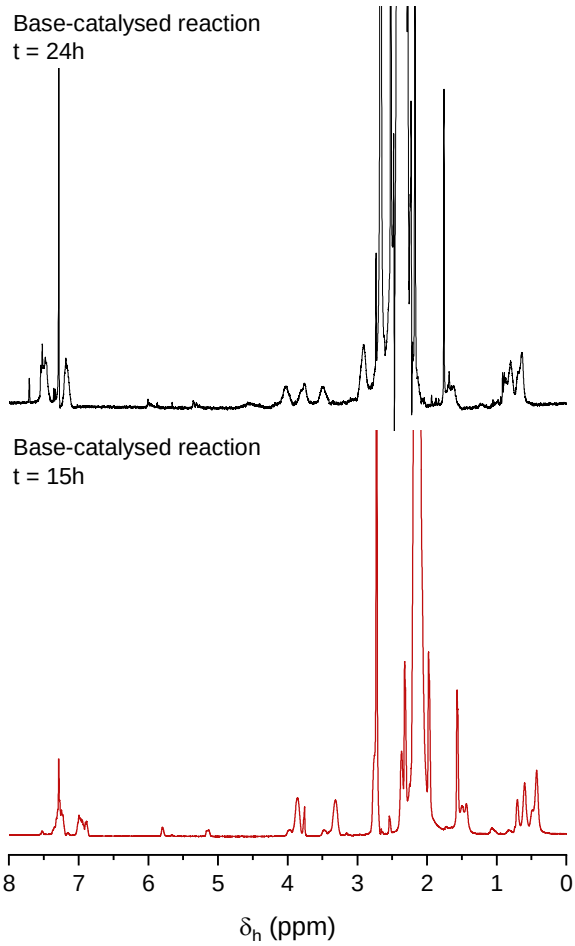


**Figure S2.11** TEA-catalysed Michael-thiol addition of dodecanethiol onto p(GMA).

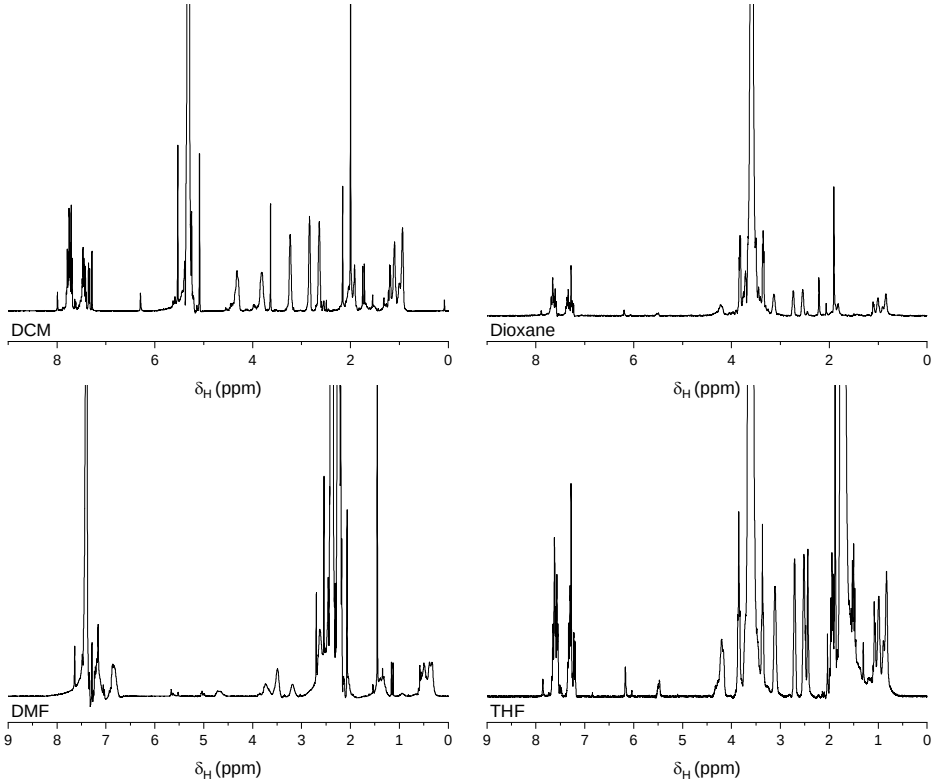


**Figure S2.12** $^{1}$H-NMR spectra ($CDCl_3$, 300 MHz at 25 ºC) of naphthalenethiol reacted with p(GMA) after 3 hours.

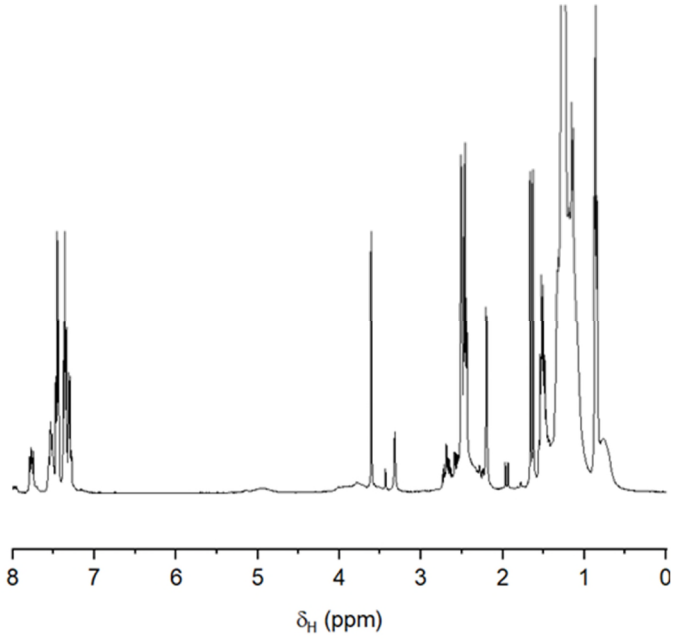


**Figure S2.13** $^{1}$H-NMR ($CDCl_3$, 300 MHz at 25ºC) spectrum of unpurified dodecanethiol functionalised p(GMA) after 12 hours of storage, with disappearance of epoxide peaks due to side-reactions.

## 2.4.2 Product Identification

**MKI range characterisation**:

**p(GMA):**

$^{1}$H-NMR, (/ppm 400 MHz at 25 °C in $CDCl_3$): 0.70-1.40 (backbone $CH_3$), 1.70-2.20 (backbone $CH_2$), 2.64 and 2.84 (epoxide $CH_2$), 3.23 (m, epoxide CH), 3.83 and 4.31 (m, ester-C$H_2$-epoxide), 5.60-6.40 (br, terminal vinyl)

$^{13}$C-NMR, (/ppm, 400 MHz at 25 °C in $CDCl_3$): 14.83 (backbone -$CH_3$), 43.34 (backbone >C<), 47.14 (epoxide -$CH_2$-), 64.17 (epoxide –CH<), 75.68 (ester-$CH_2$-epoxide), 115.02 (-CH=$CH_2$), 124.44 (-CH=$CH_2$), 175.58-175.25-174.42 (carbonyl >C=O)

GPC ($CHCl_3$): **1**: $M_n$ = 17590 g.mol$^{-1}$, $M_w$ = 76840 g.mol$^{-1}$, $Đ$ = 4.36

**2**: $M_n$ = 6670 g.mol$^{-1}$, $M_w$ = 14500 g.mol$^{-1}$, $Đ$ = 2.17

**3**: $M_n$ = 2630 g.mol$^{-1}$, $M_w$ = 4920 g.mol$^{-1}$, $Đ$ = 1.87

**4**: $M_n$ = 2170 g.mol$^{-1}$, $M_w$ = 2204 g.mol$^{-1}$, $Đ$ = 2.32

FT-IR (neat, /cm$^{-1}$): 2962 (C-H, s, medium), 1722 (C=O, s, strong), 1622 (C=C, s, medium), 1445 ($CH_2$, medium), 1267 (s), 1141 (s, C-O), 905 (s, epoxide)

**p(GMA)$_n$(DDT)(ETA): P1/P5/P9**

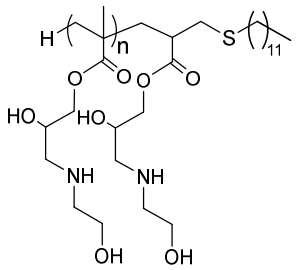

$^{1}$H-NMR, (/ppm, DMSO-$d_6$, 400 MHz at 25 °C): 0.86 (dodecyl terminal -$CH_3$), 0.70-1.10 (backbone -C$H_3$), 1.24 (dodecyl -C$H_2$-), 1.52 (-S-C$H_2$-C$H_2$-C$H_2$-), 1.86 (backbone -C$H_2$-), 2.60 (–C$H_2$-NH-C$H_2$-), 3.47 (C$H_2$-C$H_2$-OH), 3.80 (COO-C$H_2$-C$H$(OH)-), 4.46 (-$CH_2$-O$H$), 5.26 (-$CH_2$-CH(O$H$)-$CH_2$-), 5.93 ($CH_2$-N$H$-$CH_2$)

$^{13}$C-NMR, (/ppm, DMSO-$d_6$, 400 MHz at 25 °C): 14.43 (dodecyl terminal -C$H_3$), 22.59 (backbone -C$H_3$), 28.72 (backbone -$CH_3$), 29.00 – 30.00 (dodecyl -C$H_2$-), 29.69 (-S-$CH_2$-C$H_2$-), 31.79 (-C$H_2$-S-), 32.46 (-S-C$H_2$-), 35.64 (backbone >C<), 52.18-52.71 (-C$H_2$-NH-$CH_2$-), 60.71 (-$CH_2$-C$H_2$-OH), 68.20 (-COO-C$H_2$-), 177.33 (carbonyl >C=O)

GPC (DMF): P1: $M_n$ = 4652 g.mol$^{-1}$, $M_w$ = 13370 g.mol$^{-1}$, $Đ$ = 2.87

P5: $M_n$ = 5850 g.mol$^{-1}$, $M_w$ = 11750 g.mol$^{-1}$, $Đ$ = 2.00

P9: $M_n$ = 2420 g.mol$^{-1}$, $M_w$ = 4022 g.mol$^{-1}$, $Đ$ = 1.66

DLS (in water at room temperature, 5 runs average):

**P1**: d = 7.48 nm, *PDi* = 0.067 **P5**: d = 8.60 nm, *PDi* = 0.889

**P9**: d = 41.01 nm, *PDi* = 0.0961

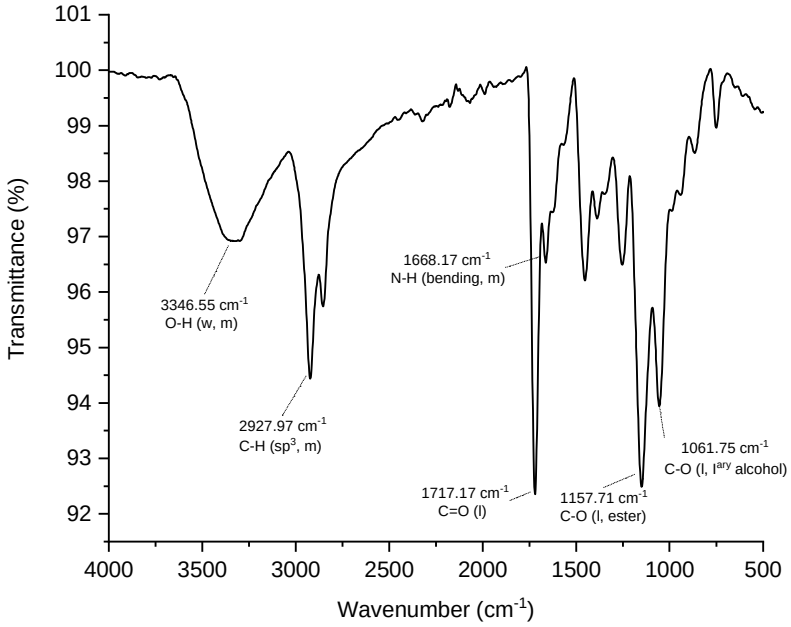


**Figure S2.14** Typical FT-IT spectra of P1/P5/P9.

FT-IR (neat, /cm$^{-1}$): 3338 (-OH, s, broad/medium), 2925 (C-H, s, strong), 1727 (C=O, s, strong), 1664 (N-H, b, medium), 1477 (C-H, b, medium), 1250 (C-N, s, medium), 1150 (C-O, s, strong)

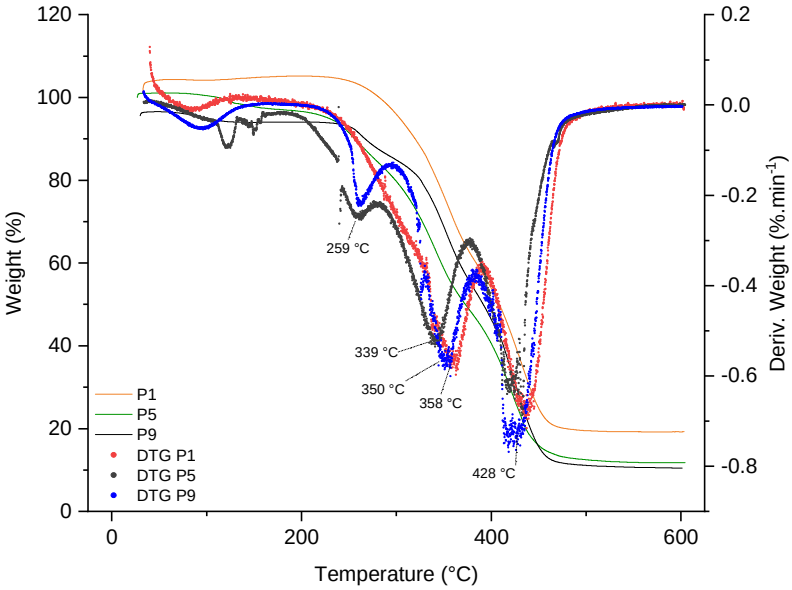


**Figure S2.15** TGA graphs of P1/P5/P9.

TGA degradation onset / °C (degradation steps temperatures):

**P1**: $d_s$ = 287 °C (356 °C, 435 °C)

**P5**: $d_s$ = 270 °C (344 °C, 424 °C)

**P9**: $d_s$ = 290 °C (265 °C, 353 °C, 421 °C)

**p(GMA)$_n$(CHT)(ETA): P2/P6/P10**

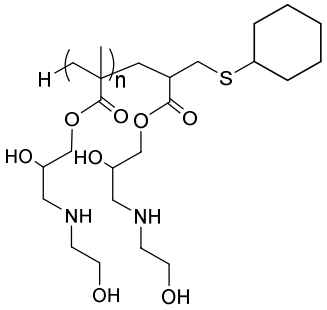


$^1$H-NMR, (/ppm, DMSO-$d_6$, 400 MHz at 25 °C): 0.70-1.10 (backbone -C<u>H</u>$_3$), 1.26 (cyclohexane para -C<u>H</u>$_2$-), 1.70 (cyclohexane meta -C<u>H</u>$_2$-), 1.85 (backbone -C<u>H</u>$_2$-), 1.93 (cyclohexane ortho -C<u>H</u>$_2$-), 2.60 (–C<u>H</u>$_2$-NH-C<u>H</u>$_2$-), 3.40 (-CH$_2$-C<u>H</u>$_2$-OH), 3.78 (COO-C<u>H</u>$_2$-C<u>H</u>(OH)-), 4.45 (-CH$_2$-O<u>H</u>), 5.27 (-CH$_2$-CH(O<u>H</u>)-CH$_2$-), 5.94 (CH$_2$-N<u>H</u>-CH$_2$)

$^{13}$C-NMR, (/ppm, DMSO-$d_6$, 400 MHz at 25 °C): 25.86 (cyclohexane meta/para -<u>C</u>H$_2$-), 33.83 (cyclohexane ortho -<u>C</u>H$_2$-), 28.72 (backbone -CH$_3$), 43.71 (Cyclohexane >C<u>H</u>-),S-<u>C</u>H$_2$-), 35.64 (backbone >C<), 52.18-52.71 (-<u>C</u>H$_2$-NH-CH$_2$-), 60.71 (-CH$_2$-<u>C</u>H$_2$-OH), 68.56 (-COO-<u>C</u>H$_2$), 177.51 (carbonyl >C=O)

GPC (DMF): **P2**: $M_n$ = 4540 g.mol$^{-1}$, $M_w$ = 8300 g.mol$^{-1}$, $Đ$ = 1.83

**P6**: $M_n$ = 2800 g.mol$^{-1}$, $M_w$ = 5330 g.mol$^{-1}$, $Đ$ = 1.91

**P10**: $M_n$ = 2560 g.mol$^{-1}$, $M_w$ = 5030 g.mol$^{-1}$, $Đ$ = 1.96

DLS (in water at room temperature, 5 runs average):

**P2**: d = 121.65 nm, *PDi* = 0.294 **P6**: d = 118.15 nm, *PDi* = 1.28

**P10**: d = 11.36 nm, *PDi* = 0.0870

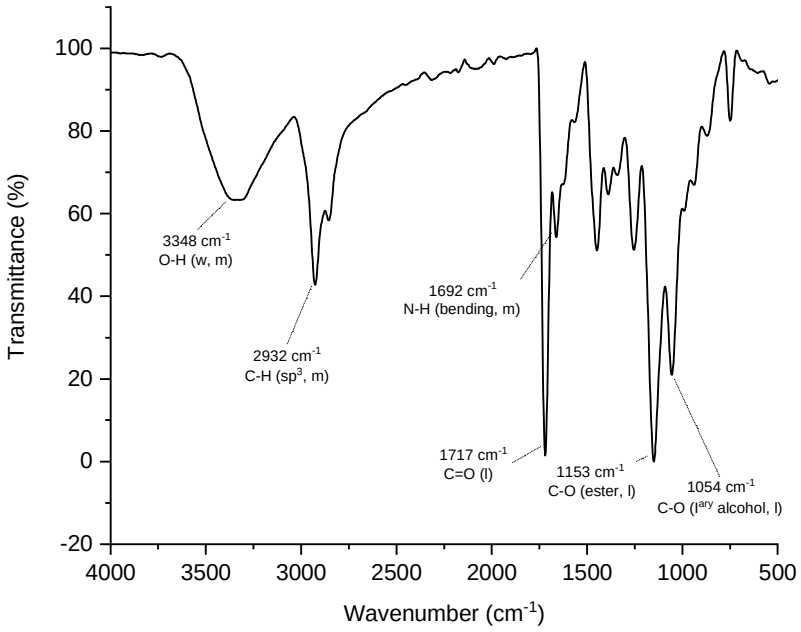


**Figure S2.16** Typical FT-IR spectra of P2/P6/P10.

FT-IR (neat, /cm$^{-1}$): 3348 (-OH, s, broad/medium), 2932 (C-H, s, strong), 1717 (C=O, s, strong), 1692 (N-H, b, medium), 1453 (C-H, b, medium), 1263 (C-N, s, medium), 1153 (C-O, s, strong)

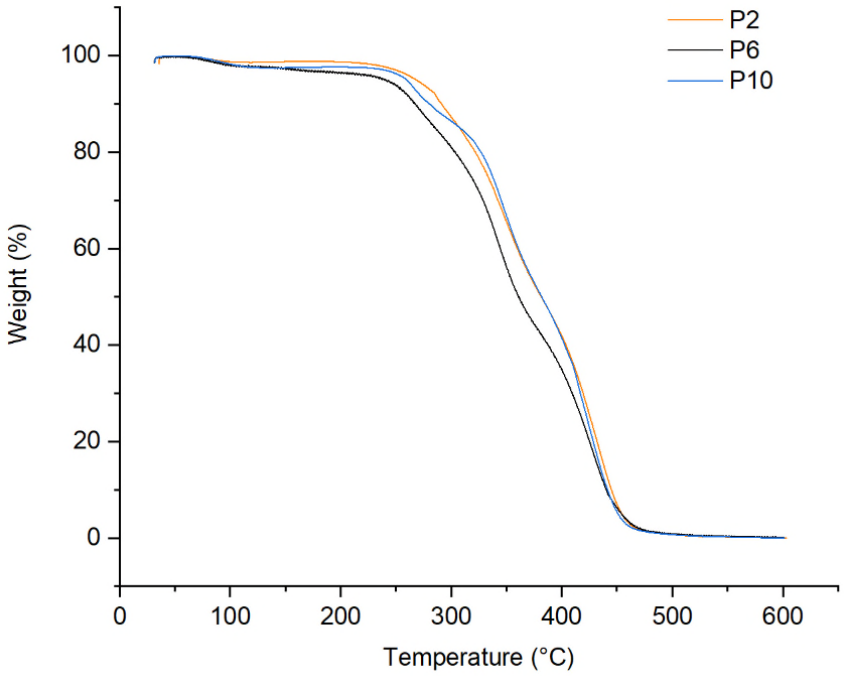


**Figure S2.17** TGA graphs of P2/P6/P10.

TGA degradation onset / °C, (degradation steps temperatures):

**P2**: $d_s$ = 286 °C (351 °C, 435 °C) **P6**: $d_s$ = 273 °C (343 °C, 429 °C)

**P10**: $d_s$ = 293 °C (265 °C, 347 °C, 421 °C)

**p(GMA)$_n$(PET)(ETA): P3/P7/P11**

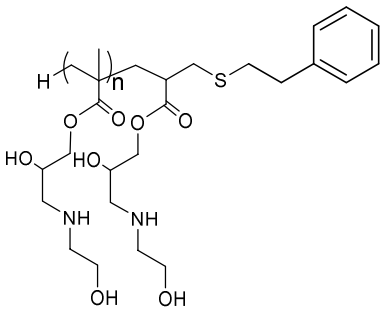


$^1$H-NMR, (/ppm, DMSO-$d_6$, 400 MHz at 25 °C): 0.70-1.10 (backbone -C$\underline{H}_3$), 1.85 (backbone -C$\underline{H}_2$-), 1.93 (cyclohexane ortho -C$\underline{H}_2$-), 2.60 (–C$\underline{H}_2$-NH-C$\underline{H}_2$-), 2.81 (-S-C$\underline{H}_2$-C$\underline{H}_2$-), 3.47 (-CH$_2$-C$\underline{H}_2$-OH), 3.83 (COO-C$\underline{H}_2$-C$\underline{H}$(OH)-), 4.44 (-CH$_2$-O$\underline{H}$), 5.22 (-CH$_2$-CH(O$\underline{H}$)-CH$_2$-), 5.91 (CH$_2$-N$\underline{H}$-CH$_2$), 7.26 (aromatic -C$\underline{H}_2$-)

$^{13}$C-NMR, (/ppm, DMSO-$d_6$, 400 MHz at 25 °C): 33.97 (-S-<u>C</u>$H_2$-<u>C</u>$H_2$-), 36.08 (backbone ><u>C</u><), 44.87 (backbone -$CH_3$), 52.12 (-<u>C</u>$H_2$-NH-$CH_2$-), 52.71 (-$CH_2$-NH-<u>C</u>$H_2$-), 60.73 (-$CH_2$-<u>C</u>$H_2$-OH), 67.76 (ester-$CH_2$-<u>C</u>H(OH)-), 68.28 (-COO-<u>C</u>$H_2$-CH(OH)-), 126.58 (aromatic para =CH-), 128.58-128.95 (aromatic ortho/meta =<u>C</u>H-), 140.94 (aromatic -C≤), 177.45 (carbonyl ><u>C</u>=O)

GPC (DMF): **P3**: $M_n$ = 5270 g.mol$^{-1}$, $M_w$ = 9050 g.mol$^{-1}$, $Đ$ = 1.72

**P7**: $M_n$ = 3250 g.mol$^{-1}$, $M_w$ = 6274 g.mol$^{-1}$, $Đ$ = 1.93

**P11**: $M_n$ = 3530 g.mol$^{-1}$, $M_w$ = 6100 g.mol$^{-1}$, $Đ$ = 1.73

DLS (in water at room temperature, 5 runs average):

**P3**: d = 119.43 nm, *PDi* = 0.306 **P7**: d = 15.27 nm, *PDi* = 0.0851

**P11**: d = 6.16 nm, *PDi* = 0.0663

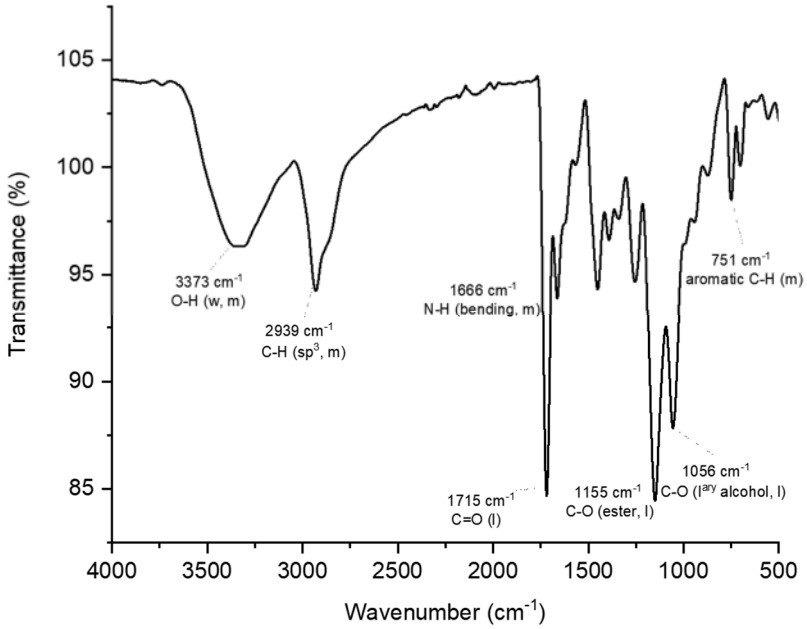


**Figure S2.18** Typical FT-IT spectra of P2/P6/P10.

FT-IR (neat, /cm$^{-1}$): 3373 (-OH, s, broad/medium), 2939 (C-H, s, strong), 1715 (C=O, s, strong), 1666 (N-H, b, medium), 1455 (C-H, b, medium), 1259 (C-N, s, medium), 1155 (C-O, s, strong), 751 (aromatic C-H, s, medium)

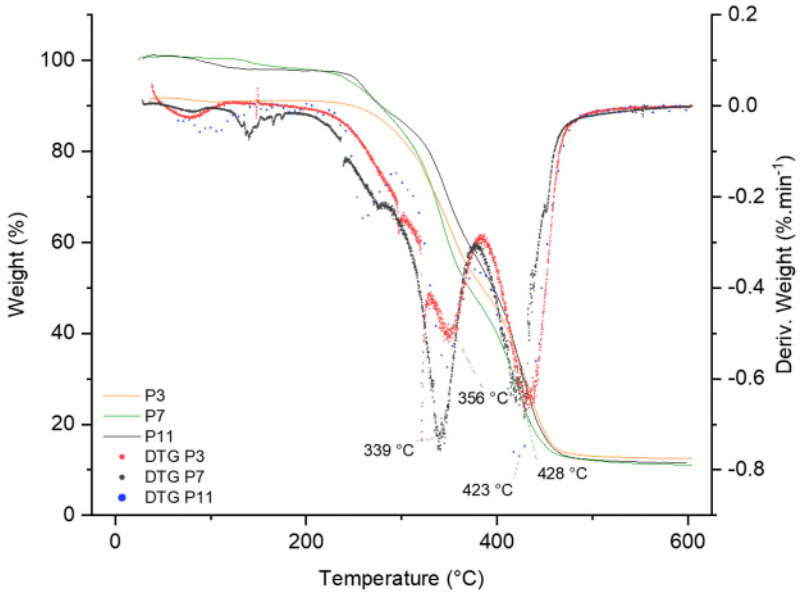


**Figure S2.19** TGA graphs of P3/P7/P11.

TGA degradation onset / °C (degradation steps temperatures):

**P3**: $d_s$ = 286 °C (351 °C, 433 °C) **P7**: $d_s$ = 270 °C (342 °C, 422 °C)

**P11**: $d_s$ = 296 °C (260 °C, 347 °C, 423 °C)

**p(GMA)$_n$(i-PT)(ETA): P4/P8/P12**

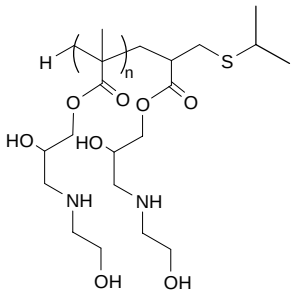

$^1$H-NMR, (/ppm, DMSO-$d_6$, 400 MHz at 25 °C): 0.78-1.07 (backbone -C$\underline{H}_3$), 1.21 (isopropyl -CH(C$\underline{H}_3$)$_2$), 1.85 (backbone -C$\underline{H}_2$-), 2.60 (-C$\underline{H}_2$-NH-C$\underline{H}_2$-), 2.98

(isopropyl -C<u>H</u><), 3.47 (-CH$_2$-C<u>H$_2$</u>-OH), 3.79 (-COO-C<u>H$_2$</u>-C<u>H</u>-), 4.45 (-CH$_2$-CH$_2$-O<u>H</u>), 5.25 (-CH$_2$-CH(O<u>H</u>)-CH$_2$-), 5.92 (br, CH$_2$-N<u>H</u>-CH$_2$), 7.59

$^{13}$C-NMR, (/ppm, DMSO-d$_6$, 400 MHz at 25 °C): 23.86 (isopropyl –CH(<u>C</u>H$_3$)$_2$), 34.19 (backbone -<u>C</u>H$_3$), 35.18 (isopropyl –<u>C</u>H<), 43.95 (><u>C</u>H-CH$_2$-S-), 52.23 (-CH$_2$-NH-<u>C</u>H$_2$-), 52.78 (-CH$_2$-NH-<u>C</u>H$_2$-), 60.75 (backbone -<u>C</u>H$_2$-), 62.60 (-CH$_2$-<u>C</u>H$_2$-OH), 67.92 (ester-CH$_2$-<u>C</u>H(OH)-), 68.38 (ester-C<u>H$_2$</u>-CH(OH)-), 177.76 (carbonyl ><u>C</u>=O)

GPC (DMF): **P4**: $M_n$ = 4510 g.mol$^{-1}$, $M_w$ = 8100 g.mol$^{-1}$, $Đ$ = 1.79

**P8**: $M_n$ = 3210 g.mol$^{-1}$, $M_w$ = 5920 g.mol$^{-1}$, $Đ$ = 1.85

**P12**: $M_n$ = 3000 g.mol$^{-1}$, $M_w$ = 4050 g.mol$^{-1}$, $Đ$ = 1.35

DLS (in water at room temperature, 5 runs average):

**P4**: d = 101.42 nm, *PDi* = 0.467 **P8**: d = 13.53 nm, *PDi* = 0.0896

**P12**: d = 9.66 nm, *PDi* = 0.0769

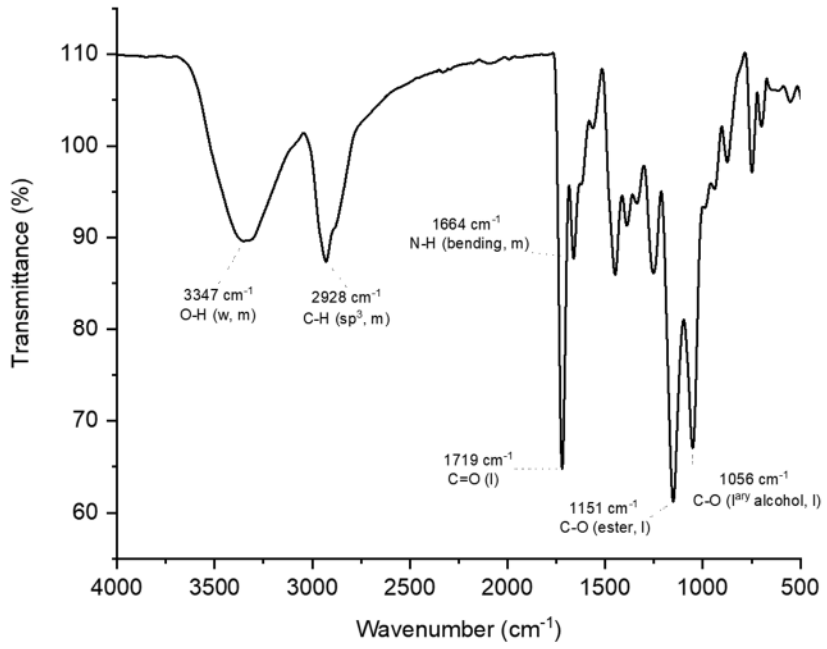


**Figure S2.20** Typical FT-IT spectra of P4/P8/P12.

FT-IR (neat, /cm$^{-1}$): 3307 (-OH, s, broad/medium), 2931 (C-H, s, strong), 1719 (C=O, s, strong), 1613 (N-H, b, medium), 1453 (C-H, b, medium), 1238 (C-N, s, medium), 1147 (C-O, s, strong)

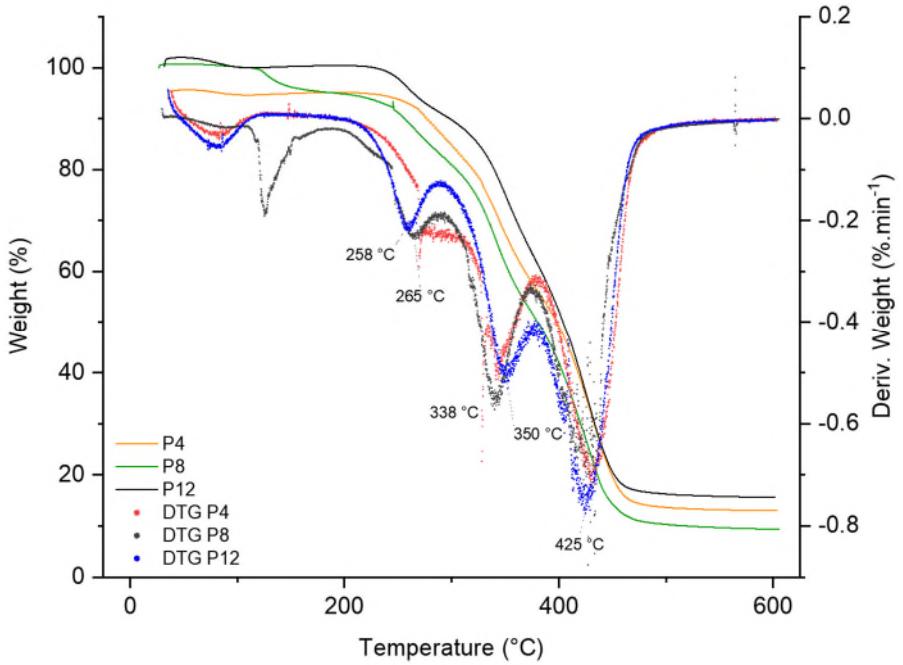


**Figure S2.21** TGA graphs of P4/P8/P12.

TGA degradation onset / °C (degradation steps temperatures):

**P4**: $d_s$ = 289 °C (344 °C, 437 °C) **P8**: $d_s$ = 267 °C (264 °C, 340 °C, 431 °C)

**P121**: $d_s$ = 292 °C (259 °C, 349 °C, 429 °C)

**MKII range characterisation:**

**p(GlyMA):**

$^1$H-NMR, (/ppm, DMSO-$d_6$, 400 MHz at 25 °C): 0.69-1.16 (br, backbone + terminal -C<u>H</u>$_3$), 1.84 (br, backbone -C<u>H</u>$_2$-), 3.67 (br, COO-C<u>H</u>$_2$-CH), 3.76 (br, CH$_2$-C<u>H</u>(OH)-CH$_2$), 3.93 (br, (OH)CH-C<u>H</u>$_2$-OH)), 4.65 and 4.90 ((O<u>H</u>)CH-CH$_2$-O<u>H</u>), 5.61 and 6.16 (terminal vinyl).

$^{13}$C-NMR (/ppm, DMSO-$d_6$, 400 MHz at 25 °C): 18.45 (backbone -$\underline{C}H_3$), 25.98 (α -$\underline{C}H_3$), 41.41 (-$\underline{C}H_2$-C=C), 43-46 (backbone >$\underline{C}$<). 59-60 (backbone –$\underline{C}H_2$-), 62.5-63.5 (HO-$\underline{C}H_2$-CH<), 65-67 (COO-$\underline{C}H_2$-CH<), 69-70 ($CH_2$-$\underline{C}$H(OH)-$CH_2$-OH), 126-127 (terminal >C=$\underline{C}H_2$), 136-137 (terminal >$\underline{C}$=$CH_2$), 176-179 (>$\underline{C}$=O)

GPC (DMF): **1**: $M_n$ = 15090 g.mol$^{-1}$, $M_w$ = 21930 g.mol$^{-1}$, $Đ$ = 1.45

**2**: $M_n$ = 8300 g.mol$^{-1}$, $M_w$ = 11670 g.mol$^{-1}$, $Đ$ = 1.40

**3**: $M_n$ = 1470 g.mol$^{-1}$, $M_w$ = 3920 g.mol$^{-1}$, $Đ$ = 2.66

FT-IR (neat, /cm$^{-1}$): 3370 (-OH, wide), 2949 (C-H, s, medium), 1713 (C=O, s, strong), 1160 (s, C-O), 1046.37 (primary alcohol)

**p(GlyMA)$_8$(PET), Q1:**

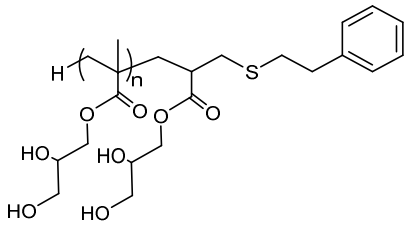


$^1$H-NMR, (/ppm, DMSO-$d_6$, 400 MHz at 25 °C): 0.70-1.10 (br, backbone + terminal -C$\underline{H}_3$), 1.80-1.90 (br, backbone –C$\underline{H}_2$-), 2.20-2.26 (>C$\underline{H}$-$CH_2$-S-$CH_2$-C$\underline{H}_2$-), 2.70-2.80 (>CH-C$\underline{H}_2$-S-C$\underline{H}_2$-$CH_2$-), 3.39 (HO-C$\underline{H}_2$-CH<), 3.68 and 3.91 (COO-C$\underline{H}_2$-CH<), 3.75 ($CH_2$-C$\underline{H}$(OH)-$CH_2$-OH), 4.70 ($CH_2$-CH(OH)-$CH_2$-O$\underline{H}$), 4.93 ($CH_2$-CH(O$\underline{H}$)-$CH_2$-OH), 7.20-2.90 (Aromatic protons)

GPC (DMF): $M_n$ = 5140 g.mol$^{-1}$, $M_w$ = 8590 g.mol$^{-1}$, $Đ$ = 1.67

DLS (in water at room temperature, 3 runs average):

d = 71.98 nm, *PDi* = 0.0289

FT-IR: N/A

TGA: N/A

**p(GlyMA)$_8$(CHT), Q2:**

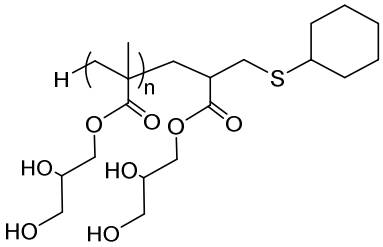


$^1$H-NMR, (/ppm, DMSO-d$_6$, 400 MHz at 25 °C): 0.70-1.10 (br, backbone + terminal -C<u>H</u>$_3$), 1.50-1.55 (cyclohexane protons), 1.80-1.90 (br, backbone –C<u>H</u>$_2$-), 3.38 (HO-C<u>H</u>$_2$-CH<), 3.68 and 3.91 (COO-C<u>H</u>$_2$-CH<), 3.75 (CH$_2$-C<u>H</u>(OH)-CH$_2$-OH), 4.69 (CH$_2$-CH(OH)-CH$_2$-O<u>H</u>), 4.94 (CH$_2$-CH(O<u>H</u>)-CH$_2$-OH)

GPC (DMF): $M_n$ = 5020 g.mol$^{-1}$, $M_w$ = 7260 g.mol$^{-1}$, $Đ$ = 1.46

DLS (in water at room temperature, 3 runs average):

d = 81.84 nm, *PDi* = 0.609

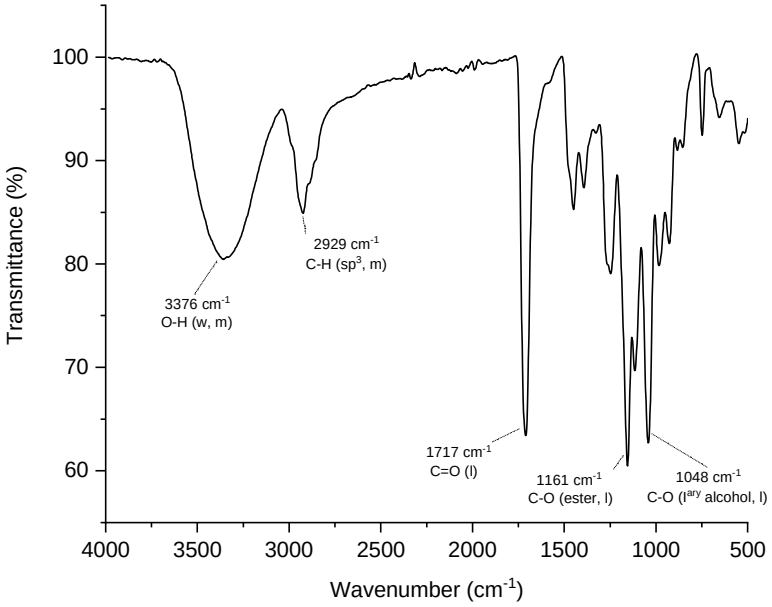


**Figure S2.22** Typical FT-IT spectra of Q2.

FT-IR (neat, /cm$^{-1}$): 3376 (-OH, wide), 2929 (C-H, s, medium), 1717 (C=O, s, strong), 1161 (s, C-O), 1048 (primary alcohol)

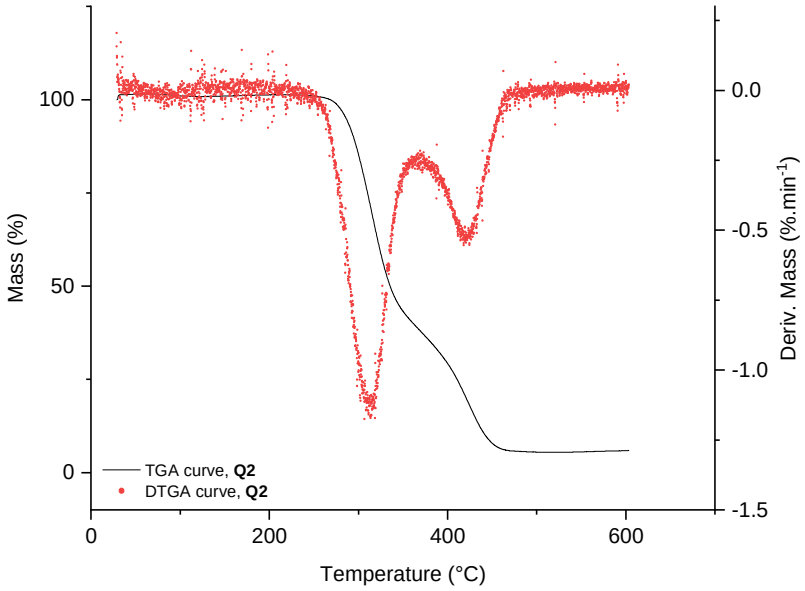


**Figure S2.23** TGA graphs of Q2.

TGA degradation onset / °C (degradation steps temperatures):

**P4**: $d_s$ = 289 °C (344 °C, 437 °C) **P8**: $d_s$ = 267 °C (264 °C, 340 °C, 431 °C)

**P121**: $d_s$ = 292 °C (259 °C, 349 °C, 429 °C)

**p(GlyMA)$_8$(i-PT), Q3:**

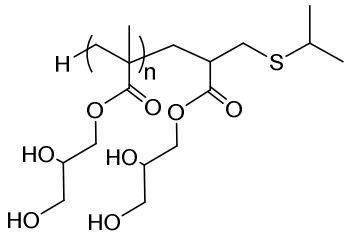


$^1$H-NMR, (/ppm, 400 MHz at 25°C in DMSO-$d_6$): 0.70-1.10 (br, backbone + terminal -C<u>H</u>$_3$), 1.15-1.25 (-S-CH(C<u>H</u>$_2$)2), 1.80-1.85 (br, backbone –C<u>H</u>$_2$-), 3.67 and 3.91 (COO-C<u>H</u>$_2$-CH<), 3.75 (CH$_2$-C<u>H</u>(OH)-CH$_2$-OH), 4.71 (CH$_2$-CH(OH)-CH$_2$-O<u>H</u>), 4.95 (CH$_2$-CH(O<u>H</u>)-CH$_2$-OH)

GPC (DMF): $M_n$ = 6180 g.mol$^{-1}$, $M_w$ = 9160 g.mol$^{-1}$, $Đ$ = 1.48

DLS (in water at room temperature, 3 runs average):

d = 106.02 nm, *PDi* = 0.274

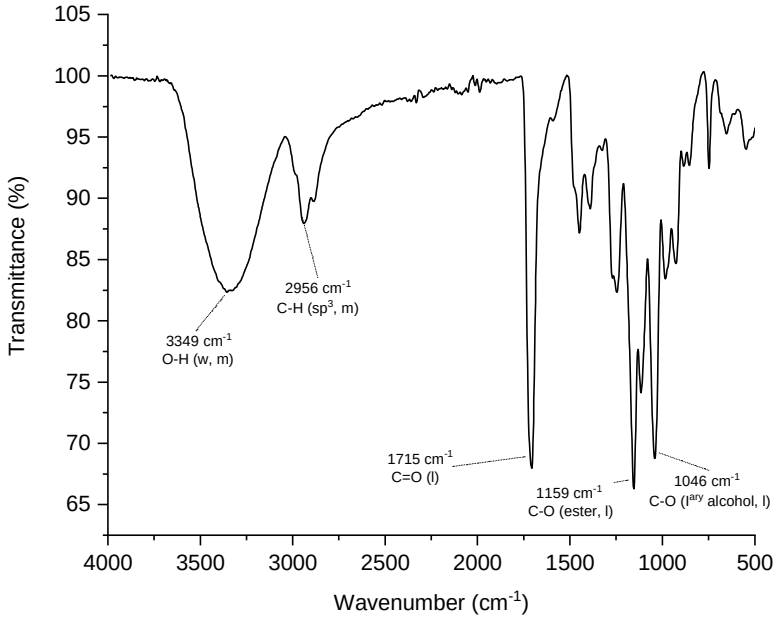


**Figure S2.24** Typical FT-IT spectra of Q3.

FT-IR (neat, /cm$^{-1}$): 3349 (-OH, wide), 2953 (C-H, s, medium), 1715 (C=O, s, strong), 1159 (s, C-O), 1046 (primary alcohol)

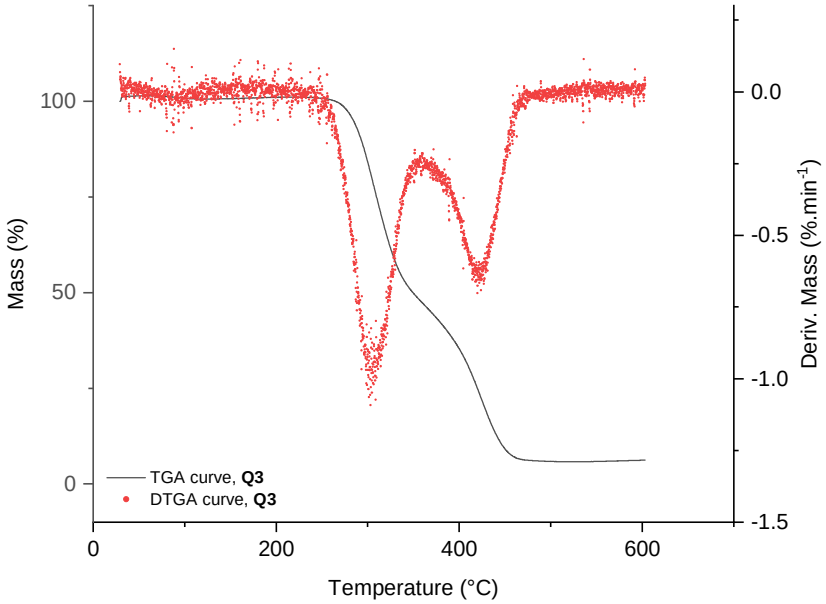


**Figure S2.25** TGA graphs of Q3.

TGA degradation onset / °C (degradation steps temperatures):

**P4**: $d_s$ = 289 °C (344 °C, 437 °C) **P8**: $d_s$ = 267 °C (264 °C, 340 °C, 431 °C)

**P121**: $d_s$ = 292 °C (259 °C, 349 °C, 429 °C)

**p(GlyMA)$_8$(linear thiol), Hexanethiol (Q4), Nonanethiol (Q5), Dodecanethiol (Q6), Tetradecanethiol (Q7), Octodecanethiol (Q8):**

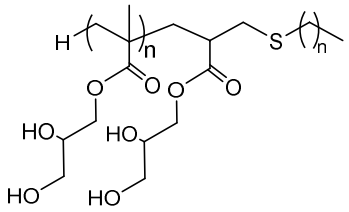


$^1$H-NMR, (/ppm, 400 MHz at 25°C in DMSO-$d_6$): 0.70-1.10 (br, backbone + terminal -C<u>H</u>$_3$), 0.86 (-S-CH$_2$-CH$_2$-CH$_2$-CH$_2$-CH$_2$-C<u>H</u>$_3$), 1.24 (-S-CH$_2$-(C<u>H</u>$_2$)$_n$), 1.40-1.50 (-S-C<u>H</u>$_2$-(CH$_2$)$_n$), 1.75-1.85 (br, backbone –C<u>H</u>$_2$-), 3.38 (HO-C<u>H</u>$_2$-CH<), c. 3.68 and 3.91 (COO-C<u>H</u>$_2$-CH<), c. 3.75 (CH$_2$-C<u>H</u>(OH)-CH$_2$-OH), c. 4.68 (CH$_2$-CH(OH)-CH$_2$-O<u>H</u>), c. 4.93 (CH$_2$-CH(O<u>H</u>)-CH$_2$-OH)

GPC (DMF): $Q_4$: $M_n$ = 5550 g.mol$^{-1}$, $M_w$ = 7460 g.mol$^{-1}$, $Đ$ = 1.34

$Q_5$: $M_n$ = 5720 g.mol$^{-1}$, $M_w$ = 7720 g.mol$^{-1}$, $Đ$ = 1.35

$Q_6$: $M_n$ = 5520 g.mol$^{-1}$, $M_w$ = 8620 g.mol$^{-1}$, $Đ$ = 1.56

$Q_7$: $M_n$ = 7650 g.mol$^{-1}$, $M_w$ = 10110 g.mol$^{-1}$, $Đ$ = 1.32

$Q_8$: $M_n$ = 2300 g.mol$^{-1}$, $M_w$ = 4930 g.mol$^{-1}$, $Đ$ = 2.15

DLS (in water at room temperature, 3 runs average):

$Q_4$: d = 78.61 nm, *PDi* = 0.0607

$Q_5$: d = 59.20 nm, *PDi* = 0.0282

$Q_6$: d = 7.329 nm, *PDi* = 0.622.

$Q_7$: d = 5.77 nm, *PDi* = 0.024

$Q_8$: d = 12.046 nm, *PDi* = 0.0754

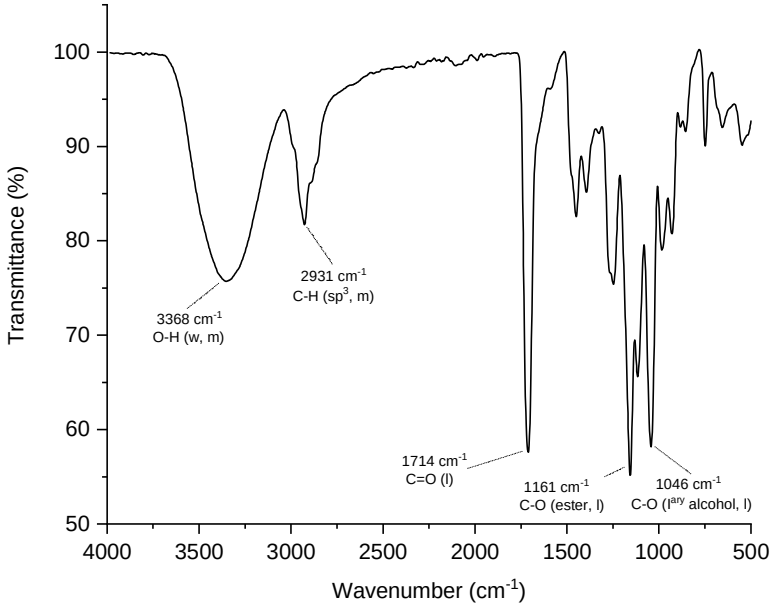


**Figure S2.26** Typical FT-IT spectra of Q4/Q5/Q6/Q7 and Q8.

FT-IR (neat, /$cm^{-1}$): 3368 (-OH, wide), 2931 (C-H, s, medium), 1714 (C=O, s, strong), 1161 (s, C-O), 1046 (primary alcohol)

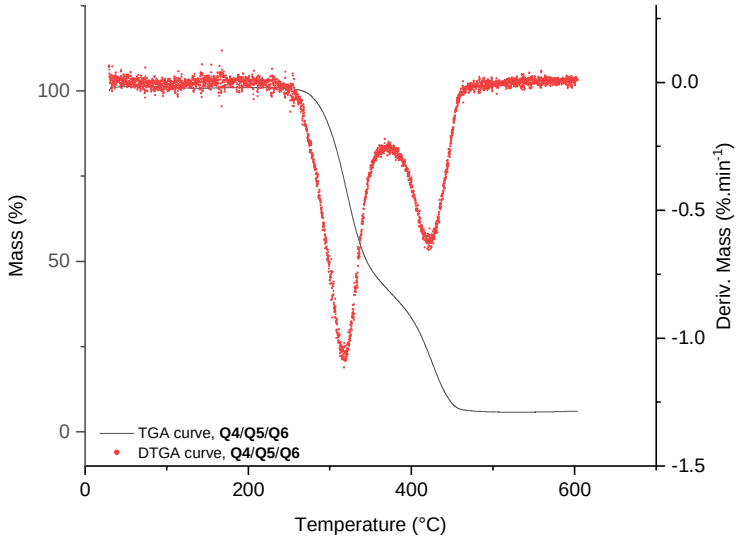


**Figure S2.27** Typical TGA graph of Q4/Q5/Q6/Q7 and Q8.

### 2.4.3 Materials

Unless stated otherwise, all chemicals mentioned were purchased from Sigma-Aldrich and were used without further purification.

Cobalt(II) acetate tetrahydrate was purchased from Riedel-de Haen / Honeywell, V-601 from Wako chemicals, glycerol monomethacrylate was kindly donated by GEO specialty chemicals. Triphenylmethanethiol, tert-dodecanethiol and heptanethiol were obtained from Acros Organics, Merck and Alfa Aesar respectively.

### 2.4.4 Instrumentation

*DMF and $CHCl_3$ Gel-Permeation Chromatography (GPC)* was carried out on an Agilent Infinity II MDS instruments equipped with differential refractive index (DRI), viscometry (VS) and dual angle light scatter (LS) detectors.

For DMF analysis the system was equipped 2 x PLgel Mixed D columns (300 x 7.5 mm) and a PLgel 5 µm guard column. 12 narrow molecular weight poly(methyl methacrylate) standards (Agilent EasiVials) were used for calibration between 955,000 – 550 g $mol^{-1}$ and data fitted with a 3$^{rd}$ order polynomial. The eluent was DMF with 5 mmol $NH_4BF_4$ additive to help prevent column interactions. Analyte samples were filtered through a 0.22 µm nylon membrane before injection and samples were run at a flow rate of 1 ml/min at 50 °C.

For $CHCl_3$ analyses the system was equipped with 2 x PLgel Mixed C columns (300 x 7.5 mm) and a PLgel 5 µm guard column. The eluent used was $CHCl_3$ with 2 % TEA (triethylamine) additive. Samples were run at 1 $ml.min^{-1}$ at 30 °C.

pMMA or polystryrene standards between 540 Da and 1000 kDa for the former and between 370 Da and 364 kDa for the latter (Agilent EasyVials) were used for

calibration. Ethanol was added as a flow rate marker. Analyte samples were filtered through a GVHP membrane with 0.22 μm pore size before injection.

In either cases, number average molecular weight ($M_{n,GPC}$) and dispersity ($Đ$) values of synthesized polymers were determined by conventional calibration using Agilent GPC/SEC software.

*Nuclear magnetic resonance (NMR, $^{1}H$ and $^{13}C$)* spectra were recorded at room temperature on a Bruker Avance III HD-300 or 400 using either deuterated solvents referenced against TMS as a reference.

*Microwave-assisted syntheses (MAOS)* were performed in a Biotage initiator+ in 2-5 or 10-20 mL Biotage vials.

*Matrix-assisted laser desorption/ionization time-of-flight (MALDI-ToF)* spectra were collected using a Bruker Autoflex Speed, equipped with a 337 nm nitrogen laser, operating in reflectron positive mode with an ion source voltage of 19 kV. Results were accumulated in 10 readings of each spot with 500 laser shots, leading to a total of 5000 laser shots per spectra. Laser power was tuned to keep noise low while maintaining the signal as to not remove any trace peaks. The samples were dissolved into the appropriate solvent at concentrations of 10 mg $ml^{-1}$, along with the cationizing agent sodium iodide (NaI) at 0.1 mg $ml^{-1}$. A matrix solution was then made up of trans-2-[3-(4-tert-Butylphenyl)-2-methyl-2-propenylidene]malononitrile (DCTB) in THF at a concentration of 40mg $ml^{-1}$, along with NaI at 0.1 mg $ml^{-1}$. 10 μl of both the matrix and sample solutions were then mixed together, and 0.5 μl of the resulting solution was then spotted on an MTP 384 ground steel target plate.

*Fourier transform infra-red (FT-IR)* spectra were recorded on a Bruker Vector 22 FT–IR Spectrometer fitted with a diamond crystal plate and a pressure tower. The instrument was set to perform 64 scans per sample at a scan speed of 0.5 $cm.s^{-1}$.

*Dynamic light scattering (DLS)* analyses were carried out on a Malvern Instruments Zetasizer Nano-ZS in water at 25 °C fitted with a 4 mW He-Ne 633 nm laser set at a back-scattering angle of 173°. Samples were prepared by dissolving 1 mg of product in 20 mL of HPLC-grade water. All solutions were sonicated for 2 minutes at 50 °C and allowed to settle for a further 10 minutes. Small aliquots were then pipetted into disposable DLS cuvettes. The equilibration time was set at 2 minutes and five measurements of eleven runs were conducted each time. Sizes are reported as averages of 5 runs and polydispersity was obtained from the zetasizer software as an average of all measurements.

*Thermo-gravimetric (TGA)* data was obtained using a Mettler-Toledo TGA/DSC1 with autosampler. Measurements were carried out under a nitrogen atmosphere from 25 to 600 °C at a rate of 10 °C/min in a 40 µL aluminium crucible.

*Transmission electron microscopy (TEM)* images were obtained on a JEOL 2100 TEM fitted with a Gatan Ultrascan 1000 camera. Samples were diluted at 0.1% v/v and one drop was cast on a carbon coated TEM copper grid. After 2 minutes the drop was blotted off with filter paper. All samples were prepared without using a stain.

### 2.4.5 Experimental Procedures

**CoBF Synthesis:**

Cobalt(II) acetate tetrahydrate was heated at 110 °C and 2 mbar for 5-6 hours in a Schlenck flask, which was removed from the oil bath when the pink powder became purple (upon becoming anhydrous).

To a second Schlenck flask equipped with a magnetic stirrer, anhydrous cobalt(II) acetate (3.14 g, 0.0126 mol) and dimethyl glyoxime (4.47 g, 0.0344 mol) were added and purged with $N_2$ for 1 hour. Separately, ethyl acetate (77.12ml, 0.87 mol) was dried with $MgSO_4$, decanted and filtered by gravity filtration. Ethyl acetate was then degassed for 30 minutes prior to addition to the mixture using de-oxygenated syringes. The mixture was stirred vigorously for 30 min. Boron trifluoride etherate ($BF_3EtO_2$) (13.03 mL, 0.09 mol) was degassed with nitrogen and added via syringe pump over a period of 10 minutes under continuous vigorous stirring. The resulting solution was heated and held at 50 °C for 30 minutes to complete the reaction. Sodium bicarbonate (3.57 g, 0.042 mol) was added in portions to avoid excessive frothing. When the bicarbonate addition was complete, the reaction mixture was cooled down to 5 °C and stirred for an hour to allow product to recrystallize. Filtration was carried out in (2 x 70 mL) $H_2O$ and (2 x 20 mL) MeOH.

**Synthesis of poly(glycidyl methacrylate):**

0.25 mg/mL stock solutions of CoBF in GMA were prepared by separately de-oxygenating 5 mg of CoBF and 20 g of GMA for 1 hour and 30 minutes respectively using nitrogen bubbling. GMA was then transferred, using degassed syringes, into the CoBF flask, previously equipped with a magnetic stirrer. The solution was then

sonicated for 10 min and left to stir for up to 1 hour to ensure proper mixing. Stock solutions were stored at 4 °C for up to two months.

All polymerisations were carried out in a similar fashion. VA-601 (0.5 mol% to monomer) was dissolved in acetonitrile (calculated to 50% solid content) and introduced into a 250 mL tri-neck round bottom flask (rbf 1) equipped with a stirrer bar. In parallel, another round bottom flask (rbf 2) was loaded with an appropriate volume of GMA, taking into consideration the volume of CoBF in GMA required from the stock solution to reach the required final CoBF concentration within the reaction mixture. The two flasks were then sealed with rubber septa and degassed for 30 minutes each. Once all components were purged of oxygen, a CoBF/GMA volume from the stock solution was transferred into rbf 2. The final CoBF in GMA solution was fed into rbf 1, which was placed in an oil bath pre-heated to 70 °C, over a 3-hour period. The reaction mixture was allowed to react for 24 hours. Samples for $^{1}$H-NMR, GPC, MALDI-ToF MS and IR were taken after termination of the reaction and removal of solvent using rotary evaporation

**Synthesis of poly(glycerol monomethacrylate):**

Due to the low chain transfer constants that were observed with GlyMA, larger amounts of CoBF were required. In addition, the relative lower solubility of CoBF in GlyMA and the high viscosity of the monomer made the preparation of CoBF in monomer solution impractical.

P(GlyMA) polymerisations were prepared using 3 different rbfs (rbf 1, 2 and 3). Initiator (ACVA, 0.5 mol% to monomer) and solvent (calculated to 50% solid content) were introduced in rbf 1, an excess of monomer in rbf 2 and CoBF (20, 30 or 40 ppm)

alongside a stirring magnet in rbf 3. Rbfs 1 and 2 were de-oxygenated for 20 minutes while rbf 3 was de-oxygenated for 35 minutes. After oxygen was removed, both the initiator in solvent and the calculated amount of GlyMA were transferred into rbf 3 using de-oxygenated syringes. Rbf 3 was finally introduced into a pre-heated oil bath (70 °C) and left to react overnight.

**Dual Functionalisation of p(GMA)$_n$: one-pot Michael-thiol Addition Followed by Epoxide Ring-Opening:**

Michael-thiol additions of p(GMA)$_n$ were carried by adapting the following protocol: 5 g of p(GMA)$_n$ (1000 Da, 1 eq) was introduced into a 10-20 mL microwave vial along with a magnetic stirrer and dissolved into 10.0 mL of acetonitrile. The vial was sealed and de-oxygenated for 15 minutes. Subsequently, 1.2 equivalents of separately de-oxygenated dodecanethiol (6.00 mmol, 1.43 mL) were subsequently added to the vial, as well as 0.8 eq of dimethylphenylphosphine (4 mmol, 0.569 mL) using de-oxygenated syringes. The reaction was then left to react at room temperature for 3 hours under vigorous stirring (500 rpm).

After the reaction was completed, the vial was opened and 9 equivalents of ethanolamine (63.3 mmol, 3.82 mL) to the number of moles of epoxide were added to the vial without intermediate purification step. The vial was sealed with a microwave cap, keeping an ambient atmosphere within the flask, and placed in the microwave for a 5-15 minutes reaction cycle at 120 °C. The sample was then taken out of the instrument and acetonitrile reduced by blowing oxygen through the clear solution for 12 hours. The resulting viscous product was dissolved with 10 mL of methanol, and dialysed against methanol for 50 hrs to remove residual acetonitrile and impurities. MeOH was removed by a combination of rotary evaporation, freeze-drying on Schlenk

lines. All products were finally placed in a vacuum oven overnight before carrying out product analysis.

**Michael-thiol Addition of Hydrophobic Thiols on p(GlyMA)$_n$:**

Michael-thiol additions of p(GlyMA)$_n$ were carried by adapting the following protocol:

p(GlyMA)$_n$ (5 g, 1400 Da, 1 eq) and a magnetic stirrer were introduced into a round bottom flask and dissolved with 20 mL of methanol. The flask was sealed and the mixture de-oxygenated for 15 min. 1.02 equivalents (3.64 mmol, 0.867 mL) of dodecanethiol and DMPP (0.8 eq, 0.607 mL) were do-oxygenated separately and added to the flask. The reaction was left to reaction was left to react for 5 min and then opened to ambient air. The reaction mixture was then transferred to a dialysis bag and dialysed against methanol for 50 hours. Methanol was evaporated *in-vacuo* to yield the product for analysis.

## 2.5 References

1 H. S. Sundaram, Y. Cho, M. D. Dimitriou, J. A. Finlay, G. Cone, S. Williams, D. Handlin, J. Gatto, M. E. Callow, J. A. Callow, E. J. Kramer and C. K. Ober, *ACS Appl. Mater. Interfaces*, 2011, **3**, 3366–3374.

2 V. P. Torchilin, V. S. Trubetskoy, K. R. Whiteman, P. Caliceti, P. Ferruti and F. M. Veronese, *J. Pharm. Sci.*, 1995, **84**, 1049–1053.

3 W. W. Yu, E. Chang, J. C. Falkner, J. Zhang, A. M. Al-Somali, C. M. Sayes, J. Johns, R. Drezek and V. L. Colvin, *J. Am. Chem. Soc.*, 2007, **129**, 2871–2879.

4 X. Qu, Y. Zou, C. He, Y. Zhou, Y. Jin, Y. Deng, Z. Wang, X. Li, Y. Zhou and Y. Liu, *Drug Deliv.*, 2018, **25**, 210–225.

5 V. V. Vasilevskaya, P. G. Khalatur and A. R. Khokhlov, *Macromolecules*, 2003, **36**, 10103–10111.

6 A. F. Miller, M. R. Wilson, M. J. Cook and R. W. Richards, *Mol. Phys.*, 2003, **101**, 1131–1138.

7 K. Kempe, R. A. Wylie, M. D. Dimitriou, H. Tran, R. Hoogenboom, U. S. Schubert, C. J. Hawker, L. M. Campos and L. A. Connal, *J. Polym. Sci. Part A Polym. Chem.*, 2016, **54**, 750–757.

8 M. Müller and K. C. Daoulas, *J. Chem. Phys.*, 2008, **128**, 32.

9 G. Kwon, M. Naito, M. Yokoyama, T. Okano, Y. Sakurai and K. Kataoka, *Langmuir*, 1993, **9**, 945–949.

10 D. Kiserow, C. Ramireddy, P. Munk, S. E. Webber, K. Prochazka and Z. Tuzar, *Macromolecules*, 1992, **25**, 461–469.

11 S. Cai, K. Vijayan, D. Cheng, E. M. Lima and D. E. Discher, *Pharm. Res.*, 2007, **24**, 2099–2109.

12 A. Choucair, C. Lavigueur and A. Eisenberg, *Langmuir*, 2004, **20**, 3894–3900.

13 J. N. Israelachvili, D. J. Mitchell and B. W. Ninham, *J. Chem. Soc. Faraday Trans. 2 Mol. Chem. Phys.*, 1976, **72**, 1525–1568.

14 F. Suriano, R. Pratt, J. P. K. Tan, N. Wiradharma, A. Nelson, Y. Y. Yang, P. Dubois and J. L. Hedrick, *Biomaterials*, 2010, **31**, 2637–2645.

15 P. S. Stayton, A. S. Hoffman, N. Murthy, C. Lackey, C. Cheung, P. Tan, L. A. Klumb, A. Chilkoti, F. S. Wilbur and O. W. Press, *Molecular engineering of proteins and polymers for targeting and intracellular delivery of therapeutics*, 2000, vol. 65.

16 F. Wang, T. K. Bronich, A. V. Kabanov, R. D. Rauh and J. Roovers, *Bioconjug. Chem.*, 2005, **16**, 397–405.

17 Z. Huang, Q. Chen, Q. Wan, K. Wang, J. Yuan, X. Zhang, L. Tao and Y. Wei, *Polym. Chem.*, 2017, **8**, 4805–4810.

18 E. Dickinson and D. Lorient, eds. E. Dickinson and D. Lorient, 2007, **0**, 20–604.

19 I. Ahmed, M. B. K. Niazi, A. Hussain and Z. Jahan, *Polym. - Plast. Technol. Eng.*, 2018, **57**, 17–27.

20 I. Sroková, V. Tomanová, A. Ebringerová, A. Malovíková and T. Heinze, *Macromol. Mater. Eng.*, 2004, **289**, 63–69.

21 A. Besheer, J. Vogel, D. Glanz, J. Kressler, T. Groth and K. Mäder, *Mol. Pharm.*, 2009, **6**, 407–415.

22 M. P. Torres, A. S. Determan, G. L. Anderson, S. K. Mallapragada and B. Narasimhan, *Biomaterials*, 2007, **28**, 108–116.

23 Y. Dai, P. Yu, X. Zhang and R. Zhuo, *J. Catal.*, 2016, **337**, 65–71.

24 B. Müller, A. Paulus, B. Lettmann and U. Poth, *J. Appl. Polym. Sci.*, 1998, **69**, 2169–2174.

25 L. Leemans, R. Fayt, P. Teyssié and H. Uytterhoeven, *Polymer (Guildf).*, 1990, **31**, 106–109.

26 P. Saindane and R. N. Jagtap, *Prog. Org. Coatings*, 2015, **79**, 106–114.

27 A. Mühlebach, S. G. Gaynor and K. Matyjaszewski, *Macromolecules*, 1998, **31**, 6046–6052.

28 J. Li, H. Chen, G. Mu, J. Sun, Y. Sun, C. Wang, Q. Ren and J. Ji, *React. Funct. Polym.*, 2013, **73**, 1517–1522.

29 M. Mertoglu, S. Garnier, A. Laschewsky, K. Skrabania and J. Storsberg, *Polymer (Guildf).*, 2005, **46**, 7726–7740.

30 H. Götz, E. Harth, S. M. Schiller, C. W. Frank, W. Knoll and C. J. Hawker, *J. Polym. Sci. Part A Polym. Chem.*, 2002, **40**, 3379–3391.

31 G. R. Jones, R. Whitfield, A. Anastasaki, N. Risangud, A. Simula, D. J. Keddie and D. M. Haddleton, *Polym. Chem.*, 2018, **9**, 2382–2388.

32 R. Whitfield, A. Anastasaki, G. R. Jones and D. M. Haddleton, *Polym. Chem.*, 2018, **9**, 4395–4403.

33 W. Ning, P. Shang, J. Wu, X. Shi and S. Liu, *Polymers (Basel).*, 2018, **10**, 214.

34 M. Destarac, *Macromol. React. Eng.*, 2010, **4**, 165–179.

35 M. Destarac, *Polym. Chem.*, 2018, **9**, 4947–4967.

36 N. G. Engelis, A. Anastasaki, G. Nurumbetov, N. P. Truong, V. Nikolaou, A. Shegiwal, M. R. Whittaker, T. P. Davis and D. M. Haddleton, *Nat. Chem.*, 2017, **9**, 171–178.

37 N. G. Engelis, A. Anastasaki, R. Whitfield, G. R. Jones, E. Liarou, V. Nikolaou, G. Nurumbetov and D. M. Haddleton, *Macromolecules*, 2018, **51**, 336–342.

38 A. Gridnev, *J. Polym. Sci. Part A Polym. Chem.*, 2000, **38**, 1753–1766.

39 A. A. Gridnev and S. D. Ittel, *Chem. Rev.*, 2001, **101**, 3611–3659.

40 K. A. McEwan, S. Slavin, E. Tunnah and D. M. Haddleton, *Polym. Chem.*, 2013, **4**, 2608–2614.

41 J. P. A. Heuts and N. M. B. Smeets, *Polym. Chem.*, 2011, **2**, 2407–2423.

42 S. Slavin, E. Khoshdel and D. M. Haddleton, *Polym. Chem.*, 2012, **3**, 1461–1466.

43 US Pat., 5,928,829, 1999.

44 K. Adamsons, G. Blackman, B. Gregorovich, L. Lin and R. Matheson, Prog. Org. Coatings, 1997, **34**, 64–74.

45 A. A. Gridnev, *Polym. Sci. U.S.S.R.*, 1989, **31**, 2369–2376.

46 A. Bakac and J. H. Espenson, *J. Am. Chem. Soc.*, 1984, **106**, 5197–5202.

47 M. A. W. Lawrence, M. J. Celestine, E. T. Artis, L. S. Joseph, D. L. Esquivel, A. J. Ledbetter, D. M. Cropek, W. L. Jarrett, C. A. Bayse, M. I. Brewer and A. A. Holder, *Dalt. Trans.*, 2016, **45**, 10326–10342.

48 M. A. Duncan, in *Physical Chemistry of Cold Gas-Phase Functional Molecules and Clusters*, Springer Singapore, 2019, pp. 157–194.

49 K. Nakamoto, in *Infrared and Raman Spectra of Inorganic and Coordination Compounds, Applications in Coordination, Organometallic, and Bioinorganic Chemistry*, 2009.

50 E. E. Lawson, H. G. M. Edwards and A. F. Johnson, *Spectrochim. Acta Part A Mol. Spectrosc.*, 1994, **50**, 1899–1907.

51 W. Henderson and J. S. McIndoe, in *Mass Spectrometry of Inorganic, Coordination and Organometallic Compounds*, John Wiley & Sons, Ltd, 2005, pp. 127–173.

52 J. P. A. Heuts, G. E. Roberts and J. D. Biasutti, Aust. J. Chem., 2002, **55**, 381–398.

53 I. F. McConvey, D. Woods, M. Lewis, Q. Gan and P. Nancarrow, *Org. Process Res. Dev.*, 2012, **16**, 612–624.

54 D. M. Haddleton, E. Depaquis, E. J. Kelly, D. Kukulj, S. R. Morsley, S. A. F. Bon, M. D. Eason and A. G. Steward, *J. Polym. Sci. Part A Polym. Chem.*, 2001, **39**, 2378–2384.

55 T. S. Bhamra and B. J. Tighe, *Contact Lens Anterior Eye*, 2012, **35**, e8.

56 D. P. Nair, M. Podgórski, S. Chatani, T. Gong, W. Xi, C. R. Fenoli and C. N. Bowman, *Chem. Mater.*, 2014, **26**, 724–744.

57 A. K. Sinha and D. Equbal, *Asian J. Org. Chem.*, 2019, **8**, 32–47.

58 I. Gadwal, M. C. Stuparu and A. Khan, *Polym. Chem.*, 2015, **6**, 1393–1404.

59 K. F. Long, H. Wang, T. T. Dimos and C. N. Bowman, *Macromolecules*, 2021, **54**, 3093–3100.

60 S. H. Frayne and B. H. Northrop, *J. Org. Chem.*, 2018, **83**, 10370–10382.

61 H. C. Kolb, M. G. Finn and K. B. Sharpless, *Angew. Chemie - Int. Ed.*, 2001, **40**, 2004–2021.

62 E. M. Muzammil, A. Khan and M. C. Stuparu, *RSC Adv.*, 2017, **7**, 55874–55884.

63 V. Majer, V. Svoboda, H. V. (Henry V. . Kehiaian and International Union of Pure and Applied Chemistry., *Enthalpies of vaporization of organic compounds : a critical review and data compilation*, Blackwell Scientific, Oxford [Oxfordshire] ;, 1985.

64 K. Hatada, T. Kitayama, N. Fujimoto and T. Nishiura, *J. Macromol. Sci. Part A*, 1993, **30**, 645–667.

65 S. Zulfiqar, M. Zulfiqar, M. Nawaz, I. C. McNeill and J. G. Gorman, *Polym. Degrad. Stab.*, 1990, **30**, 195–203.

66 M. Ferriol, A. Gentilhomme, M. Cochez, N. Oget and J. L. Mieloszynski, *Polym. Degrad. Stab.*, 2003, **79**, 271–281.

67 L. E. Manring, *A. Rev. Plast. Mod*, 1969, **19**, 1515.

68 G. Z. Li, R. K. Randev, A. H. Soeriyadi, G. Rees, C. Boyer, Z. Tong, T. P. Davis, C. R. Becer and D. M. Haddleton, *Polym. Chem.*, 2010, **1**, 1196–1204.

69 A. B. Lowe, *Polym. Chem.*, 2014, **5**, 4820–4870.

70 Q. Zhang, S. Slavin, M. W. Jones, A. J. Haddleton and D. M. Haddleton, *Polym. Chem.*, 2012, **3**, 1016–1023.

71 J. P. Menzel, D. M. Haddleton and E. Khoshdel, *Polym. Prepr.*, 2010, **51**, 721–722.

# **Chapter 3**:

# Aza-Michael Reactions for the Synthesis of Linear Amphiphilic Polymethacrylates

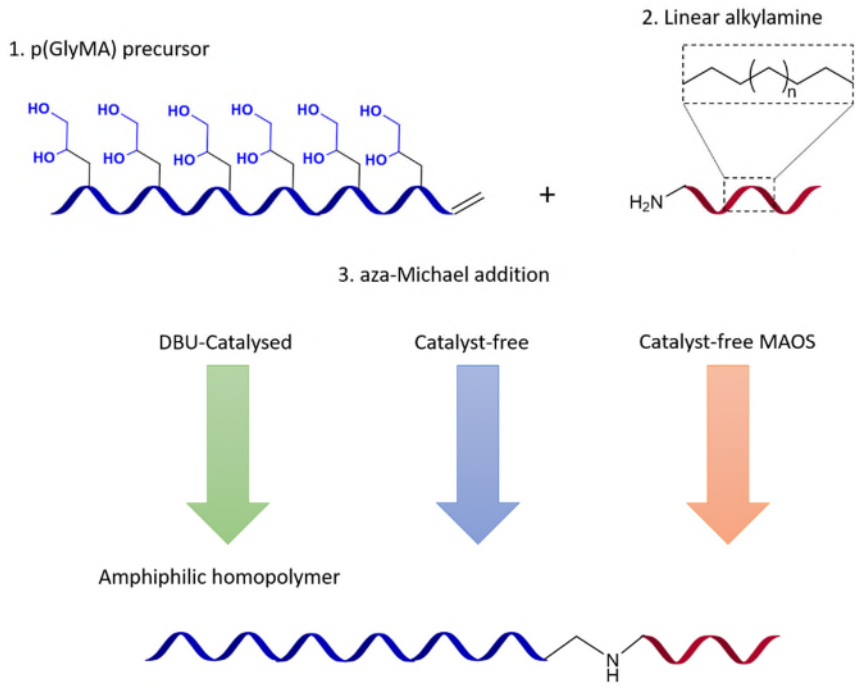

## 3.1 Introduction

Vinyl bonds substituted with electron withdrawing groups, e.g. carbonyls, can undergo addition reactions with nucleophiles. These types of reactions belong to a diverse and well-reported group of reaction labelled conjugate additions. In practice, the Michael addition, a subclass of conjugate additions, is one of the most well-known conjugate addition reaction that allows the formation of new covalent linkages under mild conditions. Its versatility stems from the fact that, while the reaction was historically developed using resonance stabilised carbanions, heteroatomic nucleophiles have also been utilised and were shown to have potential.[1] In chapter 2, the use of sulfur alcohol analogues was investigated, but because of the variety of starting reagents available, high atom economy and possible reaction conditions, aza-Michael reactions can be more attractive in the development of green / eco-friendly synthetic methods that follow the principles of green chemistry.[2]

Despite this, scientific work combining polymer chemistry and aza-Michael addition has been sporadic in the last 20 years, constituting only about 4% of the published

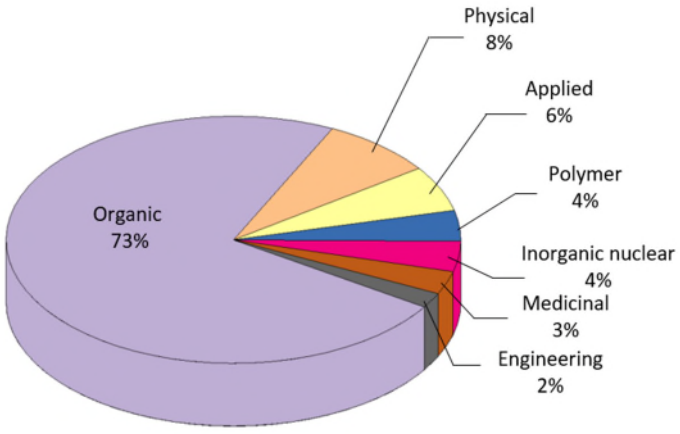


**Figure 3.1** Distribution of scientific publications on aza-Michael addition since 2000. (search performed with web of science. Keywords: “aza-Michael” OR “Michael-aza”).

literature, the vast majority being found within the field of organic chemistry, figure 3.1.

Recent literature though, illustrates this potential well. Gonzalez *et al*.[3] demonstrated an alternative route for the curing of acrylates through a 2-stage sequential reaction. The first step, an aza-Michael reaction between di/multifunctional amines and an excess of various diacrylates was carried out at room temperature, in a solvent-free environment, followed by a simple free-radical polymerisation of the excess diacrylate which led to the preparation of a new, environmentally friendly p(amino ester)-p(acrylate) family of thermosetting polymers.

Similarly, Baruah *et al*.[4] first synthesised tetraethyl-2,2′-[1,4-phenylenebis(methanyl-ylidene)]dimalonate (TPMD), a compound containing multiple esters and two internal α-β unsaturated carbonyl functionalities. Using TPMD's reactivity alongside oligoamine cross-linkers, the authors synthesised polymeric networks by creating amide linkages from the esters and aza-Michael bridges from the internal vinyl groups using aza-Michael addition. Here too, both reactions were performed solvent and catalyst-free at 25 and 50 °C. In addition to developing a green synthetic pathway, the authors also attempted to show the recyclability and self-healing properties of their gels by degrading the amides bonds through ultrasonication (at 25 °C) for 1h30 at pH 5.3. Although there was a loss of mechanical integrity, the authors did not address whether this affected aza-adducts but did observe that the aza-Michael addition using secondary amines was indeed reversible.

Lastly, Shen *et al*.[5] demonstrated the synthesis of dendrimers through a solvent-free iterative sequencing of aza-Michael addition and thiol-yne click reactions between but-3-ynyl acrylate, ethylenediamine, and cysteamine hydrochloride.

While these previous reports were some of the more prominent examples, aza-Michael addition can be found implemented in the synthesis of hydrogels,[6,7] flame retardants[8] or silicon-containing materials[9] amongst others.

Increasingly, industrial and academic research must focus attention not on what chemicals can be produced, but what processes should be employed for the synthesis of similar chemicals. One of the focus of this thesis is the synthesis of amphiphilic polymers that can efficiently act as stabilisers in water-based pigment suspensions and attempt their development in a more eco-friendly, green manner, one that can also match industrial criteria for a marketable product, should also be considered. To this end, this chapter reports the use of aza-Michael addition in combination with CCTP, as opposed to Michael-thiol addition. Several aspects of the synthesis are discussed: the shift towards more environmentally friendly solvents and their impact on the resulting polymers; the use and role of post-polymerisation modification catalysts and microwave-assisted synthesis for the reduction of reaction times. All polymers presented in this chapter (MKIII) are analysed using various techniques, namely GPC, TEM, TGA, and DSC; and their performance tested against the previously synthesised dispersant ranges (MKI & MKII) in chapter 4.

## 3.2 Results and Discussion

### 3.2.1 Initial Considerations

The synthesis of amphiphilic polymers using Michael-thiol addition was previously examined. To carry the reactions out, careful consideration was given to the selection of each compound used in the protocol. From solubility to price, different factors were taken into account and the best options were chosen for further testing. Industrial

research, however, aligns itself with market requirements. End-user feedback and sentiment plays a critical role in informing research goals.[10]

The impact of the agro-chemical industries started to be quantified in the early 2000's. The general public's awareness of the environmental repercussions of chemical processes led to increased pressure on governments to introduce regulations on the emission of volatile organic compounds.[11,12] Demand for more eco-friendly processes and the reduction of businesses' carbon footprints has had a profound impact of the industrial R&D landscape. As such, less toxic chemicals, as well as greener alternatives can be preferred to the chemically optimal ones.

In polymer chemistry for instance, certain components can have deleterious effects on health; monomers are often carcinogenic, but are safe after polymerisation. Glycerol monomethacrylate is however a biocompatible monomer that is generally considered to be safe.[13] Finally, we previously considered methanol as being the best option for the synthesis of p(GlyMA); with all components being freely soluble in the solvent, and a chain transfer constant of 540 that, while comparatively low for CCTP, could theoretically allow us to target a wide range of molecular weights. Methanol, however, is classified as having acute oral, dermal and tactile toxicity for humans while IPA is considered safer, exemplified by its extensive use during the novel coronavirus (COVID-19) pandemic.[14,15] Solvents are generally used extensively and often discarded after use, making them a concern that we wanted to focus on.

This chapter reports on the modification of the previously developed synthesis with considerations towards the impact of used chemicals on human and environmental health and the techniques used:

- Firstly, the synthesis of p(GlyMA) is modified, the solvent is exchanged with safer IPA.

- The malodorous thiols are removed from the protocol and their amine analogues introduced.
- The versatility of the aza-Michael catalyst is investigated by first optimising the reaction in its presence, and subsequently attempting reactions in catalyst-free conditions.
- Finally, the reduction in reaction times is investigated using microwave-assisted synthesis.

## 3.2.2 Synthesis of p(GlyMA) in Environmentally Benign Solvents

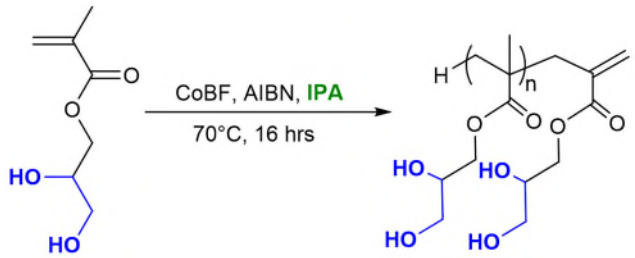


**Scheme 3.1** CCTP polymerisation conditions for the preparation of p(GlyMA).

The methodology described in chapter 2 was replicated here. For reasons explained in chapter 4, only molecular weights of 1-2.5 kDa were targeted. Initial experiments were carried out with 10 and 30 catalyst loadings and a 0.5 mol% ratio of AIBN initiator to monomer. It was, however, quickly observed that all three polymerisations resulted in relatively high molecular weight polymers. In each case, the polymers precipitated out of solution during the polymerisation, or upon cooling. Concerns over the repeatability of the reactions prompted us to test higher catalyst loadings.

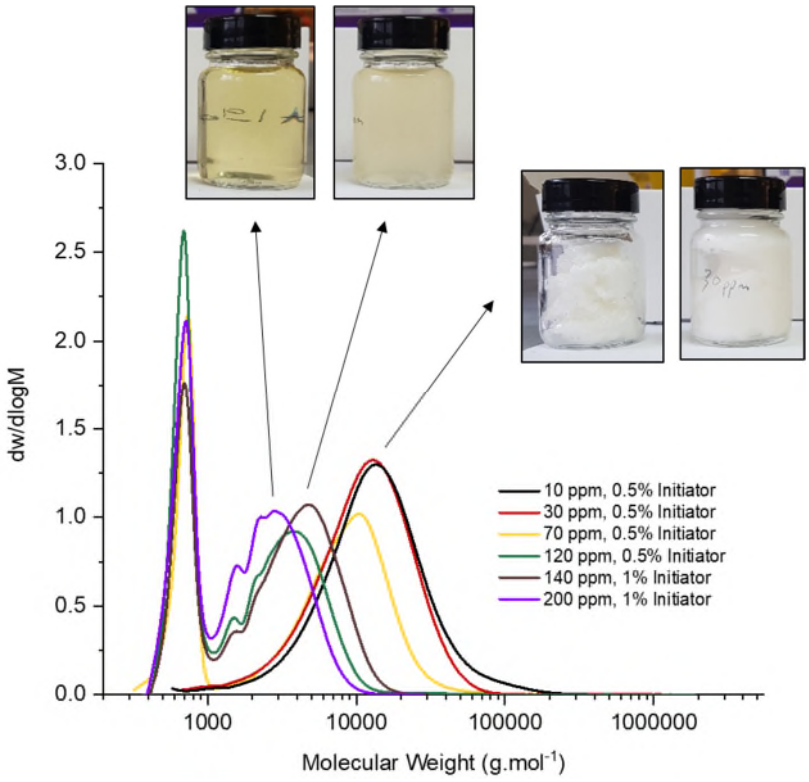


**Figure 3.2** GPC traces (DMF, 50 °C) of p(GlyMA) polymerised in IPA prepared with various catalyst loadings and 0.5 or 1 mol% initiator to monomer ratio.

| Entry | Monomer | CoBF loading / ppm | V-601 / mol% of monomer | Solvent | Percentage leftover monomer[a] | $DP_{GPC,Mw}$[b] | $M_{n,GPC}$ / kg.mol$^{-1}$ | $M_{n,NMR}$ / kg.mol$^{-1}$ | Đ |
|---|---|---|---|---|---|---|---|---|---|
| 1 | GlyMA | 10 | 0.5 | IPA | N/A | 57 | 8.9 | 9.1 | 2.00 |
| 2 | GlyMA | 30 | 0.5 | IPA | N/A | 46 | 7.8 | 7.4 | 1.88 |
| 3 | GlyMA | 50 | 0.5 | IPA | N/A | 40 | 6.4 | 6.4 | 1.99 |
| 4 | GlyMA | 70 | 0.5 | IPA | 33.14% | 31 | 6.1 | 5.0 | 1.61 |
| 5 | GlyMA | 120 | 0.5 | IPA | 45.18% | 13 | 2.7 | 2.1 | 1.31 |
| 6 | GlyMA | 120 | 1 | IPA | 6.70% | 26 | 4.1 | 4.2 | 2.10 |
| 7 | GlyMA | 140 | 1 | IPA | 31.28% | 14 | 3.1 | 2.2 | 1.43 |
| 8 | GlyMA | 200 | 1 | IPA | 33.83% | 8 | 1.9 | 1.3 | 1.35 |
| 9 | GlyMA | 20 | 0.5 | EtOAc | 18.33% | 20.1 | 3.3 | 3.2 | 1.50 |
| 10 | GlyMA | 40 | 0.5 | EtOAc | N/A | 14 | 2.5 | 2.2 | 1.81 |

**Table 3.1** GlyMA polymerisations attempted for this study. [a]determined by GPC. [b]DP = $M_w/2M_0$.

At 70 ppm, with the reduction of the average molecular weight to 5.0 kDa (calculated by NMR), there was a discernible monomeric peak, amounting to around 30% of the solution. This was a result of the increased concentration of CoBF that led to monomer being the product of the catalytic cycle. As the targeted molecular weight was not reached, higher catalyst loadings were needed and any catalyst loading beyond 70 ppm had a discernible peak arising from the monomer.

Further experiments showed that a 200 ppm CoBF loading with a 1 mol% initiator to monomer ratio were sufficient to reduce molecular weights to about 1.3 kDa, (figure 3.2 & table 3.1). Under these conditions, the product did not precipitate and around 30% of the final mixture consisted of monomer. Whilst it seemed difficult to circumvent the apparition of monomer, the polymer was easily purified by precipitation in chloroform, SI figure S3.1.

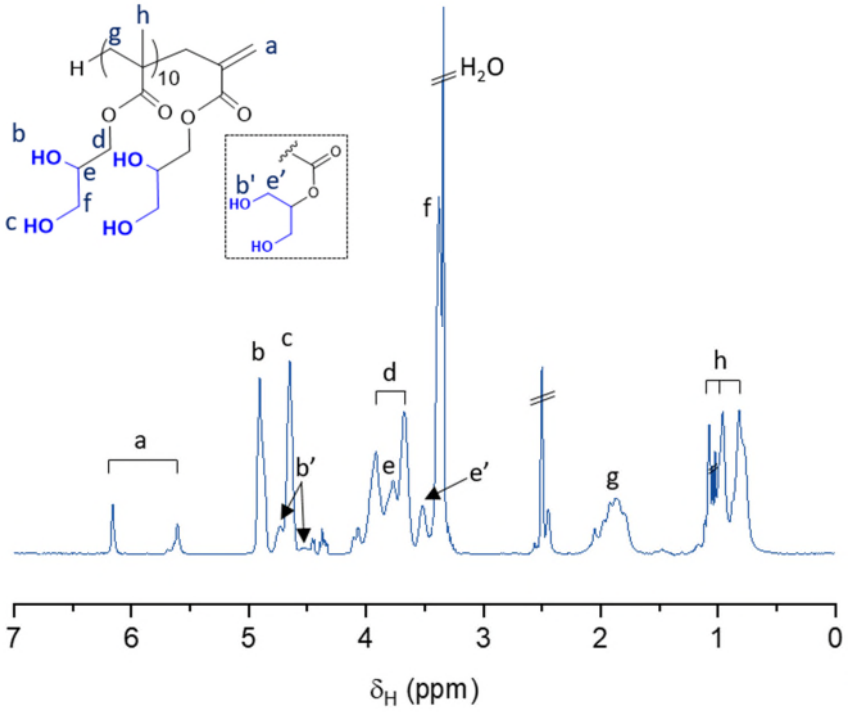


**Figure 3.3** Typical $^{1}$H-NMR (DMSO-$d_6$, 400 MHz at 25 °C) spectrum of p(GlyMA)$_{10}$ (catalyst loading: 200 ppm) prepared by CCTP in IPA.

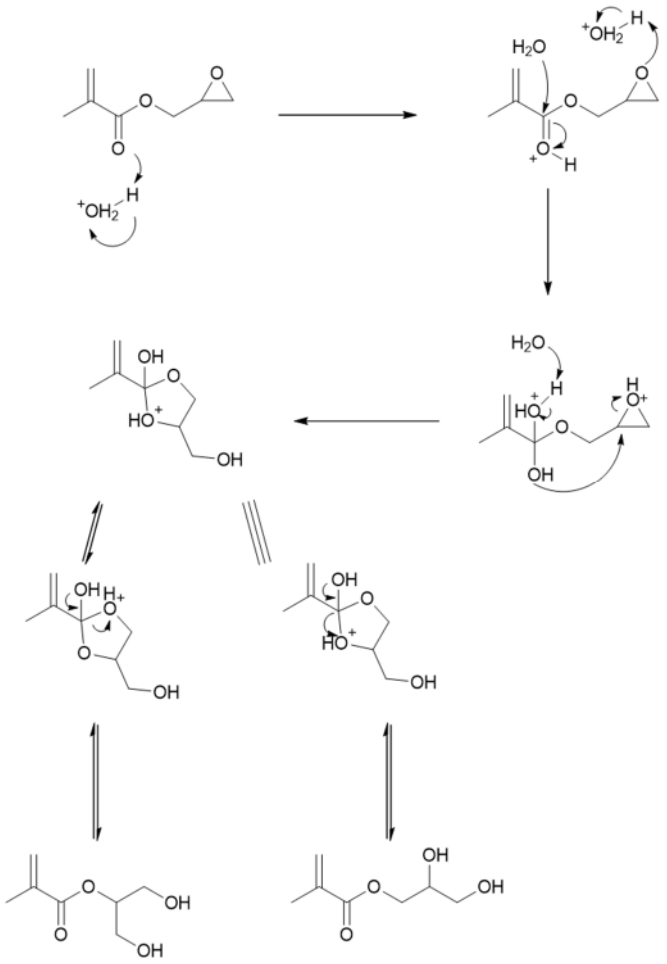

**Scheme 3.2** Mechanism of ring opening of GMA's epoxide side-chain by water.

It was further noticed that the monomer should be removed shortly after polymerisation as after a 2-week period, the crude mixture showed signs of autopolymerisation in the GPC trace, which led to the presence of high molecular weight polymers that could, if left in the mixture, interfere with further post-polymerisation modifications, SI figure S3.2.

Ethyl acetate is an interesting and low-toxicity solvent often used on industrial scales for synthesis. Several polymerisation attempts all led to the gradual precipitation mid-reaction of polymer, even under high temperatures, accompanied by significant batch-

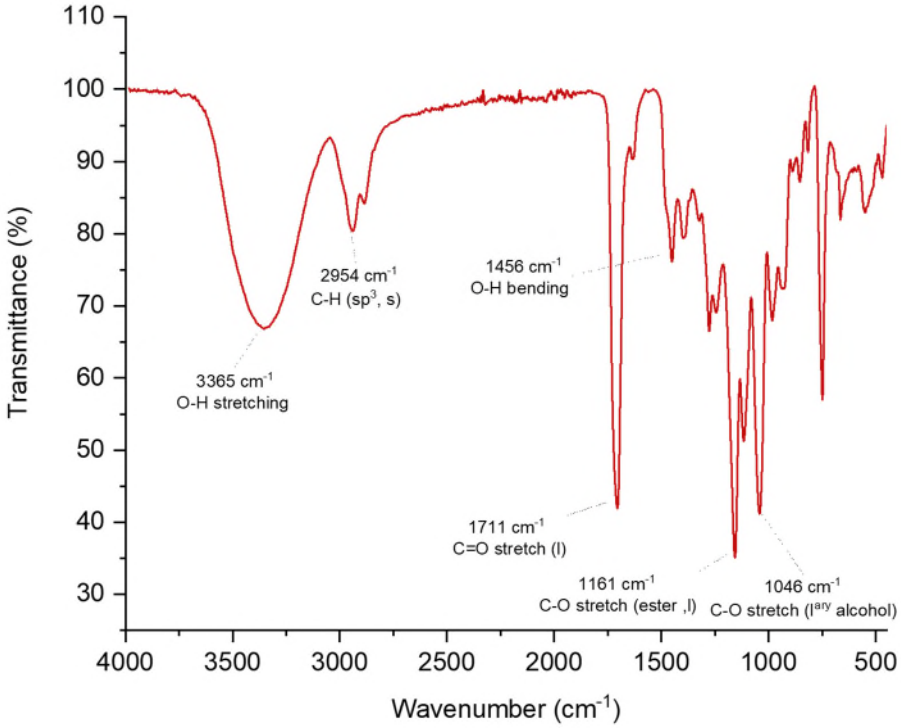


**Figure 3.4** FT-IR spectrum of p(GlyMA)$_{10}$ prepared by CCTP in IPA (catalyst loading: 200 ppm).

to-batch variance, which made EtOAc unsuitable for this polymerisation, SI figure S3.3.

The structure of the polymer (table 3.1, entry 8) can be verified using $^{1}$H-NMR (figure 3.3). Glycerol monomethacrylate is a hydrophilic monomer most often obtained by the hydrolysis of the GMA epoxide with water. The process was shown to produce two 1,3- and 2,3- isomers, by Shaw *et al.*,[16] with a mechanism following that is shown in scheme 3.2. Both isomers are identifiable through $^{1}$H-NMR with hydroxy peaks visible from 4.50 to 5 ppm and methylene peaks at 3.50 ppm. All other expected peaks are otherwise clearly visible in DMSO-d$_6$ $^{1}$H-NMR.

FT-IR shows the primary alcohol peaks at around 3365 and 1045 cm$^{-1}$, for I$^{ary}$ alcohol O-H and C-O stretching respectively, figure 3.4. We also see an -OH bending peak at 1456 cm$^{-1}$ and the ester peaks at 1711 and 1160 cm$^{-1}$.

## 3.2.3 Initial Study and Optimisation of the aza-Michael Reaction of Hydrophobic Alkylamines with p(GlyMA), MKIII

While Michael-thiol additions generally require a nitrogen or phosphorus-centered catalyst, aza-Michael can proceed without the addition of catalysts. Nevertheless, reactions can also be mediated by strong bases such as 1,8-diazabicyclo[5.4.0]undec-7-ene (DBU).

### *3.2.3.1 Initial study – DBU-Catalysed Reactions*

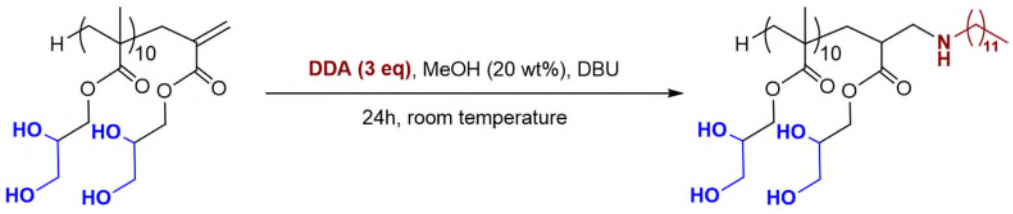


**Scheme 3.3** Initial aza-Michael conditions for the CCTP preparation of p(GlyMA)$_n$(DDA).

A series of reactions were carried out in order to assess the reactivity of p(GlyMA)$_{10}$ towards hydrophobic alkylamines. Initially, reactions were carried out on a 50 mg scale of polymer at room temperature with a 3-fold excess of dodecylamine (DDA), which was chosen as a model compound – long aliphatic chain-containing dispersants have shown promising performance as stabilisers for CB suspensions, particularly with C12 anchors, see chapter 4 – as well as equimolar amounts of DBU to DDA.[17] Methanol, which was used as a point of comparison, and IPA have been favoured as solvents as protic polar media have been shown to significantly increase rates of reaction through external proton transfer activation.[18]

Although it was found advantageous to carry out reactions under inert atmosphere with the thiol-based addition in order to avoid atmospheric oxidation of DMPP,[19] no

| Entry | Polymer | Amine | Eq amine (r ratio) | Temperature / °C | Reaction time / hr | Catalyst | Eq catalyst | Solvent | Solid content / % | Yield /% |
|---|---|---|---|---|---|---|---|---|---|---|
| 1 | $p(GlyMA)_{10}$ | DDA | 3.0 (0.33) | RT | 24 | DBU | Equimolar to DDA | MeOH | 20 | >99 |
| 2 | $p(GlyMA)_{10}$ | DDA | 1 .01 (1) | RT | 24 | DBU | Equimolar to DDA | MeOH | 20 | ≈50 |
| 3 | $p(GlyMA)_{10}$ | DDA | 3.0 (0.33) | RT | 24 | DBU | Equimolar to DDA | MeOH | 50 | >99 |

**Table 3.2** Formulations 1-3 attempted for the catalysed synthesis of $p(GlyMA)_{10}$(DDA).

such precaution was required with aza-Michael additions. While it was reported that DBU is sensitive to carbon dioxide,[20] it is unlikely that this bore any impact on our reactions ($CO_2$ only making up about 0.04% of the ambient atmosphere, discussed later). This, combined with DMPP's foul smell, made the use of DBU and aza-Michael addition more desirable. Reactions were followed by proton NMR through the disappearance of the vinyl peaks; entry 1 showed near full conversion within 24 hours, table 3.2.

Reductions of the amount of amine to 1.01 equivalent, or increases of solid content to 50%, were attempted to reduce the necessary amount of either solvent or starting reagent. In the former, conversion was limited to around 50% after 24 hours. In the latter, we observed as expected, that conversions were still > 99%, figure S3.4.

The minimum amount of DDA required to carry the reaction to > 99% conversion is found between 1 and 3 equivalents. In their review, Genest *et al.*[21] report that even though both primary and secondary amines are reactive in aza-Michael additions, primary amines can be susceptible to the formation of bis-adducts in the presence a surplus of vinyl groups, whereby amines undergo two successive Michael additions.

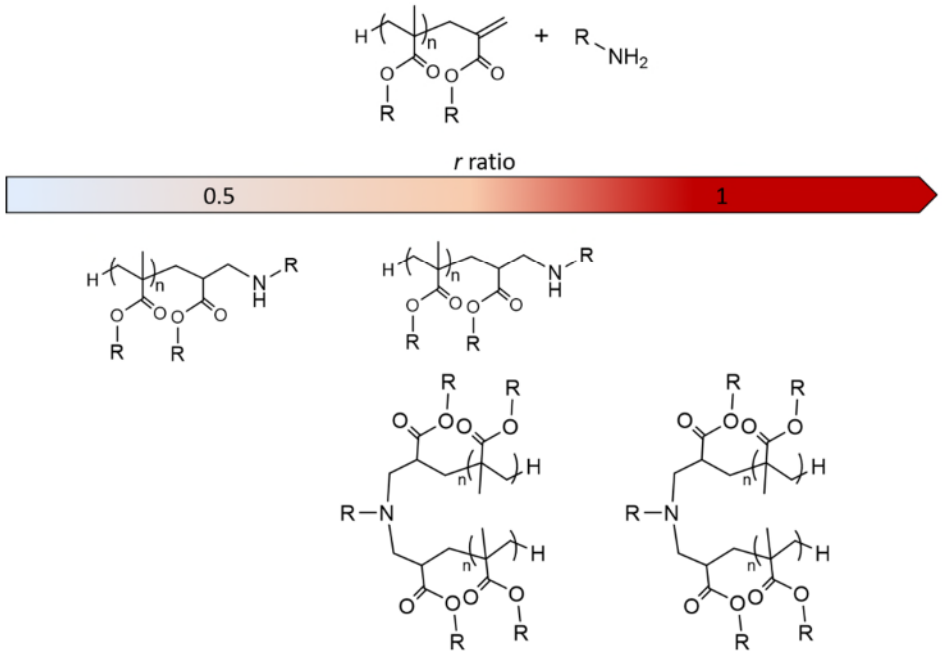


**Figure 3.5** Relationship between *r* ratio and formation of mono and/or bis adducts during aza-Michael addition of amines to CCTP macromonomers.

A ratio, *r*, can be established, with:

$$r = \frac{n(C{=}C)}{n(N{-}H)} \qquad \text{(eqn. 1)}$$

where, when $r$ = 0.5, the mono-adduct represents the majority product with low chances of bis-adduct being observed. However, as this value increases, bis-adducts are more likely to be encountered and, at any point when $r \geq 1$, the bis-adduct is the main addition product, figure 3.5.

Looking at the *r* ratios in table 3.2, it is likely that reactions from entry 2 were subject to bis-addition. A consensus must be reached where the risk of production of bis-adduct is minimised while keeping the reaction times practical. Ratios were kept within a ± 0.20 window thereafter, to minimize the risk of bis-adduct apparition.

As such, as can be seen from table 3.3, a second round of optimisation was attempted. The amount of amine was set to 1.5 equivalents; and while the reactions at room temperature (entry 4) did not go beyond 55% conversion. An increase of reaction temperature to 50 °C was enough to sustain the reaction to > 99% conversion within

| Entry | Polymer | Amine | Eq amine (r ratio) | Temperature / °C | Reaction time / hr | Catalyst | Eq catalyst | Solvent | Solid content / % | Yield / % |
|---|---|---|---|---|---|---|---|---|---|---|
| 4 | $p(GlyMA)_{10}$ | DDA | 1.5 (0.67) | RT | 24 | DBU | Equimolar to DDA | MeOH | 50 | 55.0 |
| 5 | $p(GlyMA)_{10}$ | DDA | 1.5 (0.67) | 50 | 15 | DBU | Equimolar to DDA | MeOH | 50 | >99 |
| 6 | $p(GlyMA)_{10}$ | DDA | 1.5 (0.67) | RT | 24 | DBU | Equimolar to DDA | IPA | 50 | N/A |
| 7 | $p(GlyMA)_{10}$ | DDA | 1.5 (0.67) | 50 | 15 | DBU | Equimolar to DDA | IPA | 50 | >99 |

**Table 3.3** Formulations 4-7 attempted for the catalysed synthesis of $p(GlyMA)_{10}$(DDA).

15 hours. This increase in temperature proved to be important as $p(GlyMA)_{10}$ is scarcely soluble in IPA, this made the aza-Michael reaction at room impossible, and an increase in temperature was, in those cases, necessary (entries 6 & 7).

The use of IPA offered an interesting alternative for purification by harnessing the ambivalent solubility of $p(GlyMA)_{10}$ in IPA. In repeating reactions from entry 7, heating cycles to 60 °C, followed by a cooling step to 0 °C; which respectively solubilised the product or brought it out of solution were used. The cycle was repeated several times and the precipitated polymer was subsequently filtered and volatiles removed. This technique however, did not to lend itself to the preparation of a pure product as a significant amount of leftover catalyst was found, figure S3.6. It was eventually decided to purify the polymers by precipitation in chloroform, in which the functionalised polymers were insoluble.

Our final conditions, using DBU as catalyst, consisted of a 1.5 equivalent of hydrophobic linear alkylamines, an equimolar amount of catalyst relative to the amine, with a 50% solid content IPA, at 50 °C for 15 hours. These conditions provided a starting point for the analysis of the reactions in a catalyst-free environment.

### *3.2.3.2 Optimisation – Investigation into Catalyst-Free Reactions*

Amines are both basic and nucleophilic. With a sufficiently nucleophilic amine, there is an opportunity to carry out aza-Michael reactions under catalyst-free conditions.[4,18,22,23] In general, it also seems that aromatic amines are more inert than aliphatic amines towards aza-Michael additions, as was for example reported by Duan *et al*. and Shaikh *et al*.[24,25] Moreover, linear aliphatic amines seemingly have a capacity to react without the presence of a catalyst.[22]

A catalyst-free reaction would be advantageous in that some nitrogen-containing compounds are mostly non-biodegradable[26] and DBU, in particular, is reported to have long term aquatic hazards. Its removal would bypass a potential health hazard. It has also been shown that a solid zwitterionic $[DBUH^+][HCO_3^-]$ salt can be produced by the reaction of DBU with $CO_2$ in the presence of water.[20] p(GlyMA) is hygroscopic, it is therefore possible that water molecules from solvents, or moisture from the air be retained. Removing DBU thus serves as an additional insurance that this reaction does not happen. Nine reactions with various sets of conditions were carried out, table 3.4. With 1.5 equivalent of DDA at 50 °C (entries 8 and 9), we observed conversions of 72 and 64% after 16 hours with MeOH and IPA, with little increase after an additional 8 hours, figure 3.6. It seems a doubling of the amount of amine (entry 10 & 11) is required to reach high conversion within the same 15-hour window as was observed

| Entry | Polymer | Amine | Eq amine (r ratio) | Temperature / °C | Solvent | Solid content / % |
|---|---|---|---|---|---|---|
| **8** | $p(GlyMA)_{10}$ | DDA | 1.5 (0.67) | 50 | MeOH | 50 |
| **9** | $p(GlyMA)_{10}$ | DDA | 1.5 (0.67) | 50 | IPA | 50 |
| **10** | $p(GlyMA)_{10}$ | DDA | 3.0 (0.33) | 50 | MeOH | 50 |
| **11** | $p(GlyMA)_{10}$ | DDA | 3.0 (0.33) | 50 | IPA | 50 |
| **12** | $p(GlyMA)_{10}$ | DDA | 3.0 (0.33) | 25 | IPA | 50 |
| **13** | $p(GlyMA)_{10}$ | DDA | 1.5 (0.67) | 25 | IPA | 50 |
| **14** | $p(GlyMA)_{10}$ | DDA | 1.5 (0.67) | 25 | MeOH | 50 |
| **15** | $p(GlyMA)_{10}$ | DDA | 3.0 (0.33) | 25 | MeOH | 50 |

**Table 3.4** Formulations 8-15 attempted for the catalyst-free synthesis of $p(GlyMA)_{10}(DDA)$.

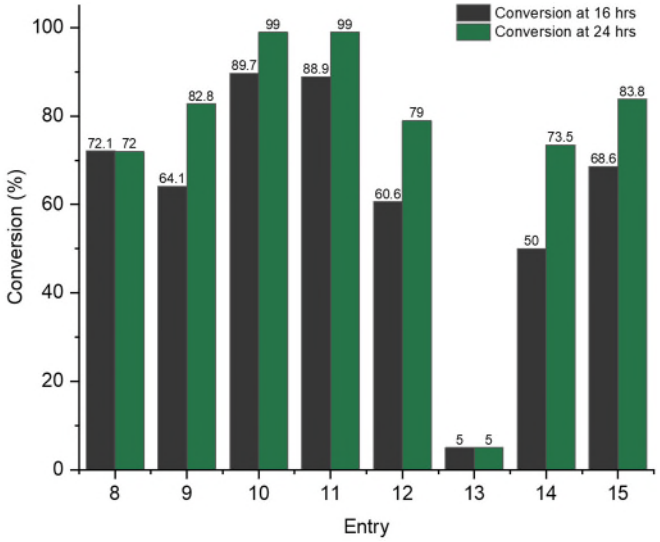


**Figure 3.6** Conversions at 16 and 24 hours for reactions 8-15.

previously with entries 5 & 7. In general, room temperature reactions did not yield satisfactory results. However, mostly similar conversions were observed, regardless of which solvent was used at elevated temperatures, which comforted us in the idea that using IPA was indeed possible without significant downsides.

#### *3.2.3.3 Microwave-Assisted Catalyst-Free Synthesis, Synthesis of MKIII*

We were curious to see whether it would be possible to use microwave reactors for these reactions which, if successful, would allow us to demonstrate the versatility of

microwave-assisted synthesis (MAOS); by carrying out different organic reactions (epoxide ring-opening or aza-Michael addition), and obtain a variety of amphiphilic polymers.

| Entry | Polymer | Amine | Eq amine (r ratio) | Temperature / °C | Solvent | Solid content / % | Time / min | Stirring | Pressure / bar | $T_{boil}$ / °C | Conversion / % |
|---|---|---|---|---|---|---|---|---|---|---|---|
| **16** | $p(GlyMA)_{10}$ | DDA | 3.0 (0.33) | 120 | IPA | 50 | 10 | N | 1 | 82.5 | 55.2 |
| **17** | $p(GlyMA)_{10}$ | DDA | 3.0 (0.33) | 120 | IPA | 50 | 30 | N | 1 | 82.5 | 75.3 |
| **18** | $p(GlyMA)_{10}$ | DDA | 3.0 (0.33) | 150 | IPA | 50 | 10 | N | 5 | 125.6 | 76.8 |
| **19** | $p(GlyMA)_{10}$ | DDA | 3.0 (0.33) | 150 | IPA | 50 | 10 | Y | 5 | 125.6 | 60 |
| **20** | $p(GlyMA)_{10}$ | DDA | 3.0 (0.33) | 150 | IPA | 50 | 60 | Y | 5 | 125.6 | 85.7 |
| **21** | $p(GlyMA)_{10}$ | DDA | 3.0 (0.33) | 150 | IPA | 50 | 120 | Y | 5 | 125.6 | >99 |
| **22** | $p(GlyMA)_{10}$ | DDA | 1 .01 (1) | 150 | IPA | 50 | 120 | Y | 5 | 125.6 | 57.2 |
| **23** | $p(GlyMA)_{10}$ | DDA | 1 .01 (1) | 160 | IPA | 50 | 120 | Y | 6 | 131.19 | 50.6 |
| **24** | $p(GlyMA)_{10}$ | DDA | 2.0 (0.5) | 150 | IPA | 50 | 120 | Y | 5 | 125.6 | >99 |

**Table 3.5** Formulations 16-24 attempted for the catalyst-free MAOS synthesis of $p(GlyMA)_{10}$(DDA).

MAOS is often touted as a benchmark tool for the 21st century. While there is still an ongoing discussion on the precise effects of microwaves, particularly regarding the non-thermal effect,[27] it is undeniable that this technique allows a significant reduction in reaction time. On a laboratory scale, sealed-vessel MAOS can be energy efficient compared to traditional heating, as was reported by Moseley *et al*.[28] Overall, the authors suggest that while efficiency at small scales can be comparatively low, MAOS can become significantly energy efficient when scaled-up and used with industrial multimodal reactors. In turn, this would go in the direction of the 6th principle of green chemistry (reactions should be designed for energy efficiency) and would be a key factor in making the process economically viable.[2]

Starting from the previous successful formulation from part 3.2.3.2 (entry 10), we started here with 3 equivalents of amine and gradually attempted various combinations of DDA equivalents, reaction temperature and time, table 3.5. $p(GlyMA)_{10}$ was solubilised in IPA in a separate vial at 60 °C prior to adding the amine and transferring the solution into a microwave vial.

If the pressure of a system develops too quickly within the reactor, an explosion might occur, calculating these limits would be an important piece of information.

Calculating the boiling point of IPA for the different reactions as was done previously using the Clausius-Clapeyron relations yields the temperatures that are reported in table 3.5. We can see that the set microwave temperatures are in most cases above $T_{boil}$, which was not observed with acetonitrile (chapter 2), and could be the reason for an uncontrolled increase in pressure during the early stages of the heating process. We therefore set to keep the set reaction temperature at, or below 150 °C.

From entry 21, it was found that 2 hours and 150 °C is sufficient to give a near-complete conversion. Subsequent reactions further revealed that a reduction to 2 equivalents of DDA was possible (entry 24) and that; interestingly, the hypothesis in part 3.2.3.1 could be verified as none of the MAOS reactions where 1 equivalent of DDA was used showed yields beyond 50% (entries 22/23).

To study the structure of the polymers and probe whether side reactions did occur, we have previously used MALDI-ToF. Usually, polymers are dissolved in volatile solvents such as THF or chloroform however, as $p(GlyMA)_{10}(DDA)$ is insoluble in these solvents, they could not be considered. Another option consisted in using DMF in water mixtures, which could allow the dissolving of the polymer. However, with these polymers and DCTB as matrix, this proved unsuccessful, figure S3.7. $^{13}$C-NMR nevertheless offered another alternative.

In order to verify whether side-reactions did or did not occur within the studied reaction systems, we carried out the following reactions:

- Reaction A, catalysed reaction: 500 mg of $p(GlyMA)_{10}$, 1.5 equivalents of amines, equimolar amounts of DBU to vinyl groups, in IPA (50% solid content) at 50 °C for 16 hours.
- Reaction B, catalyst-free reaction: 500 mg of $p(GlyMA)_{10}$, 3 equivalents of amines, IPA (50% solid content) at 50 °C for 24 hours.
- Reaction C, catalyst-free MAOS: 500 mg of $p(GlyMA)_{10}$, 3 equivalents of amines, IPA (50% solid content) at 150 °C for 2 hours.

The $^{13}$C-NMR spectra of the resulting polymers alongside a $t_0$ spectrum, figure 3.7. There are no unreacted polymers in the mixtures as no vinyl peaks are visible.

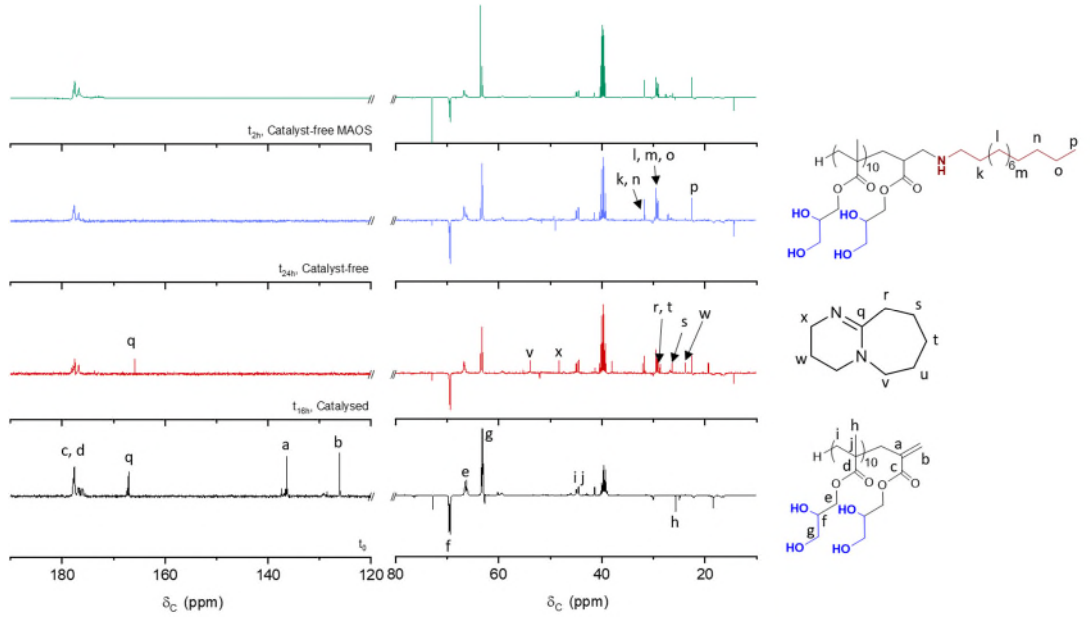


**Figure 3.7** $^{13}$C-NMR spectra (DMSO-$d_6$, 400 MHz at 25 °C) of p(GlyMA)$_{10}$(DDA) synthesised by, from top to bottom, catalyst-free MAOS, catalyst-free reaction and DBU-catalysed reaction alongside a spectrum of unreacted p(GMA)$_{10}$.

Furthermore, although products were thoroughly purified, we do observe some catalyst still present in the polymer in the case of the catalysed reaction, while the two other modes of reaction generate much cleaner spectra.

The most likely side reaction that can occur is the aminolysis of the terminal side-chain ester. This would in part be due to the aza-Michael addition mechanism that involves a delocalisation of charges to the carbonyl group, exposing it to reacting with dodecylamine. The alkoxy group is not a particularly good leaving group but this implies investigating the carbonyl groups peaks as this could provide insights.

Due to the lack of the ability to use MALDI-ToF, we cannot rule out side-reactions happening, as there is no clear indication that points to this occurring, either on the carbon $^{13}$C-NMR or GPC (discussed later).

### 3.2.4 Scaled-Up Synthesis and Characterisation of the MKIII Range Candidates

Having found a MAOS formulation that allowed us to obtain to obtain polymers with minimal side-reactions and high conversion within 2 hours, we needed to then attempt scaling up. Monomodal instruments, which are widespread in research laboratories are typically built to run vessels sequentially with the help of an auto-sampler and cannot run multiple samples simultaneously. This is because most studies focus on the optimisation of existing organic reactions. Consequently, monomodal reactor vessels are generally small, with most published research being performed on scales ≤ 1 g.[29] This reflects a current limitation of MAOS. However, because these reactions were optimised at 50% solid content, low volumes of solvent were normally required, and aza-Michael reactions were scaled up to 5 g of polymer with relative ease.

Two similar alkylamines, nonyl- and dodecylamine, were used for scaled-up reactions following the method discussed previously. The temperature was manually increased to 150 °C and the reaction left to progress for two hours. The products were subsequently purified and dried.

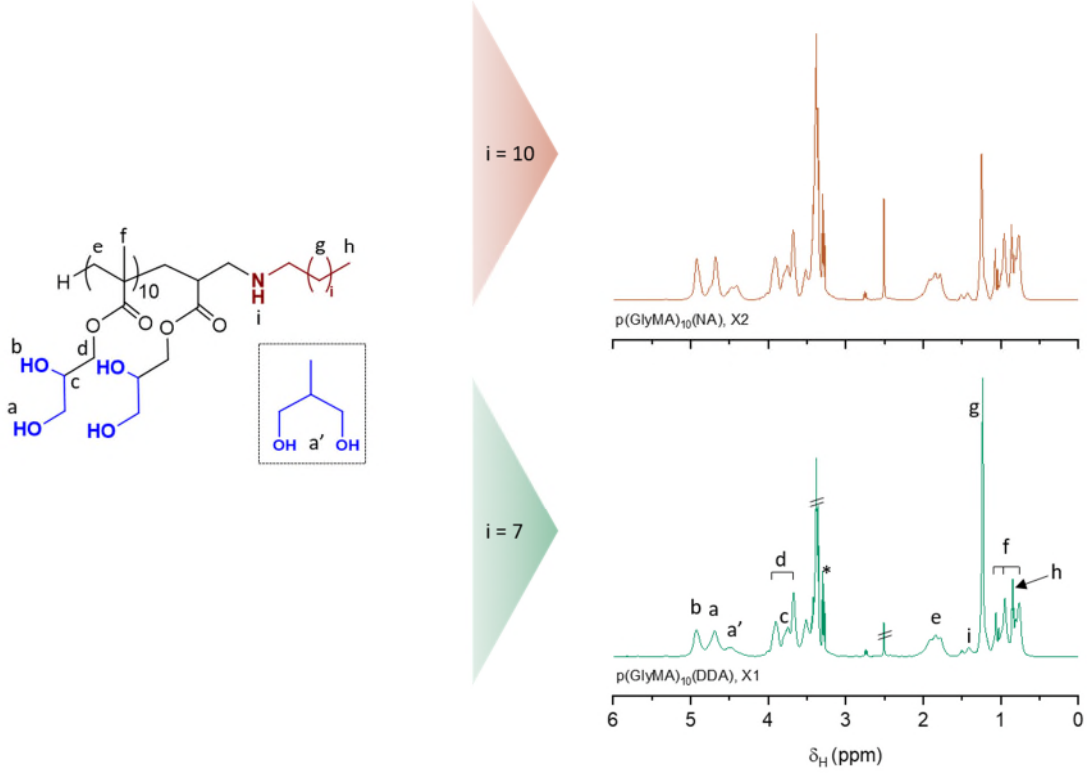


**Figure 3.8** $^{1}$H-NMR spectra (DMSO-$d_6$, 400 MHz at 25 °C) of nonyl- (bottom) and dodecylamine (top) functionalised p(GlyMA)$_{10}$. *diethyl ether impurity.

Figure 3.8 shows the $^{1}$H-NMR spectra for both purified products (**X1** = p(GlyMA)$_{10}$(DDA), **X2** = p(GlyMA)$_{10}$(NA)). Both spectra show identical peak distribution, with a difference in alkyl chain peak intensity (the C12 chain leads to a more intense peak at 1.20 ppm). $^{13}$C-NMR spectra are similar to the previously described spectra (part 3.2.3.3) and are provided in the supplementary information, figure S3.8.

DLS data was consistent with what was expected from linear aliphatic hydrophobic segments, as was discussed previously, with C9 and C12 carbons: respectively 482.5 ± 49.7 nm (PDi: 0.031 ± 0.0059) and 7.54 ± 0.17 nm (PDi: 0.055 ± 0.0024).

Similarly to what was seen with the MKII range, we do not modify the main hydrophilic block's chemistry, which leads to a positive shift in GPC traces, figure

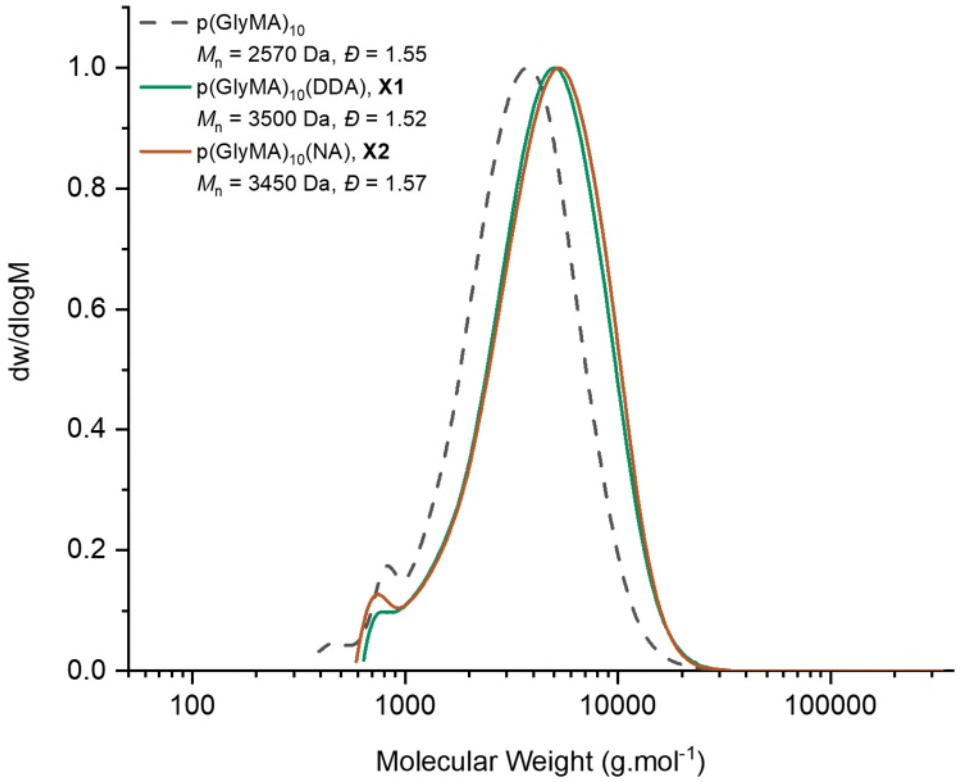


**Figure 3.9** GPC traces (DMF, 50 °C) of **X1** and **X2** compared to p(GlyMA)$_{10}$.

3.9. Moreover, high molecular weight shoulders were not detected, which could be an indicator of aminolysis or bis-addition side reactions.

Two thermal degradation inflection points were found at approximately 330 and 414 °C on the TGA curve, figure 3.10. As previously theorised, because the 3$^{rd}$ step stems from random chain scission, the peak is not expected to change. However, comparisons can be made between the **Q6**/**X1** and **Q5**/**X2** pairs, which only differ by the type of bridge linking the two blocks, respectively thiol and aza bridges. For the MKII range polymers, the 2$^{nd}$ step was found at 315 ºC, which is significantly lower than what is seen for MKIII polymers (330 ºC). Furthermore, very little amount of degradation is seen from this step for **X1** and **X2**. We theorised earlier that, in our functionalised polymers, the 2$^{nd}$ step inflection is dependent on a retro-Michael reaction first occurring which yields the vinyl-ended polymer that can undergo degradation. It seems then, that the aza-Michael adduct is more thermally stable and

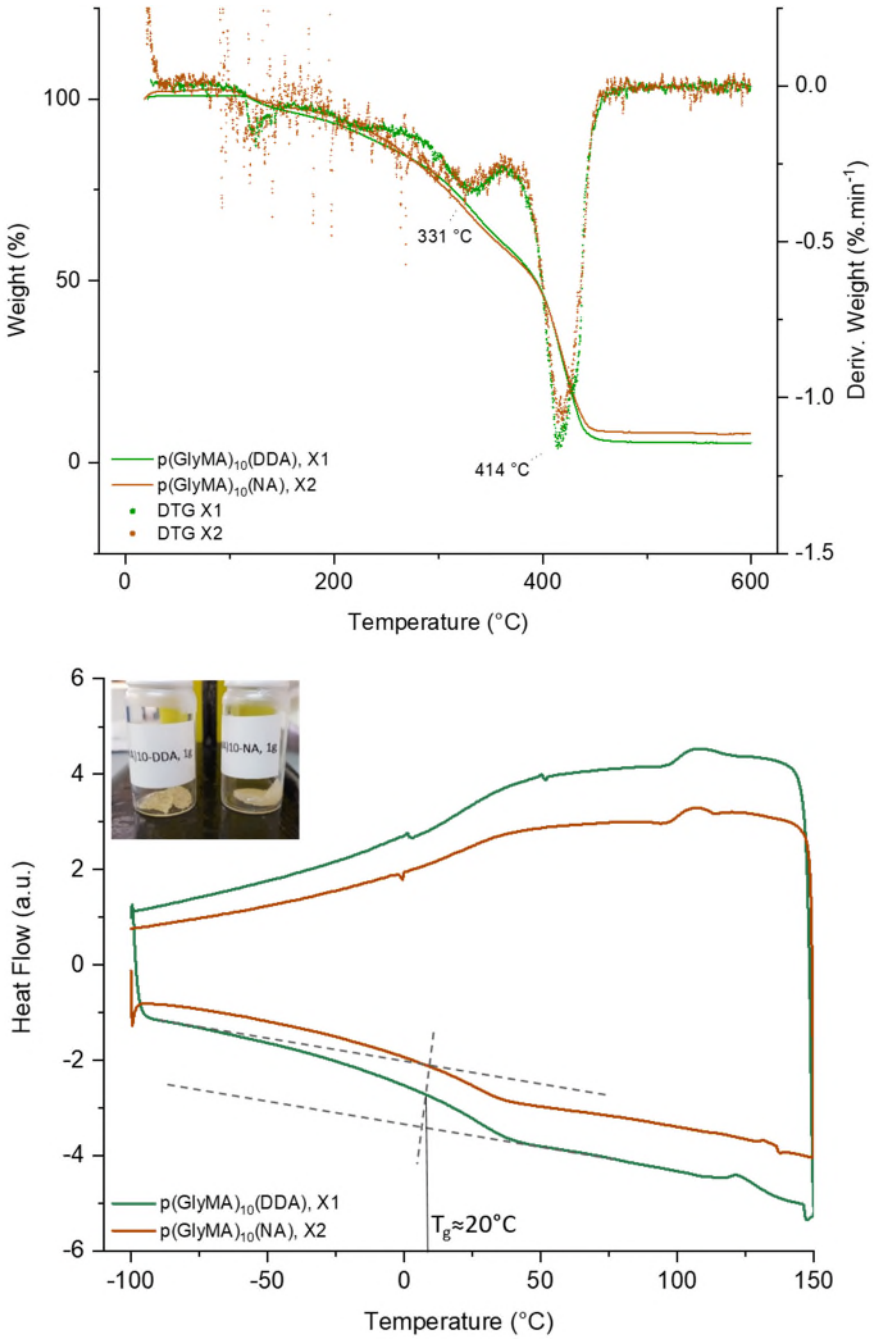


**Figure 3.10** TGA and DTG (top) and DSC (bottom) curves of **X1** and **X2**.

less prone to retro-reactions than Michael-thiol adducts. Both polymeric products are "tacky" at room temperature. This is due to the polymers' low $T_g$, around 20 °C, which is shown on the DSC curves. In addition, the TEM images, as shown in figure 3.11, do show the hallmarks of self-assembled amphiphilic polymers.

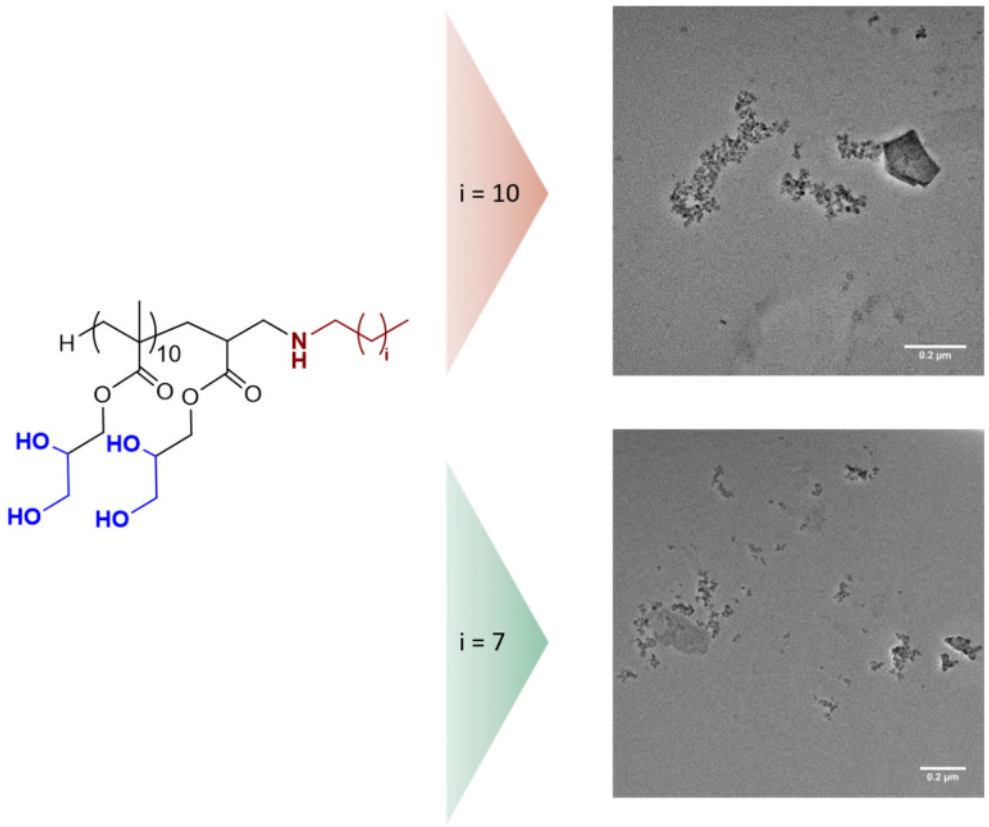


**Figure 3.11** TEM images of **X1** (top) and **X2** (bottom). Images taken by Georgios Patias.

## 3.3 Conclusions

In this work, we explore the methodology developed in the second chapter in an attempt to both produce a greener polymer synthesis process, but also make it industrially viable.

Firstly the synthesis of p(GlyMA), in isopropyl alcohol, was investigated. P(GlyMA) was found to precipitate in IPA past a threshold molecular weight, around 7 kDa. The target molecular weight, 1.5 kDa, was obtained at a combination of 215 ppm catalyst loading and a 1 mol% of initiator concentration relative to monomer. Using dodecylamine, the preparation of amphiphilic polymers through aza-Michael addition was explored as an alternative to Michael-thiol addition, which requires the use of often malodorous thiols.

Aza-Michael addition was investigated in the context of DBU-catalysed, catalyst-free and microwave-assisted catalyst-free reactions. The final approach, with a 2 hours reaction time and minimal reagents needed, offered a facile pathway to amphiphilic polymethacrylates. Finally, two final amphiphilic polymers (MKIII range) with nonyl- and dodecylamine: $p(GlyMA)_{10}(NA)$ and $p(GlyMA)_{10}(DDA)$, were prepared, and the similarities and differences with the MKI and MKII polymer ranges were established using the same array of techniques used previously. This synthetic methodology circumvents all needs for protective chemistry, but also simplifies the process of obtaining amphiphilic polymers with minimal work up and a variety of accessible primary and secondary amines.

# 3.4 Experimental Data

## 3.4.1 Additional Figures and Scheme

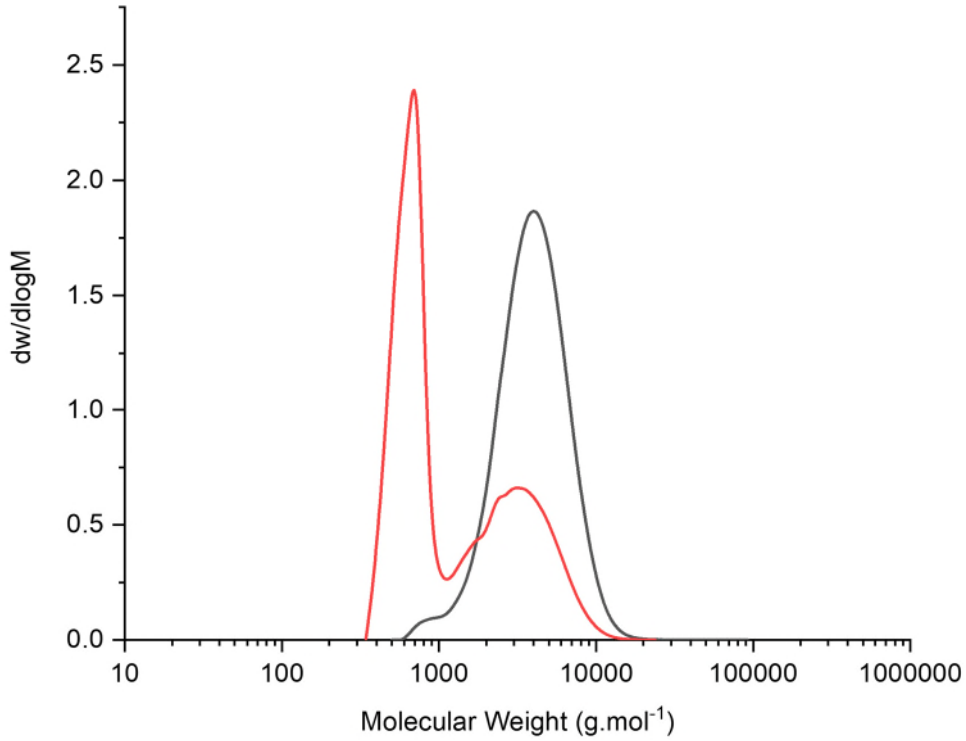


**Figure S3.1** GPC traces (DMF 50 °C) of p(GlyMA)$_{10}$ (entry 8) before (red) and after (grey) purification.

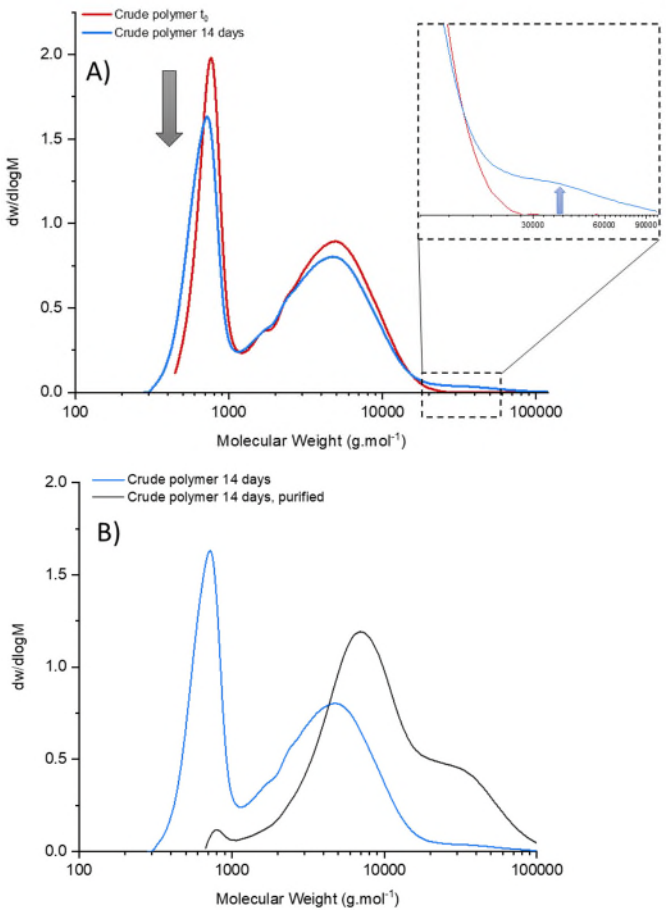


**Figure S3.2** GPC traces (DMF 50 °C) of A) crude p(GlyMA)$_{10}$ at $t_0$ and t = 2 weeks and B) purified product after being left 2 weeks without purification.

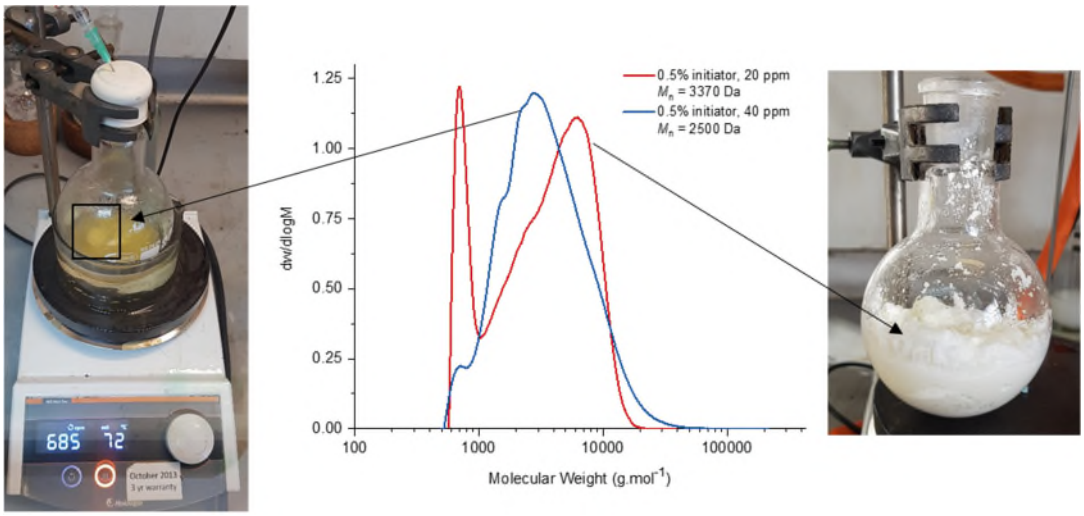


**Figure S3.3** GPC traces (DMF 50 °C) of GlyMA polymerisation attempts in EtOAc.

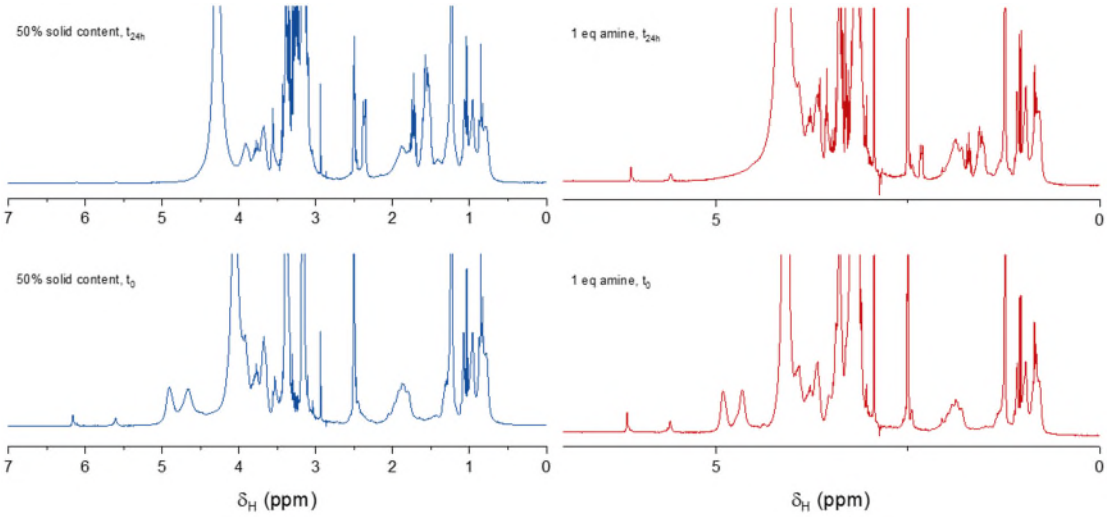


**Figure S3.4** NMR spectra (DMSO-$d_6$) of entries 2 and 3 table 3.2.

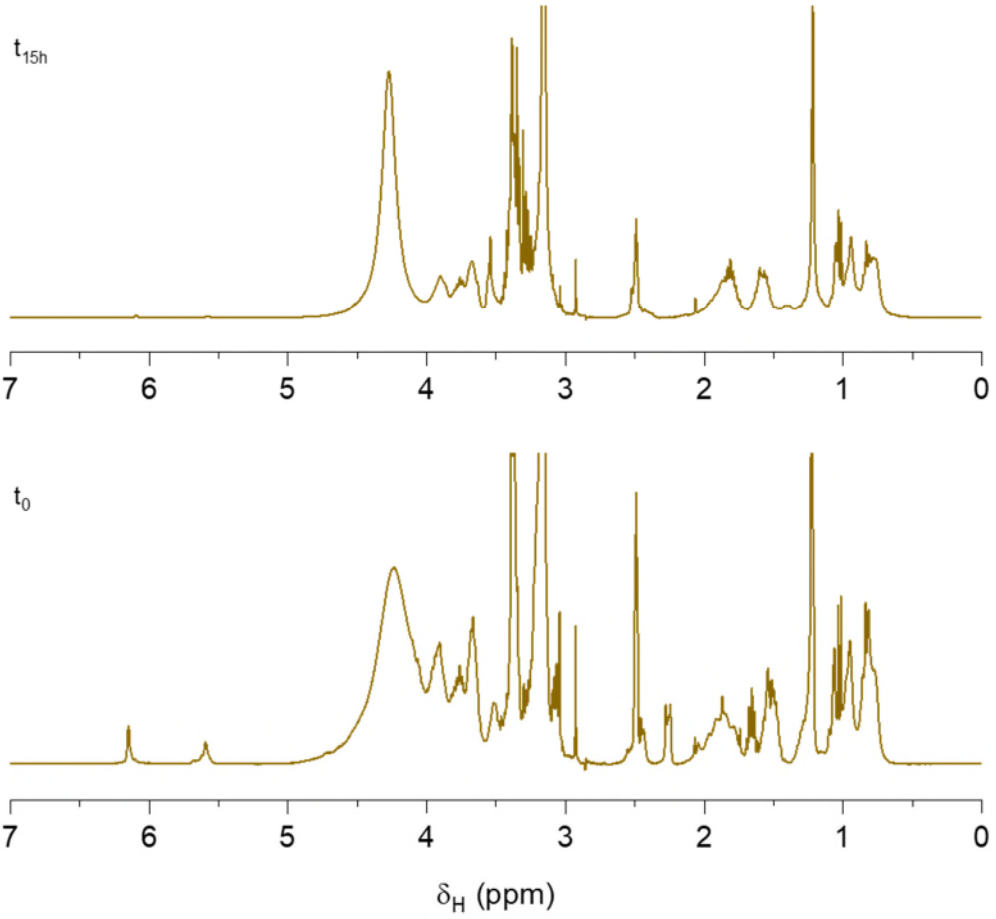


**Figure S3.5** $^1$H-NMR spectra (300 MHz, DMSO-$d_6$ at 25 °C) of aza-Michael reaction product between p(GlyMA)$_9$ and DDA at $t_o$ and $t_{15h}$ (unpurified).

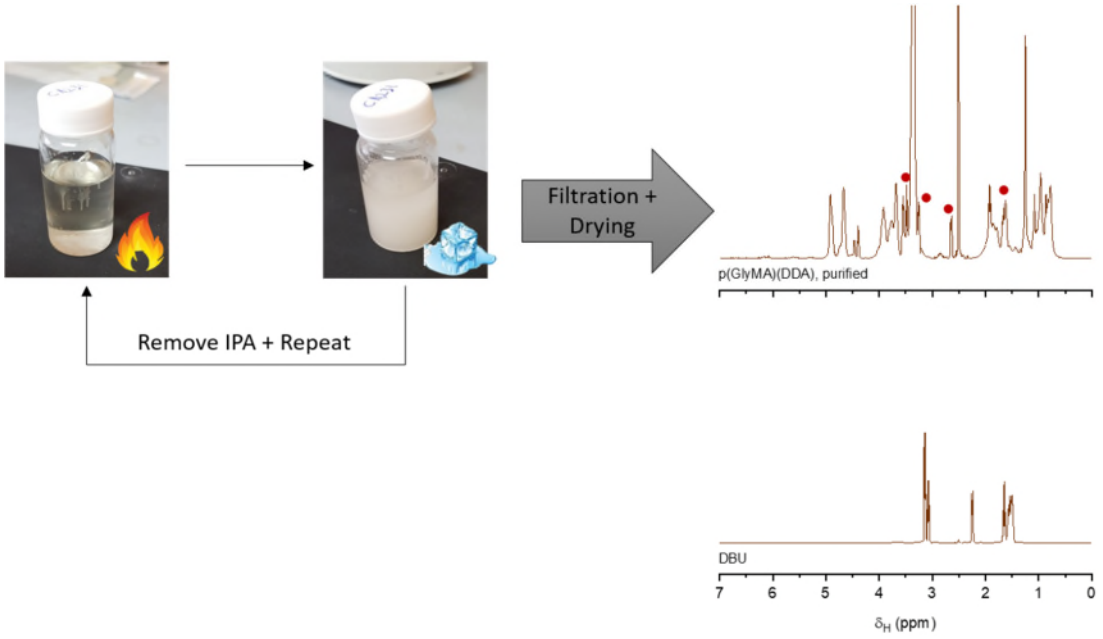


**Figure S3.6** Heating and cooling cycles attempted to purify p(GlyMA)$_{10}$(DDA) and resulting NMR spectrum (DMSO-d$_6$), DBU peaks are indicated in red.

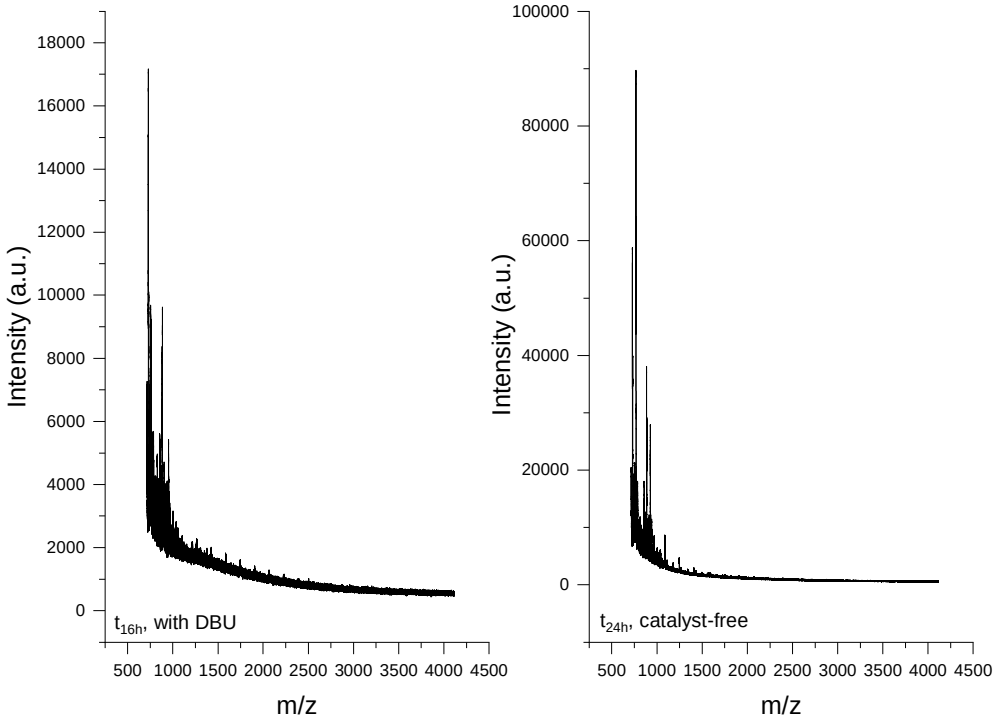


**Figure S3.7** MALDI-ToF spectra of p(GlyMA)$_{10}$(DDA) attempted in DMF/water mixtures with DCTB matrix.

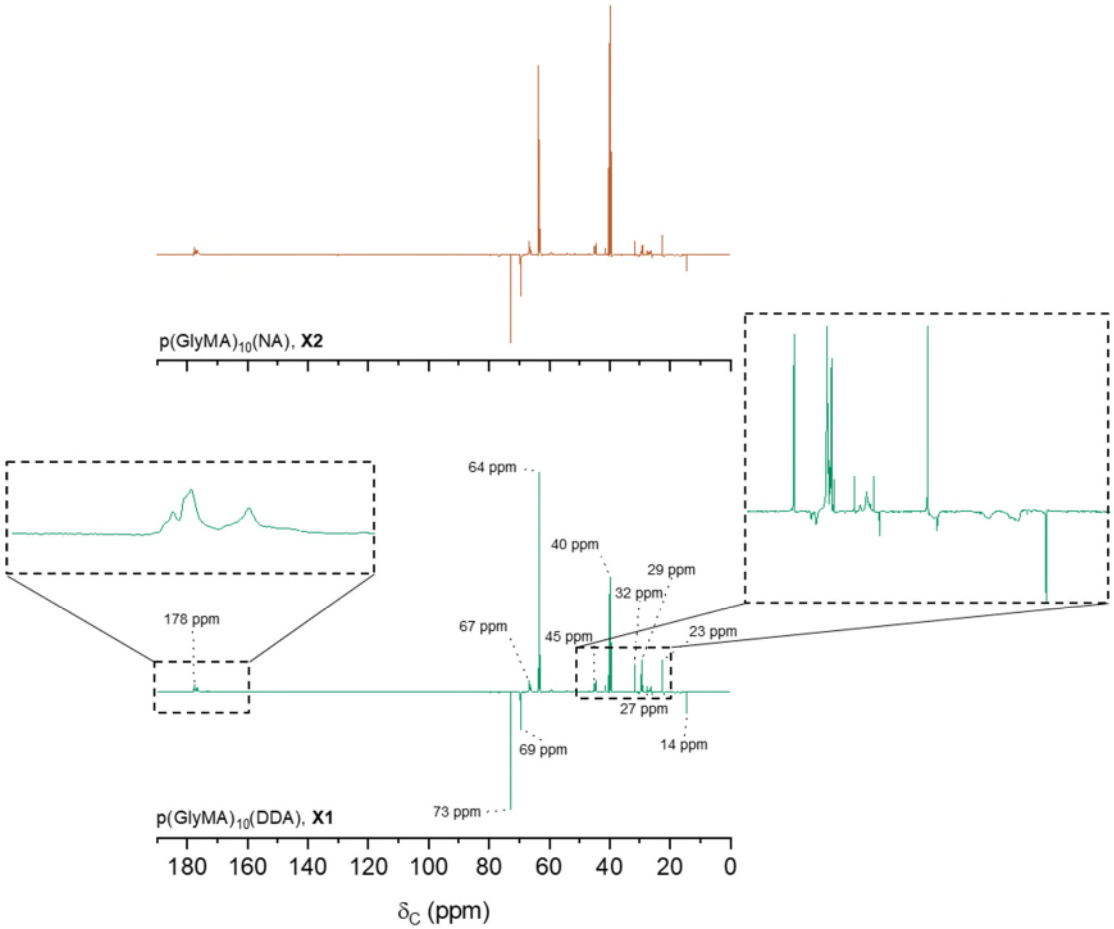


**Figure S3.8** $^{13}$C-NMR (DMSO-$d_6$ 400 MHz at 25 °C) spectra of **X1** (bottom) and **X2** (top).

## 3.4.2 Product Identification

**p(GlyMA)$_{10}$(DDA), X1 and p(GlyMA)$_{10}$(NA), X2:**

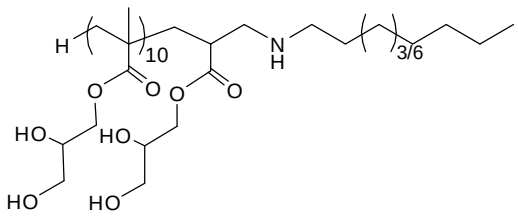


$^1$H-NMR, (/ppm, DMSO-$d_6$, 400 MHz at 25 °C): 0.85-0.86 (alkyl chain terminal -C<u>H</u>$_3$), 0.75-1.06 (backbone -C<u>H</u>$_3$), 1.23 (alkyl chain -C<u>H</u>$_2$-), 1.41 (-CH$_2$-N<u>H</u>-CH$_2$-), 1.84-1.90 (backbone -C<u>H</u>$_2$-), 3.40 (CH(OH)-C<u>H</u>$_2$-OH), 3.68 and 3.90 (COO-C<u>H</u>$_2$-CH(OH)-), 4.46 (-CH$_2$-O<u>H</u>), 3.76 (-CH$_2$-C<u>H</u>(OH)-CH$_2$-OH), 4.68 (-CH$_2$-CH(OH)-CH$_2$-O<u>H</u>), 4.92 (-CH$_2$-CH(O<u>H</u>)-CH$_2$-OH)

$^{13}$C-NMR, (/ppm, DMSO-$d_6$, 400 MHz at 25 °C): 14.11 (alkyl chain terminal -$\underline{C}H_3$), 28.43 (backbone -$\underline{C}H_3$), 28.86 (alkyl chain NH-$CH_2$-$CH_2$-$(CH_2)_n$-$\underline{C}H_2$-$CH_2$-$CH_2$-$CH_3$), 28.95-29.17 (alkyl chain NH-$CH_2$-$CH_2$-$(\underline{C}H_2)_n$-$CH_2$-$CH_2$-$CH_2$-$CH_3$), 28.95-31.45 (alkyl chain NH-$CH_2$-$CH_2$-$(CH_2)_n$-$CH_2$-$\underline{C}H_2$-$\underline{C}H_2$-$CH_3$), 31.79 (alkyl chain NH-$CH_2$-$\underline{C}H_2$-$(CH_2)_n$-$CH_2$-$CH_2$-$CH_2$-$CH_3$), 40.99 (alkyl chain NH-$\underline{C}H_2$-$CH_2$-$(CH_2)_n$-$CH_2$-$CH_2$-$CH_2$-$CH_3$), 62.92 (-$CH_2$-CH(OH)-$\underline{C}H_2$-OH), 66.44 (-$\underline{C}H_2$-CH(OH)-$CH_2$-OH), 69.12 (-$CH_2$-$\underline{C}$H(OH)-$CH_2$-OH) 176.00-178.00 (carbonyl >$\underline{C}$=O)

GPC (DMF): **X1**: $M_n$ = 3500 g.mol$^{-1}$, $M_w$ = 5340 g.mol$^{-1}$, $Đ$ = 1.52

**X2**: $M_n$ = 3450 g.mol$^{-1}$, $M_w$ = 5430 g.mol$^{-1}$, $Đ$ = 1.58

DLS (in water at room temperature, 5 runs average):

**X1**: d = 7.51 nm, *PDi* = 0.055 **P5**: d = 482.5 nm, *PDi* = 0.031

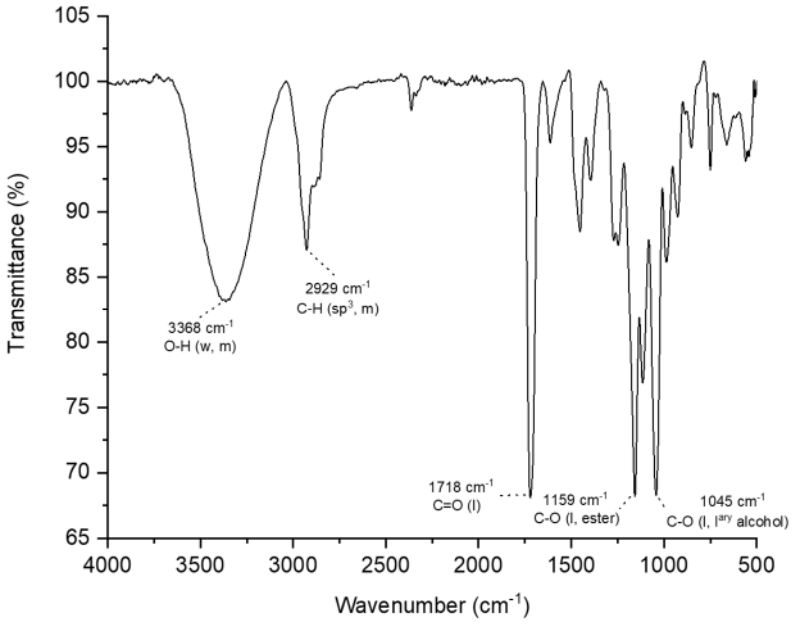


**Figure S3.9** Typical FT-IT spectra of **X1/X2**.

FT-IR (neat, /cm$^{-1}$): 3368 (-OH, s, broad/medium), 2929 (C-H, s, strong), 1718 (C=O, s, strong), 1150 (C-O, s, strong), 1046 (C-O, I$^{ary}$ alcohol)

TGA degradation onset / °C (degradation steps temperatures):

**X1**: $d_s$ = 287°C (330 °C, 414 °C) **X2**: $d_s$ = 270°C (330 °C, 414 °C)

DSC / °C:

**X1**: $T_g$ = 20 °C **X2**: $T_g$ = 20 °C

### 3.4.3 Materials

Unless stated otherwise, all chemicals mentioned were purchased from Sigma-Aldrich and were used without further purification.

CoBF was synthesised in-house, glycerol monomethacrylate was kindly donated by GEO specialty chemicals.

### 3.4.4 Instrumentation

*DMF Gel-Permeation Chromatography (GPC)* was carried out on an Agilent Infinity II MDS instruments equipped with differential refractive index (DRI), viscometry (VS) and dual angle light scatter (LS) detectors.

The system was equipped 2 x PLgel Mixed D columns (300 x 7.5 mm) and a PLgel 5 µm guard column. 12 narrow molecular weight poly(methyl methacrylate) standards (Agilent EasiVials) were used for calibration between 955,000 – 550 g $mol^{-1}$ and data fitted with a 3$^{rd}$ order polynomial. The eluent was DMF with 5 mmol $NH_4BF_4$ additive to help prevent column interactions. Analyte samples were filtered through a 0.22 µm nylon membrane before injection and samples were run at a flow rate of 1 ml/min at 50 °C. Number average molecular weight ($M_{n,GPC}$) and dispersity (Đ) values of synthesized polymers were determined by conventional calibration using Agilent GPC/SEC software.

*Nuclear magnetic resonance (NMR, $^{1}H$ and $^{13}C$)* spectra were recorded at room temperature on a Bruker Avance III HD-300 or 400 using either deuterated chloroform or deuterated dimethyl sulfoxide referenced against TMS as a reference.

*Microwave-assisted syntheses (MAOS)* were performed in a Biotage initiator+ in 2-5 or 15-20 mL Biotage vials.

*Matrix-assisted laser desorption/ionization time-of-flight (MALDI-ToF)* spectra were collected using a Bruker Autoflex Speed, equipped with a 337 nm nitrogen laser, operating in reflectron positive mode with an ion source voltage of 19 kV. Results were accumulated in 10 readings of each spot with 500 laser shots, leading to a total of 5000 laser shots per spectra. Laser power was tuned to keep noise low while maintaining the signal as to not remove any trace peaks. The samples were dissolved into the appropriate solvent at concentrations of 10 mg $ml^{-1}$, along with the cationizing agent sodium iodide (NaI) at 0.1 mg $ml^{-1}$. A matrix solution was then made up of trans-2-[3-(4-tert-Butylphenyl)-2-methyl-2-propenylidene]malononitrile (DCTB) in THF at a concentration of 40mg $ml^{-1}$, along with NaI at 0.1 mg $ml^{-1}$. 10 µl of both the matrix and sample solutions were then mixed together, and 0.5 µl of the resulting solution was then spotted on an MTP 384 ground steel target plate.

*Fourier transform infra-red (FT-IR)* spectra were recorded on a Bruker Vector 22 FT–IR Spectrometer fitted with a diamond crystal plate and a pressure tower. The instrument was set to perform 64 scans per sample at a scan speed of 0.5 $cm.s^{-1}$.

*Dynamic light scattering (DLS)* analyses were carried out on a Malvern Instruments Zetasizer Nano-ZS in water at 25 °C fitted with a 4 mW He-Ne 633 nm laser set at a back-scattering angle of 173°. Samples were prepared by dissolving 1 mg of product in 20 mL of HPLC-grade water. All solutions were sonicated for 2 minutes at 50 °C and allowed to settle for a further 10 minutes. Small aliquots were then pipetted into disposable DLS cuvettes. The equilibration time was set at 2 minutes and five measurements of eleven runs were conducted each time. Sizes are reported as averages of 5 runs and polydispersity was obtained from the zetasizer software as an average of all measurements.

*Transmission electron microscopy (TEM)* images were obtained on a JEOL 2100 TEM fitted with a Gatan Ultrascan 1000 camera. Samples were diluted at 0.1% v/v and one drop was cast on a carbon coated TEM copper grid. After 2 minutes the drop was blotted off with filter paper. All samples were prepared without using a stain.

*Thermo-gravimetric (TGA)* data was obtained using a Mettler-Toledo TGA/DSC1 with autosampler. Measurements were carried out under a nitrogen atmosphere from 25 to 600 °C at a rate of 10 °C/min in a 40 µL aluminium crucible.

*Differential scanning calorimetry (DSC)* was carried out on a Mettler Toledo DSC1-STAR$^{e}$ instrument under nitrogen flow (50 mL.min$^{-1}$) with a heating rate of 10 °C.min$^{-1}$. Samples were loaded in 40 µL aluminium pans and heated for two cycles between -50 and 150 °C. The glass transition temperature values ($T_g$) were determined from the midpoints of the thermograms obtained in each case from the 2$^{nd}$ cycle.

### 3.4.5 Experimental Procedures

**Homopolymerisation of p(GlyMA)**

As previously described p(GlyMA) polymerisations were prepared using 3 different rbf (rbf 1, 2 and 3). Initiator (AIBN, 0.5 or 1 mol% to monomer) and solvent (IPA or EtOAc, calculated to 50% solid content) were introduced in rbf 1, an excess of monomer in rbf 2 and CoBF (10, 30, 40, 50, 70, 120, 140 or 200 ppm) alongside a stirring magnet in rbf 3. Rbfs 1 and 2 were de-oxygenated for 20 minutes while rbf 3 was de-oxygenated for 35 minutes. After oxygen was removed, both the initiator in solvent and the calculated amount of GlyMA were transferred into rbf 3 using de-oxygenated syringes. Rbf 3 was finally introduced into a pre-heated oil bath (70 °C) and left to react overnight.

**Catalysed synthesis of p(GlyMA)$_{10}$(DDA)**

p(GlyMA)$_{10}$ (1.44 kDa, 1 eq, 1 g, 0.694 mmol), IPA/methanol (50% solid content, 1.51 mL for MeOH and 1.52 mL for IPA) and a magnetic stirrer were introduced in a 20 mL glass vial. The mixture was heated to 60 °C to allow the solvent to dissolve p(GlyMA)$_n$. After full solubilisation, dodecylamine (1.5 eq, 1.04 mmol, 193 mg) was introduced as well as 1,8-diazabicyclo(5.4.0)undec-7-ene (DBU) (equimolar amounts to amine, 1.04 mmol, 0.16 mL). The vial was finally caped without further de-oxygenation and reacted overnight at either room temperature, or in an oil bath (50 °C).

**Catalyst-free synthesis of p(GlyMA)$_n$(DDA)**

p(GlyMA)$_{10}$ (1.44 kDa, 1 eq, 1 g, 0.694 mmol), IPA/methanol (50% solid content, 1.51 mL for MeOH and 1.52 mL for IPA) and a magnetic stirrer were introduced in a

20 mL glass vials. The mixture was heated to 60 °C to allow the solvent to dissolve $p(GlyMA)_n$. After full solubilisation, dodecylamine (1.5 eq, 1.04 mmol, 193 mg or 3.0 eq, 2.08 mmol, 386 mg) was introduced. The vial was caped without further de-oxygenation and reacted overnight at either room temperature, or in an oil bath (50 °C).

**MAOS catalyst-free synthesis of $p(GlyMA)_n$(amine)**

Reactions for the synthesis of MKIII polymers were adapted from the following procedure:

$p(GlyMA)_{10}$ (1.44 kDa, 1 eq, 5 g, 3.47 mmol), IPA (50% solid content, 8.26 mL) and a magnetic stirrer were introduced in a 10-20 mL microwave glass vials. The mixture was heated to 60 °C to allow IPA to dissolve $p(GlyMA)_n$. After full solubilisation, dodecylamine (3.0 eq, 10.40 mmol, 1.93 g) was introduced. The vial was caped without further de-oxygenation and introduced into the microwave reactor. The instrument was set apply 160 °C for 2 hours. After reaction, the product was purified by precipitation in chloroform. The white solid was filtered off and added to a jar that was placed in a vacuum oven for 48 hours, which resulted in an off-white, highly viscous product that was used for analysis.

## 3.5 References

1 B. D. Mather, K. Viswanathan, K. M. Miller and T. E. Long, *Prog. Polym. Sci.*, 2006, **31**, 487–531.

2 S. L. Y. Tang, R. L. Smith and M. Poliakoff, *Green Chem.*, 2005, **7**, 761–762.

3 G. González, X. Fernández-Francos, À. Serra, M. Sangermano and X. Ramis, *Polym. Chem.*, 2015, **6**, 6987–6997.

4 R. Baruah, A. Kumar, R. R. Ujjwal, S. Kedia, A. Ranjan and U. Ojha, *Macromolecules*, 2016, **49**, 7814–7824.

5 Y. Shen, Y. Ma and Z. Li, *J. Polym. Sci. Part A Polym. Chem.*, 2013, **51**, 708–715.

6 C. Hoffmann, M. C. Stuparu, A. Daugaard and A. Khan, *J. Polym. Sci. Part A Polym. Chem.*, 2015, **53**, 745–749.

7 A. Southan, M. Mateescu, V. Hagel, M. Bach, C. Schuh, C. Kleinhans, P. J. Kluger, S. Tussetschläger, I. Nuss, T. Haraszti, S. V. Wegner, J. P. Spatz, H. Boehm, S. Laschat and G. E. M. Tovar, *Macromol. Chem. Phys.*, 2013, **214**, 1865–1873.

8 M. Moreno, G. Lligadas, J. C. Ronda, M. Galià and V. Cádiz, *J. Polym. Sci. Part A Polym. Chem.*, 2013, **51**, 1808–1815.

9 A. Genest, D. Portinha, E. Fleury and F. Ganachaud, *Prog. Polym. Sci.*, 2017, **72**, 61–110.

10 W. M. Cohen, R. R. Nelson and J. P. Walsh, Manage. Sci., 2002, **48**, 1–23.

11 E. P. Agency, *National Volatile Organic Compound Emission Standards For Consumer Products -- Background for Promulgated Standards*, 1998.

12 Clean Air Act 1993, https://www.legislation.gov.uk/ukpga/1993/11/contents, (accessed 7 December 2020).

13 S. Rimmer, C. Johnson, B. Zhao, J. Collier, L. Gilmore, S. Sabnis, P. Wyman, C. Sammon, N. J. Fullwood and S. MacNeil, *Biomaterials*, 2007, **28**, 5319–5331.

14 J. V. Ashurst and T. M. Nappe, *Methanol Toxicity*, StatPearls Publishing, 2020.

15 J. V. Ashurst and T. M. Nappe, *Isopropanol Toxicity*, StatPearls Publishing, 2020.

16 S. E. Shaw, T. Russo, D. H. Solomon and G. G. Qiao, *Polymer (Guildf).*, 2006, **47**, 8247–8252.

17 I. Kulai, A. Karpus, D. E. Bergbreiter, M. Al-Hashimi and H. S. Bazzi, *Macromol. Rapid Commun.*, 2020, **41**, 2000382.

18 F. Medina, N. Duhal, C. Michon and F. Agbossou-Niedercorn, *Comptes Rendus Chim.*, 2013, **16**, 311–317.

19 C. Frajerman, B. Meunier and M. E. Strem, in *Inorganic Syntheses*, Wiley Blackwell, 1984, vol. 22, pp. 133–135.

20 D. J. Heldebrant, P. G. Jessop, C. A. Thomas, C. A. Eckert and C. L. Liotta, *J. Org. Chem.*, 2005, **70**, 5335–5338.

21 A. Genest, D. Portinha, E. Fleury and F. Ganachaud, *Prog. Polym. Sci.*, 2017, **72**, 61–110.

22 G. Bosica and A. J. Debono, *Tetrahedron*, 2014, **70**, 6607–6612.

23 J. Wang, P. F. Li, S. H. Chan, A. S. C. Chan and F. Y. Kwong, *Tetrahedron Lett.*, 2012, **53**, 2887–2889.

24 Z. Duan, X. Xuan, T. Li, C. Yang and Y. Wu, *Tetrahedron Lett.*, 2006, **47**, 5433–5436.

25 N. S. Shaikh, V. H. Deshpande and A. V. Bedekar, *Tetrahedron*, 2001, **57**, 9045–9048.

26 I. J. Ochuma, R. P. Fishwick, J. Wood and J. M. Winterbottom, *Appl. Catal. B Environ.*, 2007, **73**, 259–268.

27 D. Dallinger and C. O. Kappe, *Chem. Rev.*, 2007, **107**, 2563–2591.

28 J. D. Moseley and C. O. Kappe, *Green Chem.*, 2011, **13**, 794–806.

29 J. M. Kremsner, A. Stadler and C. O. Kappe, in *Topics in Current Chemistry*, Springer, Berlin, Heidelberg, 2006, vol. 266, pp. 233–278.

# **Chapter 4**:

# Amphiphilic Polymethacrylates as Pigment Dispersants for Carbon Black

## 4.1 Introduction

Carbon black (CB) is the name given to a class of carbon particles manufactured from the incomplete combustion of heavy petroleum matter. CB particles are made up of up to 95% elemental carbon, with high aromaticity and surface area.[1] It is one of the oldest known pigments, with reports linking it to ancient Egypt and China,[2] and has historically also been used in Gutenberg's printing press as early as the 15th century in oil-based printing inks. The discovery, at the turn of the 20th century, that carbon black could be used to reinforce rubber was critical in the development of the modern tire. It enhanced the mechanical properties, reduced thermal damage, and shielded rubber from UV degradation, allowing the production of a strong material that could be used for thousands of miles.[3] This breakthrough led to an exponential increase in the production of carbon black. As of 2018, CB had a global market value of $ 17.5 billion, and is projected to reach 10 million tons per annum production within a few years.[4,5] Today, it is still predominantly used as a reinforcing filler.[6–9] 90% of the carbon black production is dedicated to reinforcement of tires and rubber products.[2] The other 10% is dedicated to special applications such as in semiconductors,[10,11] but is also used in paints and coatings.[12–15]

The introduction of legislation in the early 2000's set out to place a limit on the amount of VOCs in a wide range of consumer products, including paints and coatings.[23] Since then, there has been an increased interest in finding ways to reduce the levels of organic solvent emitted during paint application with high-solids paints, solvent-free or water-borne systems. As such, the need for research into the production of more efficient carbon black dispersants for water-borne suspensions, which could in turn increase profit margins and drive customer fidelity, is quickly rising.

In this chapter, the amphiphilic polymethacrylates synthesised in chapters 2 and 3 (ranges MKI, II and III) were screened as dispersants for waterborne carbon black dispersions. For each dispersant, immediate post milling tests were carried out (DLS, viscosity). The evaluation and comparisons of the mill bases' properties were used to detect deficiencies, which were addressed in subsequent generations. Storage stability of the mill bases was also tested with TEM studies at one and three months.

The systematic evaluation of these parameters for each successive generations allowed the identification of high-performing dispersants, whose properties were selected for. Finally, two final mill bases stemming from the final generation of dispersants were further studied by performing *let-downs*. The resulting paints' jetness, gloss and haze were finally analysed and compared.

## 4.2 Results and Discussion

### 4.2.1 Foreword on Methodology

In practice, it is more energy efficient to mill a pigment concentrate (also known as mill base), and subsequently combine it with the rest of the coating components (resin, additives) in a separate container in a step called "*let-down*".

The loading of pigment influences colour strength and viscosity but in a "*real life*" situation, having a low initial mill base pigment concentration might be helpful in that more pigment can be added (to increase colour strength or jetness of the final coating), as some customers might want to use the least necessary amount of pigment so as to minimise impact on cost. As such, in screening studies of dispersant activity such as the following, low pigment loading samples are preferred. A "10% CB loading" standard mill base production method is used here (8 g of water : 1 g of dispersant : 1 g of pigment). Glass beads are added and the samples shaken overnight. This provides

a means of imparting mechanical energy to the mill-base to break-up pigment agglomerates. Sis and co-workers found that, while ionic (electrostatic stabilisation) and non-ionic (steric stabilisation) dispersants could stabilise carbon blacks, non-ionic dispersants provided enhanced stability to the system.[24]

The 22 dispersants discussed in this chapter are summarised in table 4.1.

| Dispersant code | Dispersant generation | Hydrophilic segment | Anchor | HLB[a] | $D_{10}$ /nm | $D_{50}$ /nm | $D_{90}$ /nm |
|---|---|---|---|---|---|---|---|
| **P2** | MKI | $p(GMA)_7(ETA)$ | CHT | 18.5 | 0 | 0 | 0 |
| **P3** | MKI | $p(GMA)_7(ETA)$ | PET | 18.2 | 0 | 0 | 0 |
| **P4** | MKI | $p(GMA)_7(ETA)$ | *i*-PT | 19.0 | 0 | 0 | 0 |
| **P5** | MKI | $p(GMA)_{11}(ETA)$ | DDT | 18.4 | 68 | 201 | 304 |
| **P6** | MKI | $p(GMA)_{11}(ETA)$ | CHT | 19.0 | 83.4 | 229 | 320 |
| **P7** | MKI | $p(GMA)_{11}(ETA)$ | PET | 18.8 | 129 | 243 | 397 |
| **P8** | MKI | $p(GMA)_{11}(ETA)$ | *i*-PT | 19.3 | 161 | 287 | 409 |
| **P9** | MKI | $p(GMA)_{43}(ETA)$ | DDT | 19.6 | 391 | 1109 | 1792 |
| **P10** | MKI | $p(GMA)_{43}(ETA)$ | CHT | 19.7 | 291 | 900 | 2061 |
| **P11** | MKI | $p(GMA)_{43}(ETA)$ | PET | 19.7 | 275 | 558 | 895 |
| **P12** | MKI | $p(GMA)_{43}(ETA)$ | *i*-PT | 19.8 | 336 | 615 | 1145 |
| **Q1** | MKII | $p(GlyMA)_8$ | PET | 18.1 | 132 | 194 | 305 |
| **Q2** | MKII | $p(GlyMA)_8$ | CHT | 18.3 | 135 | 193 | 325 |
| **Q3** | MKII | $p(GlyMA)_8$ | *i*-PT | 18.9 | 167 | 319 | 493 |
| **Q4** | MKII | $p(GlyMA)_8$ | HT | 18.3 | 111 | 221 | 316 |
| **Q5** | MKII | $p(GlyMA)_8$ | NT | 17.8 | 68 | 145 | 321 |
| **Q6** | MKII | $p(GlyMA)_8$ | DDT | 17.3 | 60 | 165 | 312 |
| **Q7** | MKII | $p(GlyMA)_8$ | TDT | 17.0 | 74 | 180 | 452 |
| **Q8** | MKII | $p(GlyMA)_8$ | ODT | 16.3 | 67 | 157 | 292 |
| **X1** | MKIII | $p(GlyMA)_{10}$ | DDA | 17.5 | 71 | 145 | 247 |
| **X2** | MKIII | $p(GlyMA)_{10}$ | NA | 18.0 | 85 | 163 | 280 |

**Table 4.1** Summary of the amphiphilic polymethacrylates dispersants used in this chapter. [a]Hydrophylic lipophilic balance (Griffin model, $HLB = 20*(M_{hydrophilic}/M_{tot})$. [b] / nm

### 4.2.2 Analysis of Raven 5000 ultra 3

There is a wide variety of carbon blacks available on the market whose properties vary depending on the feedstock and manufacturing process.[25] The one used in this study is Birla's Raven 5000 ultra 3, which is typically used in the automotive industry.[26] Given the hydrophobicity of the pigment, it is not readily wetted when introduced in water, figure S4.1. In order to evaluate the quality of a dispersion, it is necessary to first learn about the properties and behaviour of undispersed carbon black. To this end, multiple analytical tools are available. Brunauer-Emmett-Teller (BET) surface area analysis is one such technique.

BET theory is used to accurately determine particle surface area, including irregularities, by studying the adsorption of inert gases such as nitrogen on particles' surface. Generally, the experiments are carried out under isothermal conditions at cryogenic levels (77K), while the gas pressure is increased. This creates an adsorption

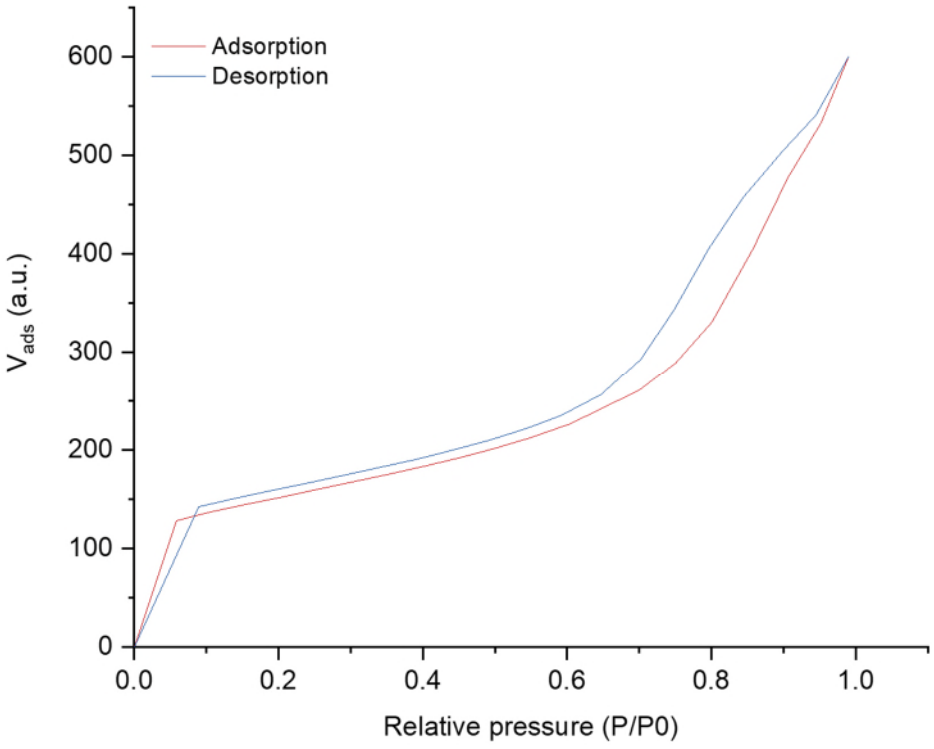


**Figure 4.2** BET isotherm of undispersed Raven 5000 ultra 3 carbon black. BET measurements by Tom Chamberlain.

isotherm that, when studied, and in conjunction with the knowledge of the adsorbed molecule's cross-sectional area, can help determine the overall specific surface area of the sample.

A BET isotherm is generally divided into two segments, figure 4.2. The bottom curve shows the $N_2$ adsorption onto the surface of the carbon black particles, while the top shows desorption. The hysteresis observable between the two curves indicates the existence of mesoporosity, usually meaning that pores exist in the range of 20-500 Å and is typical of what is referred to as type IV isotherms. In particular, the isotherm of the studied carbon black lacks the apparition of a plateau at higher $P/P_0$ that usually indicates pore volume. When no plateau is visible, the hysteresis loop can be classified as an H3 loop. H3 hysteresis loops do not allow for pore size distribution to be reliably assessed by single-point BET, but is also relevant as it is an indicator of aggregation of plate-like particles forming slit-like pores, which allows us to paint a more precise picture of the structure of the pigments themselves. Carbon black pigments are generally spherical, but are constituted paracrystalline carbon layers, which can be assimilated to graphite. The amount of gas used for creating the first monolayer at the surface of the particles can be calculated from the adsorption isotherm using the BET equation:

$$\frac{1}{W\left(\frac{P_0}{P}-1\right)} = \frac{C-1}{W_m C}\left(\frac{P}{P_0}\right) + \frac{1}{W_m C} \qquad \text{(eqn. 1)}$$

where W is the volume of gas adsorbed, $P/P_0$ the relative pressure, $W_m$ the volume of adsorbate as monolayer and C the BET constant.

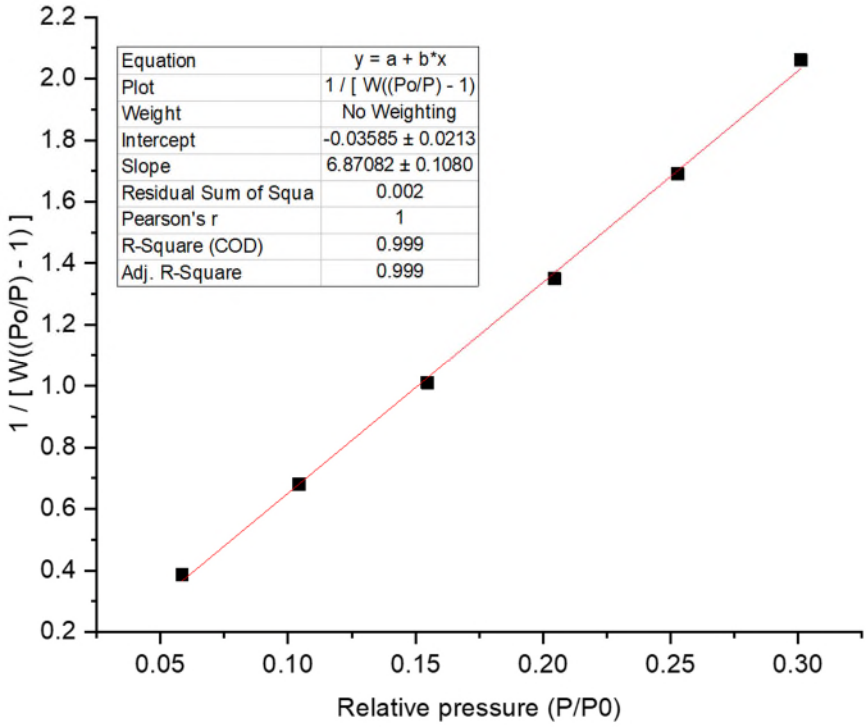


**Figure 4.3** Multi-point BET plot of Raven 5000 ultra 3 carbon black.

W is measured at various $P/P_0$ values, and the BET equation can then help describe a linear plot of $1/W(P_0/P)-1$ against $P/P_0$. After regression, the data is usually considered usable when $r^2 > 0.995$. Figure 4.3, which shows the regressed multi-point plot for Raven 5000 ultra 3, has an acceptable set of data points with $R^2 = 0.999$.

$W_m$ can then be found with:

$$W_m = \frac{1}{\text{Slope+intercept}} = \frac{1}{6.87-0.036} = 0.15 \qquad \text{(eqn. 2)}$$

And the total surface area, $S_t$, is calculated with:

$$S_t = \frac{W_m N_A A_{N_2}}{M_{N_2}} \qquad \text{(eqn. 3)}$$

with $N_a$ the Avogadro number, $A_{N2}$ the cross sectional area of the nitrogen adsorbate (in $m^2$) and $M_{N2}$ the molecular weight of nitrogen. We then obtain:

$$S_t = \frac{0.15 \times 6.02e10^{23} \times 1.62e^{-19}}{28}$$

We obtain a total surface area of 509.7 $m^2.g^{-1}$. This value is in good accordance with that of the pigment manufacturer, who cites a surface area of 583 $m^2.g^{-1}$.[26]

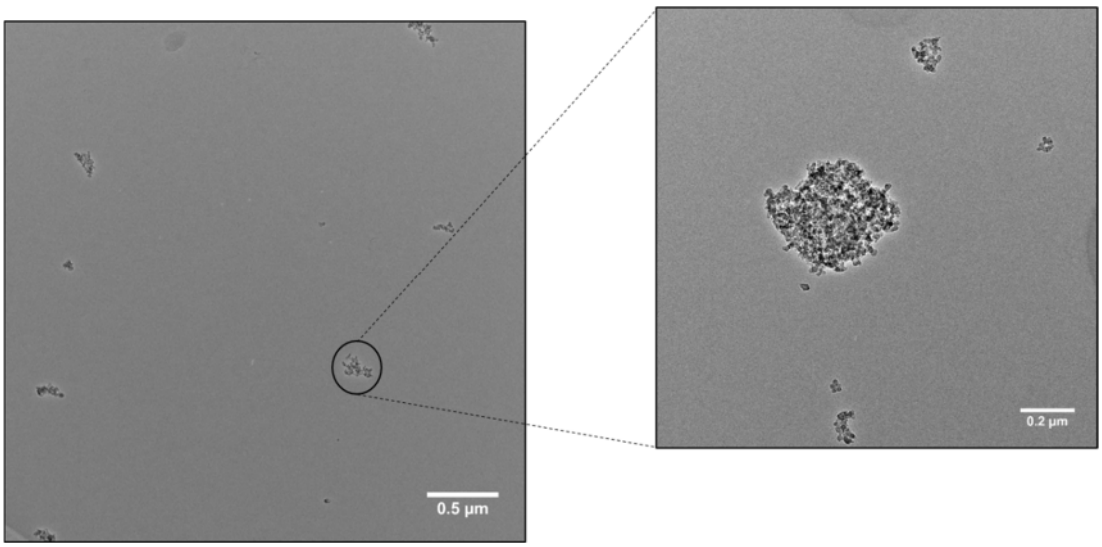


**Figure 4.4** TEM images of undispersed carbon black with focus on agglomerate cluster.

Generally, the optimum amount of dispersant required is a function of the pigment's surface area. Too little means stabilisation will be lesser and exposes users to bridging flocculation while, If too much is used, the thickness of the protective barrier is actually reduced as a result of overcrowding on the pigment surface. Film properties such as adhesion or hardness can also be affected by the use of an excess of dispersants because of the presence of free dispersant molecules in the drying film.

A general rule of thumb consists in using 2 mg of polymeric dispersant per square metre of pigment surface area, which will be close to the optimum amount required. Percentage Agent On Weight of Pigment (%AOWP) is a formula used in industry to achieve the 2 mg.m-² loading where:

$$\%AOWP = \frac{Surface\ Area_{BET}}{5} \qquad \text{(eqn 4)}$$

Here we therefore have %AOWP ≈ 100%. This means that for 100 g, around 100 g of dispersant is required, hence the 1:1 ratio of dispersant to pigment.

Observing these same particles under TEM allows for a closer look at the structure of the undispersed pigment powder, figure 4.4. Easily visible are amassments of spherical particles ranging from 0.1 to 0.3 μm in diameter.

Indeed, as discussed in chapter 1, carbon black's primary particles (or nodules) are not usually present in isolated form. Instead, they frequently fuse together to form tightly bonded aggregates that vary in size, shape, and number of constituting nodules. Loosely bonded agglomerates can then be formed by the physical interaction of primary particles with aggregates. The breaking up of agglomerates is the process that is at the core of the dispersion process and can be done by sonication, or mechanical grinding as discussed previously.

## 4.2.3 The MKI Dispersant Range

### *4.2.3.1 MKI Post-Milling Analysis*

The relationship between agglomerate size and coating properties is a critical aspect of coating science. With carbon black, the size of the dispersed particles will have a direct impact on gloss, hue, colour intensity or jetness of the dry coating. A milled sample should generally be analysed within a few hours of being prepared as this provides an accurate state of the system, comparable to that which occurs when the paints are being prepared by customers before application. The use of DLS is common and *in-situ* measurements are preferred as they minimize disturbance of the sample.[24] One of the widespread descriptors of the quality of milled samples is the median, or $D_{50}$. It is the point in the size distribution below and above which 50% of the sample is contained and is obtained using the cumulative plots. Figure 4.5 shows $D_{50}$ data for

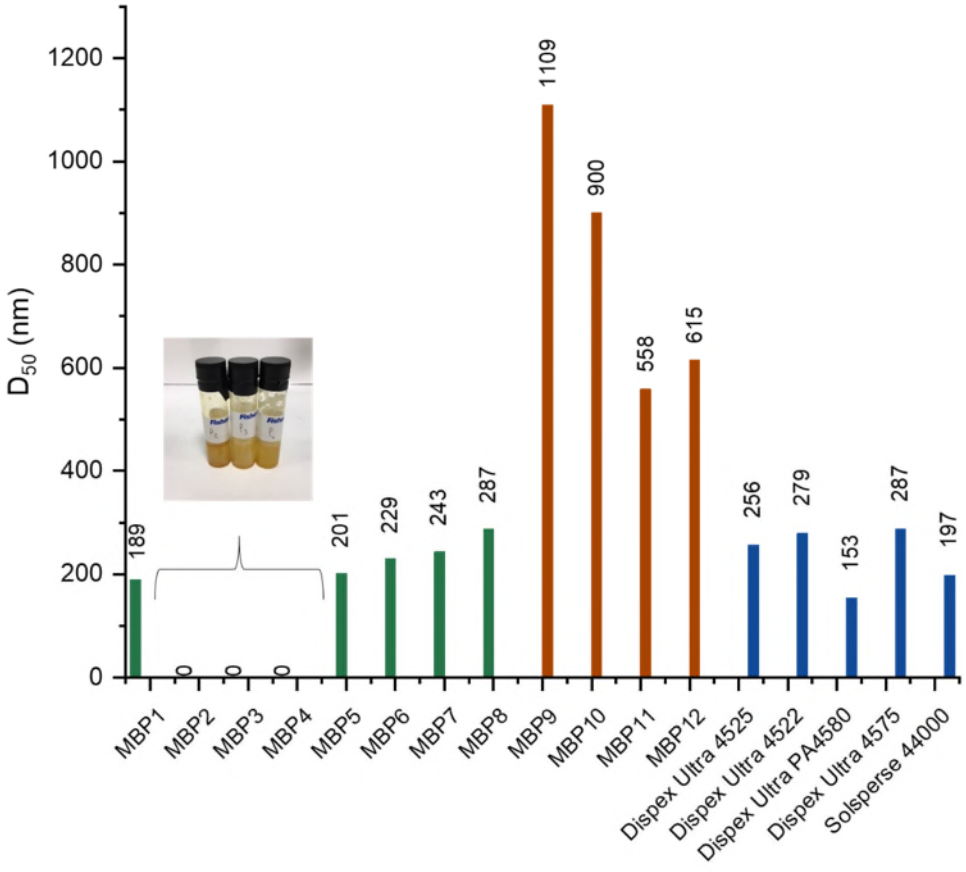


**Figure 4.5** $D_{50}$ data of aqueous carbon black suspensions stabilised by MKI and commercial dispersants. (MB = mill base)

the MKI range dispersants, along with five commercial samples (Dispex® ultra 4525, 4522, PA4580 and 4575 by BASF, as well as Solsperse$^{TM}$ 44000 by Lubrizol).

There are several trends observable. Firstly, **P2**, **P3** and **P4**, even when placed in an oven, could not properly be dispersed and formed masses that proved difficult to break up. **P1** performed well with a 189 nm $D_{50}$, only being outperformed by the commercial Dispex® ultra PA4580. Dispersants **P5** to **P8** performed reasonably well, in a similar fashion to the commercial samples, while samples **P9** to **P12** failed to stabilise the

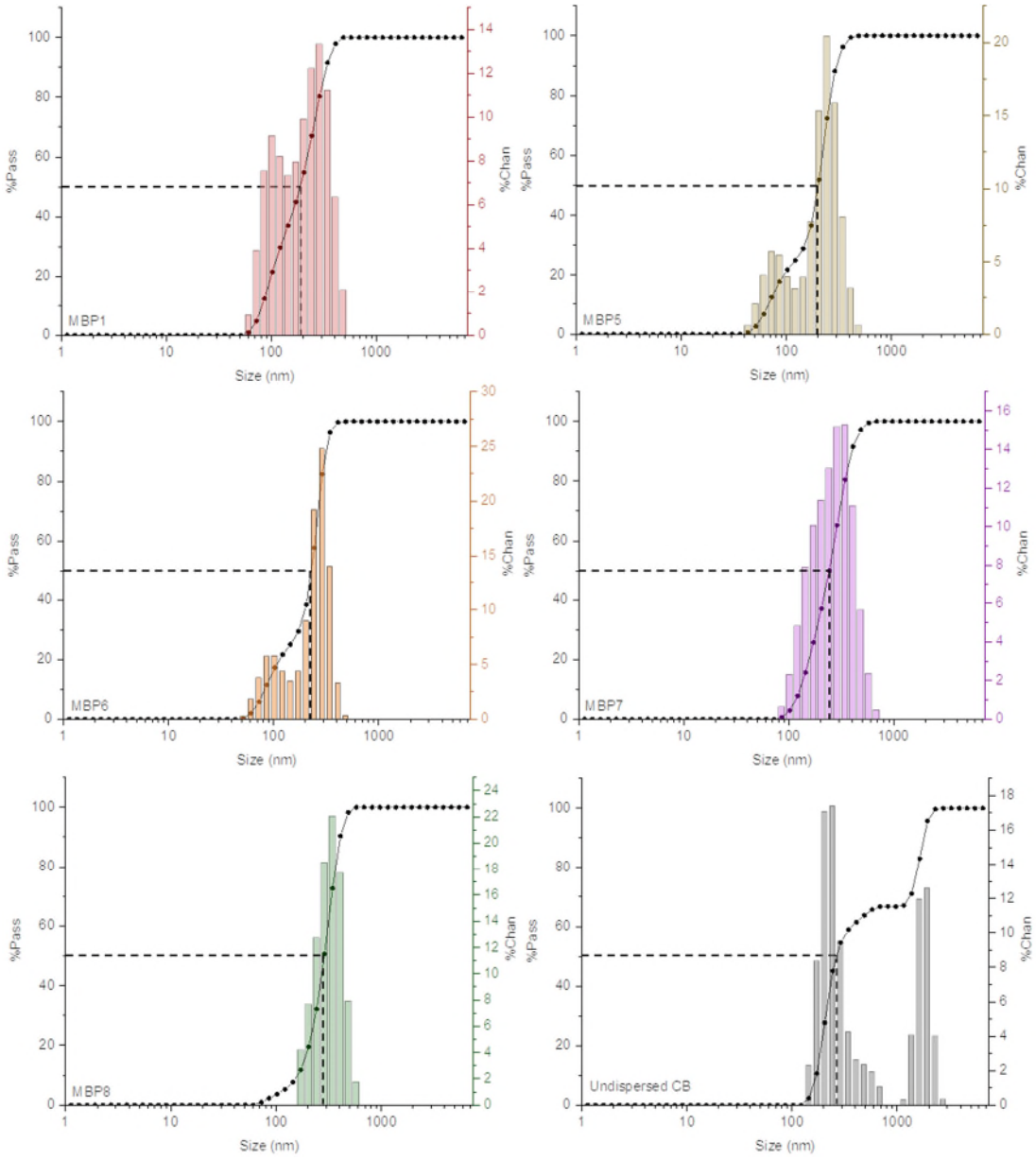


**Figure 4.6** In-situ DLS measurements of intensity distribution and cumulative plots of **MBP1**, **MBP5**-**MBP8** and undispersed carbon black.

pigment suspension almost entirely. A high $D_{50}$ is an indicator of a flocculated system which here might be a due to the high molecular weight of the stabiliser bloc (degree of polymerisation = 42).[27] The stabilisation of the system depends on the steric barrier thickness. The dispersants' solvophilic segments must be enough to overcome attractive Van der Waals forces, however, excessively long polymeric chains such as those found in **P9** to **P12** will lead to particle bridging throughout the sample and, as was explained by Farrokhpay *et al.*,[28] will also have a tendency to fold back onto themselves which in both case can lead to flocculation of the particle, and is likely the reason for the poor performances of dispersants **P9**-**P12**, figure S4.2.

Figure 4.6 shows the intensity based population histogram distribution and cumulative passage plot for **MBP1**, **MBP5**-**MBP8** (MB = mill base).

Pigment samples dispersed with **P1**, **P5** and **P6** yielded bimodal distributions. In each case the populations centred on 100 and 240 nm. There are two potential reasons why this would happen. It could be due to incomplete dispersion, but no agglomerate was found in the size range of undispersed carbon black. It could also stem from early flocculation occurring very shortly after dispersion.

**P1**, **P5** and **P6** gave indications of being able to stabilise carbon black more efficiently than other dispersants. Comparing with **MBP7** and **MBP8**, these samples are only showing one population centred at 240 nm. This could be because they are less able to prevent this early re-agglomeration.

#### *4.2.3.2 MKI Dispersant aging analysis*

One of the main issues during storage of paints is dispersant desorption which can lead to flocculation of the mixture. As such, shelf-life / storage stability is an important

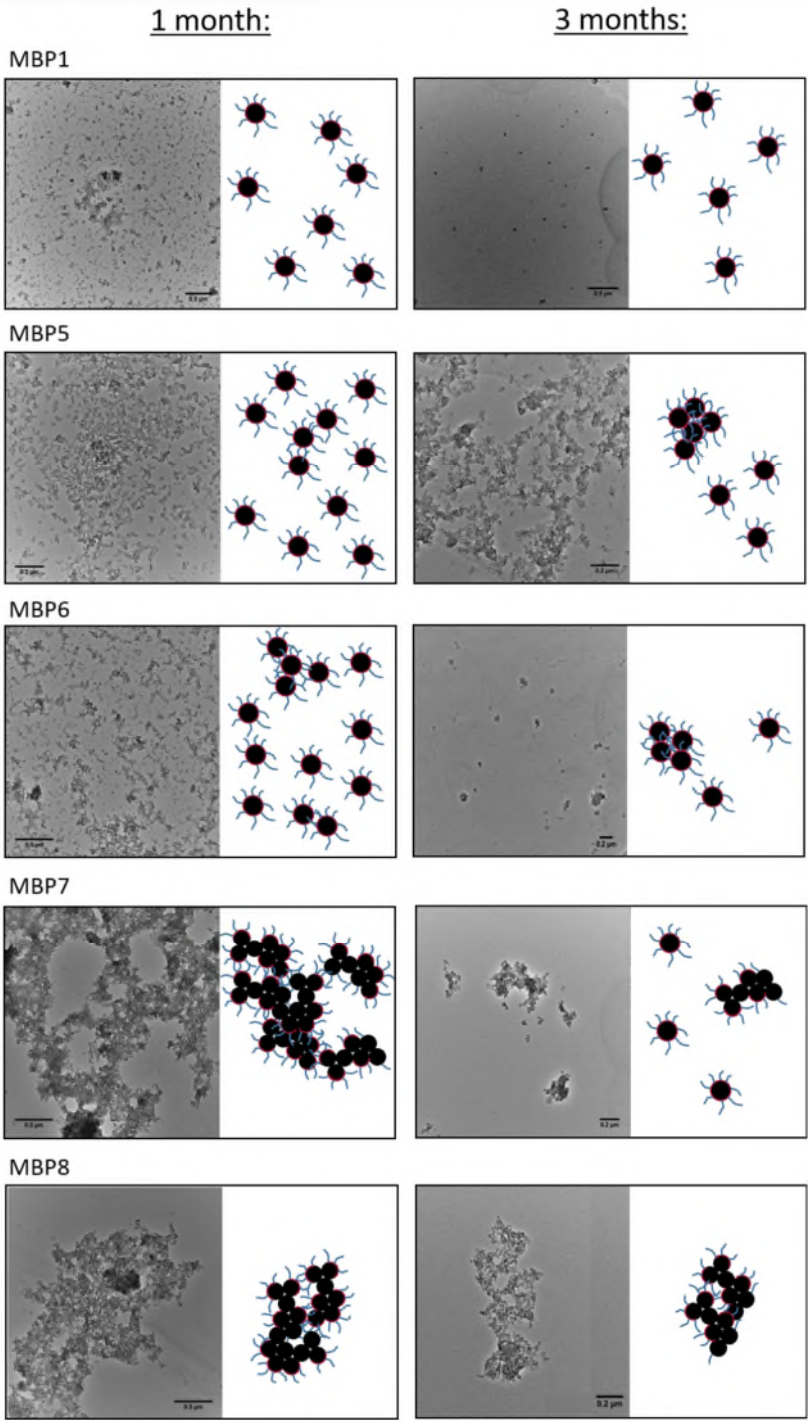


**Figure 4.7** TEM images of successful mill bases **MBP1** and **MBP5** to **MBP8**, 1 and 3 months after dispersion.

variable, from a commercial perspective, that should be taken into account when developing products. An evaluation of the viability of the mill bases is necessary and was achieved by recording TEM images at key dates after the milling was performed and comparing the different mill base formulation with one another.

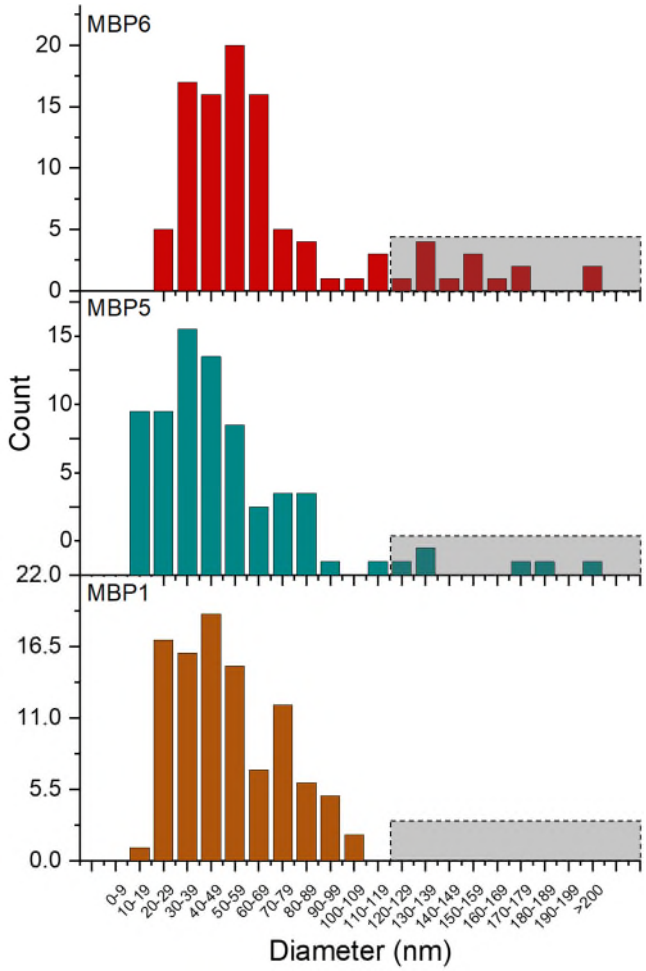


**Figure 4.8** TEM–based size histograms of mill bases **MBP1**, **MBP5** and **MBP6** (collected from 100 measurements), 1 month after dispersion.

After a month **MBP1**, **MBP5**, **MBP6** and **MBP7** were still free flowing, while the other suspensions had completely flocculated and CB crashed out of solution.

TEM images of the free-flowing mill bases are shown in figure 4.7. **MBP1** still showed very good stability of the carbon black agglomerates after 1 month while large, mostly flocculated agglomerates were visible for **MBP7** and **MBP8**. This issue was also observed, to a lesser extent, with **MBP5** and **MBP6**. Desorption of the dispersants likely plays a role in the observed aging of the samples. Iso-propyl anchors (**MBP8**) were not expected to have a strong affinity to carbon black particles' surface. Such cannot be said for phenylethylthiol anchors. Indeed, as discussed previously, the surface of CB can be likened to that of graphite with high aromaticity, and π-π stacking

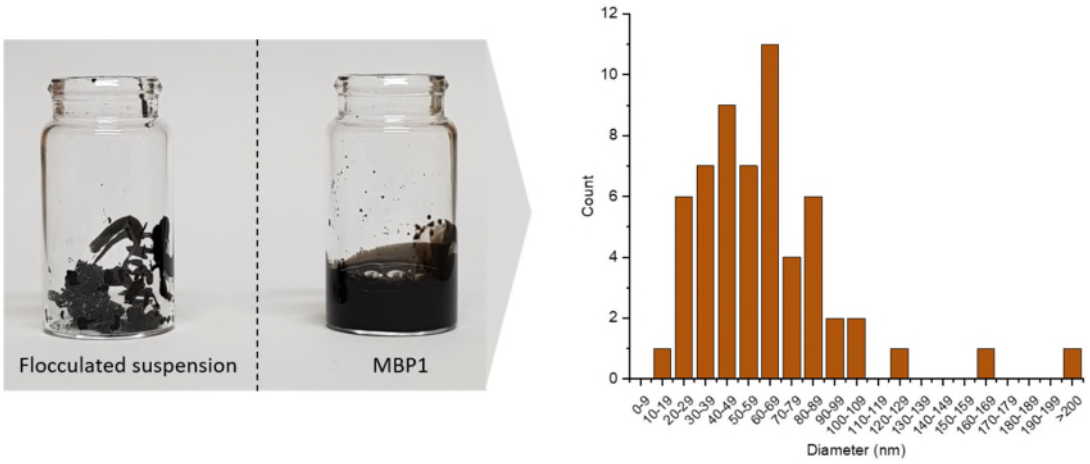


**Figure 4.9** (left) Images of typical flocculated suspensions and **MBP1** after 3 months. *Measurements were obtained from multiple images.

was expected to provide an additional non-covalent force that would increase the dispersant anchor's pigment affinity.

Size distribution of the particles can help provide additional information on the state of the mill bases. To do so, measurements from 100 randomly selected agglomerates were taken (from one or more images) and arranged into size distribution histograms, figure 4.8. (It should be noted that the TEM and DLS size distributions are not directly comparable. This is because, beyond the differences in measurement conditions, DLS assumes a spherical shape of the particle while TEM allows for a more direct measurement).

**MBP5** and **MBP6**'s size histograms (average agglomerate sizes of 54.91 ± 41.35 and 69.19 ± 44.71 nm respectively) show more heterogeneous populations, with particle clusters of increased size (i.e. > 120 nm), which are not present in **MBP1**'s population (average size = 51.72 ± 22.037 nm).

After 3 months, all mill-bases but **MBP1** were re-agglomerated. Interestingly, even if free flowing, as was the case with **MBP5**, TEM reveals widespread flocculation in the sample, making cluster measurement impossible. **MBP1**'s population had also shown signs of aging, with an average cluster size of 62.8 ± 36.2 nm and a mode interval of

60-69 nm (as opposed to 40-49 nm after a month), as well as several clusters > 120 nm in size. As a dispersant, however, **P1** has overall shown that it can perform better than most tested commercially available dispersants, with an acceptable shelf life, figure 4.9.

Moreover, two of the best performing dispersing agents, **P1** & **P5**, had a dodecane anchor. An interesting report was published by Huffer *et al*.[29] where the authors attempted to predict the sorption efficiency of various aliphatic and aromatic compounds onto multi-walled carbon nanotubes (MWCNT). Amongst the various conclusions of the paper, it was stated that (i) the adsorption isotherm onto MWCNT was closer to linear sorption for aliphatic compounds than aromatic ones and (ii) the sorption of cycloalkanes and iso-alkanes was overall worse that the corresponding aliphatic alkanes. This therefore seems to suggest that the linear aliphatic anchor groups (DDA) would indeed be better able to disperse carbon black than the aromatic (PET), cyclic (CHT) or small (i-PT). This also raised the question of the existence of an optimal anchor length that would maximise adsorption onto CB surfaces.

Several aspects of the formulations were thereupon modified to address these issues:

(i) **P2**, **P3** and **P4** not dispersing in water indicated that, in practice, it would be advantageous to integrate a more hydrophilic segment in our dispersant candidates. This would prevent lumping of the dispersant powders, and potentially lead to a better dispersion.

(ii) An investigation of the optimal linear aliphatic anchor length should be conducted.

(iii) Particle bridging becomes an issue with higher molecular weight dispersants. Having seen no indication of such issue with dispersants **P1**, **P5**-**P8**,

further dispersant synthesis should target molecular weights ranging from 1 to 2.5 kDa.

## 4.2.4 The MKII Dispersant Range

### *4.2.4.1 MKII Post-Milling Analysis*

In the second generation of dispersants, the issues above were addressed by (i) using poly(glycerol monomethacrylate) (GlyMA) as a stabiliser block. GlyMA is a very hydrophilic monomer and thus circumvents the need for a ring-opening step. This monomer was also shown to be non-toxic and antifouling.[30–33] Finally, the side-chain is functional and its –OH groups can be derivatised to, for example, "encapsulate" the particles. (ii) We wished to study linear aliphatic anchors in more depth. Accordingly, 6 aliphatic chains of varying carbon lengths, *i*, were employed (with *i* = 3, 6, 9, 12, 14, 18). (iii) Finally, all CCTP macromonomers retained for post-polymerisation functionalisation had average number molecular weights of 1.5 kDa (degrees of polymerisation between 8 and 15). Eight dispersant candidates (**Q1** to **Q8**) were

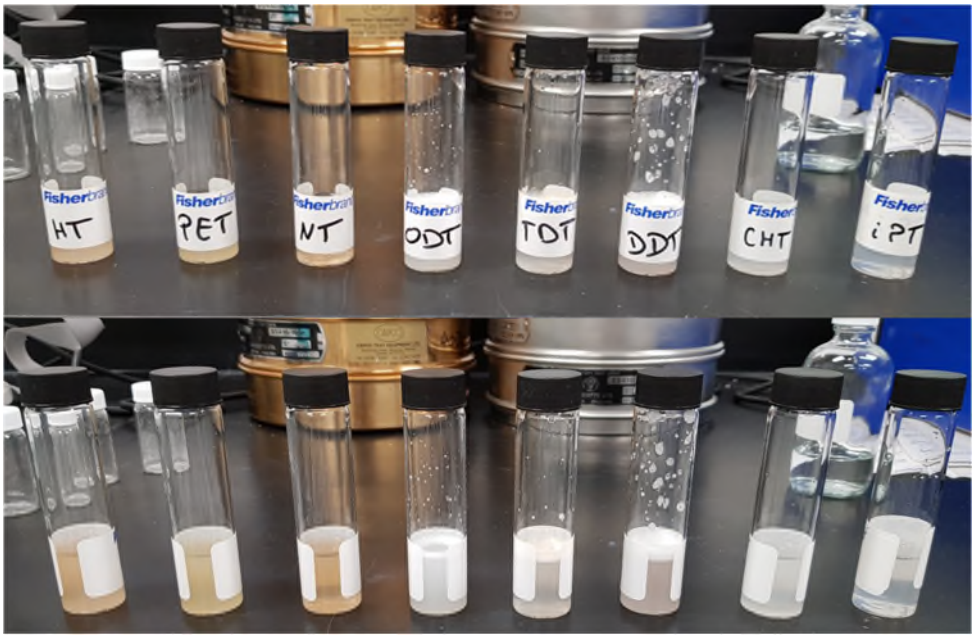


**Figure 4.10** Images of MKII surfactants dispersed in water.

prepared for testing. All samples were dispersed in water with relative ease, figure 4.10. $D_{50}$ data comparing the MKI and MKII range shows a much improve performance across the whole range, figure 4.11.

Examining the **MBP1**/**MBQ6**, **MBP6**/**MBQ2** and **MBP7**/**MBQ1** pairs can be useful, as the main difference will lie in the stabiliser block. This allows a comparison of

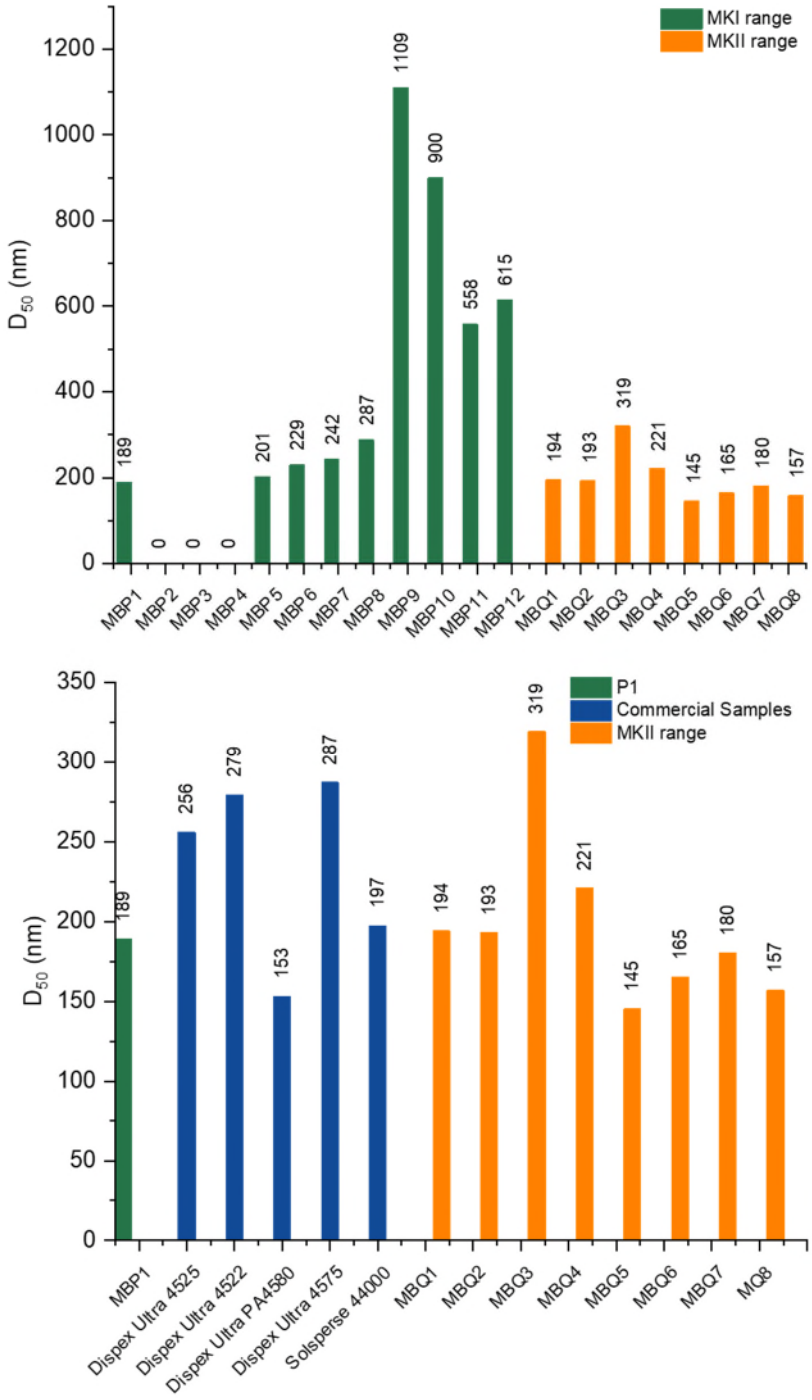


**Figure 4.11** $D_{50}$ data of aqueous carbon black mill bases stabilised with (top) MKI and MKII dispersants and (bottom) **P1**, MKII and commercially available pigment dispersants.

p(GlyMA)$_8$'s performance as opposed to that of p(GMA)$_{11}$(ETA). We can observe a difference in $D_{50}$ of 23, 33, and 48 nm, respectively in favour of the MKII dispersants. This then suggests that p(GlyMA) is a better stabiliser. Polymer solvation is an important factor to consider. This result could be due to the increased hydrophilicity of p(GlyMA) over that of p(GMA)(ETA). Auschra *et al.*[34] claim that aminic moieties have a high affinity to, and work well with many pigments. While still hydrophilic, this would imply that for similar polymer lengths, the MKI dispersants could arrange themselves more compactly, leading to a thinner steric barrier than in the case MKII MBs, figure 4.12. **MBQ3** performed the poorest ($D_{50}$ = 319 nm), likely owing to its insufficiently affinic iso-propyl anchor (which was also seen with **MBP8**). It is **MBQ5** (C9 anchor) that, in contrast, performed best with a 145 nm $D_{50}$. Overall, the results imply that an ideal anchor could be found where $9 \leq i \leq 12$.

The particle size distribution was also much more homogenous for **MBQ5**, and is much closer to a normal distribution with a mode at 144 nm. **MBQ6** displays the same bimodal distribution as was seen with **MBP1** and **MBP5**, with local modes at 78 and 290 nm, figure S4.4.

The flow behaviour of pigment dispersion can be an important practical assessment tool of the quality of the dispersion. The better the wetting and stabilising of the pigments, the more the mill bases are expected to express a Newtonian flow

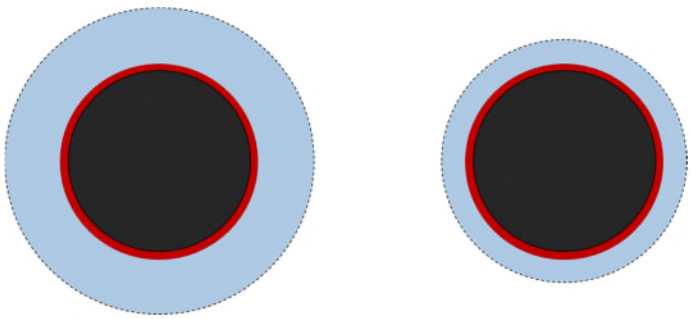

**Figure 4.12** Dispersed CB pigments with both adsorbed layer in red and steric barrier in blue.

behaviour.[35,36,37] On the other hand, less efficiently dispersed systems will have higher viscosities with shear-thinning behaviour due to shear-induced disaggregation of agglomerates that were not broken up during the milling process, or that appeared due to pigment flocculation. As mentioned previously, in order to produce a coating, it is more energy efficient to mill a pigment concentrate, or mill base, then "let down" into the coating. This mill base should be easily mixable with the resin; and low mill base viscosity is often preferred.

The flow curves of all dispersions using MKII dispersants are shown as log-log plots of viscosity or shear stress against a 1 to 2400 $s^{-1}$ shear rate range, figure 4.13.[37]

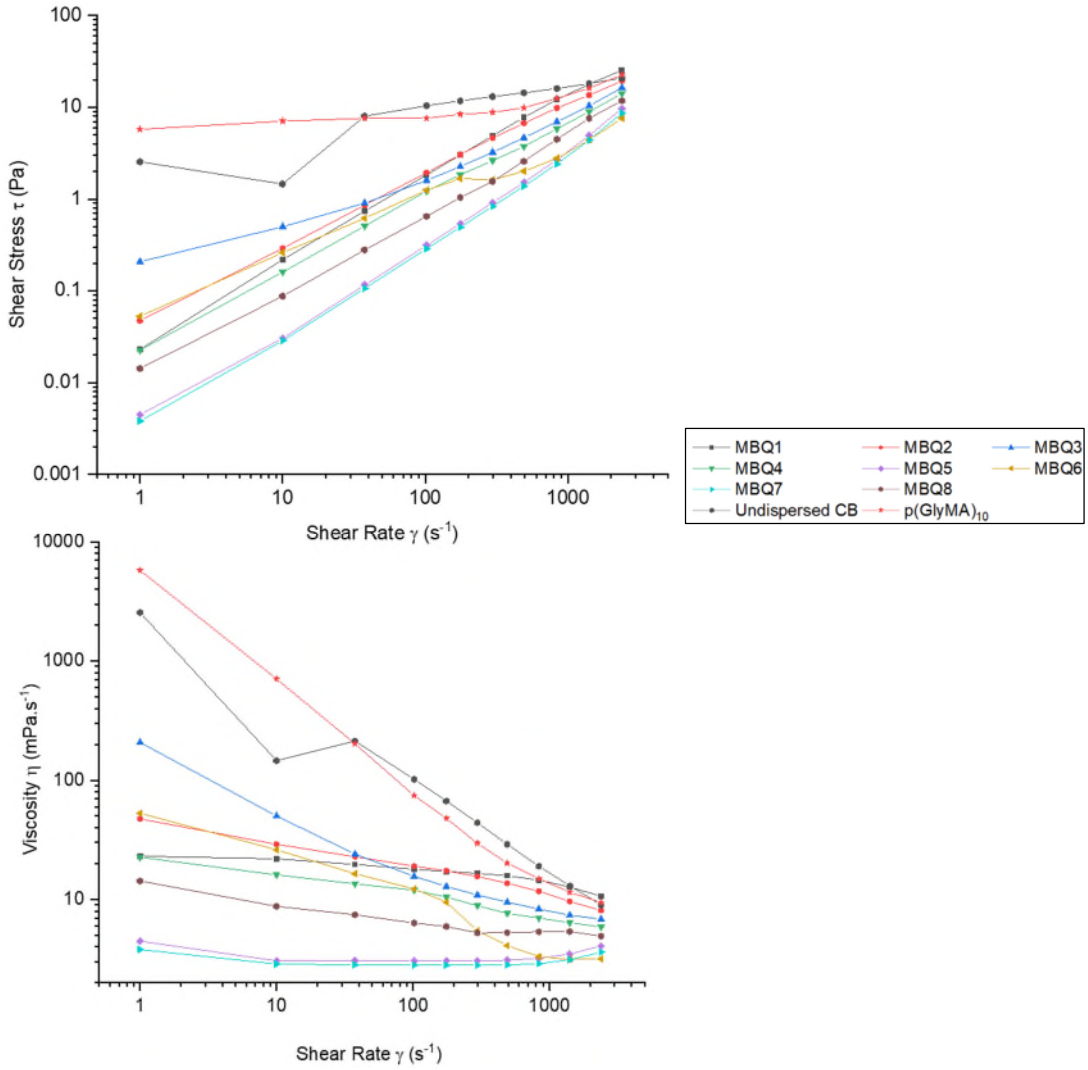


**Figure 4.13** Log-log flow curve plots of MKII dispersants-stabilised aqueous carbon black suspensions, undispersed CB and $p(GlyMA)_{10}$.

Initially most dispersions showed relatively low viscosities 15 $mPa.s^{-1} < \eta < 100$ $mPa.s^{-1}$, comparable to those of inkjet printing ink formulations,[38] and tended towards 9-10 $mPa.s^{-1}$ when shear rate approached 2400 $s^{-1}$.[39,40] This is a product of shear-thinning, as is expected for most suspensions, but which indicates incomplete dispersion. Also visible are an increase is in viscosity at high shear rates for **MBQ5** and **MBQ7**, as well as a downturn in viscosity for **MBQ6** at around 175 $s^{-1}$, which are likely measurement artefacts. Interesting behaviour can however also be observed. **Q5** and **Q7** based dispersions largely displayed Newtonian behaviour (between 10 and 1000 $s^{-1}$), with

viscosity remaining relatively constant and hints of shear thinning at lower shear rate, going from, respectively 4.47 and 3.81 mPa.s$^{-1}$ (at $\gamma$ = 1 s$^{-1}$) to 3.06 and 2.87 mPa.s$^{-1}$ (at $\gamma$ = 10 s$^{-1}$). This behaviour is usually preferred at this step over shear-thinning, as the mill base can be "*let-down*" into the resin more easily. However, it is important to note that none of the dispersions studied would pose a significant issue with regards to low shear rate viscosity given the low viscosities and yield point.

The yield point is defined as the stress required to set the fluid in motion. It is not measured directly. Instead, various mathematical curve fitting models have been developed to measure it.[41–44] As such, the yield point is not a constant and largely depends the model used. Here, it was elected to use the Casson model, which was first used to describe the behaviour of pigment-oil suspensions. This mathematical model is generally more suited to shear thinning material, with a Casson equation that can be written as

$$\sqrt{\tau} = \sqrt{\tau_c} + \sqrt{\eta_c . \gamma} \qquad \text{(eqn. 4)}$$

Where $\tau$ is the shear stress (Pa), $\tau_c$ the Casson yield point (Pa), $\eta_c$ the Casson viscosity (Pa.s$^{-1}$) and $\gamma$ the shear rate (s$^{-1}$). The yield point is then calculated as the

| Mill base | $R^2$ | Casson Yield Stress /mPa |
|---|---|---|
| MBQ1 | 0.987 | 75.1 |
| MBQ2 | 0.978 | 190.9 |
| MBQ3 | 0.998 | 239.1 |
| MBQ4 | 0.992 | 67.6 |
| MBQ5 | 0.994 | 4.8 |
| MBQ6 | 0.960 | 191.8 |
| MBQ7 | 0.994 | 3.4 |
| MBQ8 | 0.999 | 6.7 |

**Table 4.1** Casson yield stress values of carbon black mill bases dispersed using MKII dispersants.

square of the intercept obtained from the $\tau^{0.5}$ against $\gamma^{0.5}$ plot. The yield points for our mill bases are reported in table 4.1. The Casson model seems to provide a good fit, with high coefficients of determination ($R^2$), which indicates >90% of values that will fall within the regression line. Across the board, we observe low yield points for all mill bases but it is interesting to point out that **MBQ6**, which was based on a C12 anchor, has the highest yield point of all tested mill bases. **Q6** was one of the better dispersants. Intuitively, this mill base would be expected to have lower resistance to flow, similar to that of **MBQ5**. This discrepancy, along with the measurement artefact, warrants more testing.

### *4.2.4.2 MKII Dispersants aging analysis*

We wished to focus on the **Q5** and **Q6** dispersants. After a month, **MBQ5** showed little signs of flocculation, figure 4.14 (note: due to external factors, 1 month TEM measurements of **Q6** based suspensions could not be recorded).

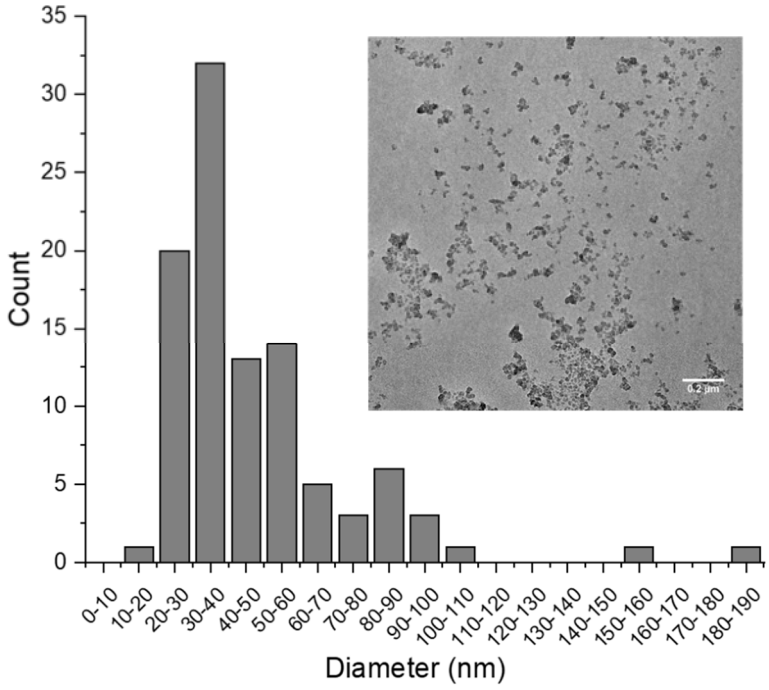


**Figure 4.14** TEM image and population size distribution of **MBQ5** one month after milling.

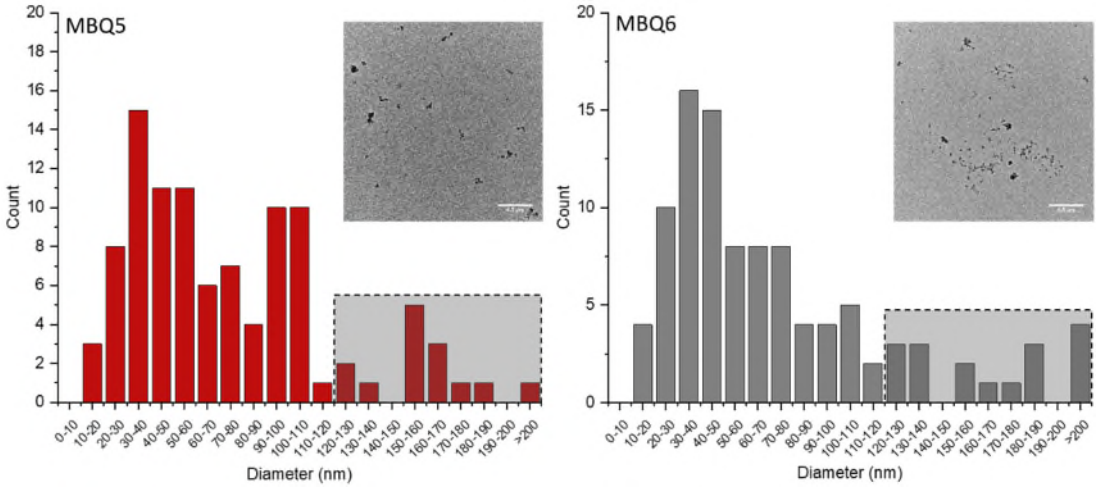


**Figure 4.15** TEM image and population size distribution of **MBQ5** and **MBQ6** three months after milling.

Comparisons after three months, however, show clear indications of flocculation for both MBs (**MBQ7** and **MBQ8**'s histogram are provided in figure S4.5). With **MBQ5**/**6** having mean agglomerate sizes of 74.2 ± 43.8 and 73.7 ± 52.5 nm, as well as medians of 63 and 53 nm respectively, both dispersions appeared to age relatively similarly, figure 4.15. However, overall, both **Q5** and **Q6** dispersants possessed imparted improved stabilisation to carbon black suspensions than commercial products. Both mill bases had low viscosities needed at this step of the paint formulation process.

Dispersants with C9 and C12 anchors needed a more in-depth analysis as potential ideal Raven 5000 ultra 3 pigment dispersant. More testing is also needed to address the observed visco- and rheometric discrepancies.

There are, however, a few reasons for not wanting to use thiol-based anchors, chief amongst which is the odour/smell of the compounds.

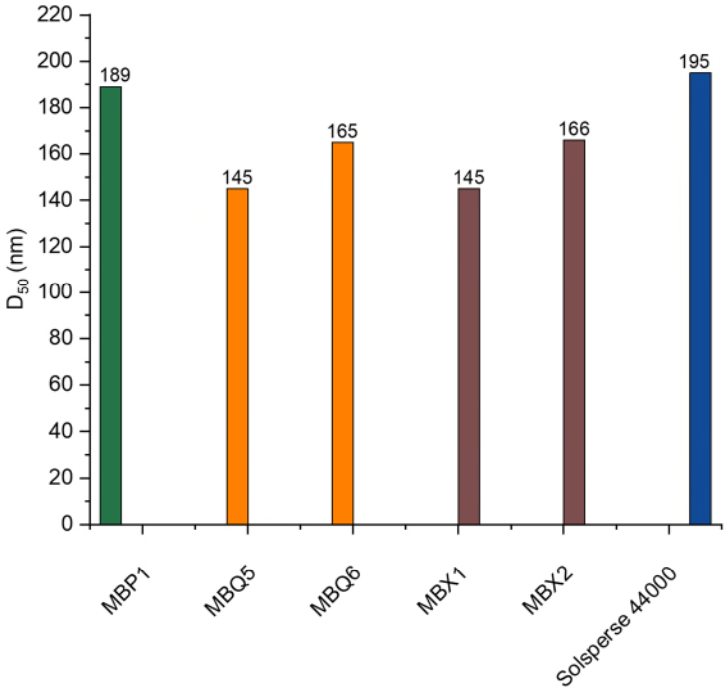


**Figure 4.16** $D_{50}$ data of the MKIII-based dispersions compared to **MBP1**, **MBQ5**/**6** and Solsperse 44000.

## 4.2.5 The MKIII Dispersant Range: Producing a Paint Formulation

### *4.2.5.1 MKIII Dispersants Analysis*

The MKIII range was developed in order to, primarily, substitute the thiol-based anchors to their respective amine counterparts, here, nonylamine and dodecylamine. This range of dispersants was, in addition, produced in view of addressing the increasing need of coating manufacturers to produce their goods in an eco-friendly manner. All dispersant synthesis steps were carried out in IPA, which is generally considered a safe solvent that is not classified as dangerous for the environment. The use of thiols was circumvented, in part due to the foul smells and health concerns. Finally, amines such as dodecylamine were used in the optic that, in higher industrial scales, the chemicals could be sourced from the purification of organic pollutants.

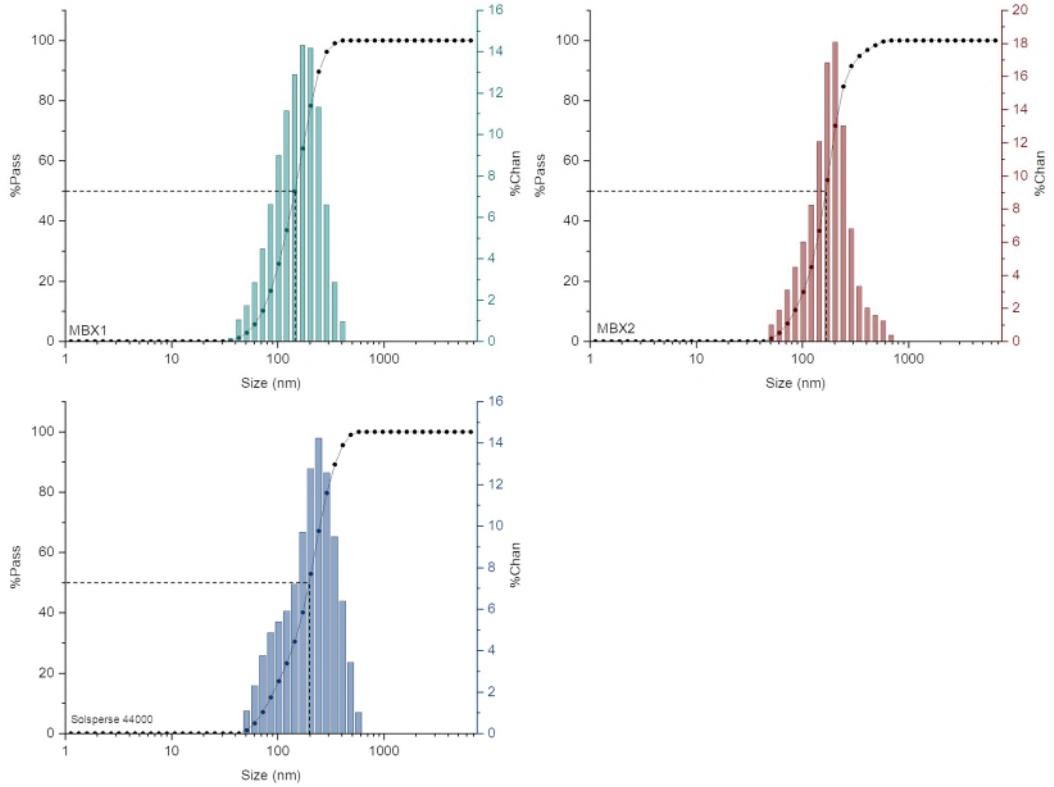


**Figure 4.17** DLS intensity histograms of **MBX1**, **MBX2** and Solsperse 44000.

Dodecylamine hydrochloride, for instance, is a cationic surfactant that is widespread in pigments and dye stuff manufacture, and is often discarded in waste waters.[45]

Looking at the $D_{50}$ data, we see a reversal in performance, with $p(GlyMA)_{10}(DDA)$ (**MBX1**, $D_{50}$ = 144.5 nm) performing better than $p(GlyMA)_{10}(NA)$ (**MBX2**, $D_{50}$ = 163.1 nm), figure 4.16. Moreover, DLS population histograms shows mono-modal distributions for both dispersions (**MBX1** mode = 172 nm, **MBX2** mode = 204 nm), not dissimilar to that of the commercially available product Solsperse 44000. Repeats of the dispersion of carbon black using **X1** (4 in total) showed excellent repeatability which confirmed DLS ($D_{50}$ = 150.9 ± 4.8 nm) and rheology analyses (average Casson yield point = 28.86 ± 3.05 mPa, discussed later), figures 4.17, S4.6 and S4.8.

**MBX1** had a much-improved viscosity over its homologous **MBQ6** suspensions throughout the investigated shear rate range, figure 4.17. It is unclear exactly why this difference in behaviour is observed, but one potential explanation is the introduction

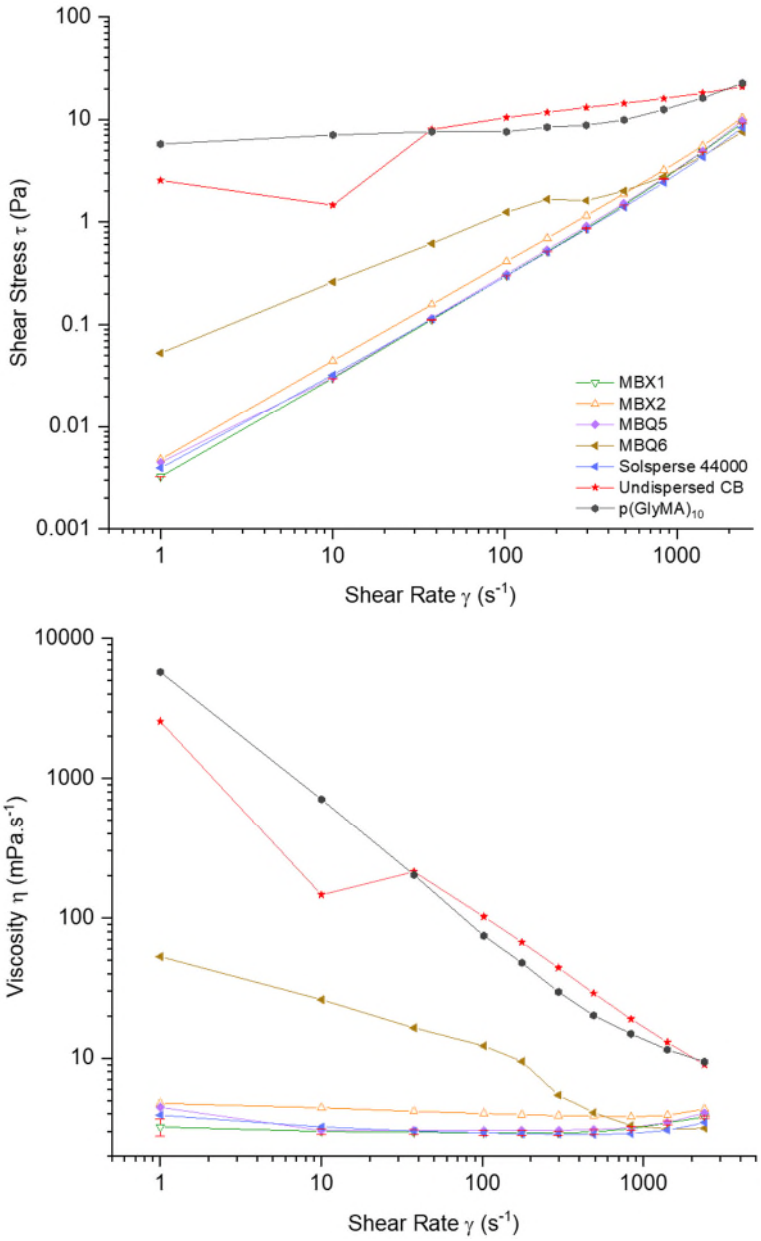


**Figure 4.18** Log-log flow curve plots of MKIII dispersants, **MBQ5**, **MBQ6** and Solsperse 44000 and $p(GlyMA)_{10}$-stabilised carbon black suspension, alongside measurements for undispersed CB.

of an amine-based anchor which, as discussed previously, is quite affinic towards the pigment surface and could impart an at least marginal improvement in attraction of the anchor to carbon black. It is also interesting to observe that both **MBX1** and **MBX2** displayed Newtonian flow behaviour, with yield points of 4.9 and 0.324 mPa (as opposed to 1.6 mPa for Solsperse 44000-based suspensions), figure S4.7.

Both **X1** and **X2** dispersants displayed low $D_{50}$ values (145 and 166 nm respectively), indicating good dispersing performance, but also showerd good aging of the mill bases with minimal flocculation (SI, figure S4.9, S4.10 and S4.11. *note*: due to COVID-19 restrictions, the 3 months measurement point could not be met, images were taken at 4 months, but size histograms were not produced). Furthermore, the low mill bases viscosities and Newtonian-flow behaviours can facilitate the let-down step in either case. Both dispersants dispersed CB better than pre-existing commercial products, while still having pendant hydroxyl groups available for further modification. However, dodecylamine, at £76/1L is two orders of magnitude less expensive than nonylamine (£425/100 g). The synthesis involves a polymerisation step and a single post-polymerisation modification step. It is expected that the overall cost of production of the synthesis of **X1**, even at higher scales, will remain low. The monomer, GlyMA, can be prepared from the hydrolysis of glycidyl methacrylate, an inexpensive, widely available monomer (£59/500mL). DDA is also solid at room temperature, therefore easier to handle. This makes **X1** preferable from economic and synthetic viewpoints. As such, **X1** will be chosen as final dispersant candidate for this project and will be the subject of further work.

### *4.2.5.2 Colorimetry*

In addition to DLS and viscosity measurements, other requirements need to be satisfied when designing carbon black dispersants. Looking further ahead after the mill base production step, is the "*let-down*" step that leads to the production of the final coating formulation and presupposes colorimetric assessments of said coatings. Black coatings, technically, do not impart colour to surfaces, but serve more as a way to hide the surface, the perceived degree of blackness can be measured and is typically called "jetness". The colour properties can be quantitatively measured using industry standard methodology. In this work, the method is adapted from DIN 6174. This

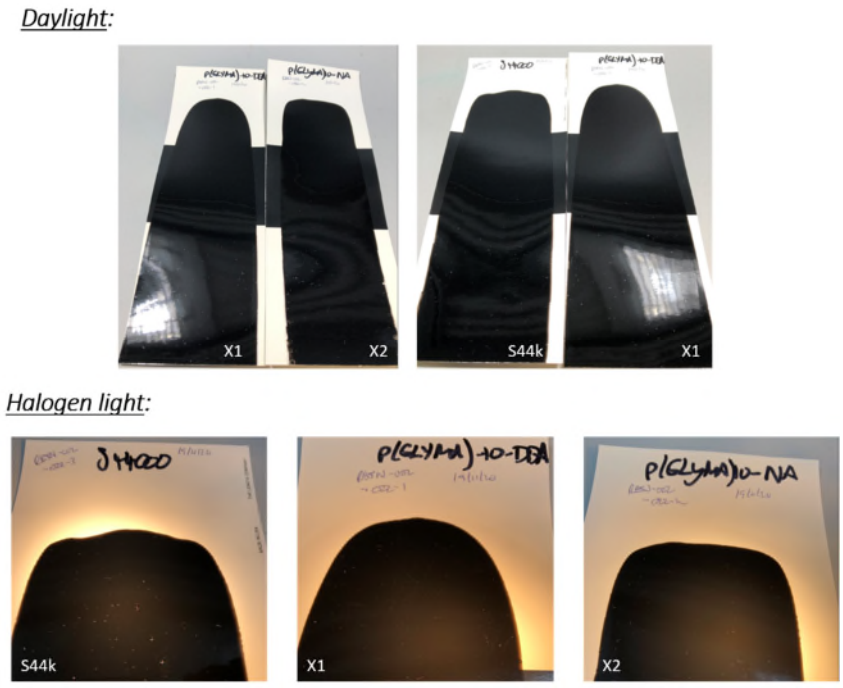


**Figure 4.19** Coatings of **X1**, **X2** and Solsperse 44000 stabilised paints spread onto black & white card with K-bar. Measurements by Robert Jennings.

| Jetness | My | Mc | dM |
|---|---|---|---|
| *MBX1* | 266 | 262 | -3 |
| *MBX2* | 268 | 265 | -3 |
| *S44k* | 274 | 274 | -0.3 |
| *p(GlyMA)$_{10}$* | 270 | 269 | -1.0 |
| *Undispersed CB* | 176 | 173 | -2.3 |
| **Gloss/Haze** | **Haze** | **20° Gloss** | **60° Gloss** |
| *MBX1* | 35.7 | 89.8 | 95.9 |
| *MBX2* | 32.4 | 86.8 | 94.1 |
| *S44k* | 38.2 | 87.6 | 91.4 |
| *p(GlyMA)$_{10}$* | 106.0 | 91.5 | 95.2 |
| *Undispersed CB* | 263.0 | 59.5 | 84.2 |

**Table 4.2** Colorimetric, gloss and haze data of let-down samples prepared using **X1**, **X2**, Solsperse 44000 and p(GlyMA)$_{10}$ with an undispersed carbon black control.

methodology allows the measurement of three parameters $M_y$ and $M_c$, respectively the hue independent and dependant degree of jetness and dM the absolute contribution of hue, table 4.2. Figure 4.18 shows natural and halogen images of the dry coatings plates used to evaluate colorimetric properties (images from control measurements are shown in figure S4.12). It is seen that Solsperse 44000 based coatings, having higher $M_y$ and $M_c$ values, would be perceived as having higher blackness the MKIII based formulation. Hue can be evaluated from the difference between the two jetness parameters, usually when:

- dM < 0: coatings have brownish undertones
- dM ≈ 0: coatings are achromatic
- dM > 0: coatings have blueish undertones

In the automotive industry, blue undertones are perceived as a lusher, vivid colour and is used for exteriors, while brown/red undertones will be warmer and preferred for

interiors. Here, both of the MKIII dispersants impart a brown undertone to the coating, against the achromaticity of the Solsperse based coating, which could make them good candidates for interior applications. Finally, we see that our developed dispersant also contribute towards both lower haze, and higher gloss than what the commercial product, which in either case is favourable towards our product.

To confirm the repeatability of our results we, here too, repeated the let-down step for the favoured **X1** dispersant (three times) and measured jetness, haze and gloss, which generally confirmed our previous measurements with average values of $M_y$, $M_c$ and dM of 263 ± 2.2, 260 ± 1.3 and -2 ±0.7, as well as average haze and 20o gloss of 33.15 ± 2.00 and 90.6 ± 0.53, see figure S4.13. With every polymeric product that is considered for commercial applications comes the need to consider the weatherability of said product. Polymer degradation comes with the presence of labile groups such as esters or amides. Therefore, the backbone of our dispersants should remain stable. The side chains, with the presence of ester functionalities, however, might be susceptible to hydrolysis reactions. However, having established that the resulting paints would be better suited for interiors due to their colourimetric properties, exposure to water, and weatherability, are less likely to occur during the lifecycle of the product.

## 4.3 Conclusions and Outlook

The reports of the application of CCTP to carbon black and coating science, is mostly found in the academic and patent literature of the 1990's and, if infrequent in the last decade, found little success. In this body of work, three generations of amphiphilic polymethacrylates synthesised in previous chapters, namely MKI, II and III, were here tested as stabilisers in carbon black aqueous suspensions.

Dispersants from the MKI range were tested first. It was found that an increase to the hydrophilicity of the stabilising segment would be necessary, but also that linear aliphatic anchors could potentially adsorb onto the pigment surface better than other types of tested anchors (aliphatic ring, short aliphatic, aromatic) according to in-situ DLS and TEM measurements. Finally, particle bridging started to occur at higher molecular weights, which prompted the use thereafter of dispersants with targeted molecular weights ranging from 1 to 2.5 kDa.

The MKII range was developed from the observations made during the MKI investigation. A poly(glycerol monomethacrylate) hydrophilic segment provided sufficient hydrophilicity to allow easy dispersion of the polymers in water. An investigation into the length of aliphatic linear anchors also suggested than chain lengths of 9-12 carbon provided the best stability to the systems.

The stability of aqueous pigment suspensions relies on several factors:

- The quality of adsorption of the hydrophobic segment onto the pigment surface.
- The effectiveness of the repulsion induced by the stabilising segments.
- The long-term stability of the system

Using a systematic, iterative process, stabilisers were tested and the properties that afforded increased stability of the pigment system selected for. Using a one step methodology p(GlyMA) was, in chapter 3, reacted with the hydrophobic alkylamines using microwave-assisted synthesis. Amines were used, as they are less malodorous and comparatively less toxic than thiols. Two final dispersant candidates (MKIII) with C9 and C12 anchors, were obtained. These dispersants performed best and showed excellent repeatability and aging, outperforming current commercially available products.

The dispersants developed in this body of work consisted of AB dispersants, meaning they were made up of one anchor and one stabilising segment. However, dispersants can have multiple anchors and/or stabilising segments, such that we can encounter ABA, BAB, $A(B)_n$, or $(AB)_n$ dispersants. Future work, therefore, will first allow a widening and exploration of the influence of the number of anchors or stabilising segments on the quality of the dispersion.

It is anticipated that this can be achieved using dimer amines. Dimer amines are a class of compounds increasingly found in the literature and in industry. Companies such as Croda are able to produce dimer amines from renewable sources. They are usually prepared by modification of dimer acids, themselves obtained by dimerization of unsaturated fatty acids derived from waste vegetable oil. As such, building on the methodology presented in chapter 3, the dispersant would be of the structure A-B-A, a triblock copolymer: $p(GlyMA)_n$-DA-$p(GlyMA)_n$ which combines linear aliphatic anchors and two stabilising segments, while also being partly prepared from renewable resources.

Furthermore, having hydroxyl groups radiating out of the stabilising segments also offers potential for future work. These reactive moieties can, after pigment stabilisation, be reacted in an inter-molecular fashion through esterification using diacids. This could constitute a pigment encapsulation step that could further negate pigment re-agglomeration.

# 4.4 Experimental Data

## 4.4.1 Additional Figures and Schemes

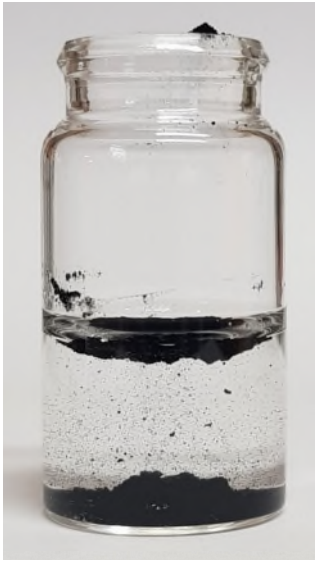

**Figure S4.1** Undispersed carbon black in water.

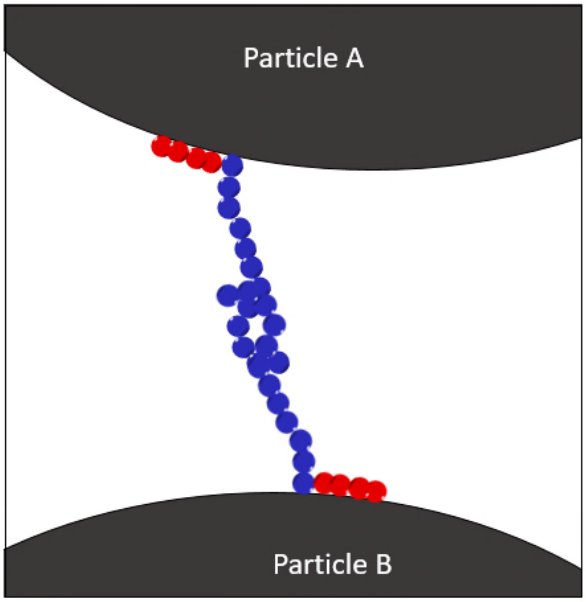


**Figure S4.2** Particle bridging from long solvophilic chains.

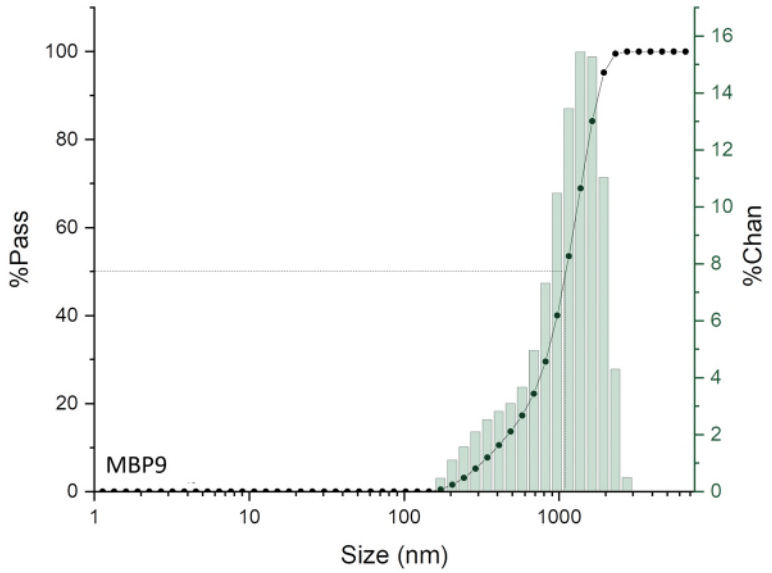


**Figure S4.3** DLS intensity histogram and cumulative plot of **MBP9**.

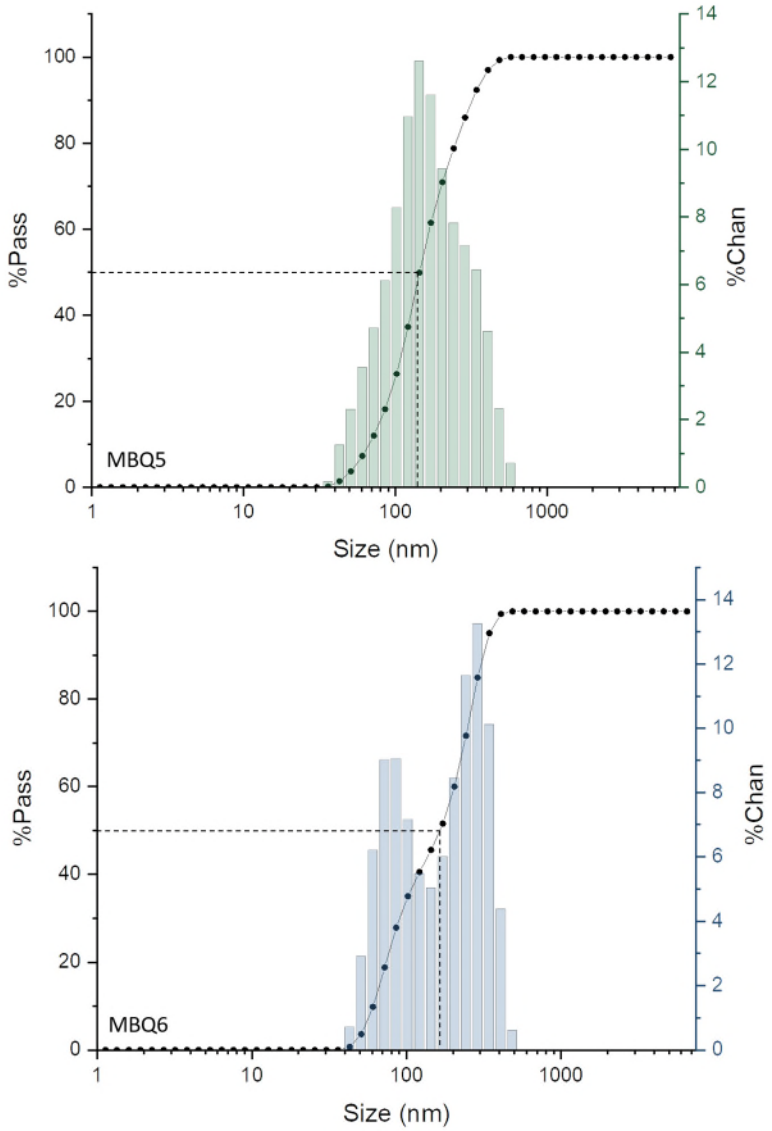


**Figure S4.4** DLS intensity histogram and cumulative plot of **MBQ5** and **MBQ6**.

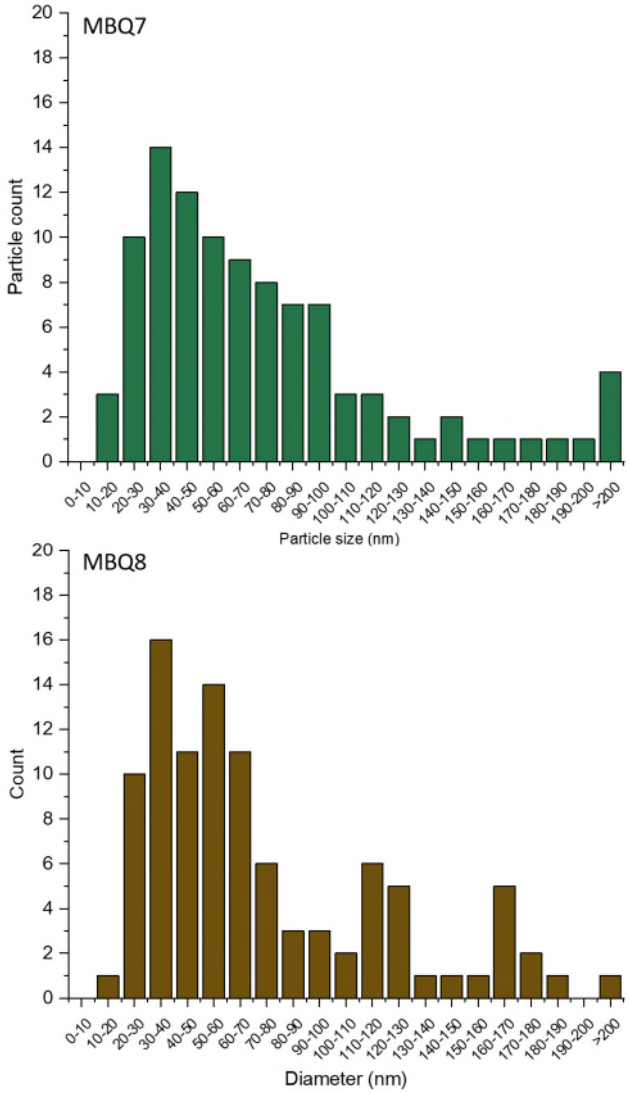


**Figure S4.5** TEM-based size histograms of **MBQ7** and **MBQ8** three months after milling.

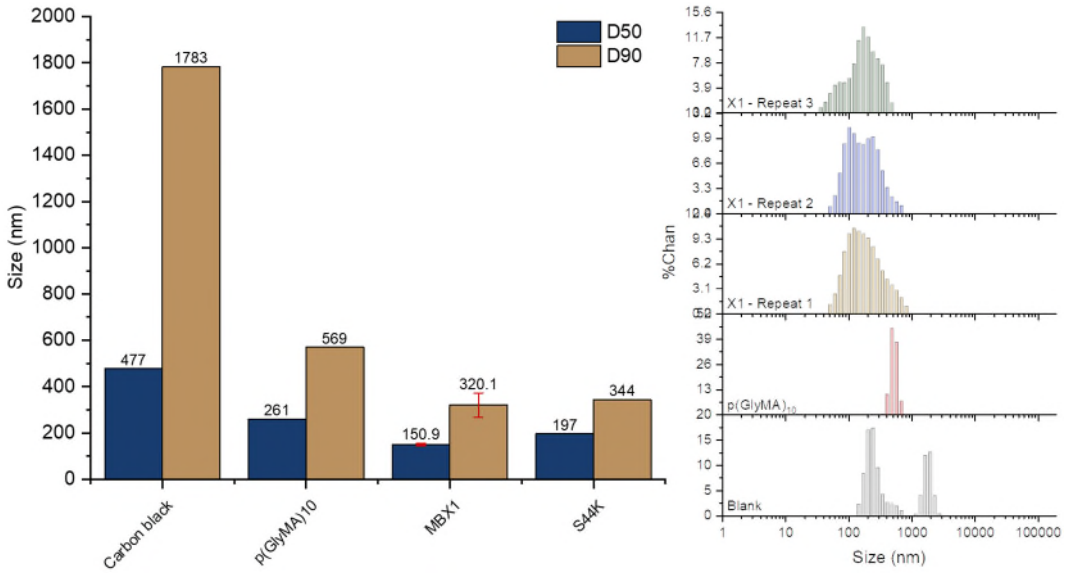


**Figure S4.6** $D_{50}$ (left) and DLS intensity histogram of **MBX1** (with repeats) and controls.

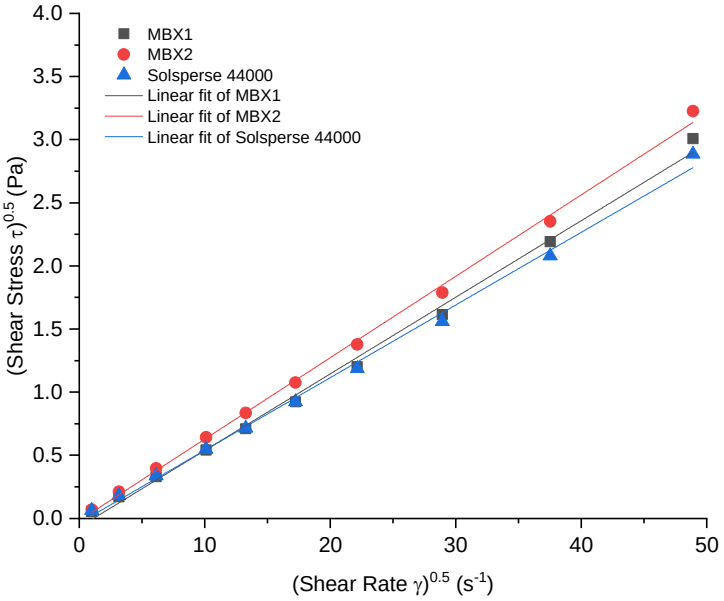


| Equation | y = a + b*x | | |
|---|---|---|---|
| Plot | MBX1 | MBX2 | Solsperse 44000 |
| Weight | No Weighting | | |
| Intercept | -0.07 ± 0.033 | -0.018 ± 0.024 | -0.037 ± 0.029 |
| Slope | 0.061 ± 0.001 | 0.065 ± 9.883E-4 | 0.058 ± 0.001 |
| Residual Sum of Squares | 0.034 | 0.017 | 0.025 |
| Pearson's r | 0.998 | 0.999 | 0.998 |
| R-Square (COD) | 0.996 | 0.998 | 0.997 |
| Adj. R-Square | 0.995 | 0.998 | 0.996 |

**Figure S4.7** Casson yield stress fitting for **MBX1**, **MBX2** and Solsperse 44000 millings.

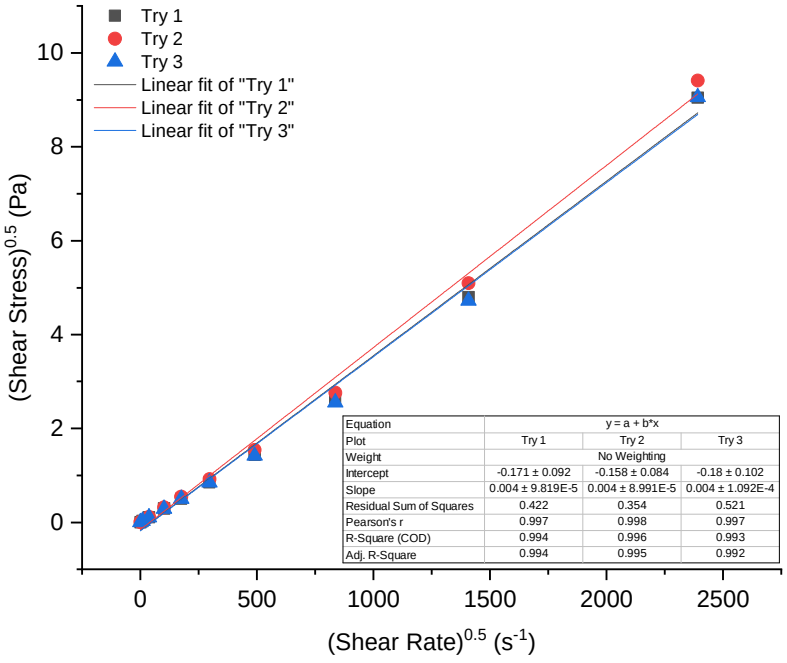


| Equation | y = a + b*x | | |
|---|---|---|---|
| Plot | Try 1 | Try 2 | Try 3 |
| Weight | No Weighting | | |
| Intercept | -0.171 ± 0.092 | -0.158 ± 0.084 | -0.18 ± 0.102 |
| Slope | 0.004 ± 9.819E-5 | 0.004 ± 8.991E-5 | 0.004 ± 1.092E-4 |
| Residual Sum of Squares | 0.422 | 0.354 | 0.521 |
| Pearson's r | 0.997 | 0.998 | 0.997 |
| R-Square (COD) | 0.994 | 0.996 | 0.993 |
| Adj. R-Square | 0.994 | 0.995 | 0.992 |

**Figure S4.8** Casson yield stress fitting for **MBX1** milling test repeats.

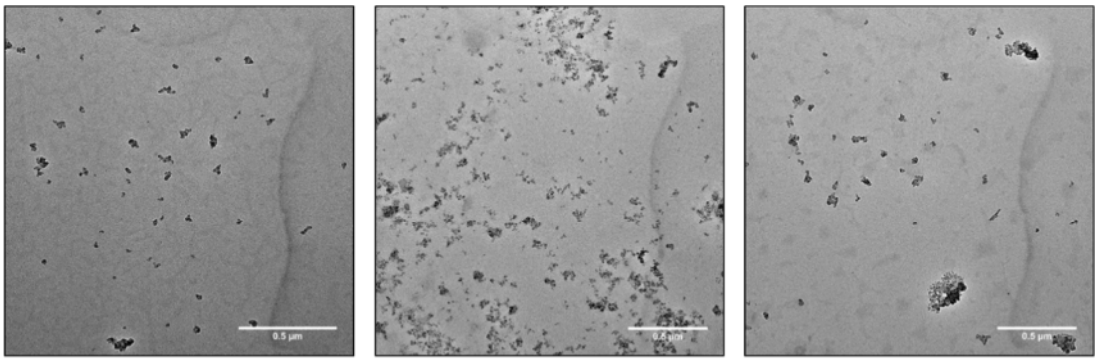


**Figure S4.9** TEM images of **MBX1**, **MBX2** and Solsperse 44000 dispersions, one month after milling.

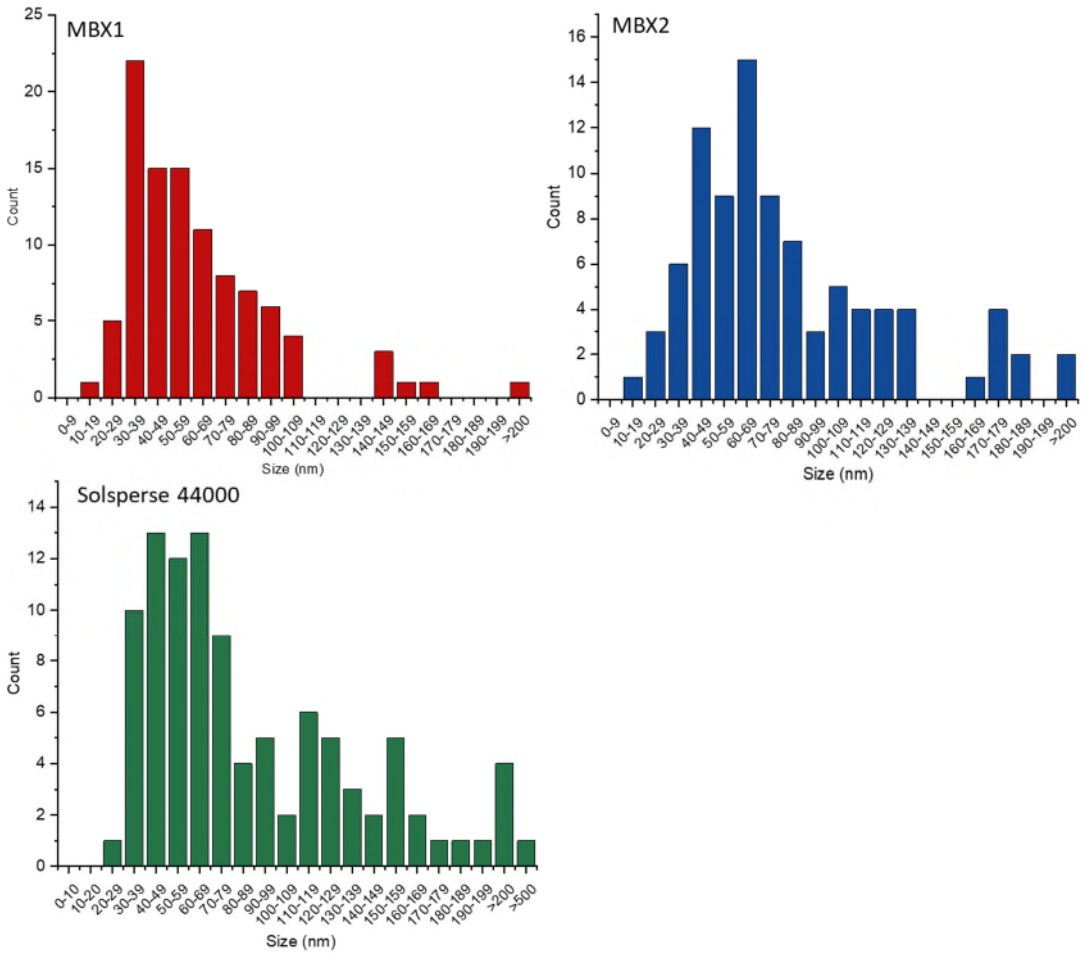


**Figure S4.10** TEM-based size histograms of **MBX1**, **MBX2** and Solsperse 44000 dispersions, one month after milling.

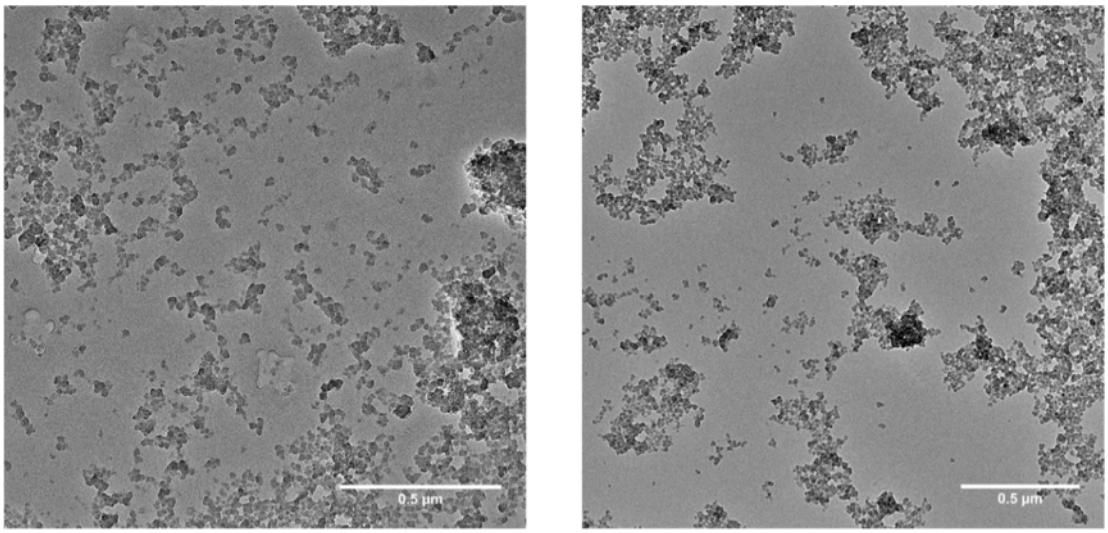


**Figure S4.11** TEM images of **MBX1**, **MBX2** and Solsperse 44000 dispersions, four months after milling.

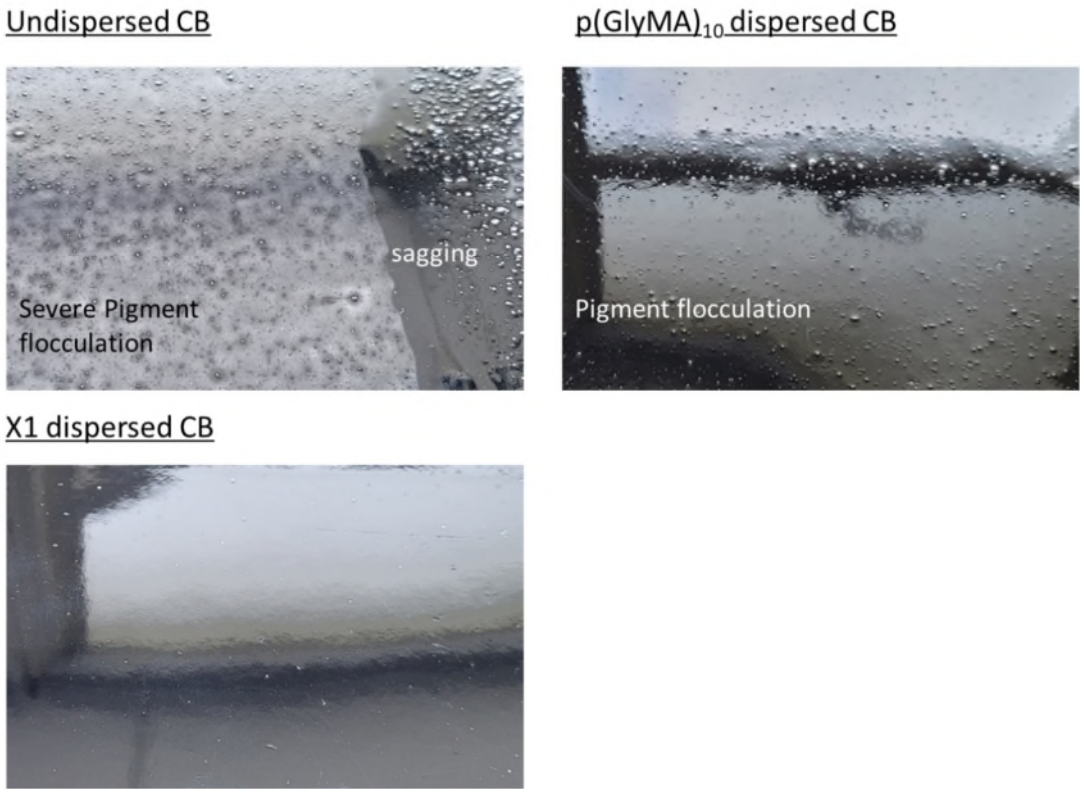


**Figure S4.12** Images of the coating plates used for gloss and jetness measurements of undispersed carbon black, as well as $p(GlyMA)_{10}$ and **X1**-stabilised carbon black under natural light.

| | My | Mc | dM |
|---|---|---|---|
| *MBX1 – original* | 266 | 262 | -3 |
| *MBX1 – 2* | 264 | 260 | -3 |
| *MBX1 – 3* | 260 | 258 | -1.8 |
| *MBX1 – 4* | 262 | 260 | -1.8 |

| | Haze | 20o Gloss | 60o Gloss |
|---|---|---|---|
| *MBX1 – original* | 35.73 | 89.80 | 95.93 |
| *MBX1 – 2* | 31.2 | 90.5 | 95.5 |
| *MBX1 – 3* | 34.5 | 91.1 | 96.0 |
| *MBX1 – 4* | 31.2 | 91.1 | 96.0 |

**Figure S4.13** Jetness and gloss data obtained from all **X1**-based dispersions.

### 4.4.2 Materials

Unless stated otherwise, all chemicals mentioned were purchased from Sigma-Aldrich and were used without further purification.

Carbon black Raven® 5000 ultra® 3 pigment was purchased from Birla Carbon.

### 4.4.3 Instrumentation

*BET surface area* measurements of samples were performed using a Quantachrome Quadrasorb-evo. Samples were degassed at 200 °C for 6 hours prior to analysis to remove surface contaminants. Then known amounts of $N_2$ were introduced into the evacuated sample tubes and adsorbed onto the particle surface at cryogenic temperature whilst measuring the change in relative pressure from which the surface area is determined based on the theory by Brunauer, Emmett and Teller

*In-situ dynamic light scattering (DLS)* measurements were carried out on a nanotrack flex by microtrac. Milling samples were transferred into 20 mL vials. Each measurement consisted of 1x30 seconds run time.

*Transmission electron microscopy (TEM)* images were obtained on a JEOL 2100 TEM fitted with a Gatan Ultrascan 1000 camera. Samples were diluted at 0.1% v/v and one drop was cast on a carbon coated TEM copper grid. After 2 minutes the drop was blotted off with filter paper. All samples were prepared without using a stain.

*Rheology* measurements were carried out with a discovery HR1 rheometer. Measurements were made at room temperature with 0.0 sec Soak time. 10 shear rates values were selected for measurement (1.0, 10.0, 37.6, 102.1, 176.0, 297.0, 491.0, 837.0, 1408.0, 2392.0 1/s). Max equilibration time was set at 60 with a sample period of 10.0 seconds and a 5% tolerance.

A datacolour 550 was used to measure the *XYZ values* (in the 1976 colour space. The following formulae were used to determine jetness parameters:

$$M_y = \log_{10}\left(\frac{1}{\frac{Y}{100}} * 100\right)$$

$$M_C = 100 \times \left(log_{10}\left(\frac{1}{\frac{X}{94.81}}\right) - log_{10}\left(\frac{1}{\frac{Z}{107.34}}\right) + log_{10}\left(\frac{1}{\frac{Y}{100}}\right)\right.$$

$$dM = M_c - M_y$$

Finally, *Gloss/haze* were measured with a Byk gardner haze/gloss meter, calibrated against the standard tile.

### 4.4.4 Experimental Procedures

**Mill base preparation**

A 10% carbon black loading protocol was followed for the preparation of the studied mill bases. In glass vials were first dispersed 1 g of dispersant (from MKI, MKII, MKII or commercial ranges) in 8 g of distilled water. After full dispersion, 1 g of carbon black and 17 g of glass beads (3 mm in diameter) were added. The vials were subsequently capped, tapped, and shaken horizontally for 16 hours.

**Let-down preparation**

To prepare let-down samples, 1 g of mill base was added to 5 g of Setaqua 6160 (ex Allnex) acrylic resin. The mixture was shaken thoroughly and then coated onto black and white cards with K-bar 6 (wet film thickness ≈ 60 µm). The plates were then air dried for 3 hours and then oven cures at 120 °C. for 30 min (dry film thickness ≈ 25 µm).

## 4.5 References

1 ORION Engineered Carbons, *What is Carbon Black?*, 2014, https://www.orioncarbons.com/what_is_carbon_black, (accessed 5 February 2021).

2 M.-J. Wang, C. A. Gray, S. R. Reznek, K. Mahmud and Y. Kutsovsky, in *Encyclopedia of Polymer Science and Technology*, John Wiley & Sons Inc., 2003, 761-803.

3 Orion Engineered Carbons GmbH, Carbon Black in Tires, https://www.orioncarbons.com/tire, (accessed 5 February 2021).

4 Carbon Black Market Report: Global Industry Analysis, 2025,

https://www.ceresana.com/en/market-studies/chemicals/carbon-black/ceresana-market-study-carbon-black.html, (accessed 5 February 2021).

5 A. Choudhary and E. Prasad, Carbon Black Market Size, Share | Industry Growth & Forecast, 2026, https://www.alliedmarketresearch.com/carbon-black-market, (accessed 5 February 2021).

6 N. Rattanasom, T. Saowapark and C. Deeprasertkul, *Polym. Test.*, 2007, **26**, 369–377.

7 Y. Fukahori, *Rubber Chem. Technol.*, 2003, **76**, 548–565.

8 Y. hu Song, L. bin Zeng and Q. Zheng, *Chinese J. Polym. Sci. (English Ed.*, 2017, **35**, 1436–1446.

9 E. M. Dannenberg, *Rubber Chem. Technol.*, 1986, **59**, 512–524.

10 M. Knite, V. Teteris, A. Kiploka and J. Kaupuzs, *Sensors Actuators, A Phys.*, 2004, **110**, 142–149.

11 US Pat., 3,862,056, 1975.

12 F. Tiarks, K. Landfester and M. Antonietti, *Macromol. Chem. Phys.*, 2001, **202**, 51–60.

13 A. I. Medalia and L. W. Richards, *J. Colloid Interface Sci.*, 1972, **40**, 233–252.

14 M. A. Bhakare, P. H. Wadekar, R. V. Khose, M. P. Bondarde and S. Some, *Prog. Org. Coatings*, 2020, **147**, 105872.

15 M. Mozetič, A. Zalar, P. Panjan, M. Bele, S. Pejovnik and R. Grmek, *Thin Solid Films*, 2000, **376**, 5–8.

16 US Pat., US4530961A, 1985.

17 H. Sis and M. Birinci, *Colloids Surfaces A Physicochem. Eng. Asp.*, 2009, **341**, 60–67.

18 European Patent Office, EP1826247B1, 2014.

19 T. Liu, S. Jia, T. Kowalewski, K. Matyjaszewski, R. Casado-Portilla and J. Belmont, *Macromolecules*, 2006, **39**, 548–556.

20 W. Li, Z. Xie and Z. Li, *J. Appl. Polym. Sci.*, 2001, **81**, 1100–1106.

21 M. Sharif Sh., F. Golestani Fard, E. Khatibi and H. Sarpoolaky, *J. Taiwan Inst. Chem. Eng.*, 2009, **40**, 524–527.

22 H. Ridaoui, A. Jada, L. Vidal and J. B. Donnet, *Colloids Surfaces A Physicochem. Eng. Asp.*, 2006, **278**, 149–159.

23 C. of the E. Union, *Council Directive 1999/13/EC of 11 March 1999 on the limitation of emissions of volatile organic compounds due to the use of organic solvents in certain activities and installations*, 1999.

24 H. Sis and M. Birinci, *Colloids Surfaces A Physicochem. Eng. Asp.*, 2009, **341**, 60–67.

25 J. B. Donnet and R. C. Bansal, *Carbon Black: Science and Technology, Second Edition*, 1993.

26 *Raven ® and Conductex ® Carbon Blacks for Specialty Applications*, .

27 V. Vajihinejad, S. P. Gumfekar, B. Bazoubandi, Z. Rostami Najafabadi and J. B. P. Soares, *Macromol. Mater. Eng.*, 2019, **304**, 1800526.

28 S. Farrokhpay, *Adv. Colloid Interface Sci.*, 2009, **151**, 24–32.

29 T. Hüffer, S. Endo, F. Metzelder, S. Schroth and T. C. Schmidt, *Water Res.*, 2014, **59**, 295–303.

30 S. Rimmer, C. Johnson, B. Zhao, J. Collier, L. Gilmore, S. Sabnis, P. Wyman, C. Sammon, N. J. Fullwood and S. MacNeil, *Biomaterials*, 2007, **28**, 5319–5331.

31 R. Haigh, S. Rimmer and N. J. Fullwood, *Biomaterials*, 2000, **21**, 735–739.

32 K. Mequanint, A. Patel and D. Bezuidenhout, *Biomacromolecules*, 2006, **7**,

883–891.

33 E. Patrucco, S. Ouasti, D. V. Cong, P. De Leonardis, A. Pollicino, S. P. Armes, M. Scandola and N. Tirelli, *Biomacromolecules*, 2009, **10**, 3130–3140.

34 C. Auschra, E. Eckstein, A. Mühlebach, M. O. Zink and F. Rime, in *Progress in Organic Coatings*, 2002, **45**, 83–93.

35 H. R. Hamburg and W. M. Morgans, *Hess's Paint Film Defects*, Springer Netherlands, 1979.

36 R. Bhavsar, R. Raj and R. Parmar, *Prog. Org. Coatings*, 2013, **76**, 852–857.

37 R. R. Eley, *J. Coatings Technol. Res.*, 2019, **16**, 263–305.

38 J. Duffy, *Analytical strategies for ink formulation*, 2015.

39 L. Dintenfass, *Rheol. Acta*, 1962, **2**, 187–202.

40 P. V Liddell and D. V Boger, *Ind. Eng. Chem. Res.*, 1994, **33**, 2437–2442.

41 E. C. Bingham, *Fluidity and plasticity*, New York McGraw-Hill Book Company, Inc., 1922.

42 E. C. Bingham, *An investigation of the laws of plastic flow*, Washington, D.C. : U.S. Dept. of Commerce, Bureau of Standards, 1916, 309-353.

43 W. H. Herschel and R. Bulkley, *Kolloid Zeitschrift*, 1926, **39**, 291–300.

44 N. Casson, *Br. Soc. Rheol. Bull.*, 1957, **52**, 5–6.

45 P. Chen, H. Li, S. Song, X. Weng, D. He and Y. Zhao, *Results Phys.*, 2017, **7**, 2281–2288.

# **Chapter 5**:

# Branched Macromonomers from Catalytic Chain Transfer Polymerisation (CCTP) as Precursors for Emulsion-Templated Porous Polymers

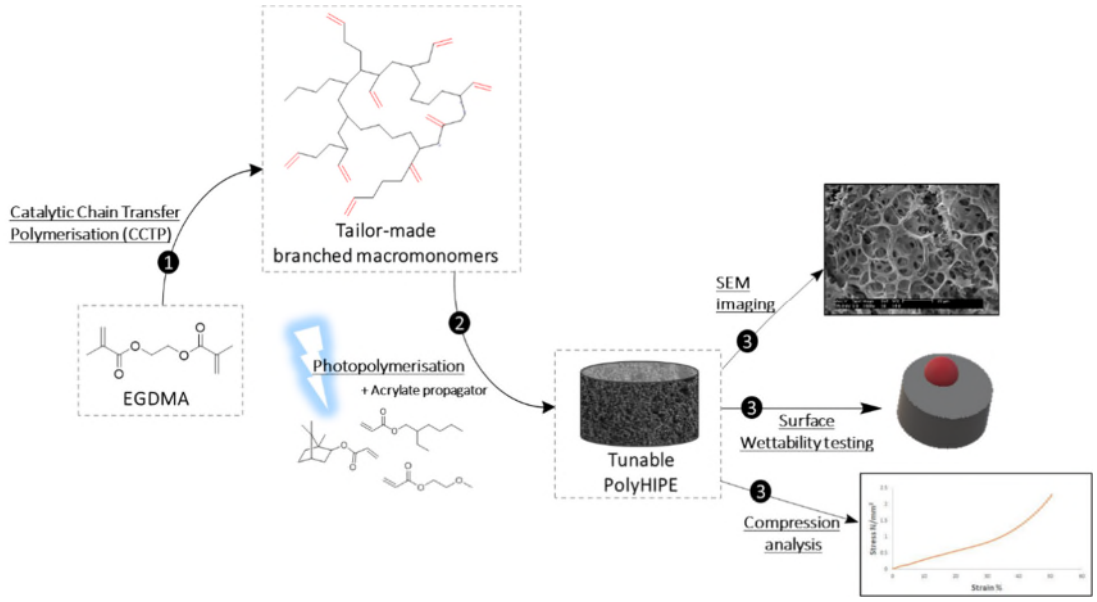


*Data in this chapter has been published:*

C. J. Atkins, D. K. Seow, G. Burns, J. S. Town, R. A. Hand, D. W. Lester, N. R. Cameron, D. M. Haddleton and A. M. Eissa, *Polym. Chem.*, 2020, **11**, 3841–3848.

*Work was carried out with the help of MChem student David Seow*

## 5.1 Introduction

Macroporous polymers have garnered increasing interest over the last few years.[1–4] Such materials can be used for energy and gas storage,[5,6] heat insulation[7] and cell culture[8,9] applications.

One of the ways that was developed to obtain such materials uses high internal phase emulsions (HIPEs).[10] HIPEs are "water in oil" inverse emulsions whereby the continuous phase is generally made up of monomer(s), initiator, crosslinker and a surfactant. The internal, droplet phase is added dropwise under vigorous stirring and, to satisfy the HIPE requirements, must take up a volume of at least 74% with regards to the continuous phase, figure 1.14. From this HIPE can then be produced polyHIPEs when the continuous phase is polymerised. FRP is the traditionally used method, but other techniques can be employed. Deleuze *et al.*[11] used ring-opening metathesis polymerisation of a norbornene derivative to prepare easy to handle, non-brittle polyHIPEs, but the use of ATRP[12] or RAFT[13] has also been reported.

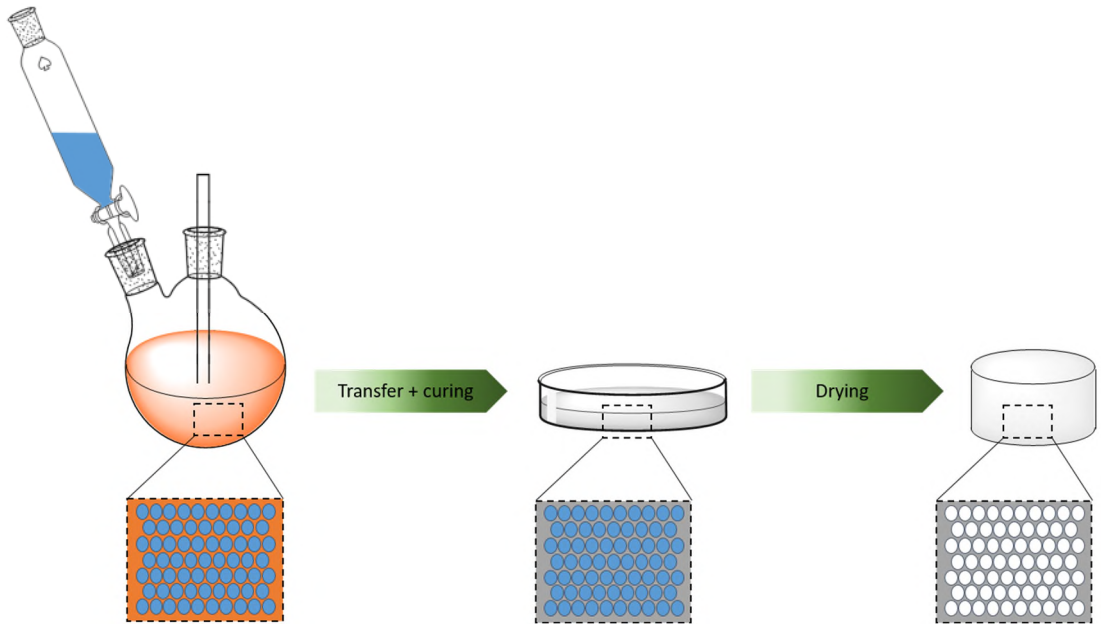


**Figure 5.1** PolyHIPE synthesis process.

Chen *et al.*[14] synthesised thiol-ene/-yne-based polyHIPEs using a commercially available multifunctional thiol with multi-functional acrylic, allyl ether- or alkyne-based monomers. It has been previously shown that the mechanical properties of polyHIPE materials correlate with the degree of functionality of monomers used. PolyHIPEs made from pentaerythritol tetraacrylate produced material with higher yield strengths than those made from 1,6-hexanediol diacrylate or trimethylolpropane triacrylate.[14] Other reactions such as Diels-Alder and copper-catalysed azide-alkyne cycloaddition click reactions have been successfully implemented in the preparation of polyHIPE materials.[15,16] Careful consideration in the selection of monomers helps tune the properties of the final polyHIPE material. Therefore, the development of synthetic approaches that allow wider access to bespoke multifunctional macromonomers and/or crosslinking agents that can be incorporated into polyHIPE preparations are desirable.

CCTP is a facile and interesting controlled polymerisation technique that has been employed for the preparation of low molecular weight functional polymethacrylates.[17–20] Much of our current knowledge of CCTP comes from investigations carried out by commercial organisations such as DuPont[21] and ICI/Zeneca,[22,23] complemented in academia by Gridnev,[24,25] Heuts,[26] Davis and Haddleton.[27-28]

McEwan *et al.*[29] for instance utilised CCTP to produce relatively low molecular weight branched polymers containing high levels of terminal vinyl functionalities that showed potential as reactive sites for further chemistries.

The current work was designed to combine CCTP with emulsion templating techniques to produce polyHIPE materials with tuneable properties. CCTP provides control over branching and molecular weight of the CCTP derived branched

macromonomer crosslinkers, which can in turn lead to the generation of polyHIPE materials where functionality and rigidity can be tailored.

In this chapter, we describe the free radical polymerisation of ethylene glycol dimethacrylate (EGDMA) *via* CCTP to produce vinyl-terminated branched EGDMA-based macromonomers, which are then used as crosslinking agents in the formulation of HIPEs containing various acrylic co-monomers. Photochemical curing of these HIPEs led to well-defined polyHIPE materials. Morphological and mechanical properties of the synthesised materials were studied.

## 5.2 Results and Discussion

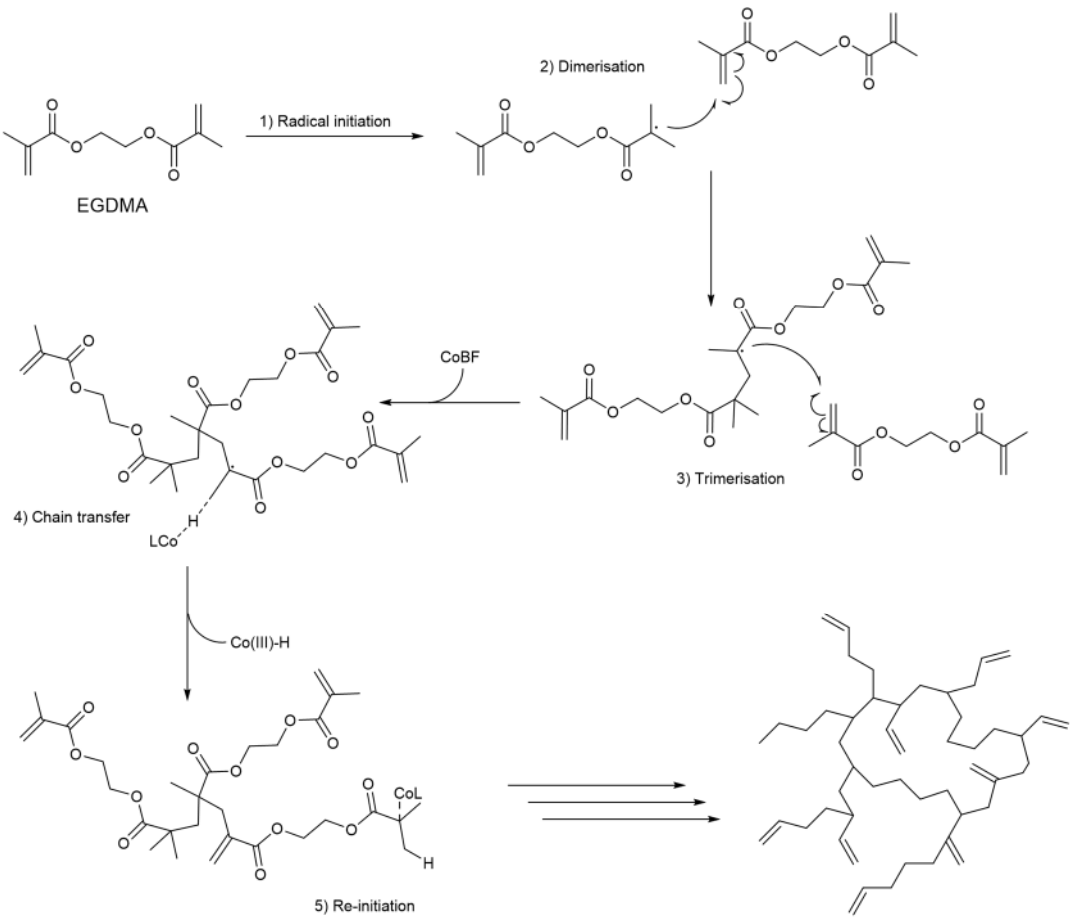


**Scheme 5.1** CCT mechanism for the homopolymerisation of EGDMA.

### 5.2.1 Branched p(EGDMA) Macromonomer Synthesis

Free-radical polymerisation of multi-vinyl monomers usually yields insoluble crosslinked materials. It can however, result in the formation of branched polymers when using chain transfer agents, such as cobaloximes within a CCTP process, as shown in scheme 5.1. Sherrington and co-workers developed a free radical one-step process to access branched polymers whereby vinyl monomers are polymerised in the presence of a crosslinking comonomer and balancing levels of a chain transfer agent, often referred to as the *Strathclyde methodology*.[30]

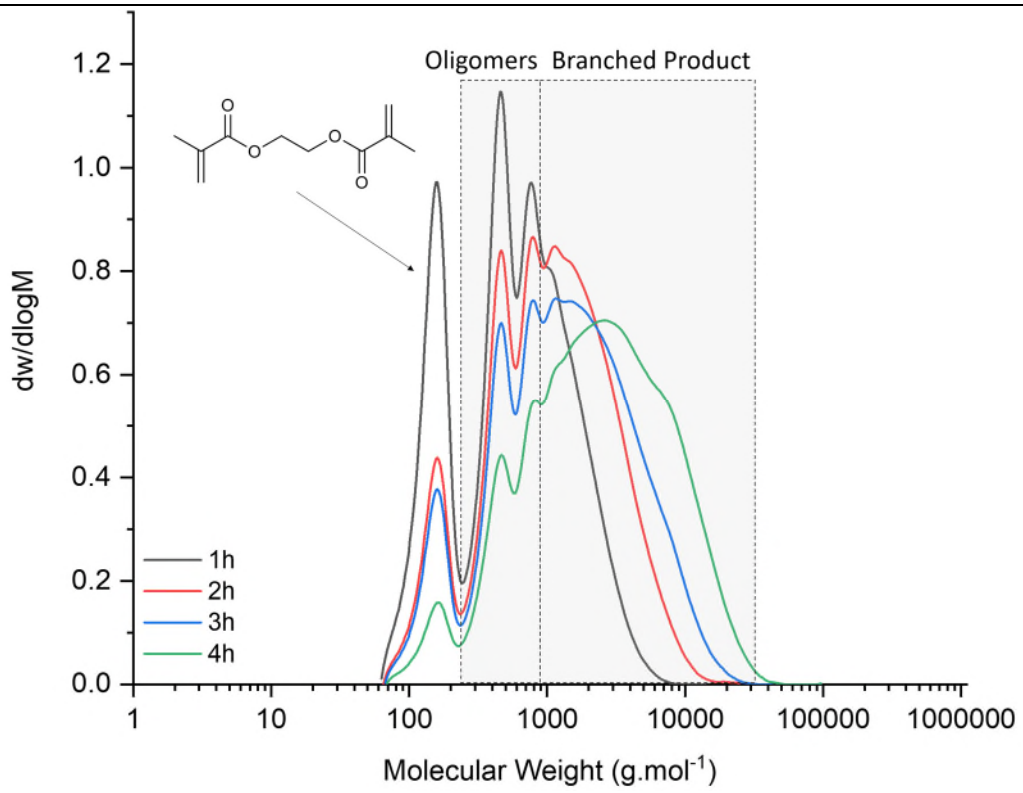


**Figure 5.1** Overlay of GPC ($CHCl_3$, 30 °C) traces for p(EGDMA) (**P1**, 0.0490 mol% CoBF) prepared by CCTP monitored hourly. Measurements by David Seow.

The strategy of balancing the level of a crosslinking comonomer with that of a free-radical chain transfer agent prevents gelation and allows control over the degree of branching to the polymer architecture.[31] However, in this Strathclyde methodology, both large amounts of chain transfer agents, typically > 10%, are required and adverse organic functionalities (e.g. thiols) are incorporated into the polymer backbone.

| Entry | CoBF loading / mol% | $M_n$ / g.mol$^{-1}$ | $M_w$ / g.mol$^{-1}$ | $Đ$ | Conversion / % | $Ext_{db}/Int_{db}$[a] |
|---|---|---|---|---|---|---|
| **P1** | 0.0490 | 1000 | 4090 | 4.0 | 89.7 | 1.41 |
| **P2** | 0.0735 | 650 | 2150 | 3.3 | 92.8 | 1.21 |

**Table 5.1** p(EGDMA) branched homopolymers synthesised in this study. [a]Determined from $^1$H-NMR.

Conversely, CCTP offers a convenient and efficient method to control the branching topology of the polymeric product by regulating chain transfer without having to use excessive quantities of chain transfer agent, i.e. ppm levels as opposed to > 10 wt%.[30–35] The branched polymers formed from these reactions exhibit low solution viscosity with high surface functionalisation using relatively low levels of chain transfer agents making CCTP of EGDMA an ideal candidate for branched polymer synthesis. Homopolymerisation of EGDMA *via* CCTP has been previously carried out under some specific conditions.[29]

Two different concentrations of CoBF were used for the polymerisation of EGDMA; 0.049 and 0.0735 mol% (475 and 710 ppm respectively) with respect to EGDMA, table 5.1. Low molecular weight branched oligomers were obtained, along with oligomeric products as seen by GPC, figure 5.1. As the reaction proceeds, molecular weight and dispersity increased whilst the number of dimers, trimers and oligomeric

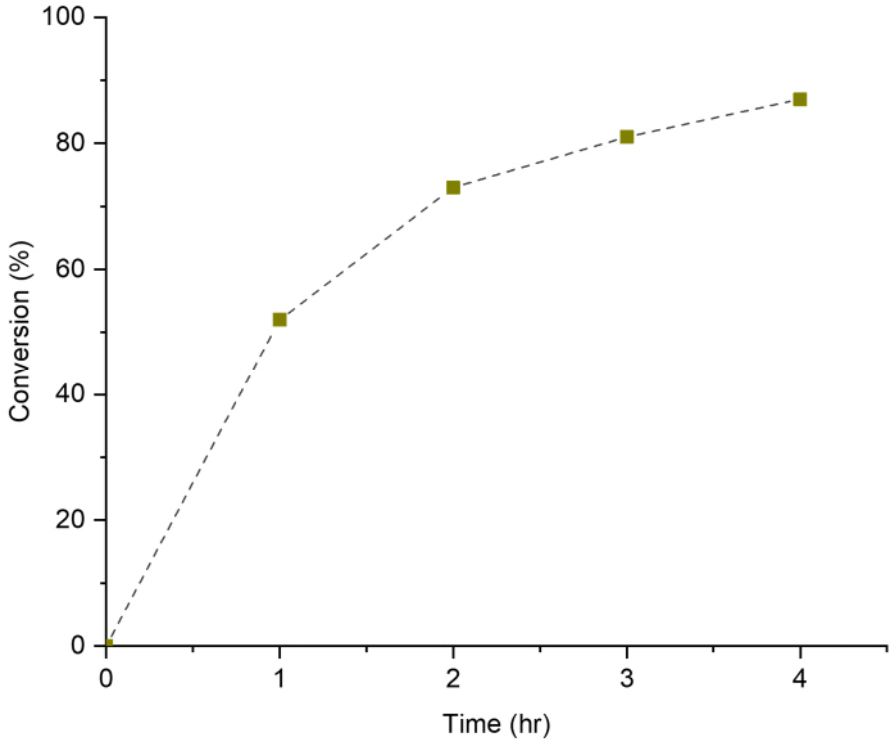


**Figure 5.2** GC-FID monitored conversion for the homopolymerisation of EGDMA by CCTP (**P1**, 0.0490 mol% CoBF).

products decreased in conjunction with the increase of the number of branched products. Polymerisation was quenched after four hours. Attempts to increase the timeframe of the reaction to 6 hours or more all resulted in gelation thus limiting monomer conversion to < 90%. This, along with the drift to higher molecular weight could be indicative of the catalyst being degraded during the reaction. A reaction time of 4 hours was chosen for all subsequent reactions, limiting catalyst decomposition.

Conversion of EGDMA to p(EGDMA) was also monitored using GC-FID, figure 5.2. Rapid monomer consumption was observed within the first hour, which subsequently began to plateau, leading to final conversions of around 85-90% without observable crosslinking after 4 hours. A linear increase in molecular weight was also observed, reaching values for $M_n$ of approximately 4100 g.mol$^{-1}$ with dispersities increasing to 4, figure 5.3. As expected, decreasing the concentration of CoBF led to an overall

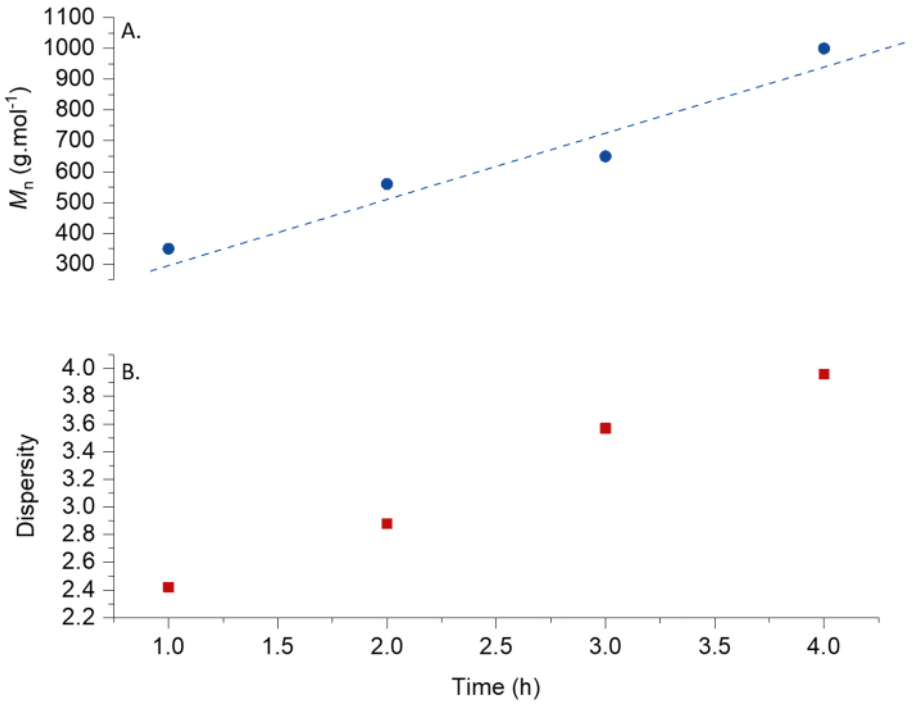


**Figure 5.3** Evolution of (A.) number average molecular weight ($M_n$) and (B.) dispersity with respect to polymerisation time obtained from GPC ($CHCl_3$, 30 °C) analysis of the homopolymerisation of **P1** by CCTP.

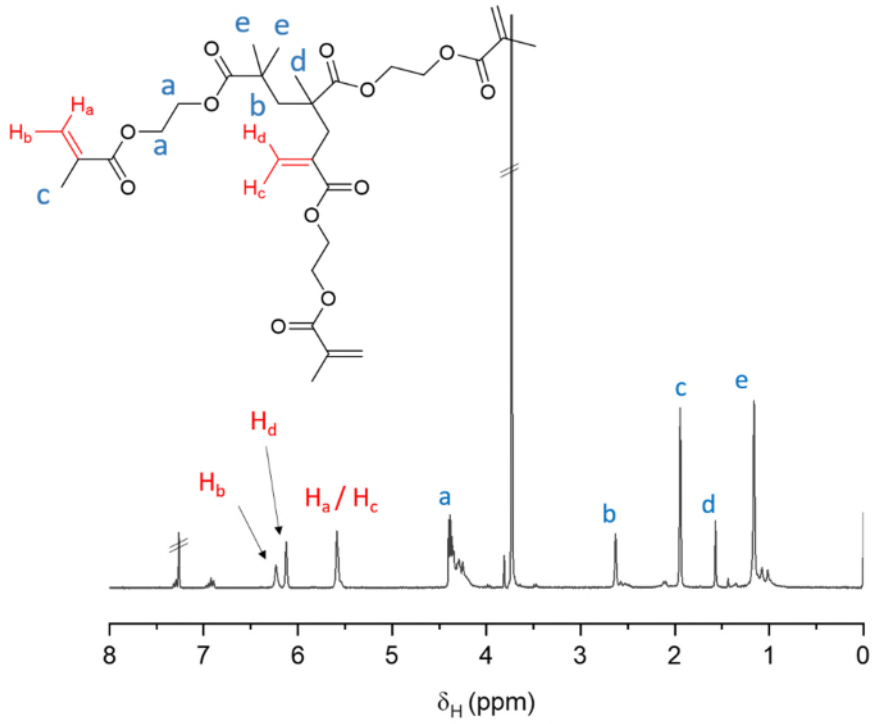


**Figure 5.4** $^1$H-NMR ($CDCl_3$, 400 MHz at 25 °C) spectrum of the **P1** macromonomer prepared by CCTP.

increase in molecular weight, however, no significant variation in monomer conversion was observed.

$^1$H-NMR confirmed the successful synthesis of the p(EGDMA) branched products, with external and internal vinyl hydrogen environments characterised by the appearance of peaks observed at 5.6, 6.1 and 6.2 ppm, figure 5.4. The ratios of external vinyl groups to internal vinylidene were calculated, for p(EGDMA) crosslinker **P1** as approximately 1.40. Similarly, for **P2**, the ratio was calculated as 1.20 (table 5.1). Each EGDMA addition to the propagating branched EGDMA provides a further locus from which to branch from as this is a "cascade polymerisation"; hence, the probability of branching increases with molecular weight.

Finally, figure 5.5 shows a MALDI-ToF spectrum of p(EGDMA). Two series of peaks are observed separated by 198.1 Da and corresponding, for each population, to the EGDMA repeat unit (with $Na^+$ or $K^+$ ions respectively). The highest intensity peak at

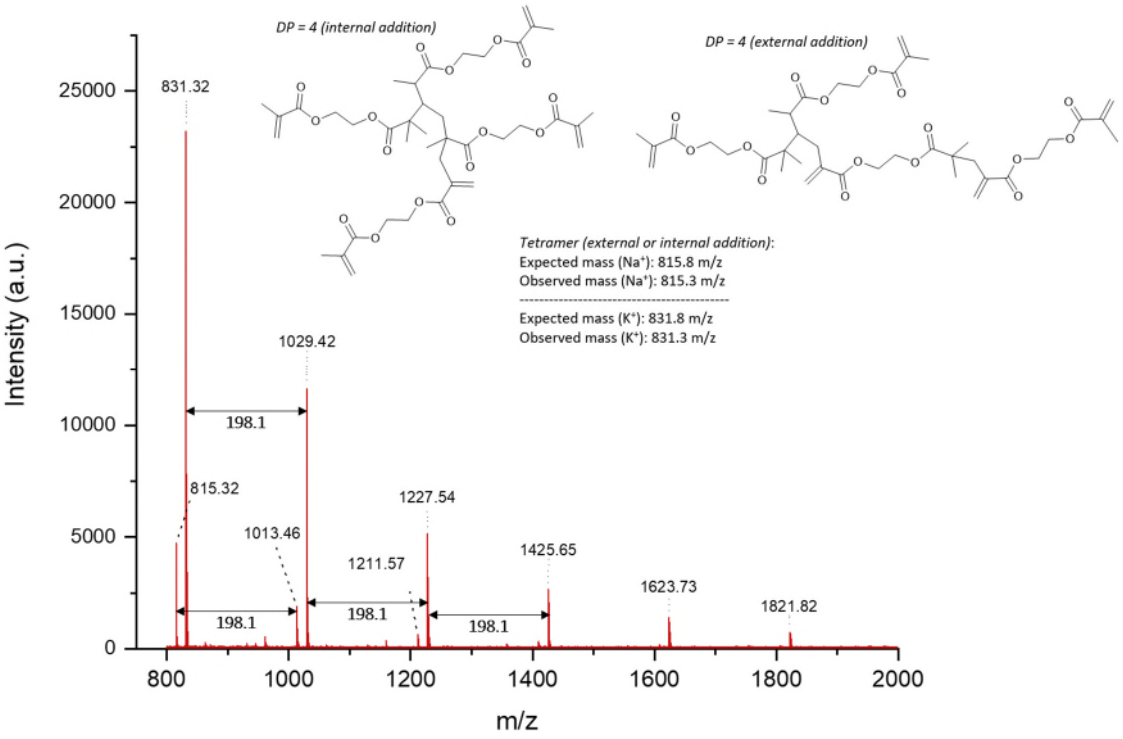


**Figure 5.5** MALDI–ToF spectrum of branched **P1** after 4 hours. Spectrum taken by Dr James S. Town.

831.3 m/z corresponds to the tetramer. The peak that contains the lowest isotope conformation of all atoms in the species indicates that each chain contains a number of vinyl terminations equal to the degree of polymerisation plus one, indicating that the CCTP synthesis has end group fidelity and all crosslinking points have been preserved.

### 5.2.2 PolyHIPE Synthesis

Water-in-oil high internal phase emulsions (HIPEs) were prepared at ambient temperature by the slow addition of deionised water, under constant mechanical stirring, to the continuous organic phase, which contained comonomers, surfactant, organic solvent and photo-initiator. A HIPE is achieved when the volume of the internal droplet phase becomes more than > 74% of the total emulsion volume.[38] The

HIPE internal phase volume fraction (φ) used in all preparations was 90% and, following transfer to a mould, the formed HIPEs were cured under UV radiation using a Fusion UV Systems Inc. *Light Hammer® 6* variable power UV curing system with LC6E benchtop conveyor and mercury discharge 'H' bulb that provides broad, high intensity UV light (200 watts/cm).

Branched p(EGDMA) macromonomers **P1** and **P2** were used in the preparation of polyHIPEs with the aim of exploiting their vinyl chain ends allowing for the synthesis of highly porous, mechanically stable polymeric networks. Dichloroethane (DCE) has in the past been successfully employed as a porogen in polyHIPE preparation.[39] The optimal porogen to monomer ratio has been previously reported to be between 40-50 w%, which closely matched the monomer to solvent ratio used in the CCTP of EGDMA. It was therefore reasoned that a one-pot reaction could be employed for the polyHIPE synthesis, which would not only be convenient and cost-effective, but may also lend interesting properties to the material. In order to produce stable HIPEs from EGDMA branched macromonomers, a number of formulations were tested under various conditions and monomer contents (figure S5.2). Moreover, due to EGDMA's hydrophilicity making the production of stable HIPEs challenging, UV photochemical curing was chosen over thermal curing as it provided higher reaction rates and shorter polymerisation times, thus minimising potential phase separation. In these HIPE formulations, a photoinitiator was used consisting of a blend of diphenyl(2,4,6-trimethylbenzoyl)phosphine oxide and 2-hydroxy-2-methylpropiophenone and a polymeric surfactant (PEG 30-dipolyhydroxystearate -Hypermer B246-; HLB = 6) was employed as steric stabiliser, kinetically hindering coalescence and agglomeration.[40,41]

Despite the prolonged exposure to high intensity UV light, initial curing experiments of HIPEs made from p(EGDMA) macromonomers **P1** and **P2** proved unsuccessful. Acrylate monomers have propagation rate coefficients, $k_p$ that are up to one order of magnitude higher than methacrylates and are therefore able to enhance curing of HIPEs.[42] Consequently, three different acrylate comonomers: 2-ethylhexyl acrylate (EHA), isobornyl acrylate (IBOA) and 2-methoxyethyl acrylate (MEA) were separately investigated as propagation promoters in the preparation of polyHIPEs.

HIPEs prepared with propagation promoters were found to cure efficiently without any noticeable phase separation. However, it was observed that the polyHIPE materials formed displayed different morphologies (discussed later). The morphology of the polyHIPE plays a key role in determining their suitability for different applications. EHA-based HIPE prepared at a 25% volume ratio of EHA with respect to the crosslinker solution were found to yield a stable HIPE that cured into a polyHIPE material. However, HIPE formulations with low EHA content were unable to cure. Upon an increase of EHA content, very stable, polymerisable HIPEs were formed (figure S5.3). This could be potentially attributed to the hydrophobic character of EHA monomer, offering resistance to droplet coalescence in emulsions. Similarly, IBOA-based polyHIPEs were successfully synthesised. IBOA is a hydrophobic monomer, and can also offer stability to the emulsion through resistance to droplet coalescence.

Due to the rapid curing time provided by photo-polymerisation, an opportunity was presented to attempt the use of unconventional monomers, such as those that may form less stable HIPEs.[18] Therefore, once reliable polyHIPE formulations were established using hydrophobic monomers, polyHIPE synthesis using a hydrophilic monomer such as 2-methoxyethyl acrylate (MEA) was explored. MEA is a water-soluble monomer

and its resulting polymer is moderately hydrophobic. It has been reported that MEA polymers exhibit excellent blood-compatibility and therefore have been explored as a coating material for biomedical devices.[43,44] MEA-based HIPEs were found to be significantly less viscous than their EHA- or IBOA-based counterparts. This is likely to be due to the enhanced partitioning of MEA stemming from its polar nature, thereby increasing the droplet size of the internal phase and reducing the viscosity of the HIPE. Furthermore, it is possible that there is some diffusion of MEA monomer into the aqueous phase, lowering the concentration of MEA in the continuous oil phase and causing destabilisation of the emulsion. This can, in turn, decrease the rate of polymerisation, therefore impeding the formation of a 3D network. The comparatively low propagation rate of methacrylates as well as the added steric hindrance surrounding the macromonomers' vinyl groups are thought to be the reasons why no polyHIPEs were formed without the addition of the acrylate propagation promoters. While the addition of propagation promoters enable the synthesis of the polyHIPE, it is unknown whether all, or some of the vinyl bonds are first reacted with propagation promoters before reaction with other cross-linkers. This, in turn, implies the formation of linear "bridges" between cross-linkers composed of one or more acrylates. Whether all acrylates are reacted can be investigated by grinding of the polyHIPE, followed by the soaking of the resulting powder in an NMR solvent, which would dissolved any unreacted material.

As it is an important factor in the synthesis of polyHIPEs, we also wished to investigate the effects p(EGDMA) crosslinkers' size. To this effect, polyHIPE preparations were carried out with **P2** as crosslinker (figure S5.4). A correlation between the hydrophobicity of the monomer and the ability to form a polyHIPE was

identified. The difference in curing ability between the EHA and IBOA compositions is likely due to the difference in propagation rates of the respective monomers.

The bulky IBOA monomer has a lower propagation rate coefficient while EHA propagates significantly faster, typically around 10 and 17 kL.mol$^{-1}$.s$^{-1}$ at ambient temperature, respectively.[45]

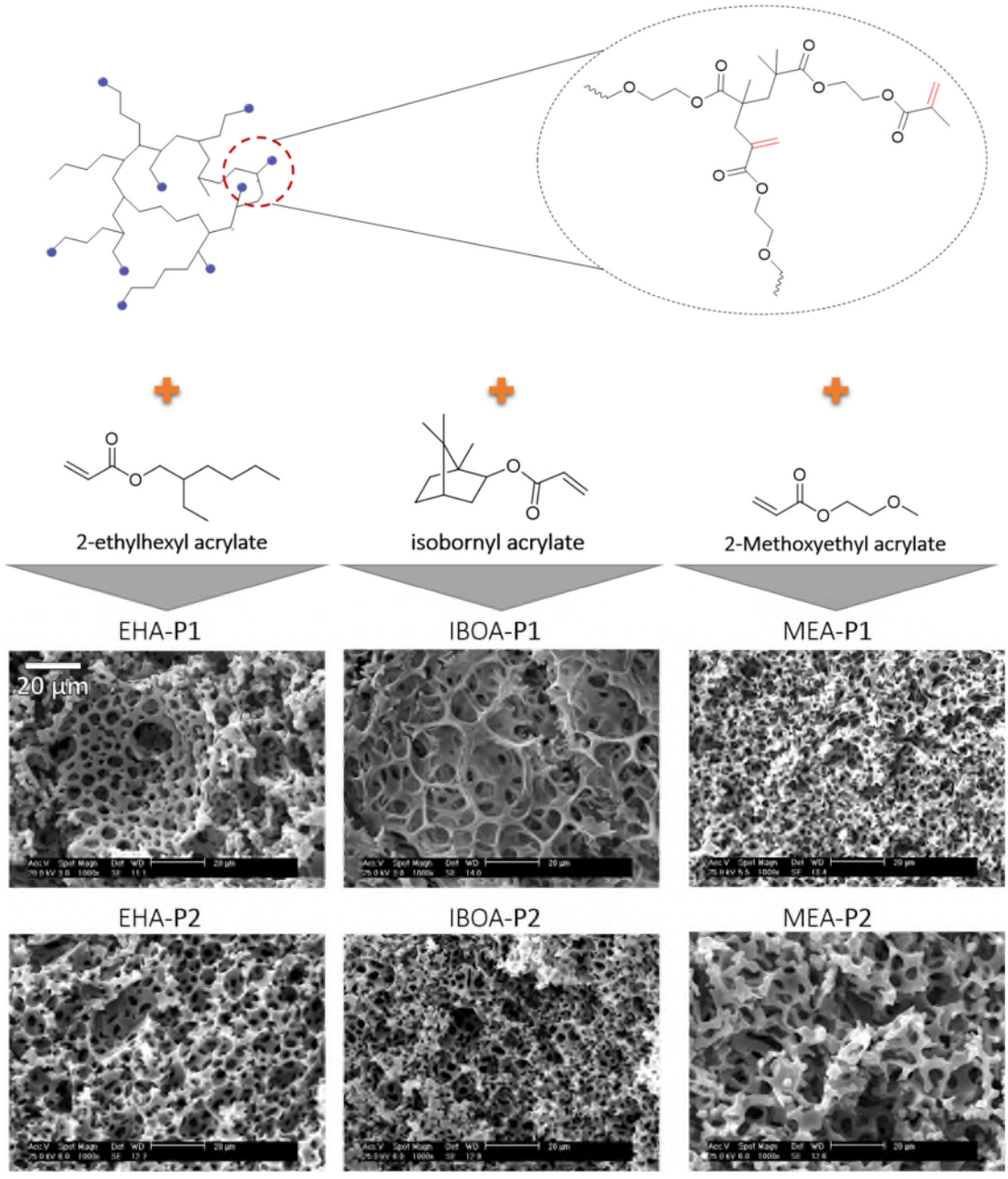


**Figure 5.6** SEM images of polyHIPEs synthesised using **P1** or **P2** as cross-linking agents. Images taken by Dr Ahmed M. Eissa.

### 5.2.3 PolyHIPE Characterisation

Morphologies of EHA-, IBOA- and MEA-based polyHIPEs were studied using scanning electron microscopy (SEM), figure 5.6, which showed that all prepared polyHIPE materials possessed an interconnected network of pores. PolyHIPEs that exhibit highly interconnected voids have previously been utilised in 3D cell culture and tissue engineering applications as such morphology allows cell infiltration into the material as well as free movement of nutrients and waste products to and from cells.[46–48] It is known that the morphology and pore size distribution of polyHIPEs are governed by both the emulsion droplet diameter at the gel point and the polymerisation rate. The droplet diameter is determined by the emulsion stability and shear during emulsion preparation. Polymerisation rate affects morphology as a slow polymerisation allows emulsion coarsening to occur before gelation, resulting in a larger droplet diameter. The morphologies of polyHIPEs obtained from EHA and IBOA show little variation from each other, most likely due to the fact that these monomers have similar hydrophobicity character and therefore their corresponding emulsions will have approximately the same emulsion stability and droplet diameter. Conversely, as all comonomers used are acrylates, it is assumed that their propagation rate constants are similar. However, polyHIPEs made from MEA were found to have a more closed-cell structure compared to those made from EHA and IBOA, presumably due to the hydrophilic character of MEA and hence the lower stability of its emulsions, as discussed above. It seems that comonomer type has a considerable influence on void diameter. PolyHIPEs made from macromonomer crosslinker **P1** and comonomer IBOA exhibited the most well-defined, open cellular morphologies for this set of monomers used in this work. All other polyHIPE materials lacked defined cellular structures, instead resembling macroporous polymer morphologies

| | | *Propagation promoter* | | |
|---|---|---|---|---|
| | | **EHA** | **IBOA** | **MEA** |
| *EGDMA Crosslinker* | **P1** | 3.37 ± 1.47 | 33.50 ± 6.80 | 9.17 ± 3.40 |
| | **P2** | 9.50 ± 3.27 | 45.77 ± 12.22 | 21.40 ± 6.58 |

**Table 5.2** 3 samples average Young's moduli (kPa, ± SD) of the polyHIPEs prepared in this study.

consequently, attempts to determine void diameter distributions for these materials were not successful. However, where possible the majority of voids in these materials were found to be in the range of 5 – 20 µm in diameter. A plausible explanation for the loss of cellular morphology is the collapse of the HIPEs before gelation. Nevertheless, no apparent evidence of phase separation of emulsions was observed. An alternative explanation could be due to the influence of the porogen, DCE. Previous work by Cameron *et al.*[49] concluded that the porogen in an emulsion mixture can act as a co-surfactant, lowering the interfacial tension. This induces phase separation of the monomeric continuous phase during polymerisation. This is accompanied by the enlargement of the window to such an extent that the cellular structure is no longer obvious.

Good mechanical properties of polyHIPEs are essential in determining their end-applications. Fabrication of polyHIPEs with tuneable mechanical properties proves to be advantageous in the investigation for new applications of these porous materials. For instance, Owen *et al.*[50] showed that stiff pure IBOA-based polyHIPE promoted osteogenic differentiation of mesenchymal cells much better than other types of softer, acrylate-based polyHIPE. Consequently, compression tests were performed on all prepared polyHIPE materials. Stress-strain curves for all materials revealed typical rigid foam behaviour where curves with an initial linear elastic region followed by a

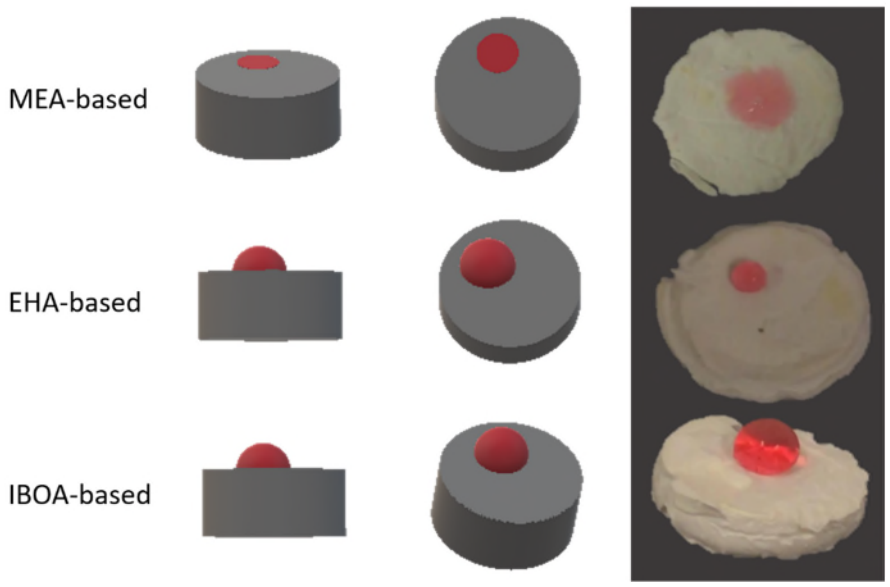


**Figure 5.7** Surface wettability of polyHIPEs at room temperature using dyed water, with images taken after 15 seconds.

plateau were observed. Compressive (Young's) moduli values for all polyHIPE materials are presented in table 5.2. Moduli values were calculated from the slope of the linear elastic region at low strain (< 10 %), and each measurement was repeated 3 times for increased accuracy. Results showed that EHA- and MEA-based polyHIPEs are quite flexible and could recover almost completely to their original dimensions after compression. However, IBOA-based polyHIPEs are relatively rigid, showing irreversible deformation as a result of brittle crushing of the foam microstructure. Results also showed that the compressive (Young's) moduli values for polyHIPE materials derived from macromonomer crosslinker **P1** are lower than those for polyHIPE materials derived from **P2**. This can be attributed to the formation of stronger networks when a lower molecular weight macromonomer crosslinker **P2** is used.

Due to extreme surface roughness and high porosity of polyHIPEs, contact angle measurements cannot be related to surface tension and therefore yields unreliable results. Instead, surface wettability has been investigated by depositing a drop of deionised water coloured with red food dye, onto dry polyHIPE surfaces, figure 5.7. Immediately after application, the coloured water droplet had dispersed on the surface of a MEA-based polyHIPE, with the bulk of the droplet quickly penetrating through the surface, verifying the hydrophilic nature of the polyHIPE. However, the low hydrophilicity of the EHA-based polyHIPE allowed the droplet to maintain its shape for several seconds, before it began to spread across the surface. Conversely, the water droplet did not disperse on the IBOA-based polyHIPE surface and the water droplet held its spherical shape for at least 15 min, remaining on the surface and was not absorbed into the material through capillary action. These results suggest that hydrophilic / hydrophobic properties of the starting comonomers can be retained in the resulting polyHIPEs, highlighting the tailored surface functionality of these materials.

## 5.3 Conclusions and Outlook

The preparation of a range of polyHIPE materials by combining catalytic chain transfer polymerisation (CCTP) and emulsion templating using branched macromonomers and a range of commercially available functional acrylates has been described. CCTP was first employed for the synthesis of EGDMA-based branched macromonomers to be used as crosslinkers in HIPE formulations. Control over branching and molecular weight was achieved by using different CoBF concentrations. One-pot preparation of polyHIPEs without any need for purification

of CCTP macromonomers was also demonstrated, highlighting the potential of this approach for industrial scale-ups.

It was found necessary to employ acrylate comonomers (EHA, IBOA and MEA) to promote propagation and hence favour the formation of crosslinked networks. These comonomers with various hydrophobic characteristics were shown to retain their properties in the resulting polyHIPE, highlighting the tunability of the material. Further, by varying the crosslinker size, the propagation promoter type or ratio thereof, a wide array of polyHIPEs could be obtained with varying degrees of hydrophilicity and mechanical properties, opening the door to the synthesis of products with finely tuned properties for targeted applications. This was first shown by the surface wettability experiments, while SEM confirmed that the prepared polyHIPEs possessed high levels of porosity and interconnectivity. Finally, their mechanical behaviour under compression was studied and correlated with the nature of the monomer as well as the molecular weight and degree of branching of the crosslinker, higher molecular weight branched crosslinkers leading to weaker crosslinking and therefore a more brittle material.

With the results of this preliminary study, more tailoring of polyHIPEs can be envisaged. The described synthetic approach can be used as a route to produce the next generation of polyHIPE materials where functionality and rigidity can be tightly tailored for a wide range of applications. These applications would, in part, comprise the test of these polyHIPEs as scaffolds for cell growth such as primary human endometrial cells, as was shown by Eissa *et al.*,[8] while p(EGDMA) could be investigated as crosslinker in similar network-creating applications, for instance 3D printing technology.

# 5.4 Experimental Data

## 5.4.1 Polymer Characterisation

**p(EGDMA)**:

$^1$H-NMR (400 MHz, $CDCl_3$ at 25 °C): δ 6.20- 6.35 (internal $CH_a\underline{H}_b$=C), 6.05-6.15 (terminal $CH_a\underline{H}_b$=C), 5.50-5.60 (terminal $C\underline{H}_aH_b$=C + internal $CH_aH_b$=C), 4.15-4.45 ($OC\underline{H}_2C\underline{H}_2O$), 2.45-2.60 (backbone $CH_2$), 2.15-2.20 (backbone $CH_2$), 1.85-2.05 (terminal $CH_3$), 1.00-1.50 (backbone $CH_3$),

| Code | CoBF / mg | CoBF / mol% |
|---|---|---|
| **P1** | 20 | 0.049 |
| **P2** | 30 | 0.0735 |

**Figure S5.1** Amount of CoBF used in EGDMA homopolymerisations.

GPC ($CHCl_3$, 30°C): **P1**: $M_n$ = 1030 g mol$^{-1}$, $M_w$ = 4090 g mol$^{-1}$, $Đ$ = 4.0; **P2**: $M_n$ = 660 g.mol$^{-1}$, $M_w$ = 21500 g mol$^{-1}$, $Đ$ = 3.3

| ***Entry*** | ***P1 / mL*** | ***Distilled Water / mL*** | ***Photo Initiator / mL*** | ***Surfactant / g*** | ***$H_2O$ Rate of addition / mL.min$^{-1}$*** | ***HIPE*** | ***PolyHIPE*** |
|---|---|---|---|---|---|---|---|
| **1** | 2.5 | 22.5 | 0.4 | 0.4 | 4.5 | Not Stable | N/A |
| **2** | 2.5 | 22.5 | 0.4 | 0.4 | 1.125 | Stable | No |
| **3** | 2.5 | 22.5 | 0.8 | 0.4 | 1.125 | Stable | No |
| **4** | 2.5 | 22.5 | 0.8 | 0.4 | 1.125 | Stable | No |

**Figure S5.2** Initial HIPE formulations with **P1**.

| *Entry* | *Propagation promoter* | *P1 / mL* | *propagation promoter / mL* | *Distilled Water / mL* | *Surfactant / g* | *HIPE Stability* | *PolyHIPE* |
|---|---|---|---|---|---|---|---|
| **1** | EHA | 0.5 | **0.5** | 9 | 0.1 | Not stable | No |
| **2** | EHA | 0.5 | **0.5** | 9 | 0.2 | Not stable | No |
| **3** | EHA | 0.6 | **0.15** | 6.75 | 0.1 | Stable | No |
| **4** | EHA | 2.4 | **0.2** | 23.5 | 0.2 | Stable | No |
| **5** | EHA | 2.4 | **0.4** | 25 | 0.2 | Stable | Yes |
| **6** | EHA | 2.4 | **0.6** | 27 | 0.2 | Stable | Yes |
| **7** | EHA | 2.4 | **0.8** | 29 | 0.2 | Stable | Yes |
| **8** | IBOA | 2.4 | **0.6** | 27 | 0.2 | Stable | Yes |
| **9** | IBOA | 2.4 | **0.8** | 29 | 0.2 | Stable | Yes |
| **10** | MEA | 2.4 | **0.6** | 27 | 0.2 | Stable | Yes |
| **11** | MEA | 2.4 | **0.8** | 29 | 0.2 | Stable | Yes |
| **12** | MEA | 2.4 | **1** | 30 | 0.2 | Stable | Yes |
| **13** | MEA | 2.4 | **1.4** | 33 | 0.2 | Stable | Yes |
| **14** | MEA | 2.4 | **1.8** | 37 | 0.2 | Stable | Yes |
| **15** | MEA | 2.4 | **2.2** | 41 | 0.2 | Semi-stable | No |

**Table S5.3** PolyHIPE formulations using **P1** and acrylate propagation promoters.

| *Entry* | *Propagation promoter* | *P2 / mL* | *propagation promoter / mL* | *Distilled Water / mL* | *Surfactant / g* | *HIPE Stability* | *PolyHIPE* |
|---|---|---|---|---|---|---|---|
| **1** | EHA | 2.4 | **0.8** | 29 | 0.2 | Stable | Yes |
| **2** | IBOA | 2.4 | **0.8** | 29 | 0.2 | Stable | Yes |
| **3** | MEA | 2.4 | **0.8** | 29 | 0.2 | Stable | Yes |

**Table S5.4** PolyHIPE formulations using **P2** and acrylate propagation promoters.

### 5.4.2 Materials

Unless stated otherwise, all chemicals mentioned were purchased from Sigma-Aldrich and were used without further purification.

Hypermer B246 and V-601 were obtained from Croda international and Wako Chemicals respectively.

### 5.4.3 Instrumentation

*$CHCl_3$ Gel-Permeation Chromatography (GPC)* was carried out on an Agilent Infinity II MDS instruments equipped with differential refractive index (DRI), viscometry (VS) and dual angle light scatter (LS) detectors. The system was equipped with 2 x PLgel Mixed C columns (300 x 7.5 mm) and a PLgel 5 µm guard column. The eluent used was $CHCl_3$ with 2 % TEA (triethylamine) additive. Samples were run at 1ml/min at 30 °C. PMMA standards between 540 Da and 1000 kDa (Agilent EasyVials) were used for calibration. Ethanol was added as a flow rate marker. Analyte samples were filtered through a GVHP membrane with 0.22 µm pore size before injection. number average molecular weight ($M_{n,GPC}$) and dispersity ($Đ$) values of synthesized polymers were determined by conventional calibration using Agilent GPC/SEC software.

*Gas chromatography flame ionisation detection (GC-FID)* analysis was performed on a Shimadzu GC2014 equipped with a Shimadzu A0C20iautosampler, the injection temperature was 250 °C. The GC was fitted with a Restek Rxi-1ms (15 m length, 0.25 mm ID and 0.25 µm film thickness). The carrier gas was hydrogen, supplied by an external hydrogen generator. The injection volume was 1 µl with a 39 split ratio. The detector was a flame ionisation detector (FID) with a flame temperature of 320 °C, and a sampling rate of 40 ms. The heating profile was 60 °C for 1 minutes and then

heated to 320°C at 40 °C min-1where it remained for a further 2.5 minutes. Data processing was carried out using Shimadzu GC solutions software.

*Nuclear magnetic resonance (NMR, $^{1}H$ and $^{13}C$)* spectra were recorded at room temperature on a Bruker Avance III HD-400 or 300 using either deuterated chloroform or deuterated dimethyl sulfoxide referenced against TMS as a reference.

*Matrix-assisted laser desorption/ionization time-of-flight (MALDI-ToF)* spectra were collected using a Bruker Autoflex Speed, equipped with a 337 nm nitrogen laser, operating in reflectron positive mode with an ion source voltage of 19 kV. Results were accumulated in 10 readings of each spot with 500 laser shots, leading to a total of 5000 laser shots per spectra. Laser power was tuned to keep noise low while maintaining the signal as to not remove any trace peaks. The samples were dissolved into the appropriate solvent at concentrations of 10 mg $ml^{-1}$, along with the cationizing agent sodium iodide (NaI) at 0.1 mg $ml^{-1}$. A matrix solution was then made up of trans-2-[3-(4-tert-Butylphenyl)-2-methyl-2-propenylidene]malononitrile (DCTB) in THF at a concentration of 40mg $ml^{-1}$, along with NaI at 0.1 mg $ml^{-1}$. 10 μl of both the matrix and sample solutions were then mixed together, and 0.5 μl of the resulting solution was then spotted on an MTP 384 ground steel target plate.

*Scanning electron microscopy (SEM)* imaging was carried out on a Zeiss SUPRA 55-VP FEGSEM operating at 25 kV. Fractured polyHIPE pieces were sputter-coated with gold using a QUORUM sputter coating system. Images were taken with an OXFORD X-ray analysis system and GATAN CL system. Average void size distribution was

calculated using Image J Version 1.50i. A statistical correction factor was applied to the measured values.

The mechanical behaviour of polyHIPE materials under compression was evaluated using a Shimadzu EZ-LX compact table-top universal tester equipped with a 500 N load cell fitted with compression plates tested at ambient temperature. The polyHIPE samples were cubes of 0.5 mm in dimension. Compression was continued until a final strain of around 50% was reached. Experiments were repeated in triplicates using three different samples of each material to obtain average Young's modulus values.

### 5.4.4 Experimental Procedures

**EGDMA Homopolymerisation**

A 100 mL rbf with CoBF and a stirrer bar was de-oxygenated for 30 min via nitrogen bubbler. A separate 100 mL rbf with EGDMA (20 mL), DCE (25 mL), anisole (1 mL) and V-601 (200 mg) was immersed in an ice bath and de-oxygenated for 20 min. The liquids were transferred to the solids under positive nitrogen pressure. The solution was degassed for a further 5 min under continuous stirring. The RBF was immersed in an oil bath at 70 °C for 4 hours under nitrogen. Samples were taken hourly (approx. 0.1 ml) via degassed syringe in order to obtain GPC, GC-FID and $^{1}$H-NMR measurements. The reaction terminated by removal from heat and introduction of oxygen.

**PolyHIPE preparation**

In a 100 mL two-necked RBF covered in foil, an oil phase consisting of PEGDMA solution (2.4 mL), acrylate (EHA, IBOA or 2-methoxyethyl acrylate) and Hypermer

B246 (0.2 g unless stated) was sonicated until homogenous. The photoinitiator (0.8 mL unless stated), a blend of diphenyl(2,4,6-trimethylbenzoyl)phosphine oxide and 2-hydroxy-2-methylpropiophenone, was added to the mixture with continuous stirring at ambient temperature using a D-shaped PTFE paddle attached to an overhead stirrer at 350 rpm. An aqueous phase of deionised water was added drop-wise to the oil phase over 20 min, with continuous stirring, to form a HIPE with an internal (aqueous) phase volume fraction of 90%. Once all the aqueous phase was added, the HIPE was transferred into cylindrical PTFE moulds (diameter 15 mm, depth; 2 mm, 3.5 mm and 5 mm) that was secured between two glass plates. The HIPE was passed under a UV irradiator (Fusion UV Systems Inc. Light Hammer® 6 variable power UV curing system with LC6E benchtop conveyor and mercury discharge 'H' bulb) 25 times on each side, at a belt speed of 5.0 m $min^{-1}$. The cured polyHIPE material was washed by immersion in acetone and dried at ambient temperature for 24 h.

## 5.5 References

1 A. M. Eissa, P. Wilson, C. Chen, J. Collins, M. Walker, D. M. Haddleton and N. R. Cameron, *Chem. Commun.*, 2017, **53**, 9789–9792.

2 T. N. Gao, T. Wang, W. Wu, Y. Liu, Q. Huo, Z. A. Qiao and S. Dai, *Adv. Mater.*, 2019, **31**, 1806254.

3 F. Huang, K. Lin, Z. Wang, Z. Hu, P. Luo, X. Yang, X. Zhang, M. Rafiq and Y. Cao, *J. Mater. Chem. A*, 2019, **6**, 1–3.

4 D. Wu, F. Xu, B. Sun, R. Fu, H. He and K. Matyjaszewski, *Chem. Rev.*, 2012, **112**, 3959–4015.

5 Y. Kou, Y. Xu, Z. Guo and D. Jiang, *Angew. Chemie - Int. Ed.*, 2011, **50**, 8753–8757.

6 US Pat., 20100326847A1, 2008.

7 J. Kwon, J. Kim, D. Park and H. Han, *Polymer (Guildf).*, 2015, **56**, 68–72.

8 A. M. Eissa, F. S. V. Barros, P. Vrljicak, J. J. Brosens and N. R. Cameron, *Biomacromolecules*, 2018, **19**, 3343–3350.

9 C. E. Severn, A. M. Eissa, C. R. Langford, A. Parker, M. Walker, J. G. G. Dobbe, G. J. Streekstra, N. R. Cameron and A. M. Toye, *Biomaterials*, 2019, **225**, 1-13.

10 M. S. Silverstein, *Prog. Polym. Sci.*, 2014, **39**, 199–234.

11 H. Deleuze, R. Faivre and V. Herroguez, *Chem. Commun.*, 2002, **2**, 2822–2823.

12 M. Lamson, Y. Epshtein-Assor, M. S. Silverstein and K. Matyjaszewski, *Polymer (Guildf).*, 2013, **54**, 4480–4485.

13 K. L. Anderson, W. Nazarov, C. S. A. Musgrave, N. Bazin and D. Faith, *J. Radioanal. Nucl. Chem.*, 2014, **299**, 969–975.

14 C. Chen, A. M. Eissa, T. L. Schiller and N. R. Cameron, *Polymer (Guildf).*,

2017, **126**, 395–401.

15 H. Zhang, Y. Zhu, J. Chen and S. Zhang, *J. Polym. Sci. Part A Polym. Chem.*, 2017, **55**, 2129–2135.

16 C. Xiao, Y. Zhu, J. Chen and S. Zhang, *Polymer (Guildf).*, 2017, **110**, 74–79.

17 C. J. Atkins, G. Patias, J. S. Town, A. M. Wemyss, A. M. Eissa, A. Shegiwal and D. M. Haddleton, *Polym. Chem.*, 2019, **10**, 646–655.

18 A. Shegiwal, A. M. Wemyss, M. A. J. Schellekens, J. de Bont, J. Town, E. Liarou, G. Patias, C. J. Atkins and D. M. Haddleton, *J. Polym. Sci. Part A Polym. Chem.*, 2019, **57**, E1–E9.

19 G. Patias, A. M. Wemyss, S. Efstathiou, J. S. Town, C. J. Atkins, A. Shegiwal, R. Whitfield and D. M. Haddleton, *Polym. Chem.*, 2019, **10**, 6447–6455.

20 A. Shegiwal, A. M. Wemyss, E. Liarou, J. Town, G. Patias, C. J. Atkins, A. Marathianos, D. W. Lester, S. Efstathiou and D. M. Haddleton, *Eur. Polym. J.*, 2020, **125**, 109491.

21 US Pat., US4694054A, 1987.

22 J. Cowie, in *Polymers: Chemistry & Physics of Modern Material*, United-Kingdom, 1991, pp. 53–81.

23 WO/1995/027737, *Polym. Chem. Phys. Mod. Mater.*, 1991, 53–81.

24 A. A. Gridnev, *Polym. J.*, 2005, **24**, 613–623.

25 A. Gridnev, *J. Polym. Sci. Part A Polym. Chem.*, 2000, **38**, 1753–1766.

26 J. P. A. Heuts and N. M. B. Smeets, *Polym. Chem.*, 2011, **2**, 2407–2423.

27 G.-Z. Li and D. M. Haddleton, *Polym. Prepr. (Am. Chem. Soc., Div. Polym. Chem.)*, 2010, **51**, 555.

28 J. P. Menzel, D. M. Haddleton and E. Khoshdel, *Polym. Prepr.*, 2010, **51**, 721–722.

29 K. A. McEwan and D. M. Haddleton, *Polym. Chem.*, 2011, **2**, 1992–1999.

30 N. O'Brien, A. McKee, D. C. Sherrington, A. T. Slark and A. Titterton, *Polymer (Guildf).*, 2000, **41**, 6027–6031.

31 P. . Costello, I. . Martin, A. . Slark, D. . Sherrington and A. Titterton, *Polymer (Guildf).*, 2002, **43**, 245–254.

32 M. H. Bouhier, P. A. G. Cormack, S. Graham and D. C. Sherrington, *J. Polym. Sci. Part A Polym. Chem.*, 2007, **45**, 2375–2386.

33 P. Besenius, S. Slavin, F. Vilela and D. C. Sherrington, *React. Funct. Polym.*, 2008, **68**, 1524–1533.

34 M. Chisholm, N. Hudson, N. Kirtley, F. Vilela and D. C. Sherrington, *Macromolecules*, 2009, **42**, 7745–7752.

35 R. M. England and S. Rimmer, *Polym. Chem.*, 2010, **1**, 1533–1544.

36 L. Jiang, W. Huang, X. Xue, H. Yang, B. Jiang, D. Zhang, J. Fang, J. Chen, Y. Yang, G. Zhai, L. Kong and S. Wang, *Macromolecules*, 2012, **45**, 4092–4100.

37 Z. Guan, *J. Am. Chem. Soc.*, 2002, **124**, 5616–5617.

38 N. D. Weiner, *J. Pharm. Sci.*, 1975, **64**, 1434.

39 N. Leber, J. D. B. Fay, N. R. Cameron and P. Krajnc, *J. Polym. Sci. Part A Polym. Chem.*, 2007, **45**, 4043–4053.

40 S. Yasin, P. F. Luckham, T. Iqbal, M. Zafar and N. Ramzan, *J. Dispers. Sci. Technol.*, 2013, **34**, 737–746.

41 A. J. Wang, T. Paterson, R. Owen, C. Sherborne, J. Dugan, J. M. Li and F. Claeyssens, *Mater. Sci. Eng. C*, 2016, **67**, 51–58.

42 S. Beuermann and M. Buback, *Prog. Polym. Sci.*, 2002, **27**, 191–254.

43 M. Tanaka, A. Mochizuki, N. Ishii, T. Motomura and T. Hatakeyama, *Biomacromolecules*, 2002, **3**, 36–41.

44 M. Kocakulak, T. Özgürtaş and H. Ayhan, *J. Biomater. Sci. Polym. Ed.*, 2006, **17**, 449–460.

45 S. Beuermann, D. A. Paquet, J. H. McMinn and R. A. Hutchinson, *Macromolecules*, 1996, **29**, 4206–4215.

46 Naranda, M. Sušec, U. Maver, L. Gradišnik, M. Gorenjak, A. Vukasović, A. Ivković, M. S. Rupnik, M. Vogrin and P. Krajnc, *Sci. Rep.*, 2016, **6**, 1–11.

47 A. R. Murphy, J. M. Haynes, A. L. Laslett, N. R. Cameron and C. M. O'Brien, *Acta Biomater.*, 2020, **101**, 102–116.

48 S. A. Richardson, T. M. Rawlings, J. Muter, M. Walker, J. J. Brosens, N. R. Cameron and A. M. Eissa, *Macromol. Biosci.*, 2019, **19**, 1800351.

49 N. R. Cameron and A. Barbetta, *J. Mater. Chem.*, 2000, **10**, 2466–2471.

50 R. Owen, C. Sherborne, T. Paterson, N. H. Green, G. C. Reilly and F. Claeyssens, *J. Mech. Behav. Biomed. Mater.*, 2016, **54**, 159–172.